JAERI-M
90-073

AN INTERMEDIATE BREAK BWR LOCA TEST (RUN 991) AT ROSA-III

— SIMULATION OF ECCS LINE BREAK LOCA PHENOMENA —

April 1990

Mitsuhiro SUZUKI, Yoshinari ANODA, Hiroshige KUMAMARU
Hideo NAKAMURA, Taisuke YONOMOTO, Hideo MURATA
and Kanji TASAKA

日本原子力研究所
Japan Atomic Energy Research Institute

JAERI-M レポートは，日本原子力研究所が不定期に公刊している研究報告書です。
入手の問合わせは，日本原子力研究所技術情報部情報資料課（〒319-11茨城県那珂郡東海村）あて，お申しこしください。なお，このほかに財団法人原子力弘済会資料センター（〒319-11 茨城県那珂郡東海村日本原子力研究所内）で複写による実費頒布をおこなっております。

JAERI-M reports are issued irregularly.
Inquiries about availability of the reports should be addressed to Information Division Department of Technical Information, Japan Atomic Energy Research Institute, Tokai-mura, Naka-gun, Ibaraki-ken 319-11, Japan.

編集兼発行　日本原子力研究所
印　　刷　いばらき印刷㈱

An Intermediate Break BWR LOCA Test (RUN 991) at ROSA-III
- Simulation of ECCS Line Break LOCA Phenomena -

Mitsuhiro SUZUKI, Yoshinari ANODA, Hiroshige KUMAMARU
Hideo NAKAMURA, Taisuke YONOMOTO, Hideo MURATA
and Kanji TASAKA

Department of Reactor Safety Research
Tokai Research Establishment
Japan Atomic Energy Research Institute
Tokai-mura, Naka-gun, Ibaraki-ken

(Received April 2, 1990)

Double failures on the emergency-core-cooling systems (ECCSs) can be resulted in a case of loss-of-coolant accident (LOCA) of a boiling water reactor (BWR) by assuming an ECCS line break and the single failure criterion on another ECCS.

In the Rig-of-Safety Assessment (ROSA)-III program, two BWR LOCA simulation tests with intermediate break areas were performed to experimentally study influences of the ECCS double failures on core cooling phenomena. As there was no break unit in the ROSA-III ECCS lines, two break locations were selected above and below the ECCS line elevation. Namely, one is a main steam line (MSL) break test of RUN 992 which was previously reported. Another one is a single-ended jet pump drive line (JPDL) break test of RUN 991. And this break location effect on the system responses was briefly studied in a report of JAERI 1307.

This report presents precise experiment results of RUN 991 with respect to the core cooling phenomena related to transient system mass and also presents additional findings on the influences of ECCS double failures in some intermediate break LOCA tests including above two tests.

Keywords: BWR, LOCA, Intermediate Break, ECCS Double Failures
ROSA-III, Experiment, Core Cooling, Break Location

ROSA－ⅢにおけるBWR中口径破断実験（RUN991）
－ECCS配管破断時のLOCA事象の模擬－

日本原子力研究所東海研究所原子炉安全工学部
鈴木　光弘・安濃田良成・熊丸　博滋・中村　秀夫
与能本泰介・村田　秀男・田坂　完二

（1990年4月2日受理）

沸騰水型原子炉において，ECCS配管破断による冷却材喪失事故（LOCA）が生じた場合，他のECCS 1系統に単一故障を仮定するとECCS二重故障が生じることになる。

ROSA－Ⅲ計画では，中口径破断面積を有する2つのBWR LOCA模擬実験を実施し，ECCS二重故障条件が炉心冷却事象に及ぼす影響を調べた。ROSA－ⅢのECCS配管系には破断位置を予定していなかったので，ECCS配管の上方及び下方に破断位置を選んだ。即ち，1つの実験は，既報の蒸気ライン破断（RUN992）である。他の1つは，ジェットポンプ駆動部配管（JPDL）の片側破断実験（RUN991）である。これらの破断位置の影響を調べた結果については，JAERI 1307に報告されている。

本報は，RUN991実験結果の詳しい報告を，特にシステム保有水量と関連づけた炉心冷却事象に着目して述べる。また，上記2実験を含む中口径破断LOCAにおいて，ECCS二重故障の影響に関して得られたその後の知見についても述べる。

東海研究所：〒319－11　茨城県那珂郡東海村白方字白根2－4

Contents

目　　次

ABBREVIATIONS

ADS	Automatic Depressurization System
AT	Air Tank
AV	Air Actuation Valve
(2)B	(2) inches Pipe of Schedule 80
BN	Boron Nitride
BWR	Boiling Water Reactor
CA	Chromel-Alumel
CCFL	Counter Current Flow Limiting
CHV	Check Valve
CP	Conductivity Prove
CV	Control Valve
CWT	Cooling Water Tank
D	Differential Pressure
d	Diameter
DF	Density of Fluid
DL(+100)	Elevation (+100 mm) from the Bottom of PV
ECCS	Emergency Core Cooling System
ESF	Engineered Safety Features
EX	Heat Exchanger
F	Flow Rate
Fig.	Figure
FS	Full Scale
FW	Feedwater
FWLF	Feedwater Line Flashing
FWP	Feedwater Pump
FWT	Feedwater Tank
HPCS	High Pressure Core Spray
HPCSP	High Pressure Core Spray Pump
HPCST	High Pressure Core Spary Tank
HPWP	High Pressure Water Pump
ID	Inner diameter
INC 600	Inconel 600
JP	Jet Pump
K	Kelvin

kg	Kilogram
kPa	Kilopascal
kW	Kilowatt
L	Liter
LB	Liquid Level in Channel Box
LBWR	Large Boiling Water Reactor
LL	Liquid Level
LOCA	Loss-of-Coolant Accident
LOCE	Loss-of-Coolant Experiment
LP	Lower Plenum
LPCI	Low Pressure Coolant Injection
LPCIP	Low Pressure Coolant Injection Pump
LPCIT	Low Pressure Coolant Injection Tank
LPCS	Low Pressure Core Spray
LPCSP	Low Pressure Core Spary Pump
LPCST	Low Pressure Core Spary Tank
LPF	Lower Plenum Flashing
LTP	Lower Tie Plate
M	Momentum Flux
m	Meter
mm	Milimeter
MLHR	Maximum Linear Heat Rate
MPa	Megapascal
MRP	Main Recirculation Pump
MSIV	Main Steam Isolation Valve
MSL	Main Steam Line
MW	Megawatt
N	Rotation Speed
OR	Orifice
P	Pressure
	Power
PCT	Peak Cladding Temperature
PV	Pressure Vessel
PWT	Pure Water Tank
QOBV	Quick Opening Blowdown Valve
QSV	Quick Shut-off Valve
RCN	Rapid Condencer
ROSA	Rig of Safety Assessment

rpm	Revolution per Minute
S	Signal
s	Second
Sch	Schedule
SUS	Stainless Steel
T	Temperature
T/C	Thermocouple
TC	Temperature of Fluid
TF	Temperature of Fuel
TS	Temperature of Structure Material
UTP	Upper Tie Plate
V	Valve
VF	Void Fraction
W	Watt
WL	Water Level
WSP	Water Supply Pump

List of Tables

List of Figures

1. Introduction

The rig-of-safety assessment (ROSA)-III program[1]-[3] was initiated in 1976 to study the thermal-hydraulic behavior of a boiling water reactor (BWR)[4] during a postulated loss-of-coolant accident (LOCA) with actuation of emergency core cooling system (ECCS), and to provide the data base to evaluate the predictability of computer codes developed for reactor safety analysis. To meet these objectives various kinds of ROSA-III tests were performed during five years until March, 1983 and most of the results have been already studied and published.[5]-[58] The ROSA-III test facility simulates a 1/424 volumetrically scaled primary system of a 3800 MW BWR/6(251-848) with an electrically-heated core, break simulators, steam and feedwater systems, instrumentations including water level trip logics and the ECCSs.

One of the test parameters is variation of primary system break locations. Three typical break locations were available in the ROSA-III facility, i.e., the suction and discharge lines of the main recirculation pump (MRP) and the main steam line (MSL). In addition to these, investigated at the last phase of ROSA-III program were ECCS line break tests, which might result in severer core heat-up than the previous test results because ECCS double failures were accounted according to the single failure criterion on the other ECCS.

As there was no break simulator in the ROSA-III ECCS lines, two break locations (see Fig.1.1) were selected above and below the high pressure core spray (HPCS) line elevation. Namely one is a 10% MSL break test of RUN 992[48] with failures on the HPCS, low pressure core spray (LPCS) and low pressure coolant injection (LPCI) (available ECCS was two LPCI systems). Another one is a single-ended break test of RUN 991 at the jet pump drive line (JPDL) assuming the same ECCS failure as RUN 992. As the fluid discharge from the pressure vessel was limitted at the jet pump drive nozzles (JPDNs) in the broken recirculation loop, an effective break area of RUN 991 was 21% of the scaled MRP suction line flow area. Thus the break elevation of RUN 991 was at the jet pump (JP) suction line level. These break areas are comparable to the scaled HPCS line flow area (approximately 13% of the MRP suction line area). The break location effects on the intermediate break LOCA phenomena were previously studied in the summary report[57] and were also analyzed[59] by using the

RELAP5/MOD1(CY1) code.

Principal objectives of this report are to present (A) precise experiment results of RUN 991 including transient system responses of pressure, mass inventory and core cooling behaviors (Chapter 5), and (B) aditional findings on the influences of ECCS double failures and break location on the peak cladding temperature (PCT) in the intermediate break LOCA tests (Chapter 6). A core spray line break (CSLB) LOCA test[60],[61] at the Two Bundle Loop (TBL) is refered in Chapter 6 to discuss influences of the ECCS double failures.

2. ROSA-III Test Facility

The ROSA-III test facility[3] is a volumetrically scaled (1/424) BWR system with an electrically-heated core designed to study the response of the primary system, the core and the ECCS during the postulated LOCA. The test facility is instrumented such that various thermal-hydraulic parameters during the test can be investigated.

The test facility consists of four subsystems ; (a) the pressure vessel (PV), (b) the steam line and the feedwater line, (c) the recirculation loops and (d) the ECCSs. Figures 2.1, 2.2 and 2.3 illustrate configuration of the test facility, the PV internals and the piping schematics, respectively. Table 2.1 compares the major dimensions of the ROSA-III test facility to the corresponding dimensions of the reference BWR system.

The ROSA-III PV includes various components simulating the internal structures of the reactor pressure vessel (RPV) in the BWR system as shown in Fig.2.4. Interior of the vessel is divided into the core, core bypass, lower plenum, guide tube simulator, upper plenum, downcomer annulus, steam separator, steam dome and the steam dryer simulator.

The core consists of four simulated fuel assemblies of half length and a control rod simulator. Each fuel assembly contains 62 heater rods (Fig.2.5) and 2 water rods spaced in a 8 x 8 square array and supported by spacers and tie plates. The heater rod is heated electrically with chopped cosine power distribution along the axis as shown in Fig.2.6. The effective heated length is 1.88 m, a half of the active length of a BWR fuel rod. A high electric power was supplied to the heater rod bundle "A" with radial peaking factor of 1.4 and another power was supplied to the other three bundles "B", "C" and "D" with radial peaking factor of 1.0. The total electric power is limitted below 4.24 MW. The heater rods in each bundle are divided into three groups with respect to heat generation rate as shown in Fig.2.7. The local peaking factors in each group are 1.1, 1.0 and 0.875. The orifice plate with 44 mm I.D. in one assembly is inserted at each core inlet to control the core inlet flow.

The steam line is connected to top of the steam dome (see Fig.4.1). In the first steam line branch, an orifice and a quick opening air valve (AV165) are installed for break simulation. A control valve (CV-130) is installed in the third branch to control the steam dome pressure in the steady state before the test initiation and to maintain the pressure above

6.7 MPa after the break time as a pressure control system (PCS). The second branch has an air valve (AV169) and an orifice to simulate the automatic depressurization system (ADS). The MSIV closure is simulated by quickly closing the control valve (CV-130) in the third line. (These valve characteristics and trip conditions are shown in chapter 4.) The feedwater is supplied from the feedwater tank (FWT) through the feedwater line (Fig.2.8) and the feedwater sparger (Fig.2.9) below the steam separator.

Figure 2.10 shows the piping layout of the broken recirculation loop, which has two jet pumps (JP3, JP4) and a main recirculation pump (MRP2). The break units for RUN 991 are installed at the MRP2 discharge line. Although a 100% break nozzle (26.2 mm I.D.) is installed in the break unit A, the primary fluid discharge from the vessel is limitted at the narrower flow area at the JP drive nozzles (two nozzles of 8.4 mm I.D. for each one).

The ROSA-III test facility is furnished with all kinds of the ECCS's available in the BWR system, i.e., the high pressure core spray (HPCS), low pressure core spray (LPCS), low pressure coolant injection (LPCI), and ADS. The HPCS and LPCS spray cooling water onto the core (however, these are not used in RUN 991). The LPCI injects cooling water into the core bypass. Each ECCS consists of a pump, a tank, pipings, and a control system. The water level in the upper downcomer, which is measured by a differential pressure transducer between DL 3.90 m (above the PV bottom) and DL 6.04 m, is used for the actuation trips (see Chapter 4) of MSIV and ECCSs.

3. Instrumentation

Instrumentation of the ROSA-III system is designed to obtain thermal-hydraulic data during a simulated BWR LOCA. Table 3.1 summarizes the instrumentations for No.4 assembly. However, almost a half of the 698 instrumentation channels were not used nor measured in RUN 991 as shown in Table A.1 in Appendix I. The measurement list and the core instrumentation list are presented in Appendix I. Instrumentation locations are shown in Fig.3.1 through Fig.3.10. Typical measured parameters in the ROSA-III are pressure, differential pressure, flow rate, electric power, pump speed, fluid and metal temperatures, collapsed liquid level, two-phase mixture level, fluid density, trip signals and so on.

Pressure and differential pressure transducers are two-wire, direct-current type which convert diaphragm displacement to electric capacitance. The pressure lead pipes are either the standard single, cylindrical pipes used in conjunction with condensate pots, or dual concentric cylinders capable of the circulation of cooling water to prevent flashing of the fluid.

The flow rate is measured by four types of instrumentations, i.e., turbine flow meter, orifice type flow meter, Venturi type flow meter and momentum flux measurement equipment depending on the fluid condition and measuring location. The turbine flow meter is used for subcooled water flow such as ECCS injection flow and feedwater flow. The orifice type flow meter is used for both flows, one is steam line flow including ADS flow and another one is jet pump discharge flow in the blowdown loop. The Venturi flow meters are used for recirculation flows in both loops and jet pump discharge flow in the intact loop.

The temperatures of the fluid, structural material and heater rod cladding are measured with chromel-alumel thermocouple (CA T/C) of 1.6, 1.0 or 0.5 mmφ. The thermocouples for heater rod cladding temperatures are imbedded at the surface of the cladding as shown in Fig.2.5. There are seven (maximum) thermocouples for one heater rod along the axial direction.

Liquid levels are measured by either differential pressure transducers, described above or needle type electric conductivity probes (CP) developed in the ROSA-III program. The probes are distributed along the vessel height to detect the existence of water or vapor at different levels.

The electric power supplied to the heater rods is controlled to follow

the predetermined power curve with function of time and measured by a fast response electric power meters. The pump speed is measured by a pulse generator integral of the pump. Trip signals such as selected valve positions and pump coastdown initiations and so on, are detected in order to record the exact actuation times of trip signals.

The fluid density in the pipe is measured by means of gamma densitometers. Preliminary studies indicate that two-beam and three-beam densitometers should be used to determine the flow regime. Figures 3.7 and 3.8 show the beam directions of the three-beam and two-beam gamma densitometers, respectively. The gamma-ray source is ^{137}Cs and the detector is a water cooled NaI(Tl) scintillation counter. The momentum flux is measured by a drag disk as shown in Fig.3.9. The combination of signals from a drag disk and a gamma densitometer is used to determine the two-phase flow rate as shown in Fig.3.10.

The data acquisition system (DATAC 2000B, Iwasaki Tsushinki Co.) scans all of signals with the frequency up to 30 Hz. The data recorded on magnetic tape were processed by the FACOM M200 system computer at JAERI by off-line control. After evaluation, for example by comparing the initial and final pressure values with standard values for the density and momentum flux data, the data were reprocessed using the correct conversion factors as determined from the consistency examination. Reduction of mass balance and mass distribution in the system is shown in Chapter 5. More detailed information on the data processing procedure is available in reference (52).

4. Test Conditions and Procedure for RUN 991

The test RUN 991 is a single-ended jet pump drive line (JPDL) break LOCA test with double failure assumption on HPCS and LPCS diesel generators. The test conditions are shown in Table 4.1. The measured initial test conditions are; steam dome pressure of 7.36 MPa, total core power of 3.96 MW (44% of 1/424 scaled BWR rated power), core inlet mass flow of 16.1 kg/s, core inlet subcooling of 10.5 K, main steam flow of 2.07 kg/s, feedwater flow rate of 2.04 kg/s, and pressure vessel water level of 4.80 m above the PV bottom (Actual downcomer water level was obtained as 4.87 m by correcting the frictional pressure loss). The initial core inlet flow was lowered to establish the same initial enthalpy distribution as in the reference BWR. The initial average fluid quality in the upper plenum was estimated as 12.5%.

RUN 991 was performed by the following procedures (ref. Table 5.1). Break was initiated by quickly opening the break valves (QOBVs) at break units A and B, and quickly closing the quick shut valve (QSV) between the break units A and B. As a blind orifice was used at the break unit B, fluid in PV discharged only through the break unit A being limitted at the jet pump drive nozzles (JPDNs) of JP-3 and JP-4. Structure of the jet pump and details of the drive nozzle are shown in Figs.4.1 and 4.2, respectively. The suction part of the ROSA-III jet pump is different from the actual BWR jet pump. Break nozzle of 26.2 mm ID (see Fig.4.3) was used at the break unit A.

At the break time, the power supply to both recirculation pumps (MRP 1, MRP2) was terminated and the pump speed rapidly started to coast down. The steady state core power was maintained for 7 s after the break and then decreased along the power curve shown in Fig.4.4, which was modified from the old power curve (reference 56) to simulate heat transfer rate of the average-power fuel bundles to coolant during a hypothetical BWR/LOCA.

The steam flow to heat up the feedwater from the third steam line branch was manually stopped immediately after the break by closing the valves CV-1 and CV-2. The feedwater line was closed between 1.5 and 4 s after the break. The MSIV trip was the same as that of the BWR/6, i.e., it is actuated by the low-low downcomer water level (L1) trip with a time delay of 3 s by quickly closing the control valve (CV-130). The L1 level

is 4.0 m above the core bottom in RUN 991. The pressure control system (PCS) was operated between the pressure of 6.6 and 6.7 MPa by closing the pressure control valve (CV-130).

The ADS was actuated by L1 level trip with time delay of 122 s. The ADS orifice (19.0 mm I.D.) was used to take account of the excess steam generation through the structural metal surfaces of the facility in the later blowdown phase. The LPCI injection flow rate in RUN 991 was assumed to 2/3 of the 1/424 scaled BWR LPCI flow rate because one of the three LPCI pumps is assumed to fail. The LPCI was actuated at 265 s after the break (at 1.6 MPa of the system pressure).

The test was performed on March 14, 1983 as a test before the last ROSA-III test (RUN 992). Most of the measured instruments functioned successfully.

5. Test Results of RUN 991

Presented in this chapter are typical test results of RUN 991, i.e., system pressure responses with timings of major events, boundary conditions of fluid mass inventory, and core thermal responses related to the fluid mass inventory. Timings of major events are listed in Table 5.1. Typical experimental data are shown in Figs.5.1 through 5.20 and Tables 5.2 through 5.4. All the experimental and calculated data are included in Appendices I through III with their measurement list and data processing method.

5.1 System Pressure and Major Events

Shown in Fig.5.1 are system pressure responses in the break flow path through the jet pump drive nozzles (JPDNs) at JP-3 and JP-4 in the broken recirculation loop, i.e., pressures at steam dome, JP-3 drive line, break-A upstream side and break-A downstream side. Timings of major events and core dryout period of RUN 991 are also shown in Fig.5.1.

After the break initiation, the steam dome pressure, which was a representative of the primary system, began to decrease gradually due to the increased steam flow through the MSL (see Fig.5.2) and water discharge through the JPDNs in the broken loop (see Fig.5.3). This break flow rate was measured by the low-range drag-disk flow meter located at the downstream side of the JPDNs (upstream side of the break-A unit). After initiation of core power decay (see Fig.5.4) at 7 s after the break, the system pressure decreased faster until initiation of the pressure control system (PCS) operation at 15 s after the break. Thereafter, the system pressure was maintained above 6.6 MPa by this PCS operation. The MSIV was tripped to close by L1 level signal (25 s) with a time delay of 3 s and was completely closed a few seconds after this time.

The system pressure began to decrease again at 40 s after the break due to an increased volumetric flow through the JPDNs because the downcomer water level reached the JP suction line elevation (DL 2.814 m). This change is shown in fluid density data at the break-A (ref. Fig.A.119) and the break flow data (ref. Fig.5.3). The ADS actuation (147 s) resulted in steam discharge through the MSL and caused further depressurization in the

system. The feedwater flashing was observed at 215 s after the break (see Fig.5.5) and resulted in slightly slower depressurization. The LPCI injection started at 265 s after the break and slightly influenced the system pressure responses.

The core dryout started at 42 s after the break at the top of average power bundle D and the whole core was uncovered within 80 s after this time. The injected LPCI water (see Fig.5.6) into the core bypass region gradually cooled the heated core from bottom to top and completely quenched the core at 462 s after the break (197 s after the LPCI actuation).

The pressures (PA 5 and PA 12) at downstream sides of the JPDNs in broken loop were significantly lower than the steam dome pressure (PA 3) for all the test period. Moreover the downstream side pressures were independent of the steam dome pressure. These mean a critical two-phase flow choking occurrence at the broken loop JPDNs (total flow area is 20.6% of the scaled recirculation loop flow area, ref.Figs.4.1 and 4.2). The pressure change between PA 12 and PA 13 (across the break-A nozzle of 26.2 mm ID, 100% area) also suggests choking occurrence at this location. However, the PV fluid discharge was controlled by the upstream side choking at the broken loop JPDNs.

5.2 Boundary Fluid Conditions and Transient System Mass

First, a transient fluid mass in the primary system is estimated by calculating the fluid boundary conditions of the feedwater, steam flow, break flow and ECC flow. Secondly, the estimated system mass is checked by a total remaining fluid mass obtained by another method. Lastly, the fluid mass distribution inside and outside the core shroud is discussed.

A transient fluid mass (M) in the primary system was controlled by an initial total mass (M_o), a temporarily injected feedwater mass (M_f), steam mass discharged through the MSL including the ADS flow (M_s), fluid mass discharged through the broken loop JPDNs (M_d) and injected ECC mass (M_e) according to the following equation:

$$M = M_o + M_f + M_e - M_s - M_d, \qquad (5.1)$$

where M_o is obtained from the previous report[48] of RUN 992 by slightly modifying the initial downcomerr level (M_o = 646 kg), and M_f, M_d, M_s and

M_e are obtained from each mass flow rate (ref.Figs.5.2 through 5.6). Table 5.2 shows the estimated remaining mass of RUN 991. The feedwater flow income after the feedwater flashing (215 s) was ass- umed as shown in the table. Namely a half of the remaining feedwater of 30 kg could contribute to the system mass during a time period (215 s to 340 s) of larger depressurizing phase.

A reliability of this transient fluid mass is checked at two points, i.e., one is the initial phase before the break and another one is a time point at the lowest mass inventory after the whole core dryout and before the LPCI injection. The initial system mass was previously studied in References (13) and (48). The last time point was chosen at 220 s after the break, at which the mixture levels were measured in the lower plenum (DL 0.73m), guide tube (DL 0.97m) and lower downcomer (DL 1.85m) as shown in Fig.5.7. Thermal properties at 220 s (steam dome pressure of 2.25 MPa and saturated temperature of 491.6 K) were saturated fluid densities of water and steam of 842.4 kg/m^3 and 11.3 kg/m^3, respectively. By assuming the following, remaining fluid mass in each primary region was calculated by using the experiment data of differential pressures. Downcomer water levels of ML 68 and ML 69 are shown in Fig.A.27 in Appendix II. Average void fraction in the lower downcomer (see Fig.5.8) increased above 50% after the ADS actuation (147 s).

The assumptions are:

(a) Frictional pressure loss included in the differential pressure data across the core (PD 21, see Fig.5.9) is estimated after the ADS actuation by assuming that steam flow through the core is proportional to the MSL steam flow (see Fig.5.2). By using an increased value of PD 21 at the ADS actuation time (147 s), the pressure loss included in PD 21 at 220 s was estimated as 1.4 kPa. The remaining fluid mass and average void fraction in the lower plenum are calculated by eliminating this frictional pressure loss from PD 21.

(b) Void fraction in the guide tube is assumed to be the same as that of the lower plenum.

(c) Main recirculation loops are assumed to be covered by two-phase mixture because the downcomer mixture level existed above the recirculation loop inlet nozzle elevation (DL 0.94m). Average void fraction in the intact recirculation loop is represented by that of the MRP1 suction line obtained from PD 36 (see Fig.A.12), i.e., 73%. Void frac-

tion in the broken recirculation loop is assumed to be the same as that in the intact loop.

(d) Collapsed water level in the intact loop JP is obtained from the differential pressure data of PD 41 (see Fig.A.15) by neglecting frictional pressure loss in PD 41.

(e) The broken loop JPs are assumed to be covered by two-phase mixture. As the differential pressures of PD 50 and PD 52 (see Figs.A.19 and A.20) include frictional pressure loss caused by the uprizing (reverse) two-phase flow, actual void fraction is higher than an estimated value of 70%, which was calculated by assuming no pressure loss in the PD 50 data. Thus, the average void fraction in the broken loop JPs is assumed to be a mean value of 70% and 100%, i.e., 85% ± 15%.

(f) Accuracy of each differential pressure data is considered as ± 0.32% of the full scale range. Uncertainty of void fractions in the guide tube, intact loop JPs and broken recirculation loop is assumed to be ± 20%.

Thus, the total fluid mass remaining in the primary system at 220 s was obtained as shown in Table 5.3, i.e.,

$$M^* = 171 \pm 26 \quad (kg) \qquad (5.2).$$

This is also expressed by using the initial system mass (M_0) as

$$M^*/M_0 = 0.265 \pm 0.040 \qquad (5.3).$$

The transient system mass at 220 s in Table 5.2 (M=186 kg) is consistent to this value of M^* within the accuracy of ± 4% of M_0. Thus the transient system mass estimated from the mass balance in Table 5.2 is consistent to the actual remaining fluid mass at two time points ($t \leq 0$ and $t = 220$ s). The largest uncertainty factor of the mass balance is that of the drag-disk flow rate. However, this consistency suggests that the uncertainty of the discharged fluid mass (M_d) derived from the low-range drag-disk flow data is very small and is comparable to those of the other terms in Equation (5.1) at any time during the test period. Therefore this consistency also suggests that the transient system mass (M) can be accurate at other time points during the test period of RUN 991.

On the other hand, the discharged mass measured by the high-range drag disk flow meter (see Fig.A.121) was largely different from the low-range data as shown in Fig.5.10. The high-range mass data was approximately 20 to 30% higher than the low-range mass data. Thus, the high-range mass data could not be used for the transient system mass calculation in RUN 991.

Fluid mass distribution inside and outside the core shroud is shown below. Shown in Fig.5.11 are the collapsed water levels in downcomer and inside the core shroud. This downcomer water level (LM 727) is a sum of the upper and lower downcomer levels of LM 68 and LM 69 in Fig.A.27. The collapsed water level inside the core shroud (LM 728) was obtained from the differential pressure between the top and bottom of PV (PD 25 shown in Fig.A.6). The rapid decrease of LM 727 just after the break initiation does not mean the level-decrease but a rapid decrease of the pressure loss due to the core flow coast-down after the break.

It is shown that the collapsed shroud level was maintained above the top of core during the first 40 s while the downcomer level linearly decreased to the JP suction elevation (DL 2.81m). Thereafter the shroud level began to decrease faster than the downcomer level. As shown in Fig.5.7, the downcomer mixture level was maintained at the JP suction level for a long time until the ADS actuation. Thus the mass distribution in PV was changed after the downcomer level reached the JP suction elevation (JP suction uncovery). After this JP suction uncovery, fluid mass discharged mainly from the core shroud through the broken loop JPs and the downcomer water level was maintained higher than the shroud water level. Fluid mass remaining in the downcomer, inside the core shroud and in both of JPs and recirculation loops were 120 kg (70%), 18 kg (11%) and 33 kg (29%) at 220 s after the break, respectively (ref. Table 5.3). These water levels commonly started to increase after the LPCI actuation.

It should be noted that the pressure balance inside and outside the core shroud is held in RUN 991 as in that of RUN 992 and that the differential pressures in the JP discharge regions are small. The collapsed water levels in the intact loop JPs were DL 0.56m above the PV bottom and this agreed well to the lower plenum collapsed water level of DL 0.60m. Thus the shroud water level did not correspond to the downcomer water level but to the JP collapsed water levels after the JP suction line uncovery (under the condition of significantly degraded system mass inventory).

5.3 Core Thermal Responses Related to Transient System Mass

Presented below are system mass responses in the blowdown and reflooding phases, heater rod temperature responses, and core mixture level responses related to the dryout and quench trajectories in RUN 991. The

core thermal responses are related to the transient mass inventory.

The transient system mass are shown in Fig.5.12 with respect to time and pressure. The JP suction uncovery (40 s) started at a system mass ratio (M/M_0) of 0.75 and thereafter the mass decreasing rate became slower. The ADS actuation (147 s) started at the mass ratio of 0.48 and resulted in faster mass decrease. The LPCI was injected at a system pressure of 1.57 MPa (265 s) at a mass ratio of 0.22 and thereafter the system mass increased. The core bottom was uncovered at a mass ratio of 0.53. The mass recovery after the LPCI actuation was, however, slower than the total amount of the injected LPCI water mass (see broken line data in Fig.5.12). This indicates that some amount of the injected ECC water mass discharged through the broken loop JPDNs. An ECC accumulation efficiency (E_a),[55] which is defined as

$$E_a = (M_e - M_s - M_d) / M_e \qquad (5.4),$$

is estimated as 0.61 between 300 and 500 s after the break. Namely, it is equivallent to the LPCI accumulation of 61%. This accumulation efficiency is controlled by the ECC flow rate and also by the break location as shown in the next chapter.

The core dryout started at the top of the average power bundle at a mass ratio of 0.74 and the heated core was finally quenched at a mass ratio of 0.57. A core dryout range is shown in the transient system mass and pressure domain (mass-pressure map). The core dryout started at a pressure of 6.63 MPa (P/P_0 = 0.90) before the lower plenum flashing initiation and the final core quench was observed at a pressure of 0.81 MPa (P/P_0 = 0.11). These data are also compared with those of the other tests in the next chapter.

Shown in Fig.5.13 are calculated system mass inside and outside the core shroud by using the collapsed water levels shown in Fig.5.11 (see Appendix II). As only the collapsed water levels were used for this system mass calculation, a sum of these data is slightly different from the transient system mass shown in Fig.5.12. For example, the total system mass increased after the ADS actuation in Fig.5.13, whereas the actual system mass decreased by the increased MSL steam flow as shown in Fig. 5.12. However, the mass inventories shown in Fig.5.13 are useful to know qualitative trend of the system mass distribution across the core shroud. Namely, most of the remaining fluid mass existed inside the core shroud than in the downcomer in RUN 991.

Shown in Fig.5.14 are the calculated flow rates at the core inlets and bottom of the guide tube. These flow rates are related to the mass transport across the core shroud and core cooling behaviors after the ADS and LPCI actuations. It is shown that the core inlet flows were positive in the early blowdown phase and that they temporarily became negative just after the JP suction uncovery at 40 s. These flow data, however, can be used to know only the relative flow behaviors after the lower plenum flashing (LPF) initiation. It is also shown that strong uprizing steam flow was induced in the four channel inlets after the ADS actuation and that some flow distribution was observed after the LPCI actuation among the four channels. After the LPCI injection, clear downward flow was observed at the bottom of the guide tube.

Shown in Figs.5.15, 5.16 and 5.17 are heater rod surface temperatures measured at seven vertical elevations of A-11, A-22 and C-22 rods, respectively. Similar dryout and quench phenomena were observed among these rods. Shown in Fig.5.18 are water rod surface temperatures of A-45 rod. The peak cladding temperature (PCT) was observed at 344 s after the break (79 s after the LPCI injection) at position 3 of A-22 rod (see Table 5.4). The PCT was not observed at the high power rod of A-11 (peripheral rod in channel A) but at the average power rod of A-22 (inner region of channel A). All the heater rods were quenched between 320 s and 462 s by the LPCI actuation.

Shown in Fig.5.19 are mixture level fronts in channels with high-power and average-power compared with collapsed water level (ref. Fig.5.11). Shown in Fig.5.20 are dryout and quench fronts of heater rods in four bundles (A-22, B-22, C-22 and D-22 rods). The dryout and quench fronts of four rods agreed well each other. Moreover, these agreed well to the core mixture level in the blowdown phase as shown in Fig.5.19. The quench fronts are slightly delayed from the core mixture level recovery. Consequently, the top-down dryout phenomena in the blowdown phase and the bottom-up quench phenomena in the reflooding phase almost perfectly agreed in all the rod bundles in RUN 991. The heater rod thermal responses were mainly controlled by the mixture level responses in each rod bundle.

6. Influences of ECCS Double Failures on Core Cooling

First, two ROSA-III tests of RUN 991 and RUN 992 are compared on the point of break location effects on system mass inventory and PCT. Secondly these results are compared with an HPCS line break test performed at the TBL facility[60]-[62] to discuss the HPCS line break LOCA phenomena in the ROSA-III. The break location effects were previously studied in the summary report[57] by comparing these two tests results with other two intermediate break LOCA tests (RUN 927 of 15% break test and RUN 930[51] of 25% break test). Additional findings with respect to the break location effects are shown in the Section 6.2.

6.1 Effects of Break Location on Intermediate Break ROSA-III Tests (RUNs 991 and 992)

In the ROSA-III program, the two intermediate break LOCA tests (RUNs 991 and 992[48]) were performed to study the effects of break location and ECCS double failures as mensioned in Chapter 1. As the test conditions of these two tests were similar except for the break condition, break location effects can be obtained from these comparisons. The break location of RUN 992 is at the main steam line (MSL, DL 6.04m above the PV bottom) and the break area simulates 10% of the 1/424 scaled BWR MSL flow area (14.9% of the scaled MRP suction line flow area). On the other hand, the effective break location of RUN 991 is at the JPDNs in the broken loop (the break elevation is DL 2.81m) and the effective break area is 20.6% of the scaled MRP suction line flow area. Major event timings of the two tests are shown in Table 6.1.

(1) Effects on Pressure Responses and Water Levels in PV

Shown in Fig.6.1 are steam dome pressures of the two tests. As the break area of RUN 992 is 72% of that of RUN 991, the time scale of RUN 992 is shortened for comparison.

In RUN 992, steam discharged through the MSL and the depressurization rate became lower with time. The ADS actuation at 594 s caused faster depressurization and followed the LPCI actuation with a time delay of 126

s. On the other hand, the system pressure of RUN 991 remained rather higher than RUN 992 in the early blowdown phase and started to decrease after the JP suction line uncovery (40 s). The ADS actuation caused rather faster depressurization in RUN 991 than in RUN 992.

In order to quantitatively compare these depressurization rates between the two tests with different break flow areas, an average depressurization rate per unit break area (P/A in unit of MPa/m^2s) is calculated as shown in Table 6.2. This value of RUN 991 between the pressure control system (PCS) termination time (30 s) and the ADS actuation time (147 s, P = 4.83 MPa) is almost the same as that of RUN 992 (see their similar depressurization curves in Fig.6.1). However, the depressurization rate of RUN 991 became slightly higher with time, which was contrary to that of RUN 992. The average depressurization rate (P/A) of RUN 992 in the lower pressure range before the ADS actuation time (4.83 MPa $\geqq$ P $\geqq$ 2.77 MPa) decreased to approximately 42% of the value in the higher pressure range. Thus the pressure resposes in the lower pressure range became largely different between the two tests as a result of break location effects (i.e., fairly degraded mass inventory and overall core dryout in RUN 991, whereas large mass inventory, high steam quality, and better core cooling in RUN 992).

An average break mass flow rate per unit break area (M_d/A) was calculated for the two tests to compare the break location effects on these break flow rates (see Table 6.3). Estimated mass balance for the two tests were refered (Table 5.2 for RUN 991 and Table 5.3 of Reference 48 for RUN 992). It is shown that the value of (M_d/A) in RUN 991 was 84% higher than that of RUN 992 in the same pressure range (P $\geqq$ 4.83 MPa) and their discrepancy became larger in the lower pressure range. This larger break mass flow rate in RUN 991 than in RUN 992 is also a result of the break location effects.

Shown in Fig.6.2 and 6.3 are calculated collapsed water levels and fluid mass inventories in PV in RUN 992, respectively. These are compared with those of RUN 991 (see Figs.5.11, A.133 and A.134). Shown in Fig.6.4 are the mixture levels inside the core shroud in RUN 992, which are compared with those of RUN 991 (see Figs.5.7 and 5.19). The downcomer collapsed water level (LM 727) is compared to the core mixture levels for the two tests in Fig.6.5. The core dryout period (from the earliest rod heatup initiation time to a final rod quench time) for each test is also shown in Figs.6.1 and 6.5.

It is shown in these figures that the PV water levels in RUN 991 were significantly lower than those of RUN 992 in the blowdown phase and that the core cooling conditions between them were largely different. The whole core was uncovered in RUN 991 even before the ADS actuation at 147 s (P = 4.83 MPa), whereas the core of RUN 992 was completely covered by mixture level in the same pressure range. And the mass recovery process after the LPCI actuation was slightly longer in RUN 991 than in RUN 992. Thus contribution of the core power generation on the system pressure responses was very small in the blowdown phase of RUN 991 in comparison with RUN 992.

It is also shown that the swelled downcomer level in RUN 992 delayed the L1 level trip and therefore it delayed the ADS actuation (476 s). On the other hand, the L1 level of RUN 991 was tripped at 25 s after the break (451 s earlier than that of RUN 992). Thus the L1 level trip timing was significantly affected by these two break locations.

On the other hand, it was commonly found in these two tests that the core mixture level, which controlled the core cooling conditions as shown later, decreased lower than the downcomer water level in the blowdown phase (except for a short time period after the ADS actuation). This indicates that it is necessary to detect the decreased core mixture (or collapsed) level rather than to measure the downcomer water level in the degraded mass inventory condition during the intermediate break LOCA.

(2) Comparison of Transient System Mass and PCT

Shown in Fig.6.6 are time responses both of the system mass inventory (M) and the injected ECC mass (M_e) normarized by the initial system mass of M_o for RUNs 991 and 992. The break location effects on the system mass responses are clearly observed in the blowdown phase and slightly in the reflooding phase. Namely, the least mass inventory ratio (M/M_o) of RUN 991 was observed as 0.22 at the LPCI actuation time, at which the shroud mixture level decreased to approximately a half of the lower plenum height. On the other hand, the least value of RUN 992 was 0.42 at the LPCI actuation time, at which the shroud mixture level was in the lower core region (approximately 1/3 height of the core).

The mass recovery rate after the LPCI actuation was slightly slower in RUN 991 than in RUN 992. Namely the system mass inentory became lower than the total amount of injected ECC mass in the later reflooding phase

of RUN 991. This means that some amount of the injected ECC mass discharged in addition to mass depletion of the remaining mass. On the other hand, most of the injected ECC mass contributed to the mass recovery in RUN 992. This is clearly shown in the comparison of the ECC accumulation efficiency (E_a), which is defined by equation (5.4) in Chapter 5. Shown in Fig.6.7 are ECC accumulation efficiencies of the two tests (ref. Table 5.2 for RUN 991 and Table 5.2 in Reference 48 for RUN 992). E_a of RUN 991 was approximately 1/2 to 2/3 of that in RUN 992. As the time responses of M_e are almost similar in the two tests, difference of this efficiency is a result of difference of (M_s + M_d) between them. Especially the break mass flow rate (M_d) after the LPCI actuation largely differed between them.

It should be noted that the break location effects consist of two components, i.e., one is an effect of break elevation in PV wall and another one is an effect of special break location, such as the jet pump drive nozzles in RUN 991. The latter effect contributed to promote the fluid mass decrease inside the core shroud because the break flow through the JPDNs caused larger depressurization in the jet pumps, which were opened to bottom of the core shroud, and resulted in increase of mass transport from the lower plenum to the broken loop JPs. However, these two break location effects on the transient system mass and system pressure responses can not be separated in these test results.

Shown in Fig.6.8 are mass-pressure trajectories of the two tests. The mass inventory ratio (M/M_o) of the tests can be compared at the same system pressure ratio (P/P_o, P_o is the initial system pressure) by using this figure. The core dryout region of each test is also shown in the figure as a shaded area. It is clear that the system mass inventory in RUN 991 was fairly lower than that in RUN 992 at the same pressure (M/M_o of RUN 991 was approximately 50 to 70% of that in RUN 992) during the blowdown phase after the lower plenum (LP) flashing initiation at P/P_o = 0.87.

The core heatup of RUN 991 started at M/M_o = 0.75 and P/P_o = 0.90, whereas that of RUN 992 started at M/M_o = 0.64 and P/P_o = 0.46. The core heatup initiation times of the two tests are significantly different as shown in Table 6.1. The final core quench of RUN 991 was observed at (M/M_o = 0.57 and P/P_o = 0.11), whereas that of RUN 992 was observed at (M/M_o = 0.51 and P/P_o = 0.19). Thus the final core quench was slightly delayed in RUN 991 than in RUN 992.

Shown in Fig.6.9 are the measured heater rod temperatures of the two tests, which recorded the PCT. The temperature of RUN 992 is shown on a shortened time scale for comparison with RUN 991. As a result of the significantly different system mass inventories between the two tests, their heater rod temperature responses and PCTs became also significantly different. The PCT of RUN 991 was 336 K higher than that of RUN 992. The PCT of RUN 991 was observed 79 s after the LPCI actuation, whereas it was observed 24 s after the LPCI actuation in RUN 992. It took 197 s to accomplish the core quench after the LPCI actuation in RUN 991, whereas it took only 40 s in RUN 992.

Thus these two break locations largely influenced the core cooling conditions in the blowdown phase. Namely, the JPDL break test of RUN 991 resulted in a severer core heatup but the heated core was finally cooled by the 2LPCI actuation. The 10% MSL break test of RUN 992 resulted in less severe heatup in the 2/3 core region despite of the same ECCS double failures and the heated core was cooled soon after the 2LPCI actuation.

6.2 Discussion on ECCS Line Break LOCA Phenomena

(1) Literatures of Experimental Studies on Other Piping Break LOCA Phenomena

A BWR system with jet pumps has many kinds of reactor vessel nozzles for pipings as shown in Fig.6.10. Major pipings are main steam lines (MSLs), feedwater line, ECCS lines, and outlet and inlet lines of the MRLs. The stub tubes for the conbtrol rod driving system and minor nozzles for instrumentation are also provided on the vessel wall. The MSLs and feedwater line are located at higher elevations than the core top level, whereas the MRLs are located at the downcomer wall lower than the core bottom level. On the other hand, the ECCS lines are opened to fluid inside the core shroud above the core top level. The control rod stub tubes, drain line nozzle and instrumentation stubs are also opened to fluid inside the core shroud. Thus, both break locations inside and outside the core shroud have a possibility of pipe rupture, which results in a LOCA.

There are many literatures reporting the BWR LOCA simulation tests with respect to the MRL breaks, whereas there are a few with respect to

the other piping breaks. In the ROSA-III program,[57] seven MSL break tests and one JPDL single-ended break test were performed, and all the remainings (44 tests) were MRL break tests in the RUN 900 series. Reference 63 shows a FIST Phase-I test for large MSL break LOCA. Reference 64 shows FIST Phase-II tests including an LPCI line break test for the BWR/6 system with HPCS failure assumption. The FIST facility is a 1/624 volumetrically scaled BWR system with one full-height heater rod bundle. Reference 65 shows FIST Phase-III tests of one MSL break, one HPCS line break and two PV bottom head breaks for an advanced BWR, which has some different design features such as the internal coolant pumps instead of the jet pumps, and the high pressure flooders (HPFLs) instead of the low pressure ECC systems comparing to the jet pump type BWRs.

In addition to these, three other piping tests were reported as to the TBL-II program, of which facility simulated 2/764 volumetrically scaled BWR/5 system with jet pumps. Namely, Reference 60 shows one HPCS line break test (RUN 315), one feedwater line break test and one PV drain line break test on the view point of analytical code assessment (the presented experimental data are only the system pressure and PCT rod temperature for each test). And one large MSL break test was briefly reported in Reference 66 on the view point of the code assessment. Reference 61 presents more experiment data of the HPCS line break test (RUN 315). As the TBL facility has a similar scaling ratio to that of the ROSA-III facility, the TBL HPCS line break test is refered below for comparison.

(2) Reported Results of TBL HPCS Line Break Test

Figure 6.11 (a) shows schematic diagram of the TBL facility presented in Reference 61. The TBL has a pressure vessel with internals including two heater rod bundles, steam and feedwater systems, all ECCSs, two recirculation loops and two jet pumps, which are provided in the downcomer as shown in Fig.6.11 (b). The TBL facility simulates a full-height vertical scale between the elevations of jet pump bottom and upper plenum. The steam dome and the lower plenum simulate those of the BWR on the point of volume scaling. The HPCS line is connected to a break unit A and isolated from the HPCS pump. Table 6.4 shows region volumes of the TBL facility and is compared with those of the ROSA-III facility (see Table 6.5), which simulates the BWR/6-251 system (848 fuel bundles) by a volumetric scaling ratio of 1/424. It is shown that these two test facilities

have the similar volume distribution in the primary system.

Shown in Table 6.6 are test conditions of the TBL HPCS line break. The break diameter is 10.0 mm ID, which corresponds to 10.4% of the scaled BWR MRL flow area (31.0 mm ID break area corresponds to 100% scaled BWR MRL area). As loss of off-site power is assumed and a single failure is assumed on the diesel generator for both of LPCS and 1LPCI pumps, the available ECCSs for the HPCS line break test are 2LPCI and ADS.

The reported HPCS line break test results are briefly shown below. Timings of the major events are shown in Table 6.7.

Shown in Fig.6.12 (a) are system pressures of the experiment and analysis which was performed by using the SAFER code. The system pressure started to decrease immediately after the break due to two-phase flow discharge through the HPCS line and turned to increase at 10 s after the break due to initiation of MSIV closure. The system pressure started to decrease again at 200 s after the break due to steam (or high quality two-phase flow) discharge through the HPCS line after the mixture level fell below the HPCS line (break uncovery). The ADS actuation at 288 s after the break caused faster depressurization and temporary mixture level swell inside the core shroud as shown in Fig.6.12 (b). It is shown that the core top was covered by the mixture level until the ADS actuation timing.

The core dryout started approximately at 360 s after the break (approximately 70 s after the ADS actuation) due to the mixture level fall into the core, and the dryout rapidly extended to the whole core. The LPCI injection started at 506 s after te break (218 s after the ADS actuation) and resulted in complete core quench within approximately 160 s. Thus the break uncovery continued from 200 s to some time after the final core quench except for a short time period after the ADS actuation. The core dryout time period was approximately 310 s for this test. The heater rod showed temperature excursion during this period as shown in Fig.6.12 (c) and the PCT was observed as 871 K (598 C) at 612 s after the break (106 s after the LPCI actuation). This PCT is obviously higher than the TBL MRL break tests with break diameters of 7 and 20 mm ID and with an HPCS single failure assumption. The reason of higher PCT (the difference is less than 100 K) in the HPCS line break test than in the MRL break tests is the additional failure mode on the LPCS and 1LPCI for the former.

The core power curve for this test is not shown. Only one power curve of the TBL tests is reported in the reference (62) as that of the large break LOCA tests (see Fig.6.13). However, this power curve is fairly different from the updated ROSA-III power curve (average-power rod-based power curve[67] shown in Fig.6.14). Moreover, this TBL power does not simulate the decay power after 30 s from the power control initiation. Thus it is supposed that this power curve was not used in the HPCS line break test, which was performed for approximately 800 s after the break. Effect of the power generation rate is indirectly checked by the heater rod temperature increasing rate after the dryout initiation in each test as shown later.

(3) Discussion on HPCS Line break LOCA Phenomena in ROSA-III

Test results of the TBL HPCS line break and ROSA-III tests of RUNs 991 and 992 are compared with each other on the point of core dryout behaviors caused by the ECCS double failure. Moreover, these results are compared with those of ROSA-III MRL break tests with intermediate break areas (5, 15 and 25% break area ratios) on the point of break location effects. These MRL break tests are RUNs 922, 927 and 930, which were performed by assuming an HPCS single failure and by using different power curve. These influences are also discussed below.

Shown in Table 6.8 are an equivallent break area (A/V) in two different test facilities, where A is a break area (in m^2) and V is a total system fluid volume (in m^3), timings of the core dryout initiation, final core quench and PCT, a core dryout time period and a PCT value of each test. Shown in Fig.6.15 are timings of events including the ECCS injection, core dryout periods and PCT values of the six tests related with their equivallent break areas. Fig.6.15 (a) shows that the break area slightly influenced the major event timings in the MRL tests. It also shows that core dryout initiation time of RUN 992 was fairly later than those of the MRL break tests, whereas that of the JPDL break test (RUN 991) was rather earlier than the MRL break tests. The TBL test shows slightly later dryout initiation than the ROSA-III MRL tests. Thus the TBL test results locate at an intermediate position between those of ROSA-III tests of RUNs 991 and 992.

A time period between the core dryout initiation and the LPCI injec-

tion of the TBL test is slightly shorter than the MRL break tests and that of RUN 992 is shortest among them. And this period of RUN 991 is the longest as a result of the break location effect. Namely, mass decrease inside the core shroud was earlist in RUN 991 and earlier in the MRL break tests rather than the higher break elevation tests of TBL test and RUN 992. Although the break elevation of RUN 991 was higher than the MRL break tests, mass decreasing rate of RUN 991 was higher than the MRL tests because water inside the lower plenum was continuously extracted through the jet pumps for all the test period.

Figure 6.15 (b) shows the core dryout time period (between the timings of core top dryout initiation and the final core quench) of each test. The core dryout period of the TBL test was clearly longer than those of the MRL break tests. This reason can be attributed to lack of LPCS and 1LPCI injections. This is also applied to RUN 991 and the core dryout period of RUN 991 became almost twice as large as those of the MRL break tests. Thus the core dryout periods of these intermediate break tests were influenced by both of the break location and ECCSs failure mode. The core dryout period of TBL test was at an intermediate position between those of RUNs 991 and 992.

Figure 6.15 (c) shows the PCT values of these tests. The PCT is affected by both of the core dryout period shown above and a heat flux of the PCT-recorded heater rod. The heat flux is, of course, controlled by the power distribution along the vertical axis and between the rod bundles, and also by the decay power simulation curve of each test.

An average temperature increasing rate of the PCT rod, which is principally controlled by the average heat flux and slightly influenced by the steam flow cooling, is obtained in each test as ahown in Table 6.8 (see items K/(H-L), where K shows increased temperature after its dryout initiation and (H-L) shows a time period between the dryout initiation time and PCT recording time). The PCT recorded position along the vertical axis is shown in the item N except for the TBL test (the TBL PCT position is guessed at the upper core region from the dryout initiation time and the mixture level data). It is shown that the average temperature increasing rate is higher in the MRL break tests with 15 and 25% break areas than the other tests. The temperature increasing rate of RUN 991 was rather lower than the others because of the temporary cooling effect of the ADS, which actuated before the LPCI injection. The increasing rate of the TBL test is rather lower than the ROSA-III tests (this also suggests the PCT location

at the upper core region with lower heat flux).

Consequently, the PCT value of each test was determined as a result of break location effects and ECCS failure mode. The PCT of TBL HPCS line break test showed an intermediate value between those of RUNs 991 and 992. An analysis(59) based on the RELAP5/MOD1(CY1) code also showed that an HPCS line break in the ROSA-III system resulted in an intermediate PCT value between those of RUNs 991 and 992.

The PCT value of TBL HPCS line break was, as a result, close to those of the ROSA-III MRL break tests with an HPCS single failure because of the slightly lower temperature increasing rate and the longer core dryout period in the TBL test than those of the latters. This suggest that a PCT of a ROSA-III HPCS line break will be rather higher than the TBL test result due to the higher temperature increasing rate in the former, and also higher than the results of ROSA-III MRL break tests due to the longer core dryout period in the former.

7. Conclusions

An intermediare break BWR LOCA simulation test (RUN 991) was performed at the ROSA-III program to experimentally study influences of an HPCS line break with a mulfunction of another ECCS. RUN 991 was a single-ended jet pump drive line (JPDL) break test and the effective break area was 20.6% of the scaled MRL flow area. In order to study the break location effects on the core cooling phenomena, the 10% main steam line (MSL) break test (RUN 992) and main recirculation line (MRL) break tests with break area ratios of 5, 15 and 25% (RUNs 922, 927 and 930) are compared with this test. Moreover, the HPCS line break test at the TBL (Two Bundle Loop) facility was compared with these intermediate break ROSA-III tests. The following are concluded.

(1) The PCT of 985 K in RUN 991 was observed at 79 s after the LPCI initiation at the high power bundle. The heated core was completely cooled by the 2LPCI systems within 197 s from its initiation. Transient system mass of RUN 991 was estimated from mass balance of the initial system mass (M_0 = 646 kg), the injected mass of the feedwater and the LPCI, and the discharged mass through the MSL and the break. A reliability of the calculated system mass was confirmed at a time point (t = 220 s) by a differently estimated remaining mass within an uncertainty of $\Delta M = \pm$ 26 kg ($\Delta M/M_0 = \pm$ 0.04). The core dryout started at M/M_0 = 0.74 and finally diminished by reflooding at M/M_0 = 0.57 in RUN 991.

(2) The PCT in RUN 991 was higher than in the MRL break tests (RUNs 922, 927 and 930) mainly due to the earlier core dryout initiation and later LPCI injection. The earlier core dryout in RUN 991 is due to the special break location at the jet pump drive nozzles, through which water inside the core shroud was extracted. The later LPCI injection is also due to the effect of break location, which resulted in slow depressurization.

(3) On the other hand, the 10% MSL break test (RUN 992) showed significantly lower PCT than those in the MRL break tests because of the larger remaining mass inside the core shroud. The core dryout of RUN 992 started at M/M_0 = 0.64 and the final core quench was observed at M/M_0 = 0.51. These are clearly lower than those of RUN 991. Thus

the break location significantly affects core cooling conditions and the PCT in the intermediate break BWR LOCA simulation tests.

(4) The TBL HPCS line break test showed later core dryout initiation and longer core dryout period than those of the ROSA-III MRL break tests. Consequently, the PCT in TBL test was similar to those in the MRL break tests at the ROSA-III. The reason of later core dryout initiation is the larger remaining system mass as in the MSL break test. The longer dryout period is mainly due to the assumption of the LPCS and 1LPCI failure. The TBL test results showed intermediate trend between those of RUNs 991 and 992.

Acknowledgment

The authors are grateful to Mr.H.ASAHI, T.ODAIRA, T.TAKAYASU, Y.KITANO and T.NUMATA of Nuclear Engineering Corporation for their assisstance in conducting the experiment, Mr.K.HIYAMA, E.UMEKI and T.NAKAJIMA of Information Laboratory Corporation for preparing the data plots and Ms.T.KUROSAWA and M.KIKUCHI of Nihon Computer Bureau for type writing.

the break location significantly affects core cooling conditions and the PCT in the intermediate break BWR LOCA simulation tests.

(4) The TBL HPCS line break test showed later core dryout initiation and longer core dryout period than those of the ROSA-III MRL break tests. Consequently, the PCT in TBL test was similar to those in the MRL break tests at the ROSA-III. The reason of later core dryout initiation is the larger remaining system mass as in the MSL break test. The longer dryout period is mainly due to the assumption of the LPCS and 1LPCI failure. The TBL test results showed intermediate trend between those of RUNs 991 and 992.

Acknowledgment

The authors are grateful to Mr.H.ASAHI, T.ODAIRA, T.TAKAYASU, Y.KITANO and T.NUMATA of Nuclear Engineering Corporation for their assisstance in conducting the experiment, Mr.K.HIYAMA, E.UMEKI and T.NAKAJIMA of Information Laboratory Corporation for preparing the data plots and Ms.T.KUROSAWA and M.KIKUCHI of Nihon Computer Bureau for type writing.

References

(1) K.TASAKA, et al., "Study on the Similarity between ROSA-III Experiment and BWR LOCA", JAERI-M 6703 (1976) (in Japanese).

(2) Y.ANODA, et al.,"ROSA-III System Description for Fuel Assembly No. 4", JAERI-M 9363 (1981) (in Japanese).

(3) General Electric Company, "General Electric Standard Safety Analysis Report, BWR/6", DOCKET-STN-50477 (1978).

(4) K.TASAKA, et al.,"ROSA-III Base Test Series for a Large Break Loss of Coolant Accident in a Boiling Water Reactor", Nucl. Technol. 57, 179-191 (1982).

(5) K.SODA, et al.,"Boiling Water Reactor Loss of Coolant Test (Single Failure Test with ROSA-III)", J. Nucl. Sci. Technol. 20, 537-558 (1983).

(6) K.TASAKA, et al.,"Simulation Experiment of Five Percent Small Break LOCA of BWR", J. Nucl. Sci. Technol. 20, 89-104 (1983).

(7) K.TASAKA, et al.,"ROSA-III Double-Ended Break Test Series for a Loss-of-Coolant Accident in a Boiling Water Reactor", Nucl. Technol. 68, 77-93 (1985).

(8) M.SUZUKI, et al.,"Recirculation Pump Discharge Line Break Tests at ROSA-III for a Boiling Water Reactor", Nucl. Technol. 70, 189-203 (1985).

(9) Y.KOIZUMI, et al., "Experiment Analysis of Power Curve Sensitivity Test Series at ROSA-III", Nucl. Eng. and Design 86, 267-287 (1985)

(10) H.KUMAMARU, et al.,"Five Percent Break BWR LOCA/ECC Test at ROSA-III without HPCS Actuation---Two Dimensional Core Thermal Hydraulic Phenomena", Nucl. Eng. and Design 86, 219-239 (1985).

(11) K.TASAKA, et al.,"Analysis of ROSA-III Break Area Spectrum Experiments on BWR Loss-of-Coolant Accident", Nucl. Technol. 71, 3, 628-643 (1985).

(12) T.YONOMOTO, et al.,"Investigation of BWR/LOCA at ROSA-III---Effect of Break Configuration on System Transient---", Nucl. Eng. and Design 92, 195-205 (1986).

(13) M.SUZUKI, et al.,"Similarity Study of Large Steam Line Break LOCAs in ROSA-III, FIST and BWR/6", Nucl. Eng. and Design 98,1, 39-56 (1986).

(14) Y.KOIZUMI et al.,"Investigation of Break Location Effects on

Thermal-Hydraulics during Intermediate Break Loss-of-Coolant Accident Experiments at ROSA-III", J. Nucl. Sci. Technol., 23 11, 1008-1019 (1986).

(15) H.KUMAMARU et al.,"Investigation of Effect of Pressure Control System on BWR LOCA Phenomena Using ROSA-III Facility", J. Nucl. Sci. Technol., 24 10, 844-858 (1987).

(16) T.YONOMOTO et al.,"Core Heat Transfer Analysis during a BWR LOCA Simulation Experiment at ROSA-III", Nucl. Eng. and Design, 103 2, 239-250 (1987).

(17) Y.KOIZUMI et al.,"BWR Small Break LOCA Counterpart Test at ROSA-III and FIST Test Facilities", Nucl. Eng. and Design, 102, 151-163 (1987).

(18) H.KUMAMARU et al.,"BWR Large Break LOCA/ECC Counterpart Test at ROSA-III and FIST", Nucl. Eng. and Design, 102 2, 223-238 (1987).

(19) Y.KOIZUMI et al.,"Effect of Heat Generation Difference among Fuel Bundles on Core Thermal-Hydraulics during 200% and 5% Loss-of-Coolant Accident Experiments", J. Nucl. Sci. Technol., 24 1, 61-74 (1987).

(20) K.TASAKA et al.,"ROSA-III Experimental Program for BWR LOCA/ECCS Integral Tests", JAERI 1307 (1987).

(21) H.NAKAMURA et al.,"Effectiveness of Automatic Depressurization System on Core Cooling in Small Break Loss-of-Coolant Accident of Boiling Water Reactor", to be published in Nucl. Eng. and Design.

(22) M.SOBAJIMA et al.,"Experiment Test Data of ROSA-III Test RUN 701 (Decay Heat Simulation Test with ECCS Actuation)", JAERI-M 8604 (1979).

(23) Y.ANODA et al.,"Experiment Data of ROSA-III Test RUN 703 (Split Break Simulation Test with ECCS Actuation)", JAERI-M 8967 (1980).

(24) Y.ANODA et al.,"Experiment Data of ROSA-III Test RUN 704 (Standard Test with ECCS Actuation)", JAERI-M 8968 (1980).

(25) M.OKAZAKI et al.,"Experimet Test Data of ROSA-III Integral Test RUN 705 (Isothermal Blowdown Test without ECCS Actuation)", JAERI-M 8723 (1980).

(26) M.SUZUKI et al.,"Experiment Data of ROSA-III Integral Test, RUN 706", JAERI-M 8737 (1980).

(27) M.OKAZAKI et al.,"Experiment Data of ROSA-III Integral Test RUN 708 (Standard Test without ECCS Actuation)", JAERI-M 8738 (1980).

(28) Y.KOIZUMI et al.,"Experiment Data of ROSA-III Integral Test, RUN 710", JAERI-M 9249 (1981).

(29) Y.ANODA et al.,"Experimet Data of ROSA-III Integral Test RUN912 (5% Split Break Test without HPCS Actuation)", JAERI-M 82-010 (1982).

(30) H.NAKAMURA et al.,"Experiment Data of ROSA-III Integral Test RUN 901 (200% Double-Ended Break with Full ECCS Actuation)", JAERI-M 84-007 (1984).

(31) H.NAKAMURA et al.,"Experiment Data of ROSA-III Integral Test RUN 926 (200% Double-Ended Break with HPCS Failure)", JAERI-M 84-008 (1984).

(32) M.SUZUKI et al.,"Experiment Data of 200% Recirculation Pump Discharge Line Break Integral Test RUN 961 with HPCS Failure at ROSA-III and Comparison with Results of Suction Line Break Tests", JAERI-M 84-045, (1984).

(33) M.SUZUKI, et al.,"Recirculation Pump Suction Line 2.8% Break Integral Test at ROSA-III with HPCS Failure, RUN 984", JAERI-M 84-100, (1984).

(34) M.SUZUKI, et al.,"Recirculation Pump Suction Line 200% Break Integral Test at ROSA-III with Two LPCI Failures, RUN 983", JAERI-M 84-135, (1984).

(35) M.KAWAJI, et al.,"A Main Steam Line Break Experiment at ROSA-III RUN 952 (Standard Run with Full ECCS)", JAERI-M 84-229, (1984).

(36) M.KAWAJI, et al.,"A Main Steam Line Break Experiment at ROSA-III, RUN 953 (100% Break with an HPCS Failure)", JAERI-M 85-029 (1985).

(37) M.SUZUKI, et al.,"BWR Recirculation Loop Discharge Line Break LOCA Tests with Break Areas of 50 and 100% Assuming HPCS Failure at ROSA-III Facility", JAERI-M 85-037, (1985).

(38) T.YONOMOTO, et al.,"ROSA-III 50% Break Integral Test RUN 916 (Break Area Parameter Test)", JAERI-M 85-109, (1985).

(39) H.NAKAMURA, et al.,"Recirculation Pump Suction Line 5% Split Break Test of ROSA-III (RUNs 922 and 932 with HPCS Failure)", JAERI-M 85-128, (1985).

(40) T.YONOMOTO, et al.,"ROSA-III 50% Break Integral Test RUN 928 (Break Configuration Sensitivity Test)", JAERI-M 85-151 (1985).

(41) K.TASAKA, et al.,"Comparison of ROSA-III and FIST BWR Loss of Coolant Accident Simulation Tests", JAERI-M 85-158 (1985).

(42) M.SUZUKI, et al.,"BWR Main Steam Line Break LOCA Tests RUNs 951, 954 and 956 at ROSA-III (Beak Area Effects with HPCS Failure)", JAERI-M 85-202 (1985).

(43) H.NAKAMURA et al.,"Recirculation Pump Suction Line 1% Split Break

LOCA Test of ROSA-III (RUNs 921 and 931 with HPCS Failure)", JAERI-M 85-209 (1986).

(44) M.SUZUKI, et al.,"BWR 200% Recirculation Pump Suction Line Break LOCA Tests, RUNs 942 and 943 at ROSA-III without HPCS (Effects of Initial Fluid Conditions on LOCA)", JAERI-M 86-038 (1986).

(45) M.SUZUKI, et al.,"BWR LOCA Integral Test Simulating a 100% Main Steam Line Break outside Reactor Containment Vessel in ROSA-III Program, RUN 955 (Analogy of Steam and Recirculation Line Small Break LOCAs)", JAERI-M 87-044 (1987).

(46) T.YONOMOTO, et al.,"ROSA-III 100% Break Integral Test RUN 914 (Break (Break Area Parameter Test)), JAERI-M 87-072 (1987).

(47) M.SUZUKI, et al.,"BWR Main Recirculation Line Break LOCA Tests, RUNs 917 and 918 without HPCS at ROSA-III Program (Effects of ADS Delay in Small Break LOCA)", JAERI-M 88-141 (1988).

(48) M.SUZUKI, et al.,"BWR LOCA Simulation Test (RUN 992) in ROSA-III Program for a 10% Main Steam Line Break with ECCS Double Failures", JAERI-M 89-034 (1989).

(49) T.YONOMOTO, et.al.,"Experiment Data of ROSA-III Integral Test RUN 913 (15% Split Break without HPCS Actuation)", JAERI-M 89-125 (1989).

(50) H.NAKAMURA, et.al.,"Loss of Off-Site Power Test of ROSA-III (RUN 971 with HPCS Failure)", JAERI-M 89-130 (1989).

(51) H.NAKAMURA et al.,"Recirculation Pump Suction Line 75 and 25% Split Break LOCA Test of ROSA-III (RUNs 929 and 930 with HPCS Failure)", JAERI-M 89-131 (1989).

(52) M.SUZUKI, et al.,"Heat Loss and Fluid Leakage Tests of the ROSA-III Facility", JAERI-M 9834 (1981).

(53) M.SUZUKI, et al.,"Characteristics of the ROSA-III Test Facility (Characteristics Test of the Jet Pumps in Normal and Reverse Flow)", JAERI-M 8670, (1980) (in Japanese).

(54) M.SUZUKI, et al.,"Evaluation of a Jet Pump Model for RELAP5 Code", JAERI-M 84-245, (1985) (in Japanese).

(55) M.SOBAJIMA et al.,"Instrumentation and Data Processing Method of the ROSA-III Test", JAERI-M 8499 (1979) (in Japanese).

(56) N.ABE et al.,"Electric Power Tansient Curve for ROSA-III Tests", JAERI-M 8728 (1980).

(57) K.TASAKA, et.al.,"ROSA-III Experimental Program for BWR LOCA/ECCS Integral Simulation Tests", JAERI 1307 (1987).

(58) H.MURATA, et.al.,"An Analysis of 100% Steam Line Break Test in the ROSA-III Program by Using RELAP5/Mod1 Code (Analysis of RUN 952, an HPCS Injection Test)", JAERI-M 83-210 (1983).

(59) M.SUZUKI, et.al.,"A BWR LOCA Simulation Test at ROSA-III (Simulation Test of HPCS Line Break and its Analysis)", Proceedings of Fall Meeting of Japan Atomic Energy Society in 1983, D-32 (in Japanese).

(60) S.MIURA, et al.,"SAFER Qualification by TBL Test Analysis", Proceedings of 13th Water Reactor Safety Research Information Meeting, NUREG/CP-0071 (1985).

(61) S.MIURA, et.al.,"Assessment of the SAFER Program for Core Spray Line Break LOCA with Data from the Two Bundle Loop (TBL)", 2nd International Topical Meeting on Nuclear Power Plant Thermal Hydraulics and Operations, Tokyo, Japan (April 1986).

(62) M.MURASE and M.NAITOH, "BWR Loss of Coolant Integral Tests with Two Bundle Loop, (I) - Thermal-Hydraulic Characteristics in Parallel Channels -", J. Nucl. Sci. Technol., 22(3), p213-224 (March 1985).

(63) Jae H.JO and H.R.Connel, "Assessment of TRAC-BD1/MOD1 Using FIST DATA", 13th Water Reactor Safety Research Information Meeting, NEREG/CP 0071 (1985).

(64) W.A.Sutherland, et.al.,"BWR Full Integral Simulation Test (FIST) Phase II Test Results and TRAC-BWR Model Qualification", NUREG/CR-4128, EPRI NP-3988, GEAP-30876 (Oct. 1985).

(65) A.B.BURGESS, et al.,"Assessment of SAFER Code for LOCA with Data from the Advanced Boiling Water Reactor Test Facility", ibid, NUREG/CP 0071 (1985).

(66) S.ITOYA and N.ABE, "Analyses of TBL Main Steam Line Break Test by SAFER03 and TRAC-BD1", 2nd Topical Meeting on Nuclear Power Plant Thermal Hydraulics and Operations, (April 1986) Tokyo, Japan.

(67) M.IRIKO, et.al.,"Updated Core Power Curves for ROSA-III Facility" JAERI-M 84-029 (Feb. 1984) (in Japanese).

Table 2.1 Primary chracteristics of ROSA-III and BWR/6

Items	Unit	BWR*	ROSA-III	BWR / ROSA-III
Number of Recirc. Loops	-	2	2	1
Number of Jet Pumps	-	24	4	6
Number of Separators	-	212	1	212
Number of Fuel Assemblies	-	848	4	212
Active Fuel Length	m	3.76	1.88	2
Total Fluid Volume	m^3	621	1.42	437
Maximum Core Power	MW	3800	< 4.40	> 864
Steam Dome Pressure	MPa	7.23	7.23	1
Total core Flow Rate	kg/s	15400	< 36.4	> 424
Recirc. Flow Rate/Loop	kg/s	2240	< 5.26	> 424
Total Steam Flow Rate	kg/s	2060	< 4.86	> 424
Feedwater Temperature	K	489	489	1

* BWR/6 (251-848)

Table 3.1 ROSA-III instrumentation summary list

ITEM	SENSOR	NUMBER	NOTE
Pressure	Pressure Transducer	20	
Differential Pressure	DP Cell	60	PV and Loop 44 Level Measurement 5 Flow Meter 11
Fluid Temperature	CA Thermocouple	129	Primary Loop 23 DTT 4 Tie Rod 28 Upper Plenum 10 Lower Plenum 10 Tie Plate 40 Bypass 14
Fuel Rod Temperature	CA Thermocouple	213	
Slab Surface Temperature	CA Thermocouple	70	Core Barrel 24 Pressure Vessel 3 Channel Box 35 Shroud Support 8
Slab Inner Temperature	CA Thermocouple	9	JP Diffuser 4 PV Wall 5
Volumetric Flow Rate	Turbine Flow Meter Venturi Flow Meter Orifice Flow Meter	3 4 6	ECCS Loop 3 Primary Loop 10
Mass Flow Rate	Turbine Flow Meter Orifice Flow Meter	4 3	Recirculation Loop 4 Main Steam Line 3
Liquid Level	Conductivity Probe Capacitance Probe	138 2	
Density	Gamma Densitometer	10	2 Beam GD 2 3 Beam GD 2
Momentum Flux	Drag Disk	4	JP Spool Piece 2 Break Spool Piece 4 Break Orifice 1
Signal	ON/OFF Switch	14	
Pump Speed	Revolution Counter	2	
Electric Core Power	VA Meter	2	
TOTAL		693	

Table 4.1 Test conditions of RUN 991

Test Parameters	Unit	RUN 991
Break Conditions		
Break Location		JP Drive Line
Break Diameter/Area	mm/%	2x8.4/20.6
Initial Conditions		
Steam Dome Pressure	MPa	7.36
Lower Plenum Temperature	K	552.7
Lower Plenum Subcooling	K	10.5
Core Inlet Flow Rate	kg/s	16.1
Total Core Power	MW	3.96
Max. Linear Heat Rate	kW/m	16.63
Upper Plenum Quality	%	12.5
Downcomer Water Level*	m	4.80
Steam Flow Rate	kg/s	2.07
Feedwater Flow Rate	kg/s	2.04
Feedwater Temperature	K	489
Transient Conditions		
MRP Trip	s	0.0
MSIV Closure Trip	s	L1+3
ECC Conditions		
HPCS Actuation		Failure
LPCS Actuation		Failure
LPCI Actuation Logic	s	L1+40
LPCI Actuation Pressure	MPa	1.57
ECC Water Temperature	K	313
ADS Actuation Logic	s	L1+120
ADS Orifice Diameter	mm	19.0
L1 Level	m	4.00
L2 Level	m	4.46

* Actual downcomer level is corrected to 4.87 m.

Table 5.1 Major events and test procedures of RUN 991

Time (s)	Event
-116	· Initiation of data recording
-10	· Initiation of data plotting
0	· Initiation of break at BU-A, MRP trip, closure of QSV and valves (CV-1,2)
7	· Core power decay
15	· Pressure control (P ≧ 6.7 MPa)
25	· L1 level trip (4.0 m)
30	· Completion of MSL closure
40	· DC level at JP suction level
	· Steam discharge at break
42	· Initiation of core dryout
147	· ADS opening
215	· Feedwater line flashing
265	· LPCI injection
344	· PCT at A-22 rod Position 3 (984.7 K)
462	· Completion of quench
690	· Completion of data plotting
981	· Completion of data recording

Table 5.2 Mass balance in RUN 991

Time	P	P/P_o	M_F *1	M_E *2	M_S *3	M_D *4	M *5	M/M_o
(s)	(MPa)	(-)	(kg)	(kg)	(kg)	(kg)	(kg)	(-)
0	7.37	1.00	0	0	0	0	646	1.00
20	6.58	0.89	6	0	38	66	548	0.85
40	6.66	0.90	6	0	40	132	487	0.75
60	6.37	0.86	6	0	40	176	436	0.67
80	6.06	0.82	6	0	40	210	402	0.62
100	5.68	0.77	6	0	40	242	370	0.57
120	5.28	0.72	6	0	40	268	344	0.53
147	4.74	0.64	6	0	40	300	312	0.48
160	4.09	0.55	6	0	53	318	281	0.43
180	3.32	0.45	6	0	71	338	243	0.38
200	2.68	0.36	6	0	88	354	210	0.33
220	2.25	0.31	10	0	102	368	186	0.29
240	2.06	0.28	16	0	115	382	165	0.26
265	1.72	0.23	17	0	129	395	139	0.22
280	1.55	0.21	18	21	137	402	146	0.23
300	1.34	0.18	19	54	147	412	160	0.25
320	1.15	0.16	20	92	156	422	180	0.28
340	1.03	0.14	21	134	163	432	206	0.32
360	0.97	0.13	21	177	170	444	230	0.36
380	0.92	0.12	21	222	176	456	257	0.40
400	0.88	0.12	21	267	183	468	283	0.44
420	0.86	0.12	21	314	189	480	312	0.48
440	0.83	0.11	21	360	196	492	339	0.52
460	0.80	0.11	21	407	201	504	369	0.57
480	0.75	0.10	21	455	207	514	401	0.62
500	0.71	0.10	21	504	212	524	435	0.67
550	0.62	0.08	21	628	223	549	523	0.81
600	0.60	0.08	21	753	234	584	602	0.93

*1 Mass income from feedwater line

*2 Injected LPCI water mass

*3 Discharged steam flow through MSL

*4 Discharged mass through break

*5 Remaining mass in system

$M=M_o+M_F+M_E-M_S-M_D$

Table 5.3 Mass distribution in RUN 991

Region*1	Free Volume	Mixture Level*2	Refered DP Data	Collapsed Level	Void Fraction	Average Temperature*3	Water Mass	Steam Mass	ΔM_L
	(m^3)	Lm (m)	-	L (m)	α	T (K)	M_L (kg)	M_G (kg)	(kg)
L. Plenum	0.166	0.73	PD 21	0.60	0.21±0.2	Ts	88	1	±10
Guid Tube	0.056	0.97	-	-	(0.21±0.2)	〃	23	-	± 7
Downcomer	0.340	1.85	ML 69	1.35	0.55±0.03	〃	14	4	± 1
I.Rec. Loop	0.047	0.94	PD 36	-1.12	0.73±0.02	〃	8	-	-
I. Jet Pumps	0.026	-	PD 41	0.56	(0.21±0.2)	〃	11	-	± 3
B. Rec. Loop	0.047	0.94	-	-	(0.73±0.2)	〃	9	-	± 1
B. Jet Pumps	0.026	2.81	PD 50,52	0.93	0.85±0.15	〃	5	-	± 4
Core	0.096	-	-	-	-	700	-	1	-
Core Bypass	0.060	-	-	-	-	550	-	1	-
Up. Plenum	0.156	-	-	-	-	530	-	2	-
Steam Dome	0.372	-	-	-	-	530	-	4	-
Total*4	1.392	-		-	-	-	158	13	±26

*1 Downcomer is defined below level of 5.0 m, upper (Up.) plenum includes steam separator, and broken recirculation (B. Rec.) loop excludes pipings ($0.015m^3$) between the break and JP3,4 drive nozzles.

*2 Level is defined above DL 0.0m.

*3 Ts = 491.6K, $\rho' = 842.4kg/m^3$, $\rho'' = 11.3kg/m^3$. $\rho_G(550K) = 9.5kg/m^3$, $\rho_G(530K) = 10.1kg/m^3$.

*4 Total mass = 171±26 (kg)

Table 5.4 Maximum cladding temperature distribution in core of RUN 991

** Order of PCT (RUN 991) **

No. 1	A-22 rod	Pos. 3	PCT =	984.7 (K)	Time =	343.7 (s)
No. 2	A-84 rod	Pos. 1	PCT =	971.0 (K)	Time =	340.2 (s)
No. 3	A-11 rod	Pos. 3	PCT =	961.9 (K)	Time =	366.8 (s)
No. 4	A-22 rod	Pos. 2	PCT =	960.7 (K)	Time =	369.6 (s)
No. 5	A-71 rod	Pos. 4	PCT =	958.7 (K)	Time =	304.5 (s)
No. 6	A-11 rod	Pos. 4	PCT =	958.3 (K)	Time =	315.7 (s)
No. 7	A-77 rod	Pos. 3	PCT =	955.8 (K)	Time =	361.9 (s)
No. 8	A-73 rod	Pos. 4	PCT =	952.0 (K)	Time =	340.9 (s)
No. 9	A-84 rod	Pos. 4	PCT =	945.4 (K)	Time =	338.1 (s)
No.10	A-31 rod	Pos. 4	PCT =	944.0 (K)	Time =	337.4 (s)

Table 6.1 Comparison of major event timings between RUNs 991 and 992

Major Events	Time (s)	
	RUN 991	RUN 992
Break Initiation	0	0
L1 Level Trip	25	476
PCS Termination	30	18
First Core Dryout Initiation	42	425
ADS Actuation	147	594
LPCI Actuation	265	720
PCT Occurrence	344	744
Final Core Quench	462	760

Table 6.2 Comparison of depressurization rates per unit break area between RUNs 991 and 992

	RUN 991	RUN 992	
Time Period (s)	30 - 147	18 - 172	172 - 594
Pressure Range (MPa)	6.63 - 4.83	6.60 - 4.83	4.83 - 2.77
Break Area (A) (m^2)	1.108×10^{-4}	8.01×10^{-5}	8.01×10^{-5}
$\dot{P}/A$ ($MPa/m^2 \cdot s$)	139	143	61

Table 6.3 Comparison of average break mass flow rates between RUNs 991 and 992

	RUN 991	RUN 992	
Time Period (s)	0 - 147	0 - 172	172 - 594
Discharged Mass (M_d, kg)	0 - 300	0 - 138	138 - 296
Break Area (A, m^2)	1.108×10^{-4}	8.01×10^{-5}	8.01×10^{-5}
$\dot{M}_d/A$ ($kg/m^2 \cdot s$)	1.84×10^4	1.00×10^4	0.47×10^4

Table 6.4 Region volumes of TBL pressure vessel (Reference 64)

Symbol	Region name	BWR/5×$\frac{2}{764}$ (m³)	TBL (m³)
A	Lower plenum	0.142	0.148
B	Guide tube	0.114	0.111
C	Fuel channel	0.091	0.094
D	Core bypass	0.075	0.075
E	Upper plenum	0.071	0.072
F	Downcomer	0.128	0.140
G	Annulus	0.189	0.193
H	Saturated liquid region	0.132	0.134
I	Separator	0.021	0.021
J	Steam dome	0.538	0.529
K	Jet pump	0.018	0.018
L	Stand pipe	0.030	0.028
	Total	1.549	1.563

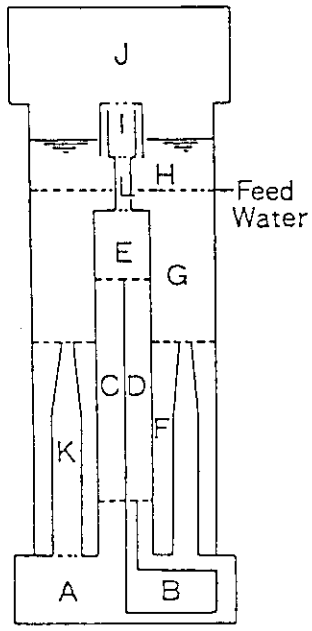

Table 6.5 Volume disrtibution of ROSA-III pressure vessel

Symbol	Region Name	BWR/6x$\frac{2}{848}$ (m³)	ROSA-III (m³)
A	Lower Plenum	0.186	0.166
B	Guide Tube	0.103	0.056
C	Fuel Channels	0.083	0.096
D	Core Bypass	0.058	0.060
E	Upper Plenum	0.124	0.124
F	Downcomer below JP Suction	0.115	0.059
G+H	Annulus below Water Level	0.175	0.281*1
I+L	Separator & Stand Pipe	0.066	0.032
J	Steam Dome	0.486	0.372
K	Jet Pump	0.016*2	0.052
	Total	1.412	1.298

*1. Water level is DL 5.0 m.
*2. 24 jet pumps are provided in BWR PV.

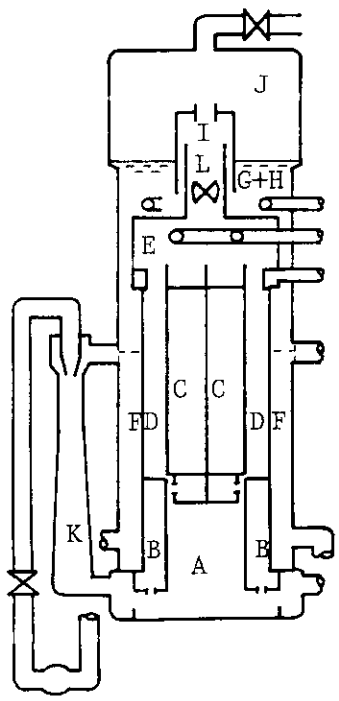

Table 6.6 Test conditions of TBL HPCS line break test (Reference 61)

Items	Unit	Test Data
Break Diameter	mm	10.0
Available ECCS	-	2LPCI + ADS
Initial Dome Pressure	MPa	7.0
Initial Core Power	MW	4.0 + 5.7
Initial Water Level	m	9.9
Initial Steam Flow	(kg/hr)	17.3×10^3

Table 6.7 Timings of major events and PCT in TBL test (Reference 61)

Events	Time(s)
Break Initiation	0
MSIV Closure	10
Break Line Uncovery	200
ADS Actuation	288
Core Dryout Initiation	(~360)*
LPCI Injection	506
PCT Recorded	612
Final Core Quench	(~670)*
PCT Value	871 K

* Timings are roughly estimated from Fig. 6.12 (b).

Table 6.8 Comparison of core dryout periods and PCTs among intermediate break LOCA tests

	TBL	ROSA-III Tests				
	RUN 315	RUN 992	RUN 991	RUN 922	RUN 927	RUN 930
A. Break Area x 10^5 (m^2)	7.85	8.01	11.08	2.73	8.01	13.48
Break Area Ratio (%)	10.4	14.9	20.6	5.1	14.9	25.0
B. PV Fluid Volume (m^3)	1.563	1.298	1.298	1.298	1.298	1.298
C. (A/B) x 10^5 (m^{-1})	5.02	6.17	8.54	2.10	6.17	10.39
D. Break Location	HPCS Line	MSL	JPDL	MRL	MRL	MRL
E. Available ECCS	2LPCI	2LPCI	2LPCI	LPCS+3LPCI	LPCS+3LPCI	LPCS+3LPCI
F. Core Top Dryout Time (s)	(360)	(425),620	42	200	(87), 167	(45), 100
G. Final Quench Time (s)	(670)	760	462	438	393	331
H. PCT Time (s)	612	744	344	431	361	275
I. Core Dryout Time (G-F)(s)	(310)	140	420	238	226	231
J. PCT Data (K)	871	649	985	830	848	867
K. ΔT of PCT Rod (K)	(355)	160	431	301	320	329
L. Dryout of PCT Rod (s)	(368)	652	68	226	194	119
M. K/(H-L) (K/s)	(1.45)	1.74	1.56	1.47	1.92	2.11
N. PCT Rod	-	A-11, P3	A-22, P3	A-17, P4	A-82, P4	A82, P4

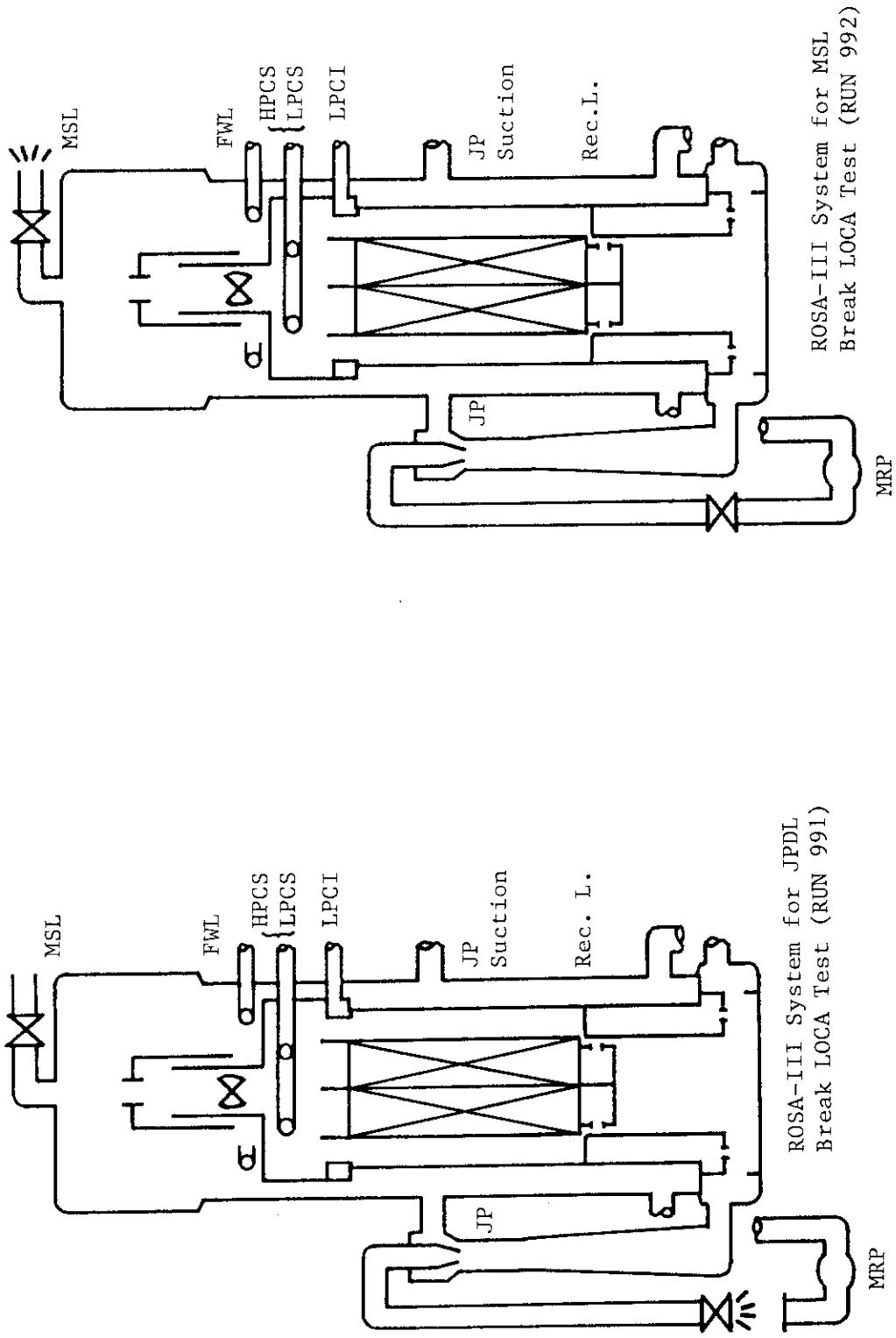

Fig. 1.1 Illustration of break locations for RUNs 991 and 992 and pipings through PV wall in ROSA-III facility

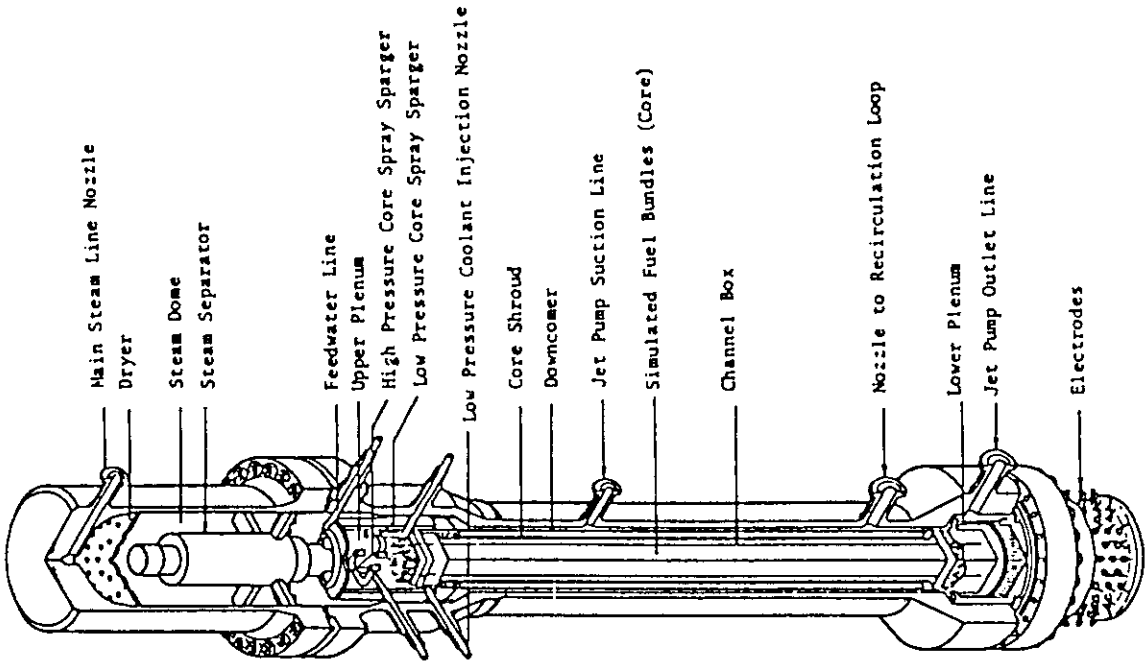

Fig. 2.2 Internal structure of pressure vessel of ROSA-III

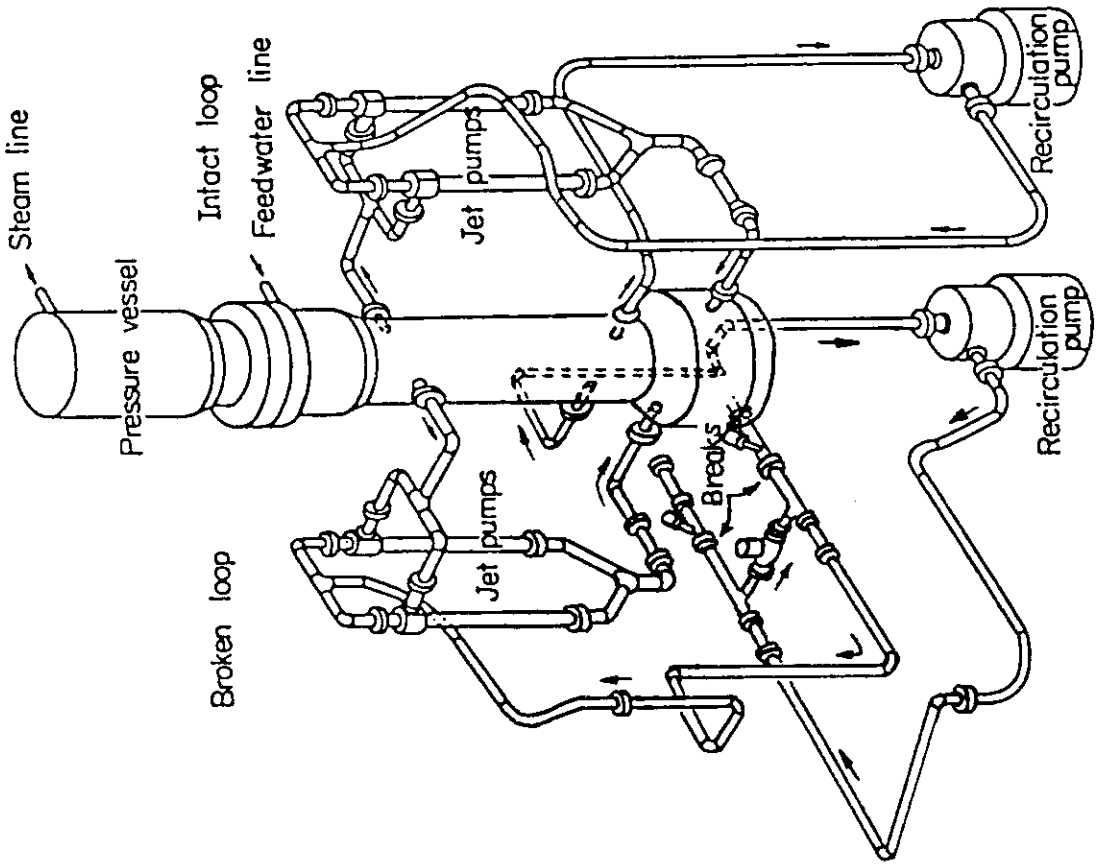

Fig. 2.1 Schematic diagram of ROSA-III test facility

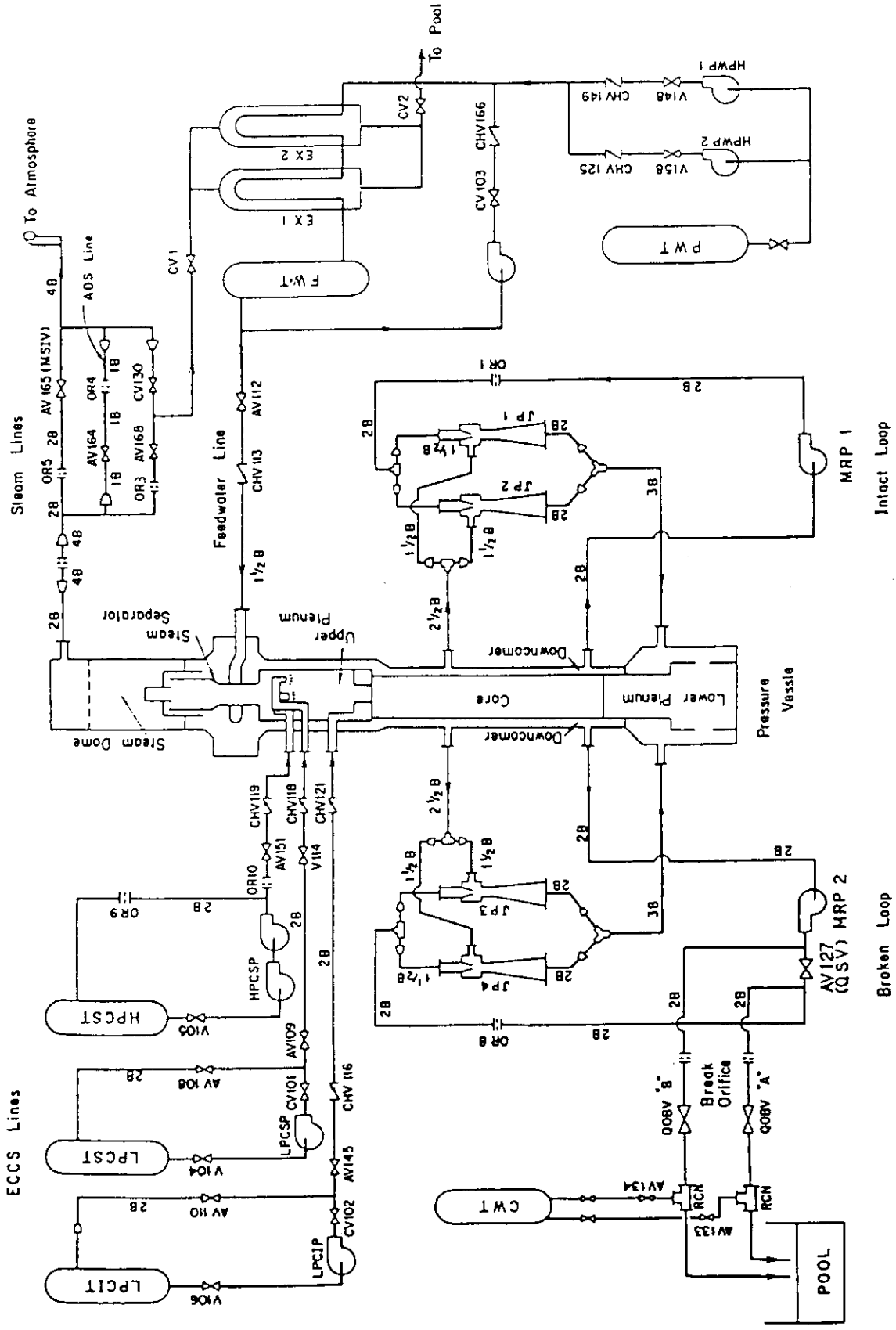

Fig. 2.3 ROSA-III piping schematic

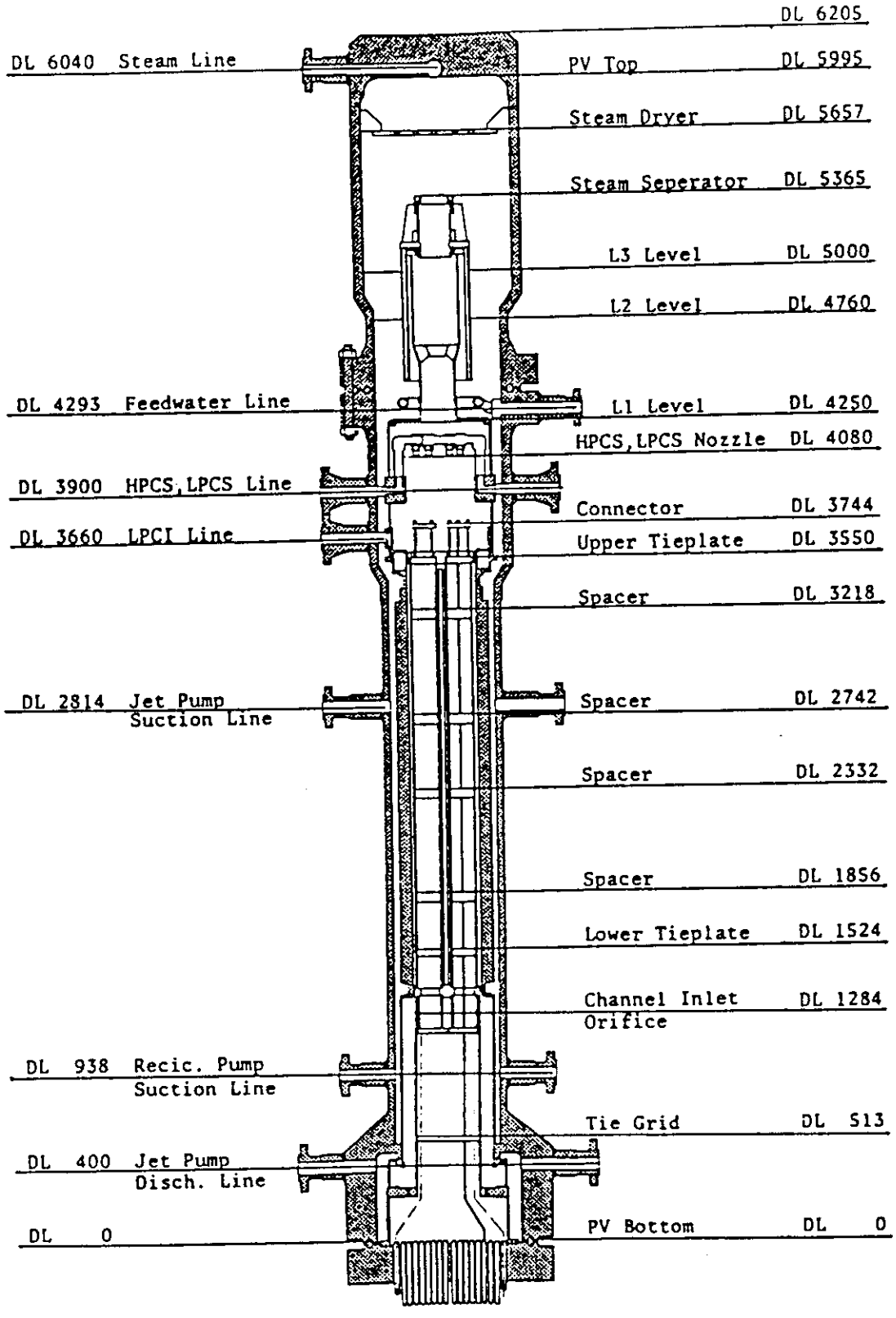

Fig. 2.4 Pressure vessel internals arrangement

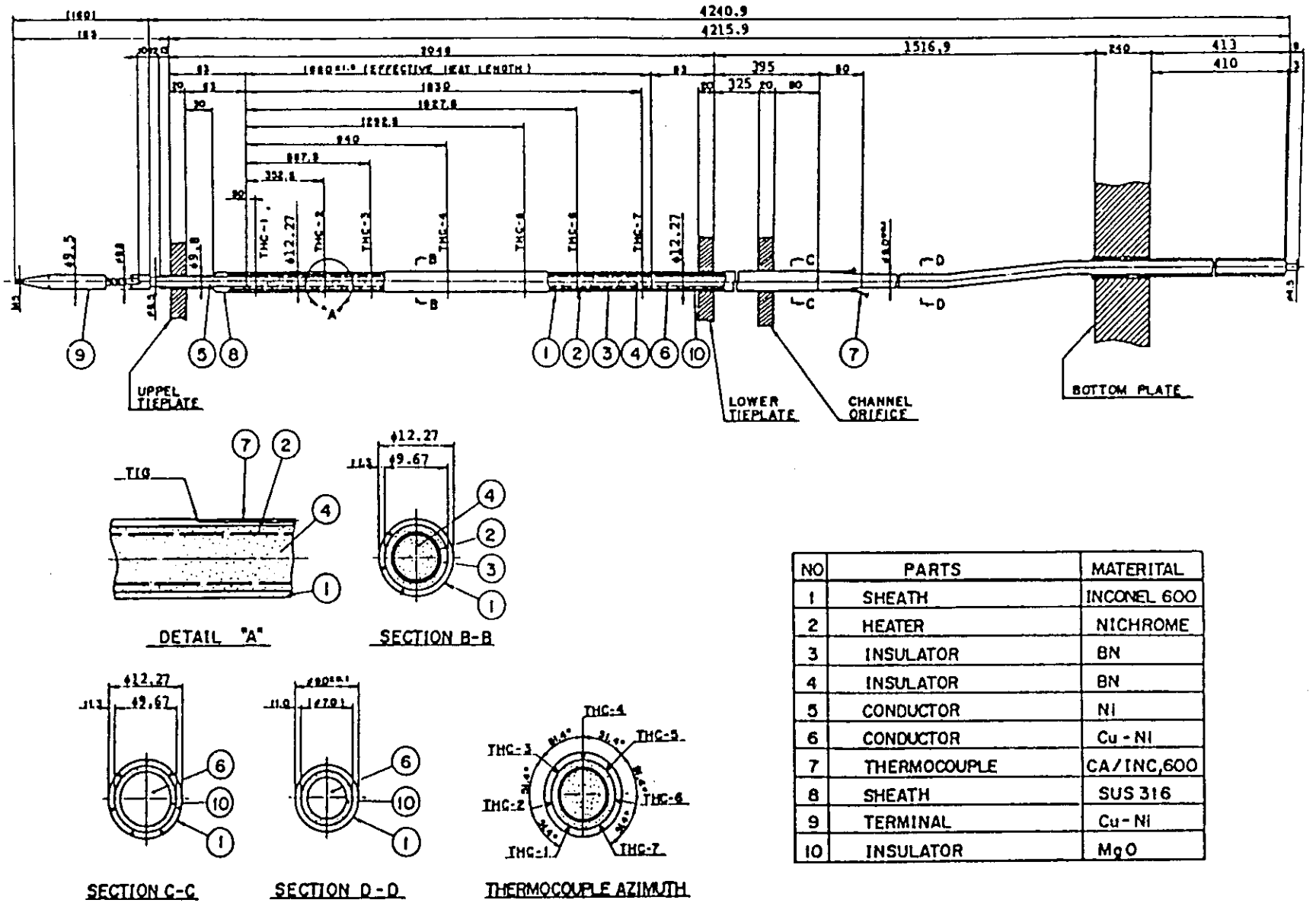

NO	PARTS	MATERITAL
1	SHEATH	INCONEL 600
2	HEATER	NICHROME
3	INSULATOR	BN
4	INSULATOR	BN
5	CONDUCTOR	NI
6	CONDUCTOR	Cu - NI
7	THERMOCOUPLE	CA/INC,600
8	SHEATH	SUS 316
9	TERMINAL	Cu - NI
10	INSULATOR	MgO

Fig. 2.5 Simulated fuel rod of ROSA-III

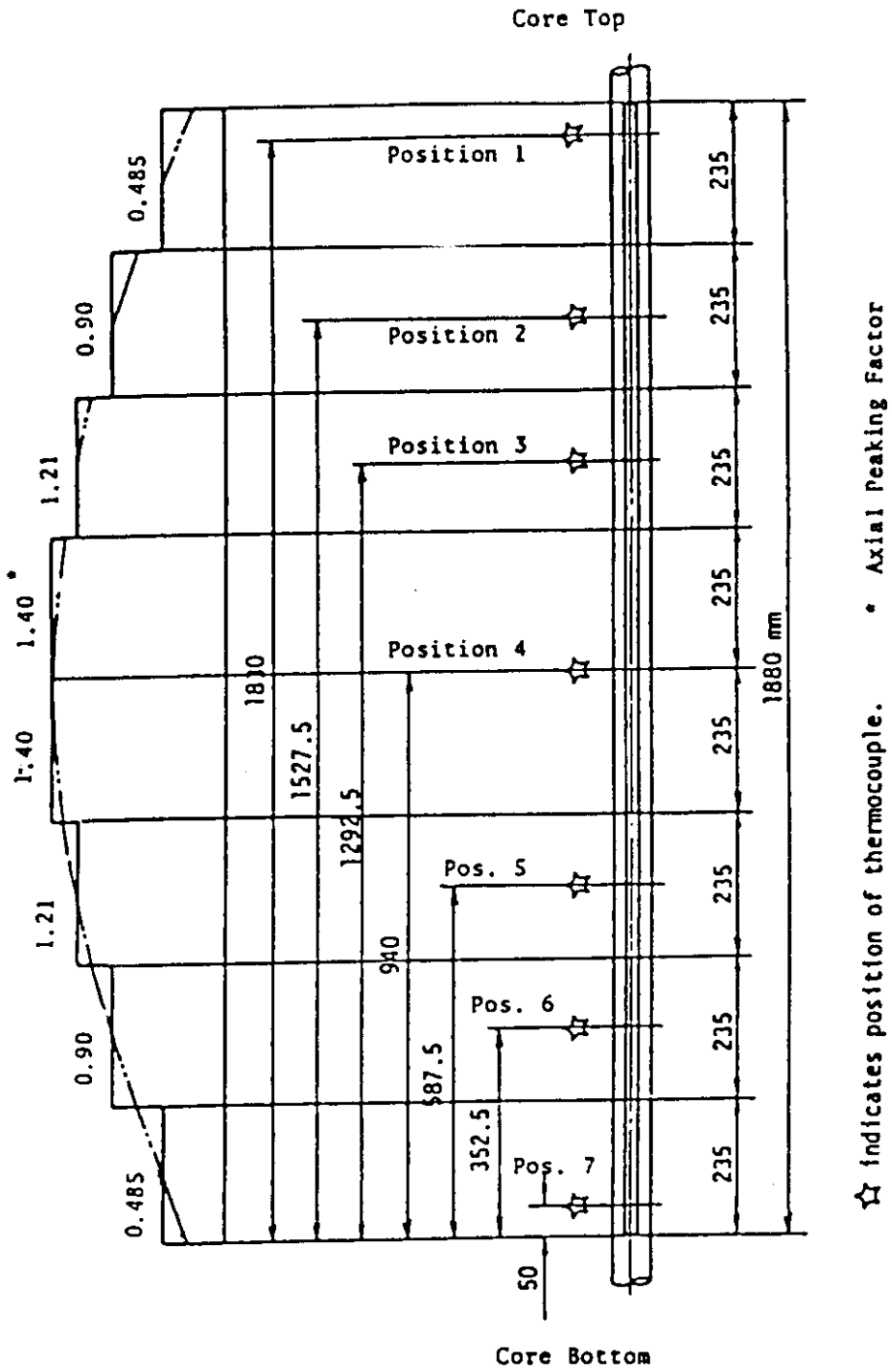

Fig. 2.6 Axial power distribution of heater rod

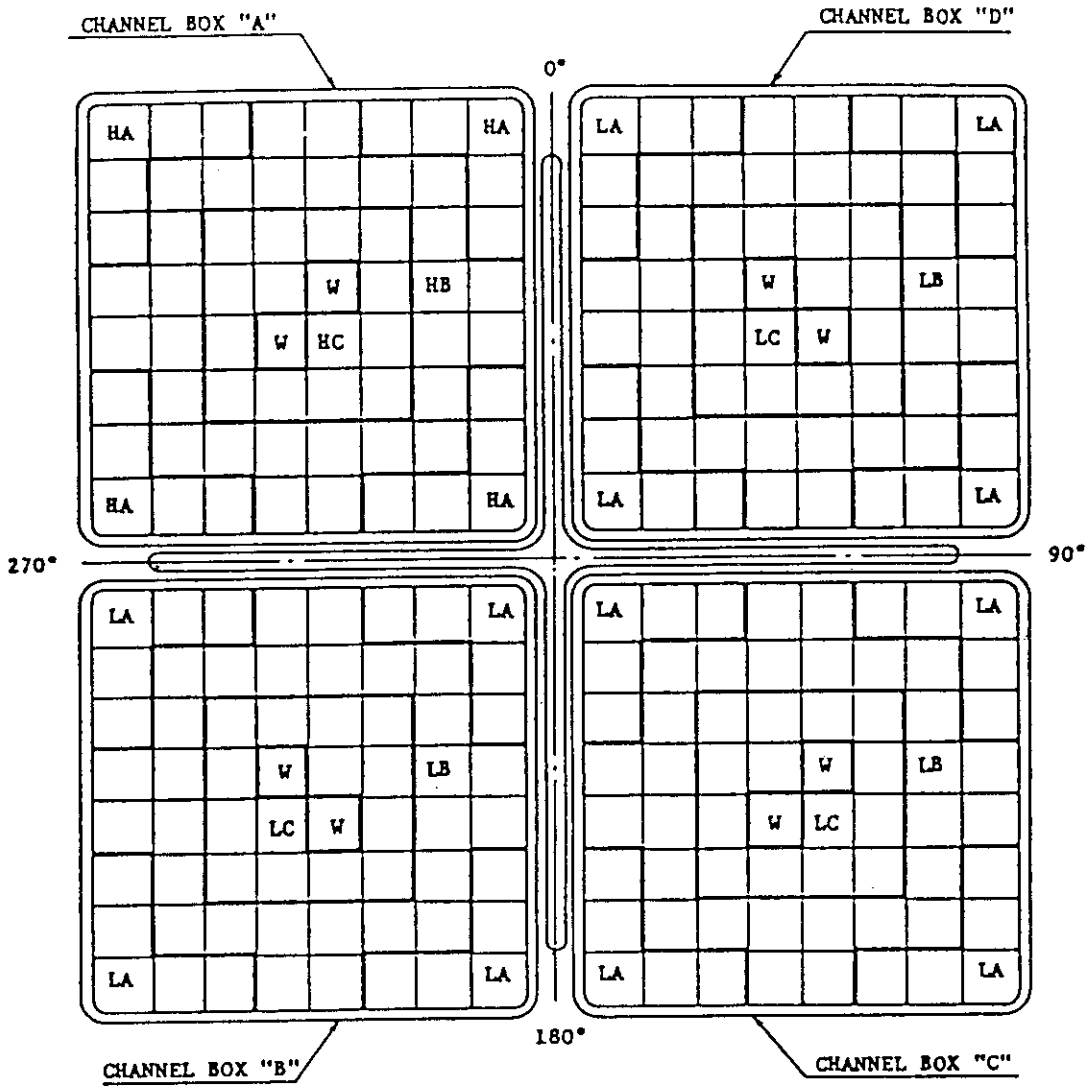

Region	HA	HB	HC	LA	LB	LC	W
Lenear Heat Rate (kW/m)	18.5	16.81	14.41	13.21	12.01	10.29	0.0
Local peaking factor	1.1	1.0	0.875	1.1	1.0	0.875	0.0
No. of Rods	20	28	14	60	84	42	8

* note : Radial peaking factor is 1.4

Fig. 2.7 Radial power distribution of core

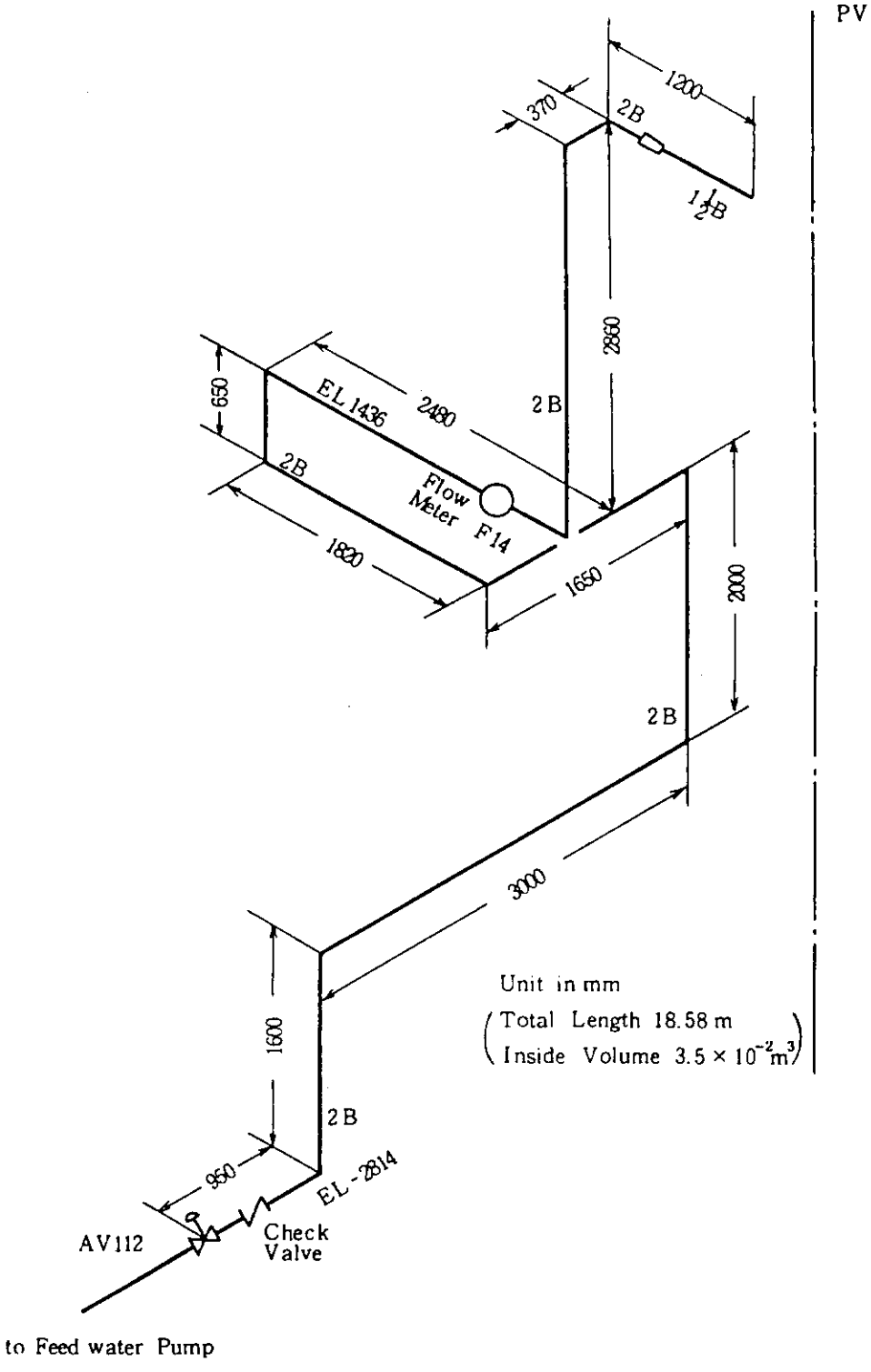

Fig. 2.8 Feedwater line between PV and AV-112

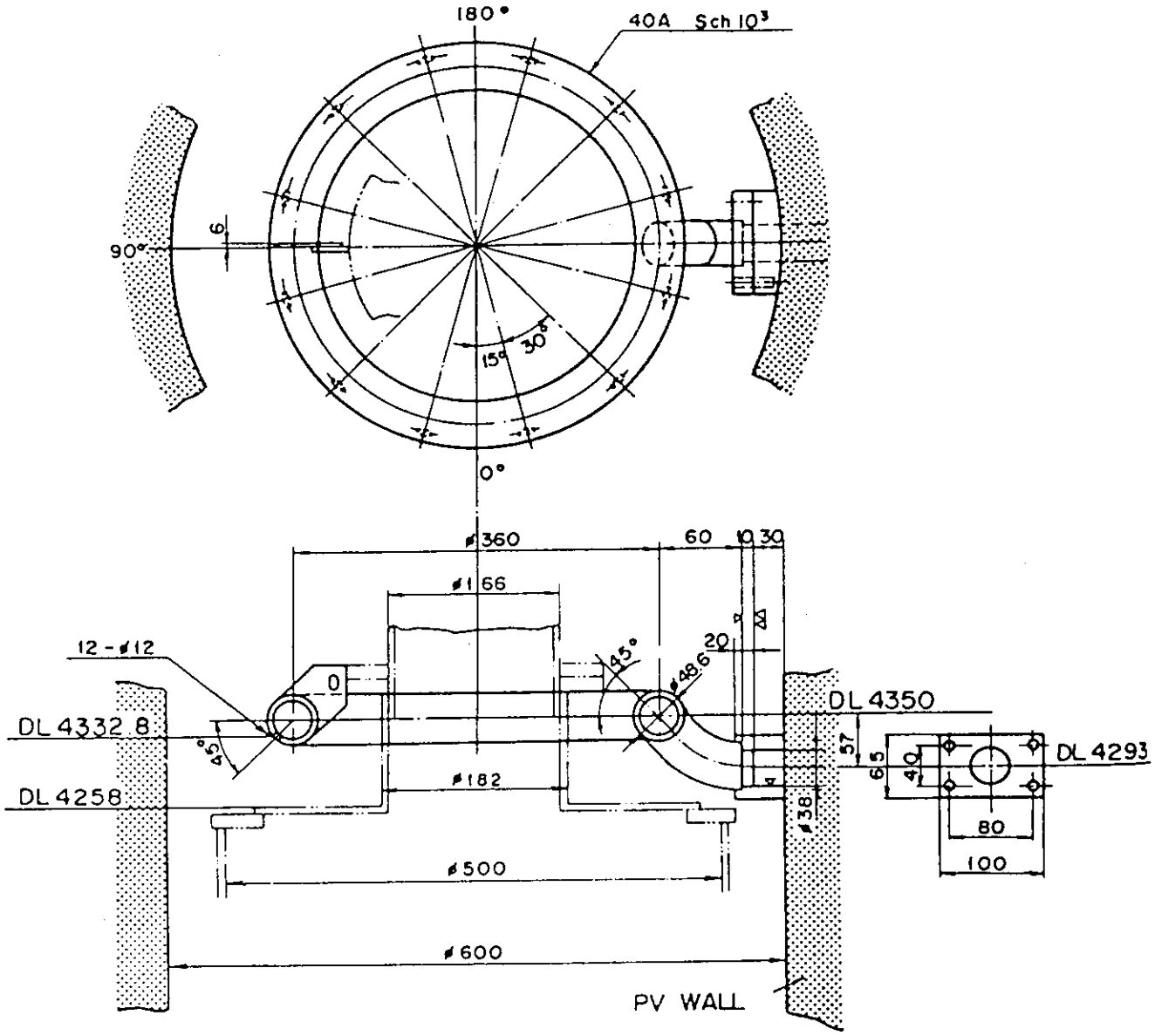

Fig. 2.9 Feedwater sparger configuration

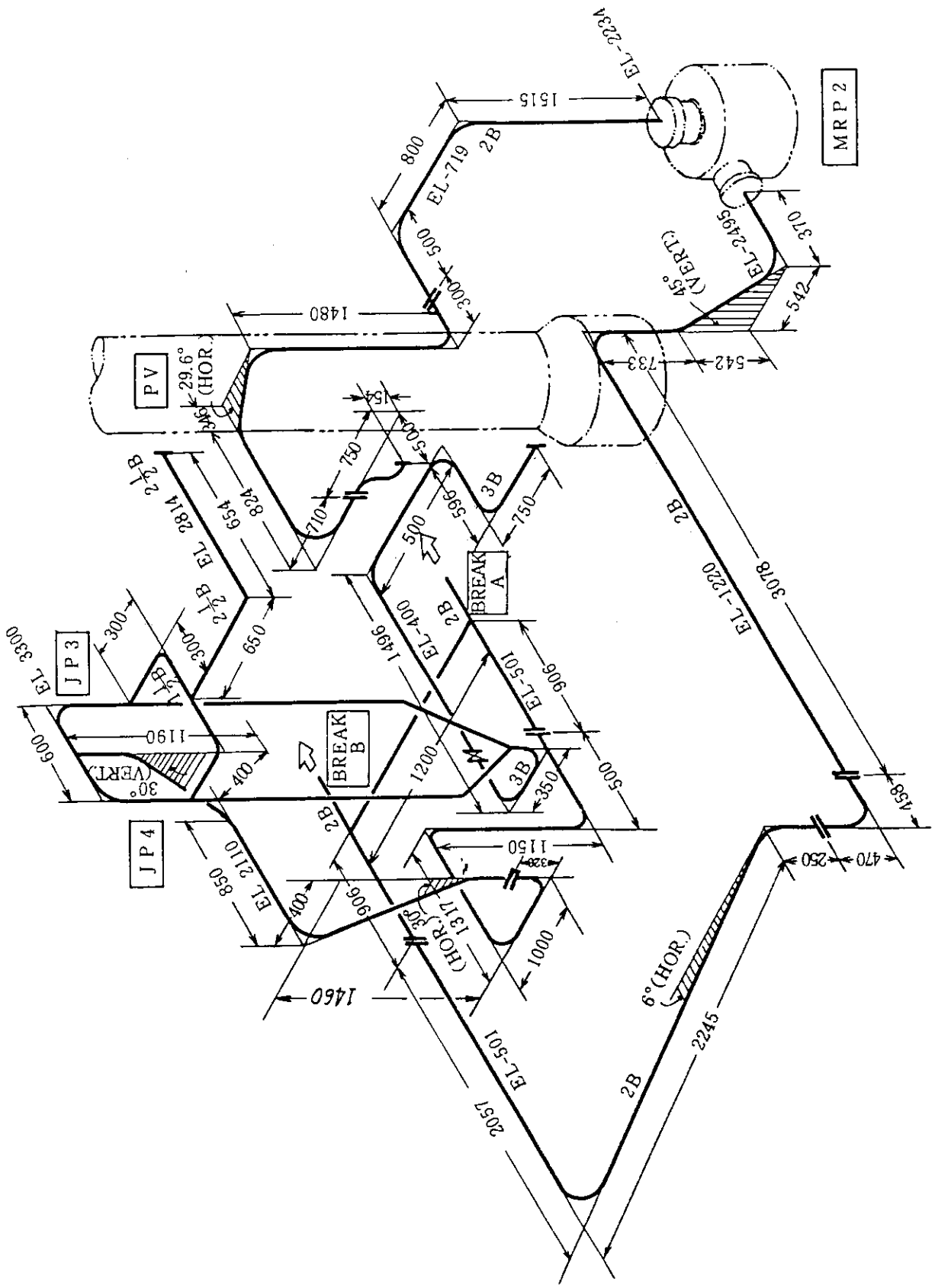

Fig. 2.10 Details of ROSA-III system piping

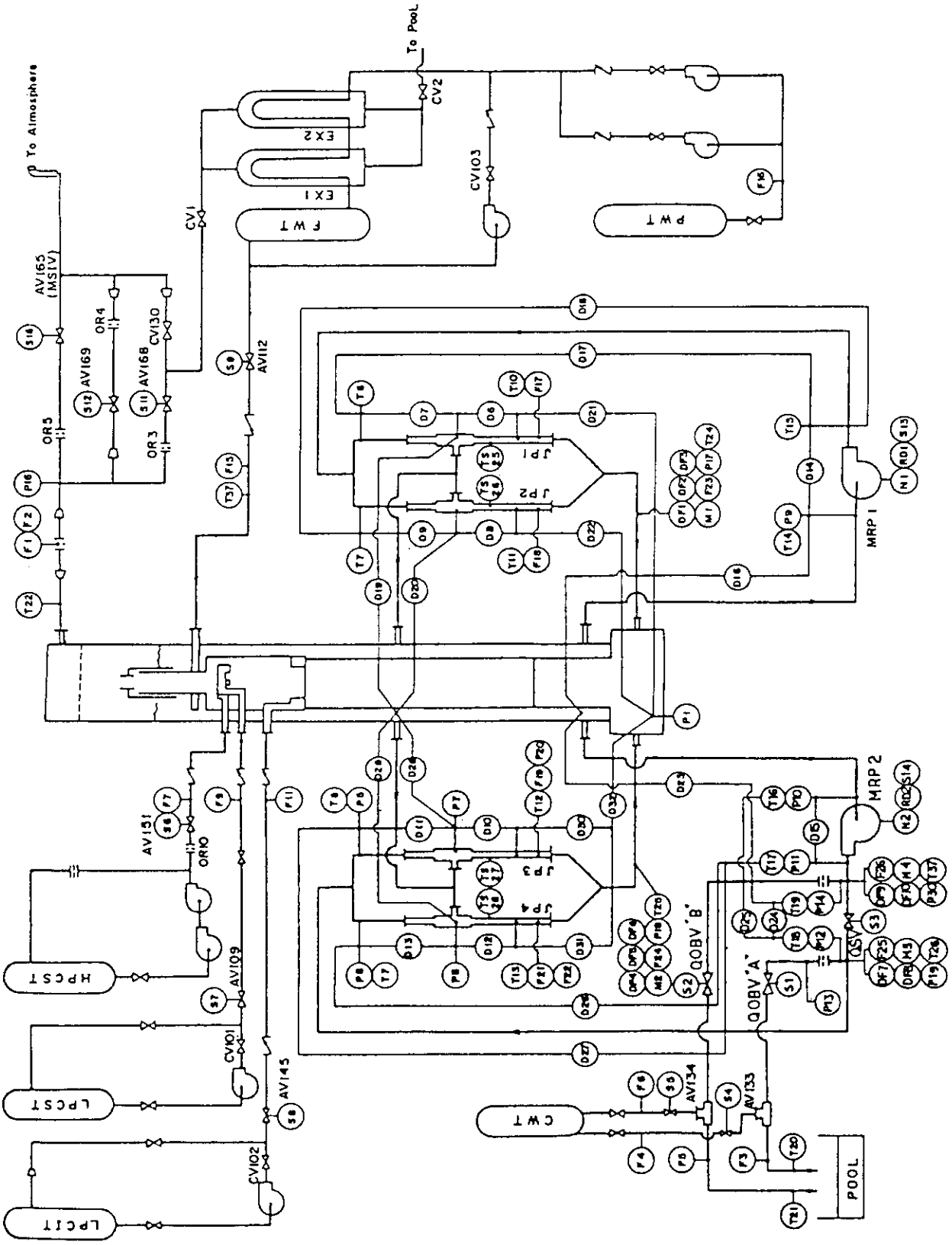

Fig. 3.1 Instrumentation location of ROSA-III test facility

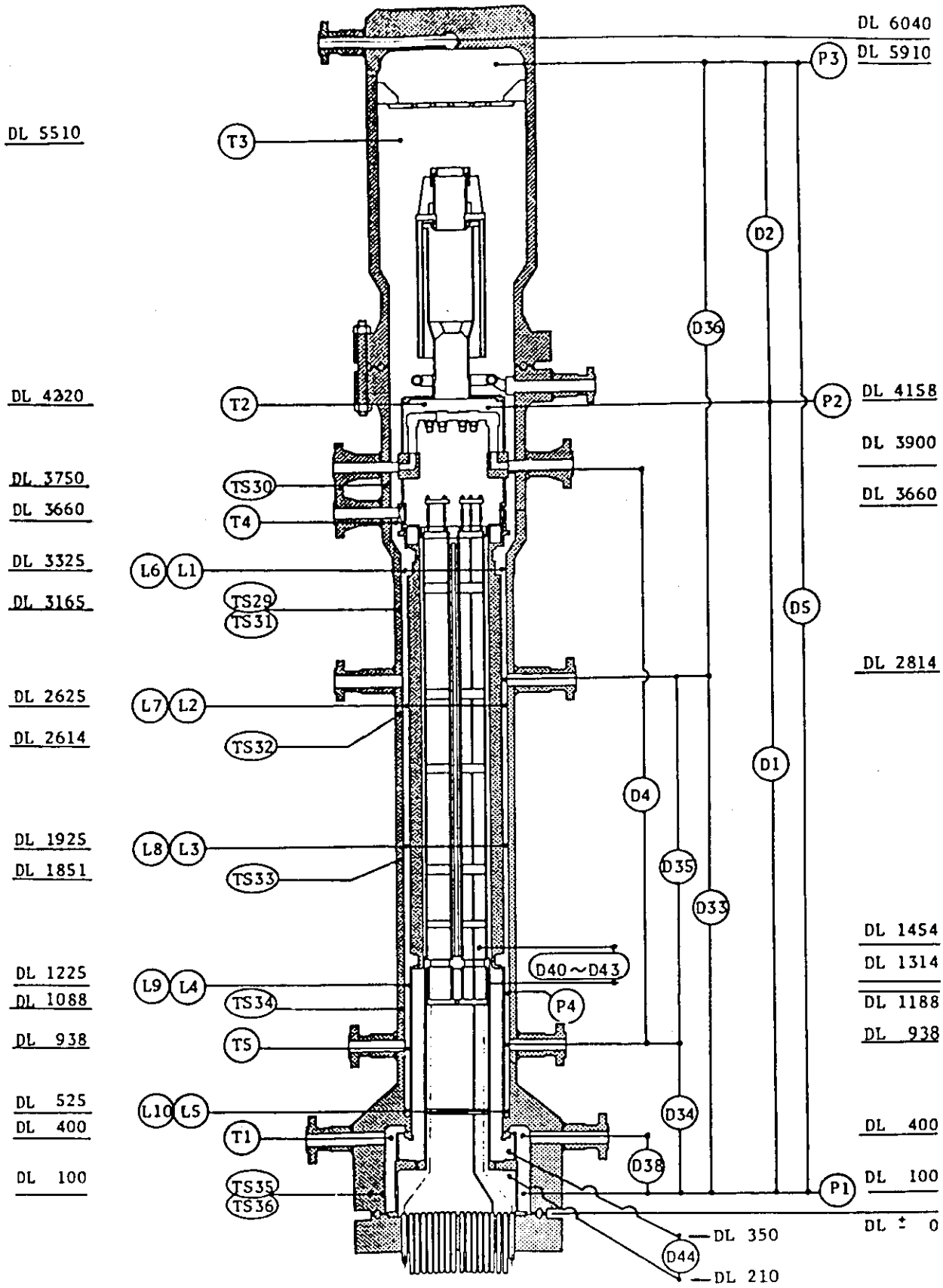

Fig. 3.2 Instrumentation location in pressure vessel

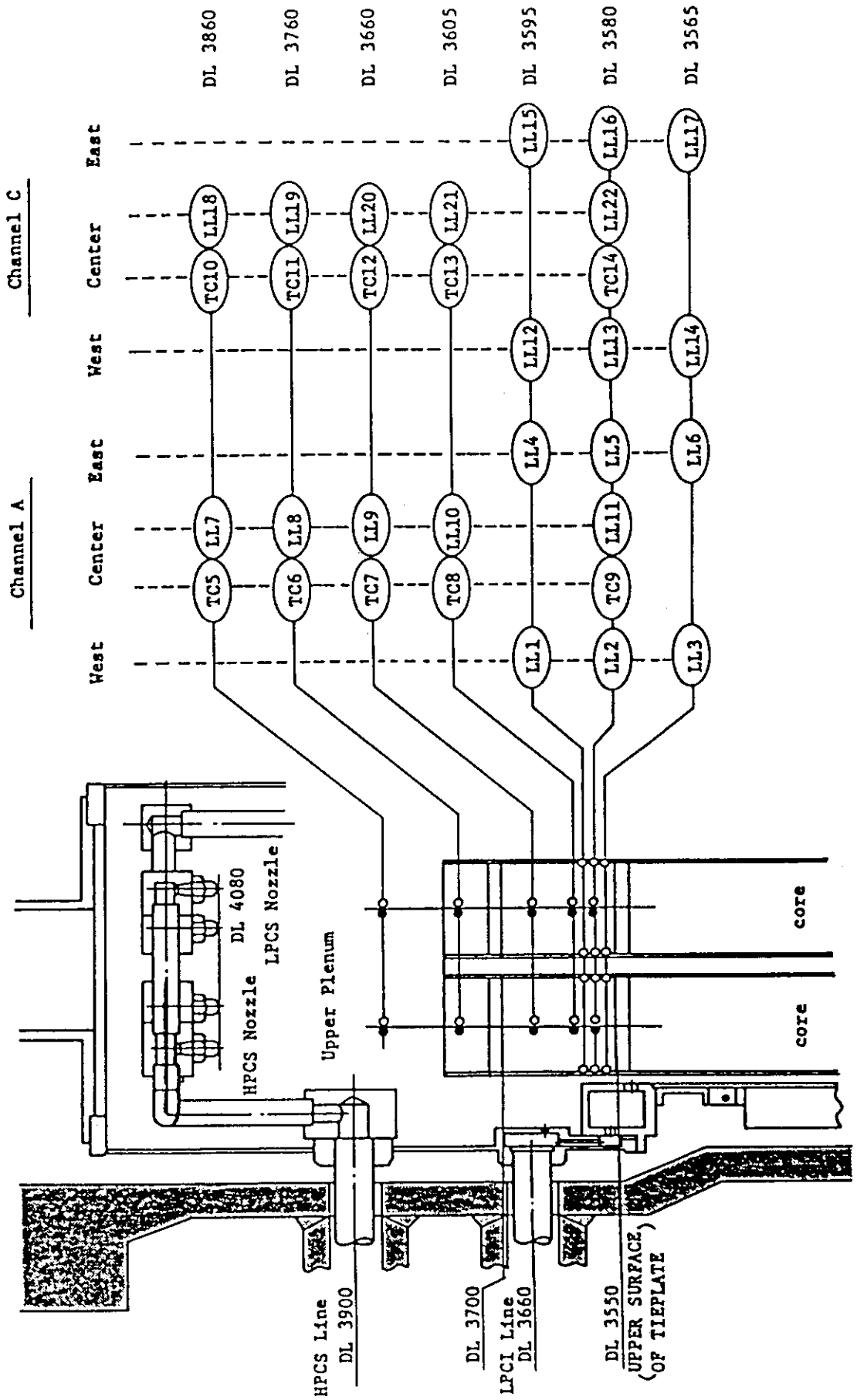

Fig. 3.3 Upper plenum instrumentation

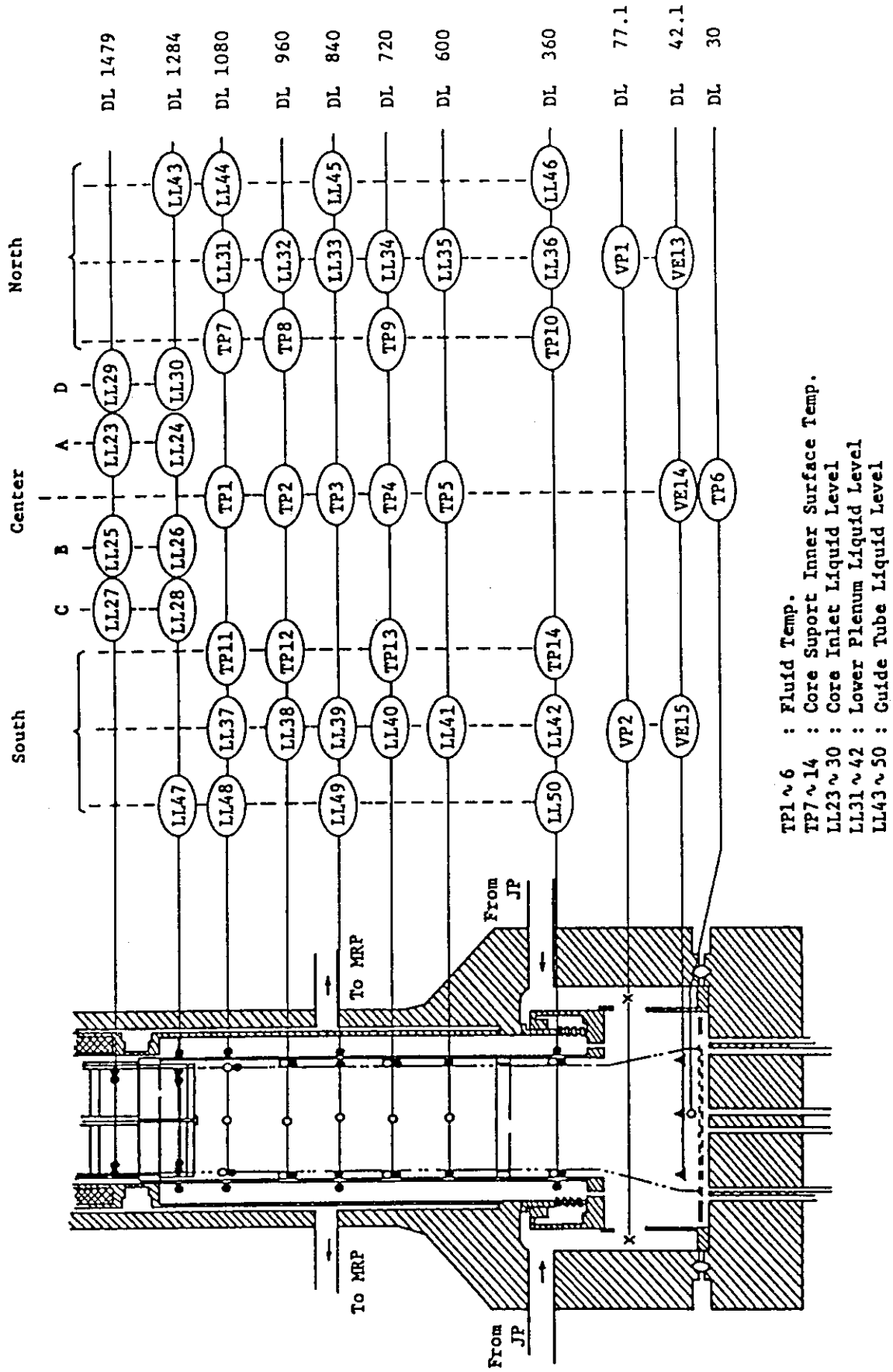

Fig. 3.4 Lower plenum instrumentation

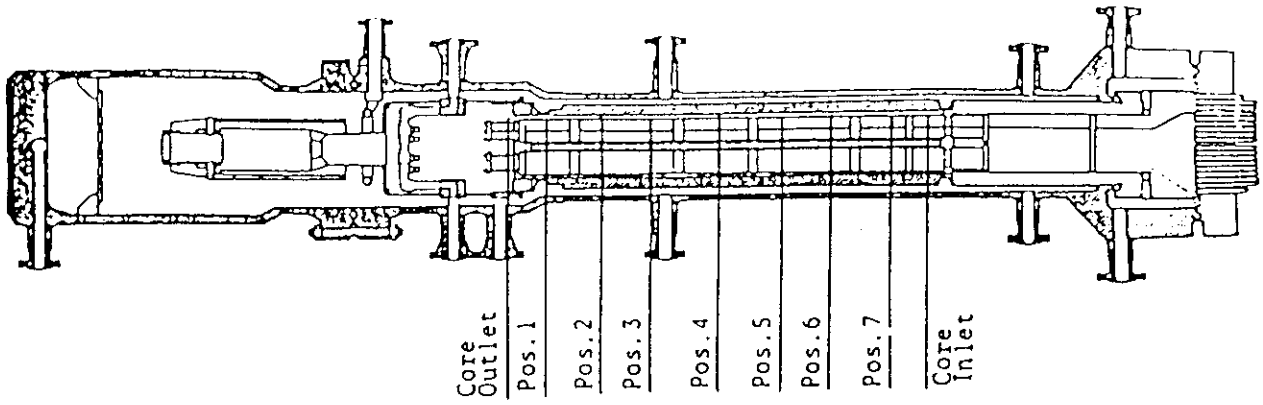

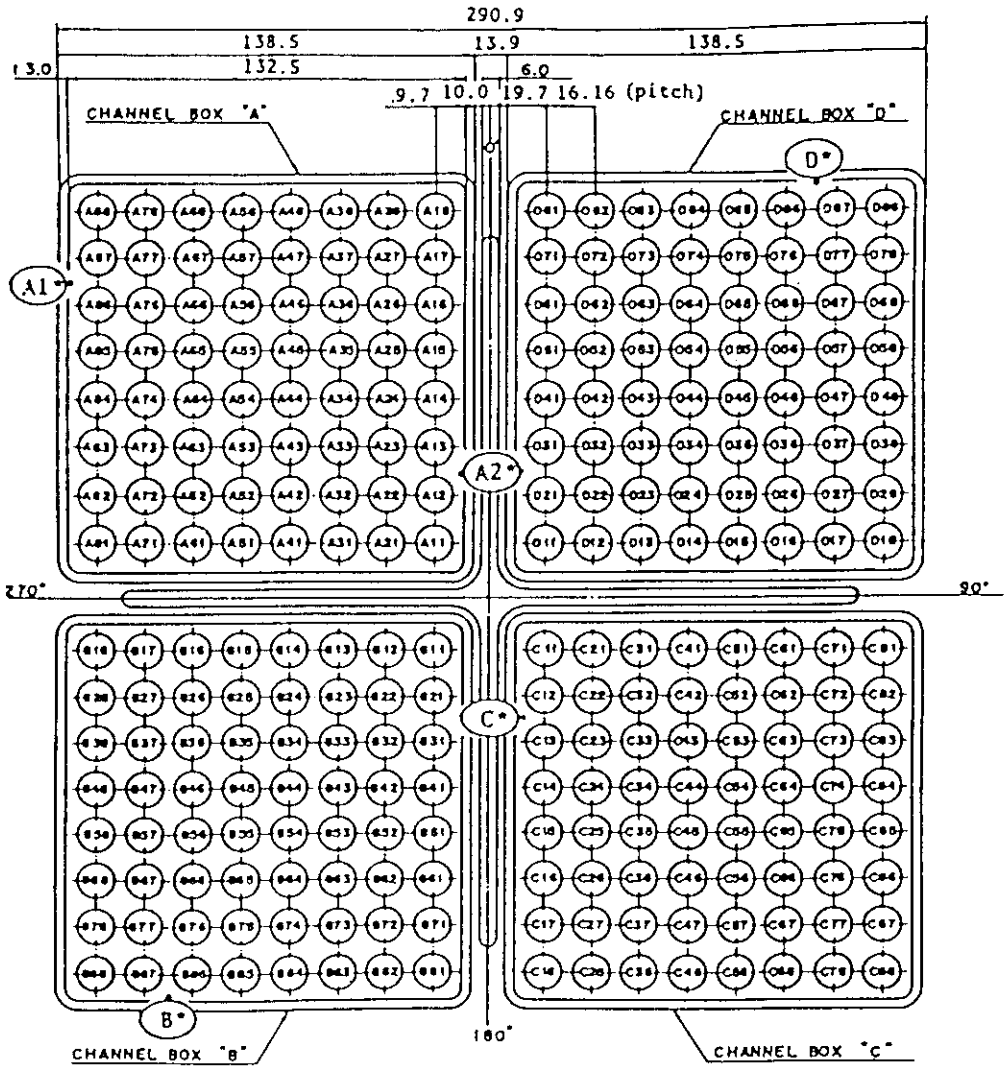

Heater rod O.D. is 12.27mm

A54,B54,C54 and D54 are water rod simulators with void probes, O.D.= 15.01mm

A45,B45,C45 and D45 are water rod simulators with thermocouples, O.D.= 15.01mm

Fig. 3.5 Core instrumentation

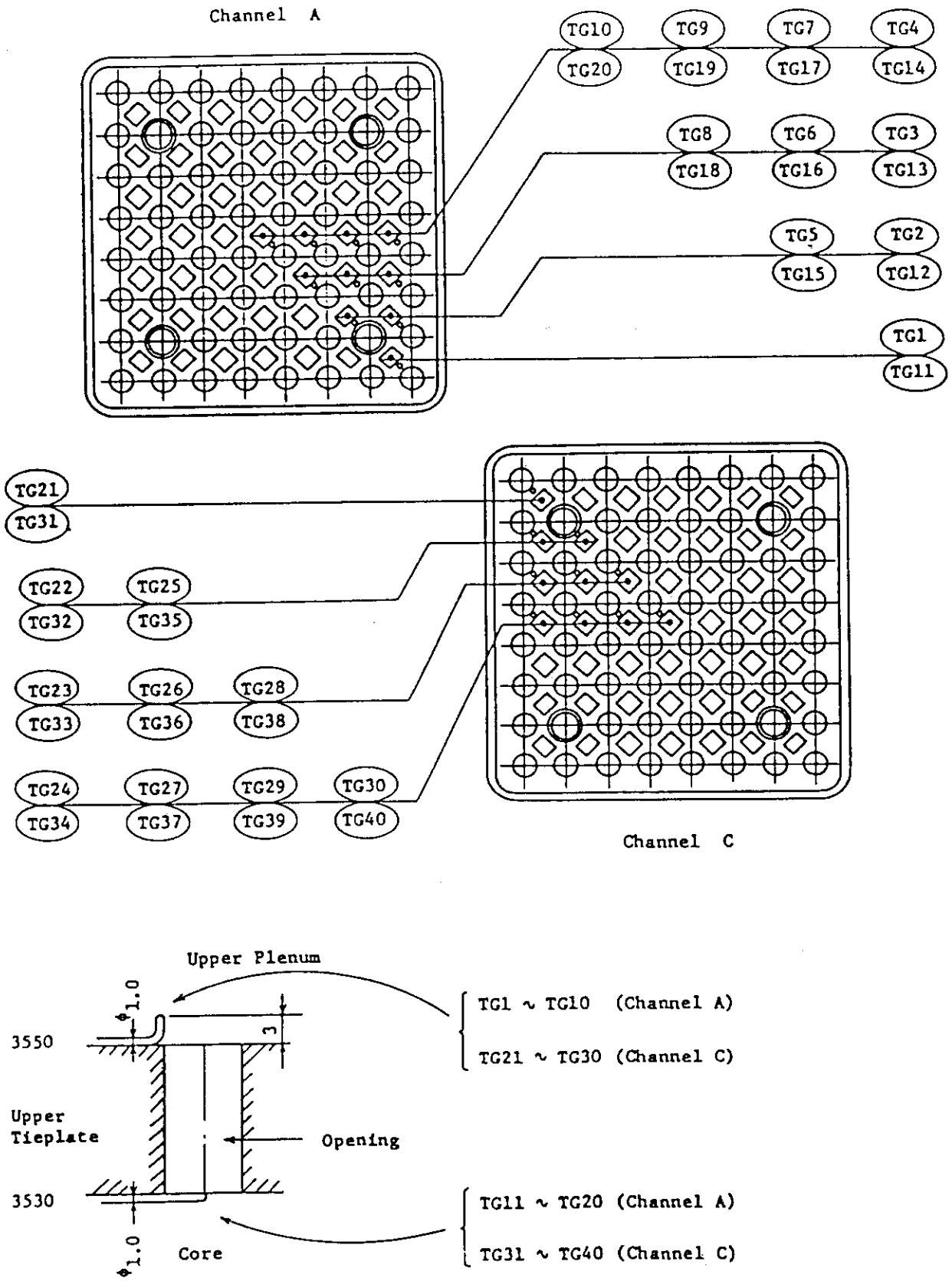

Fig. 3.6 Upper tieplate instrumentations

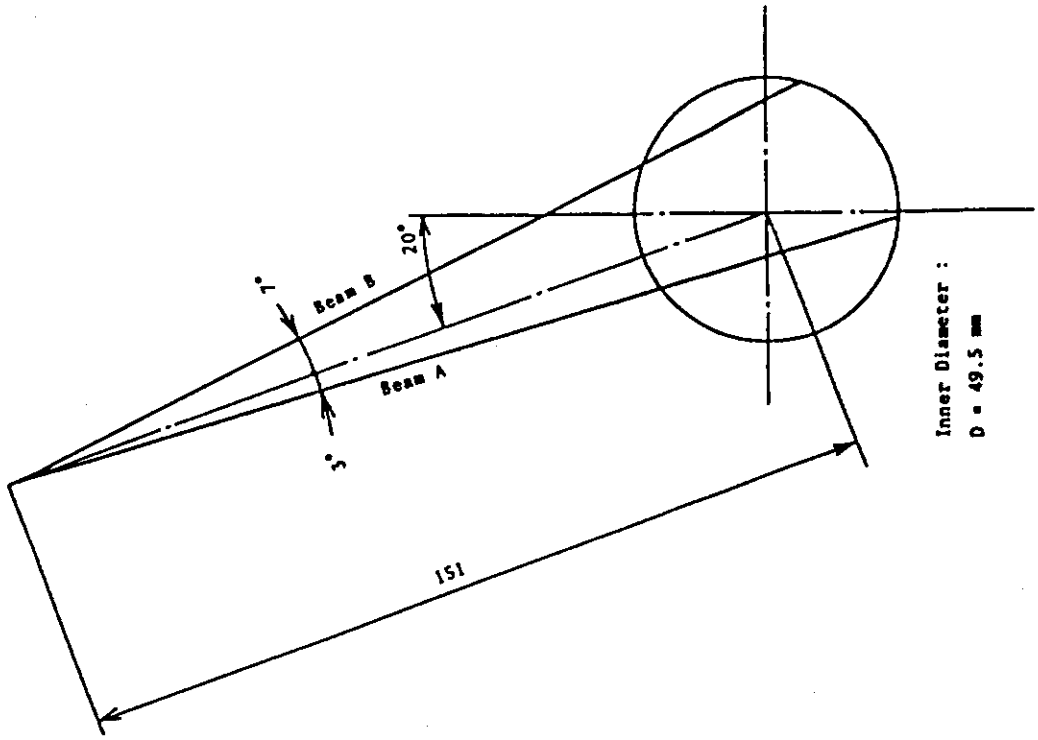

Fig. 3.8 Beam directions of two-beam gamma densitometer

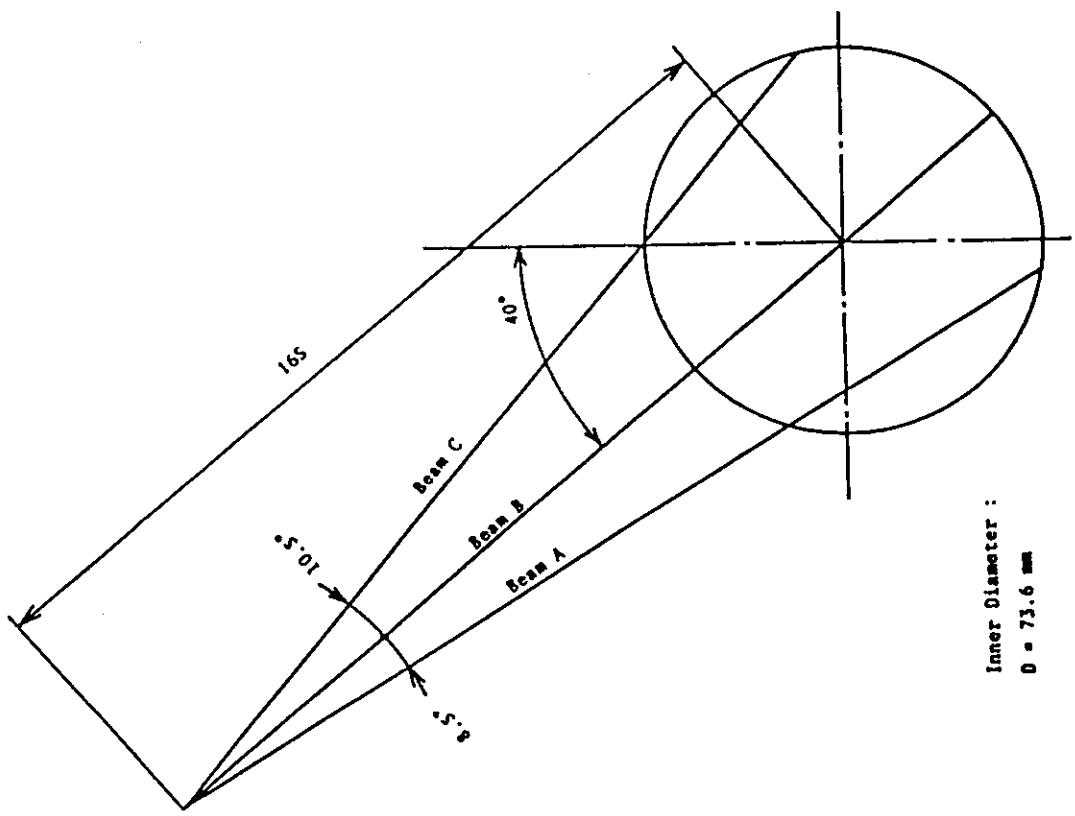

Fig. 3.7 Beam directions of three-beam gamma densitometer

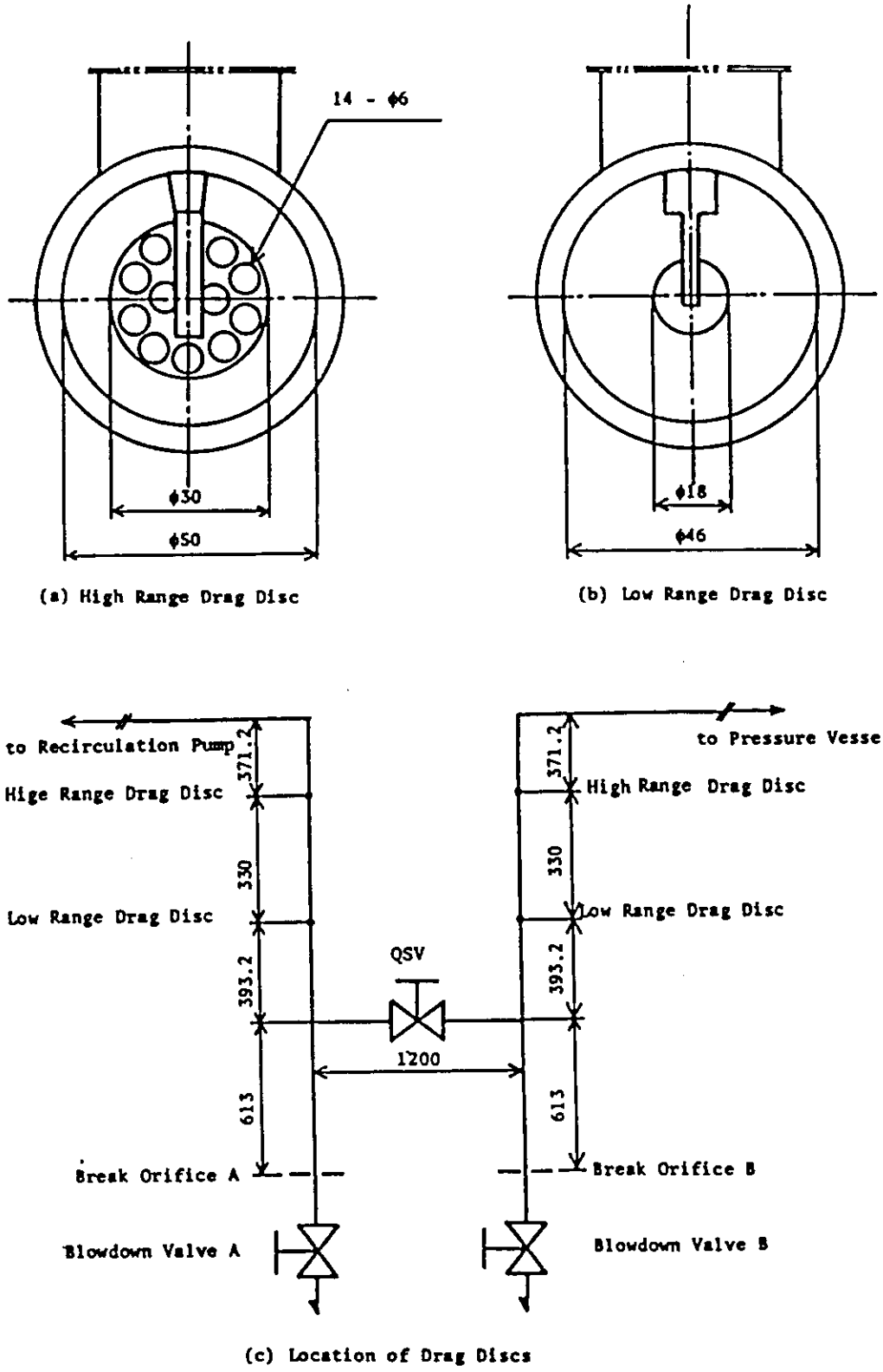

Fig. 3.9 Arrangement and location of drag disks

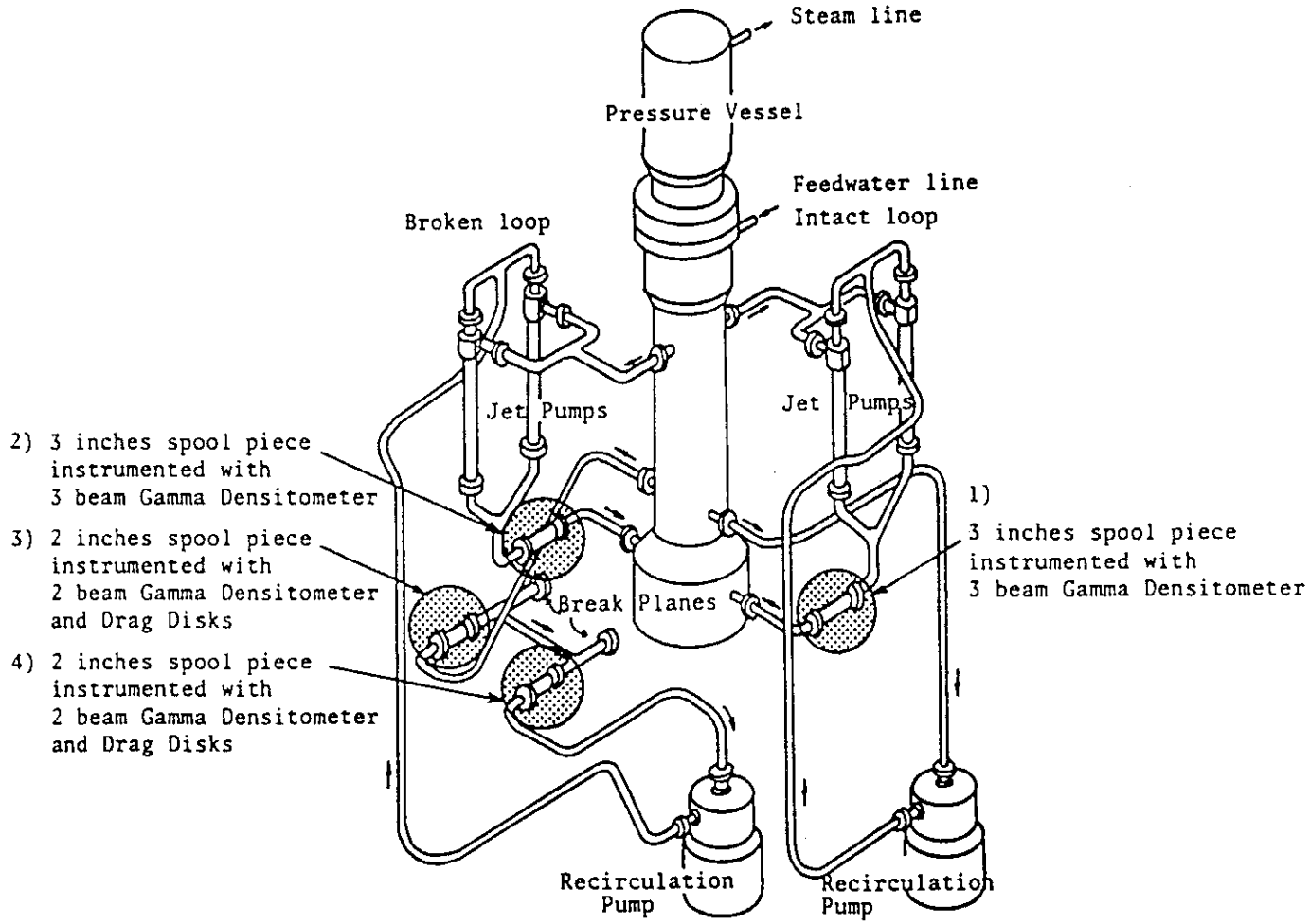

Fig. 3.10 Location of two-phase flow measurement spool pieces

(This figure shows suction line break and break unit for discharge line break is removed between the recirculation pump and jet pumps in the broken loop. However, four two-phase instrumentation spool pieces are located similarly downstream the jet pumps and near the break units.)

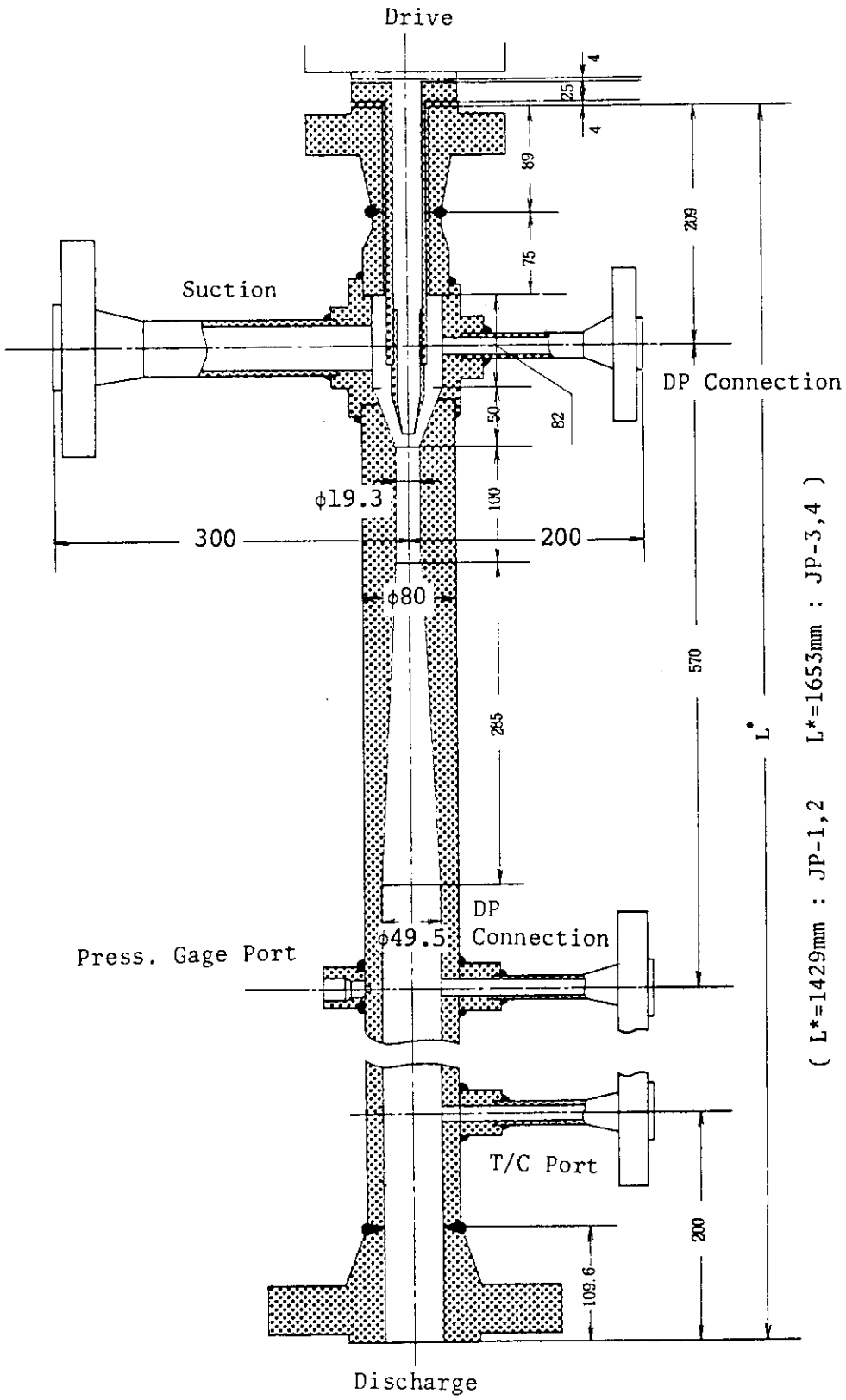

Fig. 4.1 Structure of jet pump in ROSA-III facility

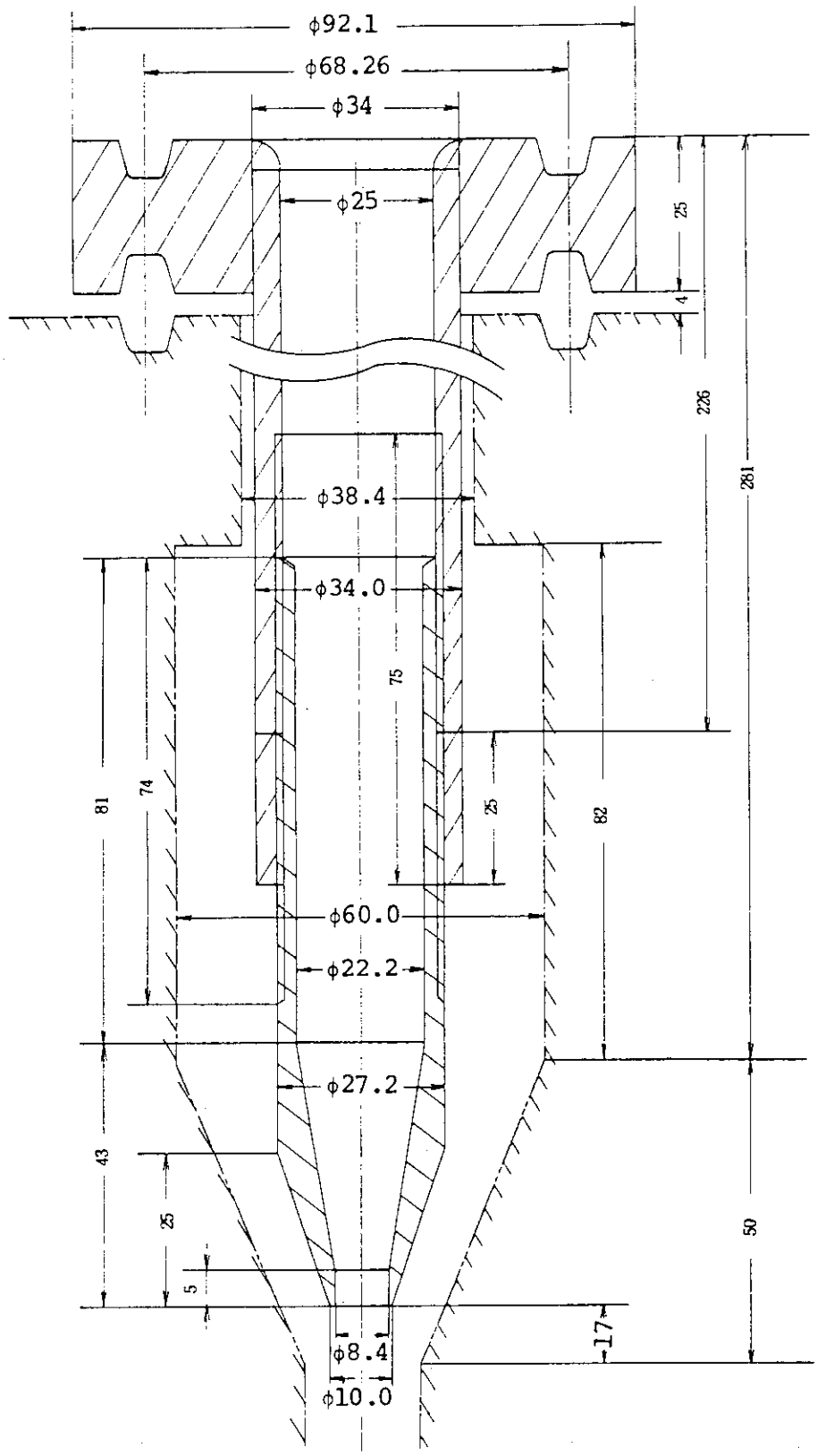

Fig. 4.2 Details of jet pump drive nozzle in ROSA-III facility

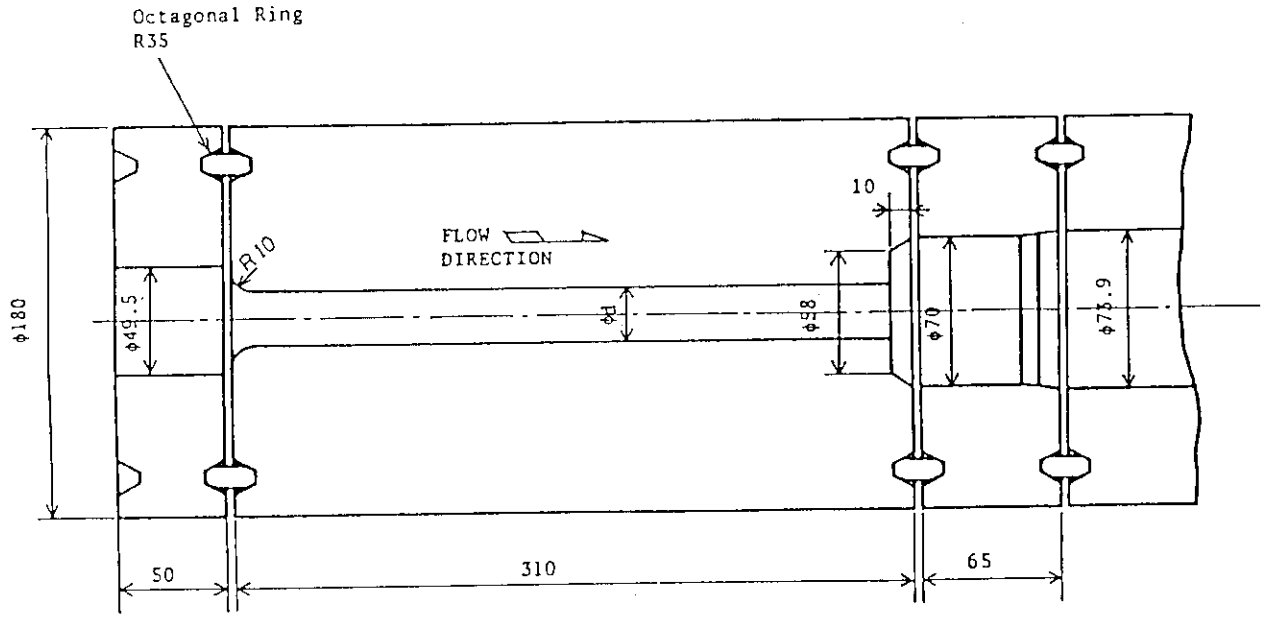

Material SUS304

Dimension in mm

Break area ratio (%)	d (mm)
100	26.2

Fig. 4.3 Break nozzle details

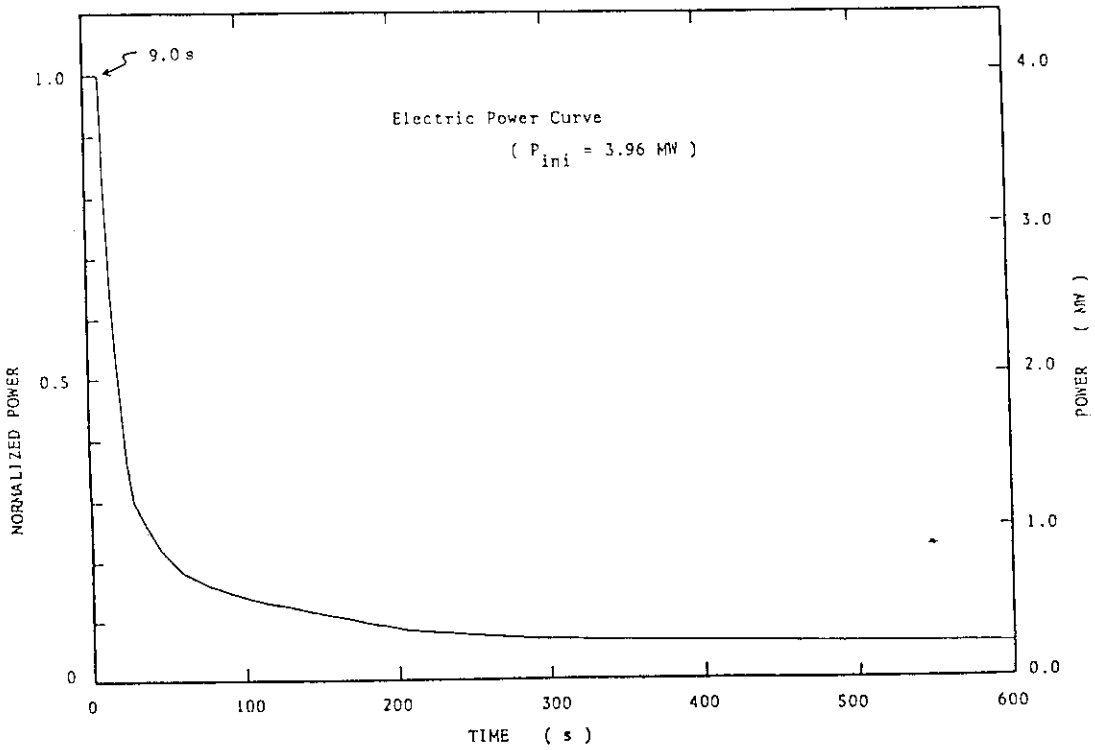

Fig. 4.4 Normalized power transient for ROSA-III test

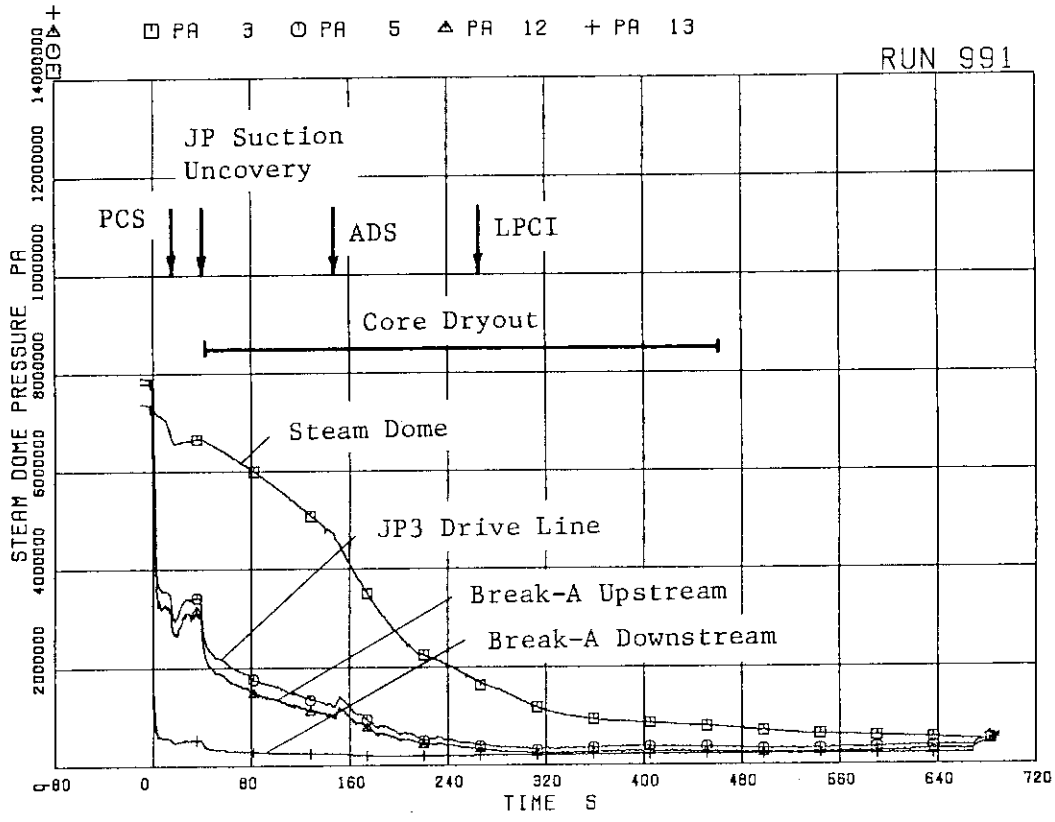

Fig. 5.1 System pressures and events in RUN 991

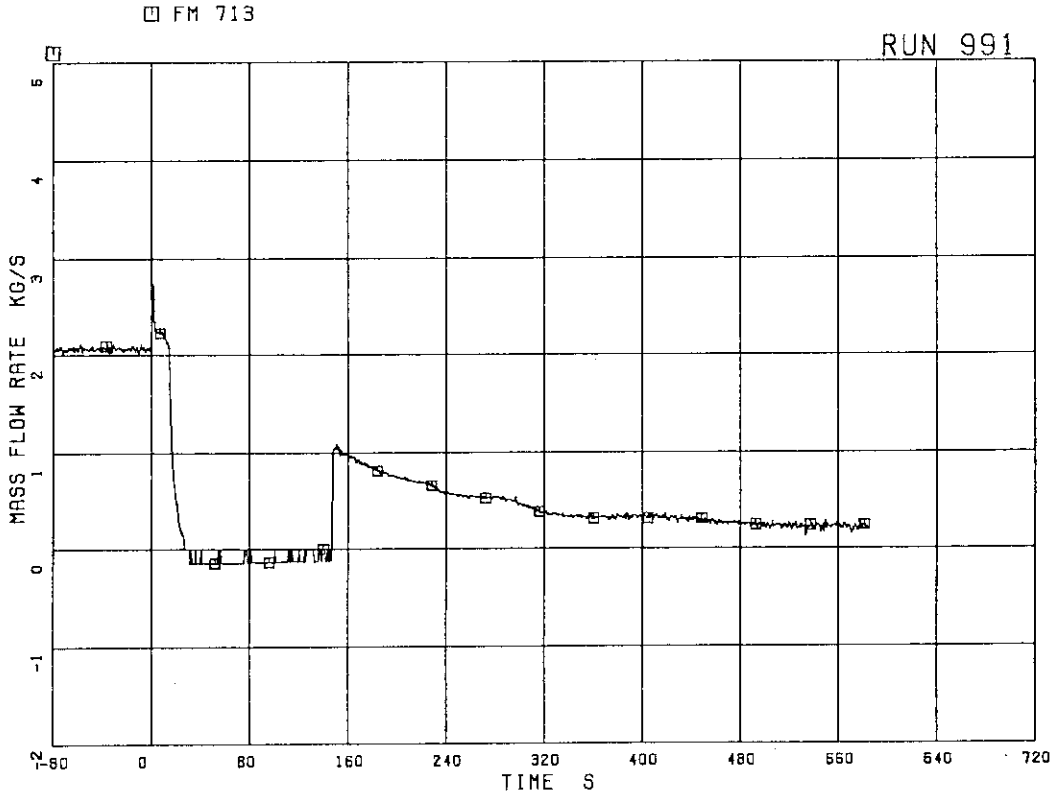

Fig. 5.2 Steam discharge flow rate through MSL in RUN 991

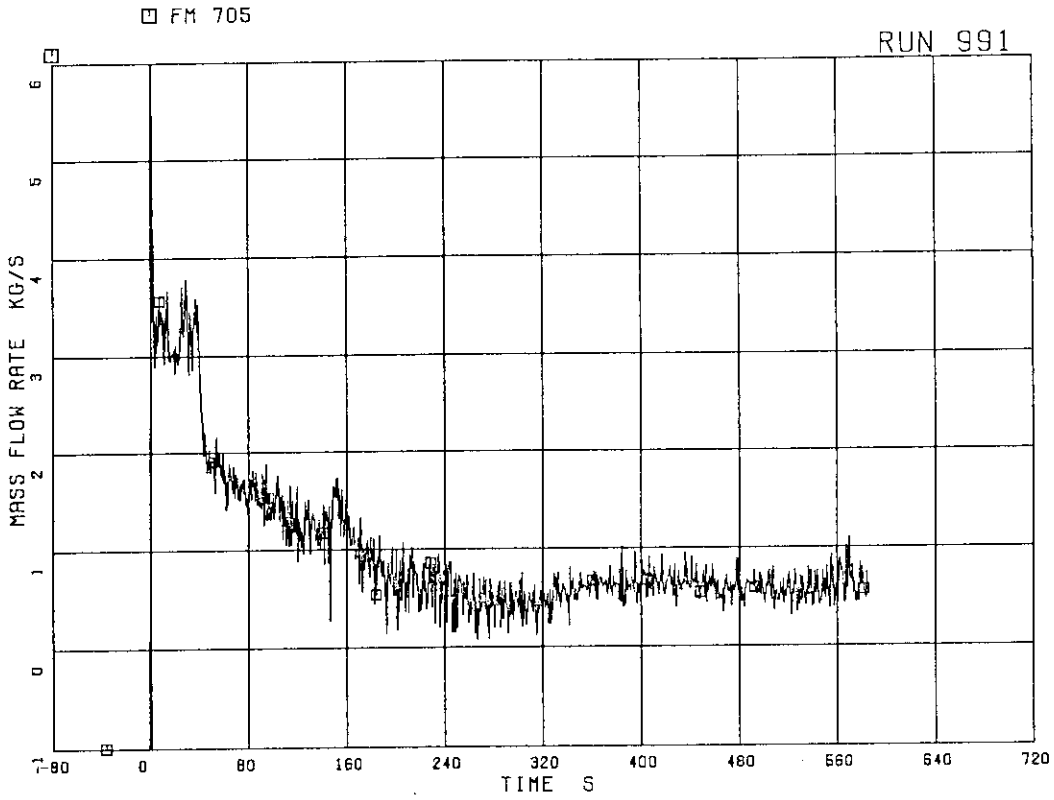

Fig. 5.3 Jet pump side break flow rate in RUN 991 (low-range drag disk data)

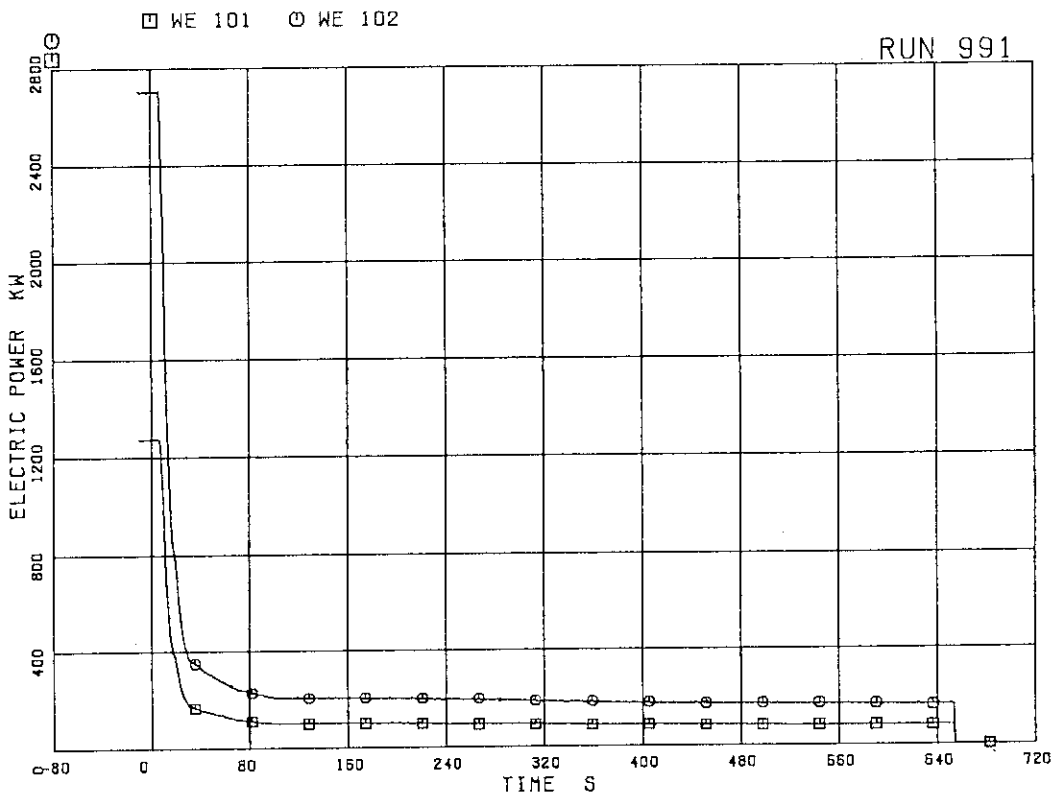

Fig. 5.4 Core power for bundle A (WE 101) and other three bundles (WE 102) in RUN 991

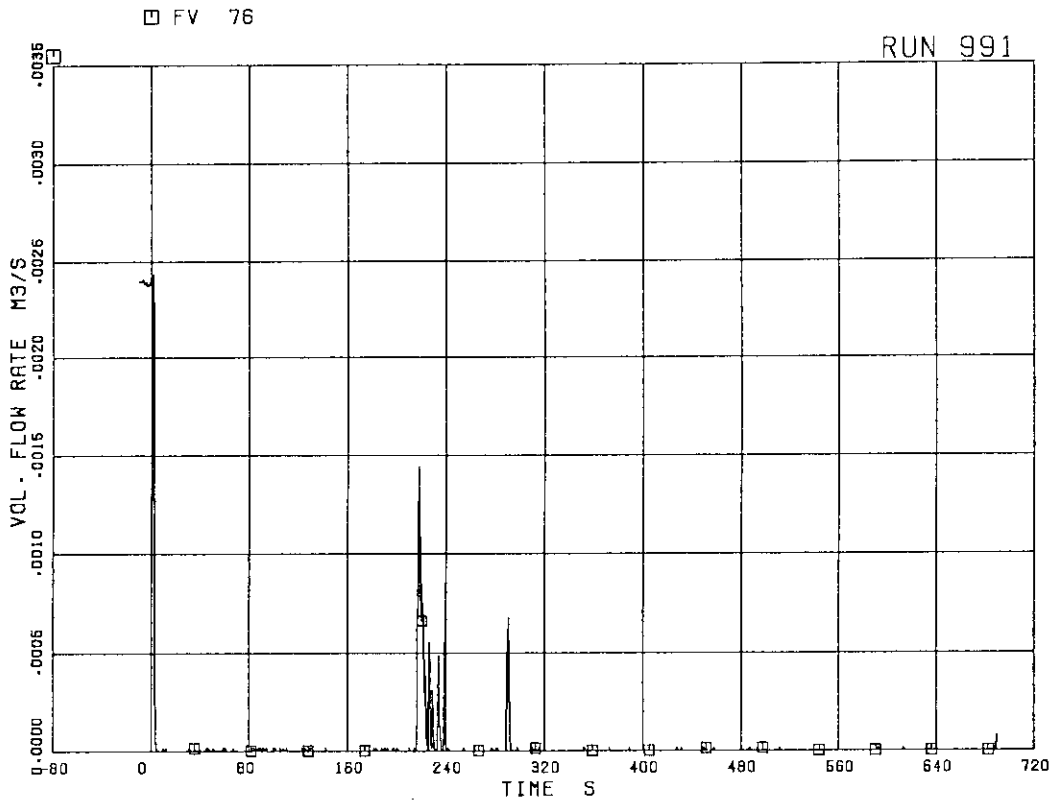

Fig. 5.5 Feedwater flow rate in RUN 991

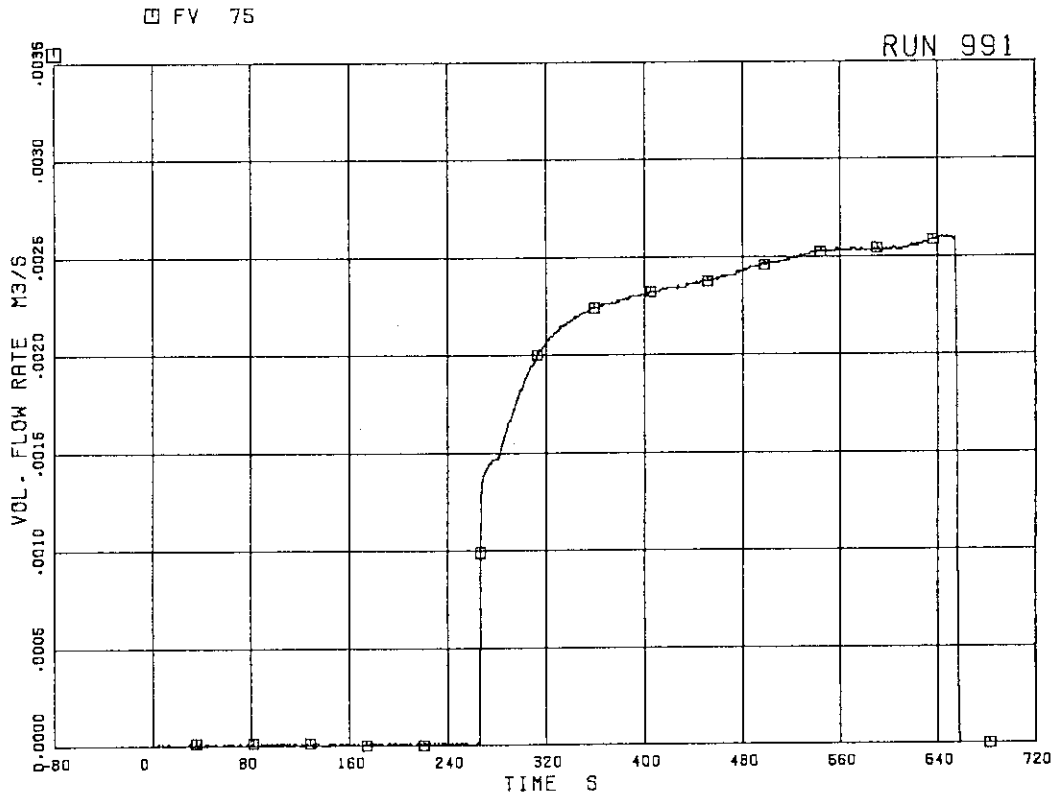

Fig. 5.6 Injection flow rate of LPCI in RUN 991

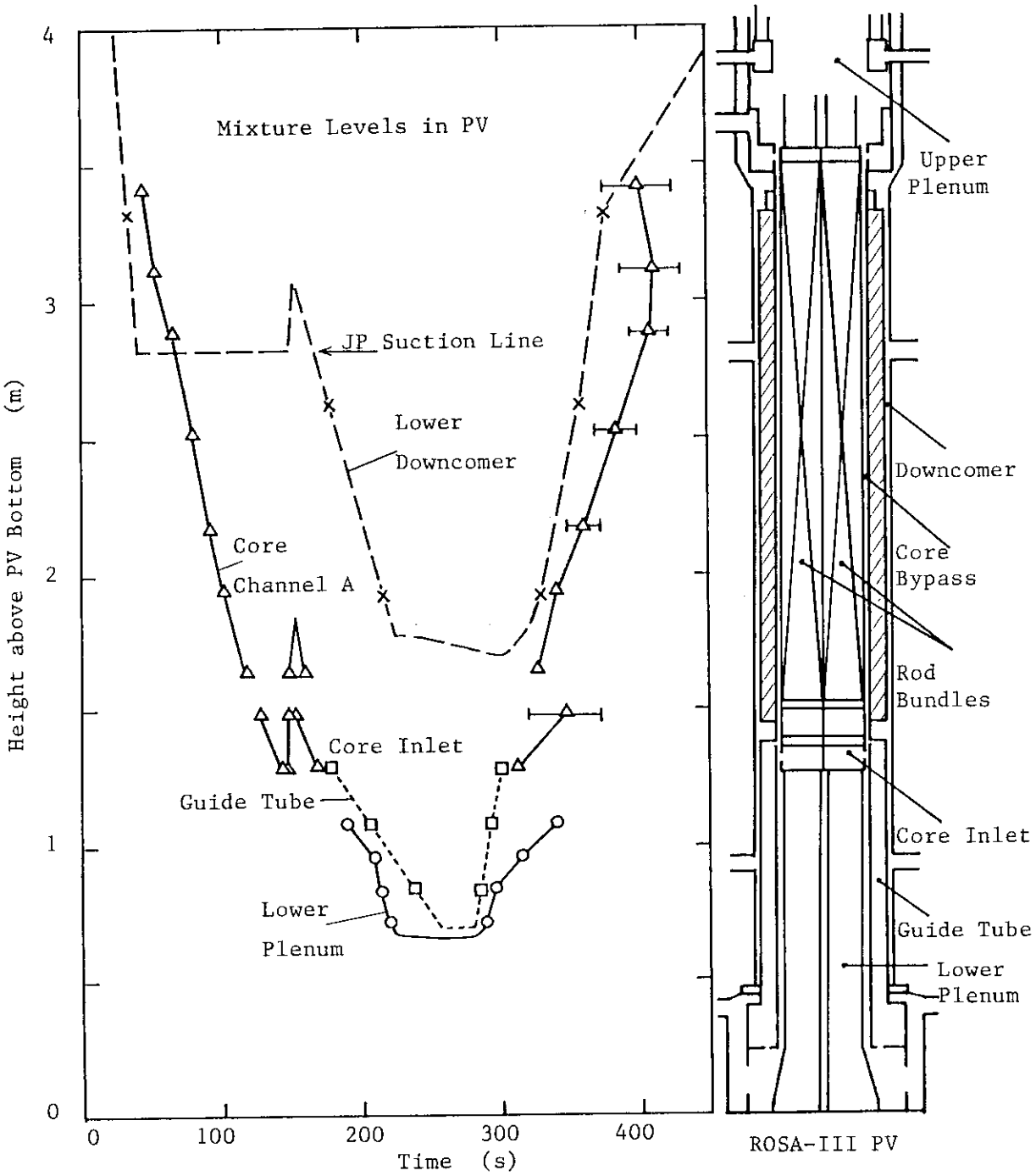

Fig. 5.7 Mixture levels in PV in RUN 991

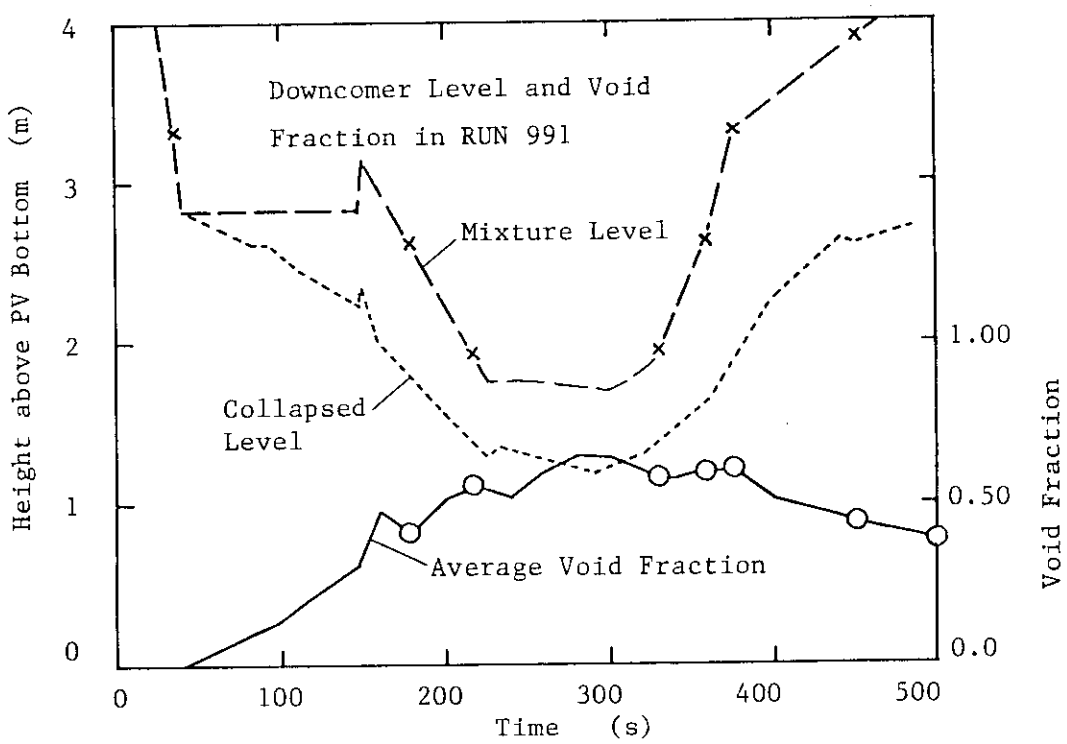

Fig. 5.8 Water level and void fraction in downcomer in RUN 991

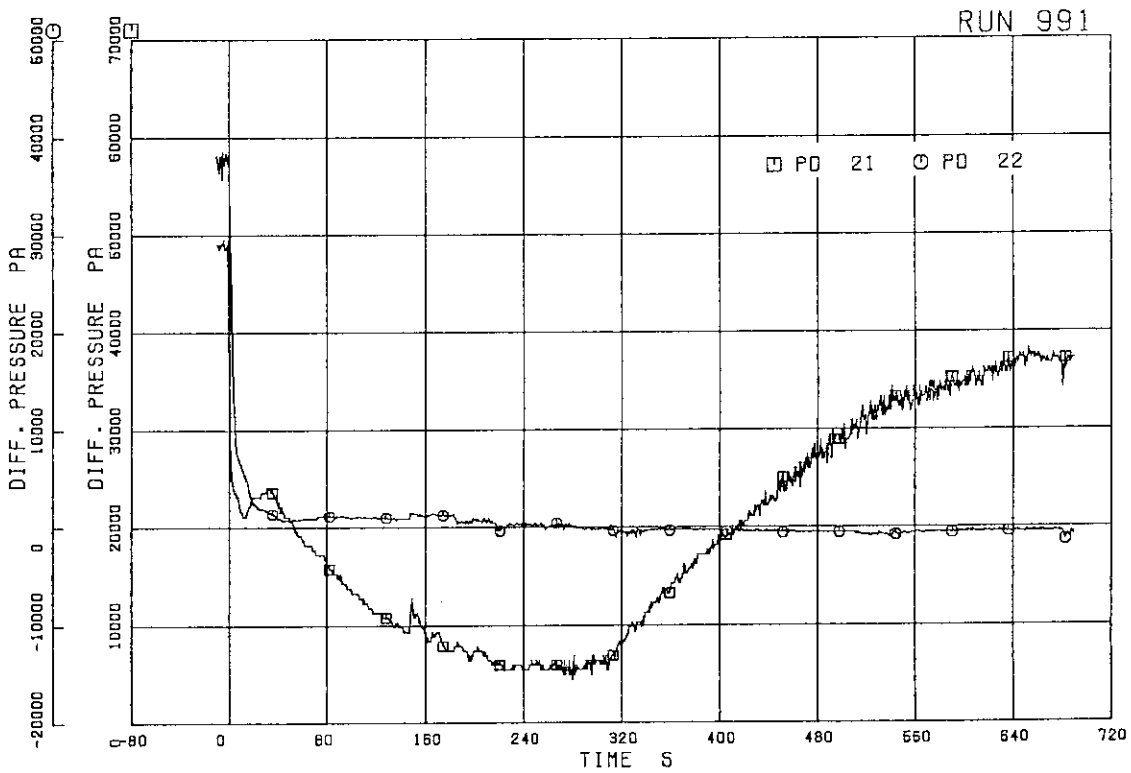

Fig. 5.9 Differential pressures inside core shroud in RUN 991

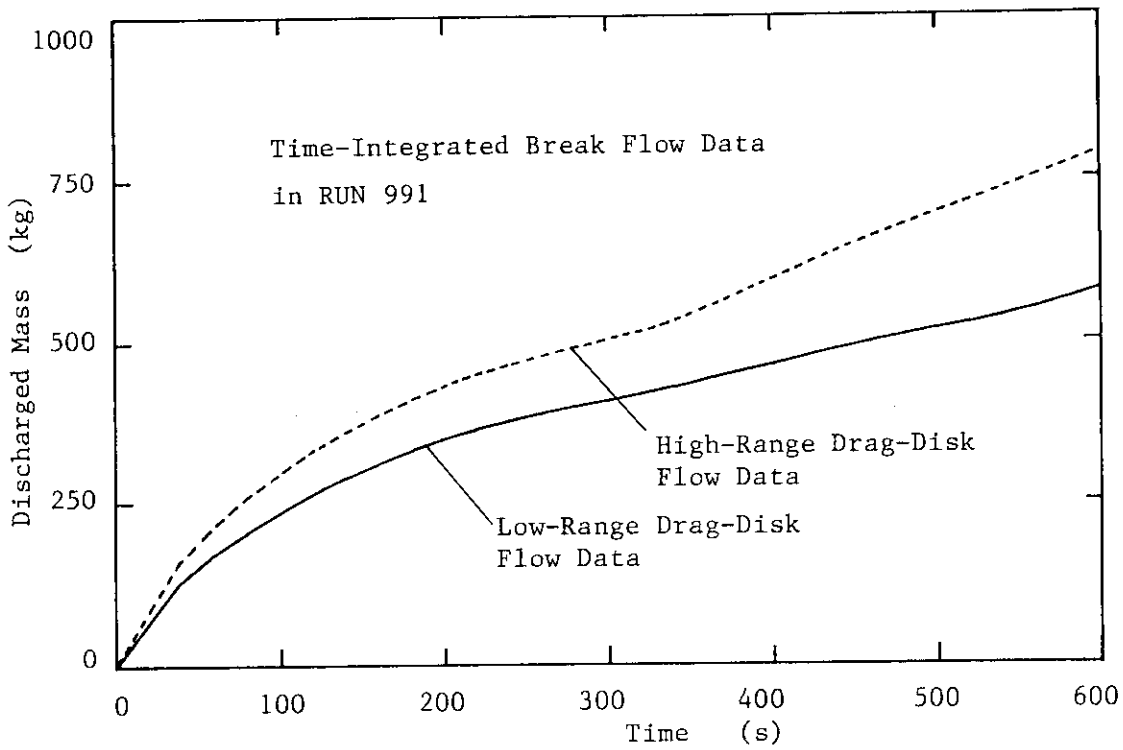

Fig. 5.10 Comparison of discharged mass between low and high range drag-disk data

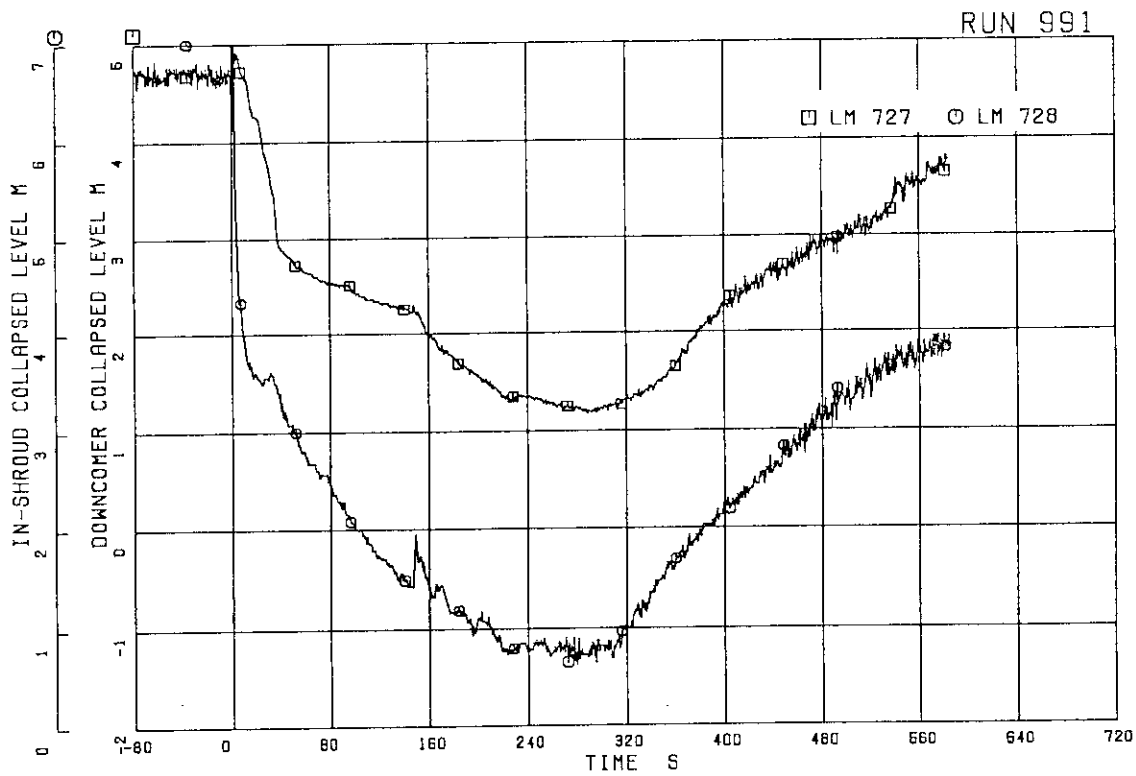

Fig. 5.11 Collapsed levels in downcomer and shroud in RUN 991

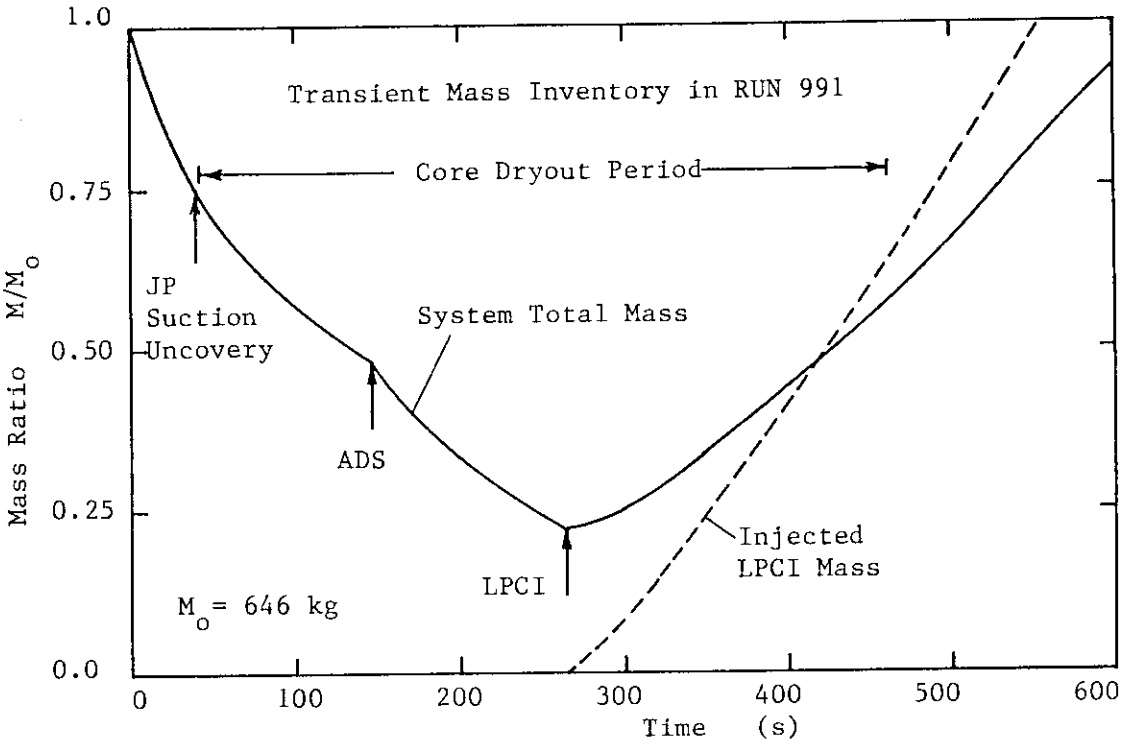

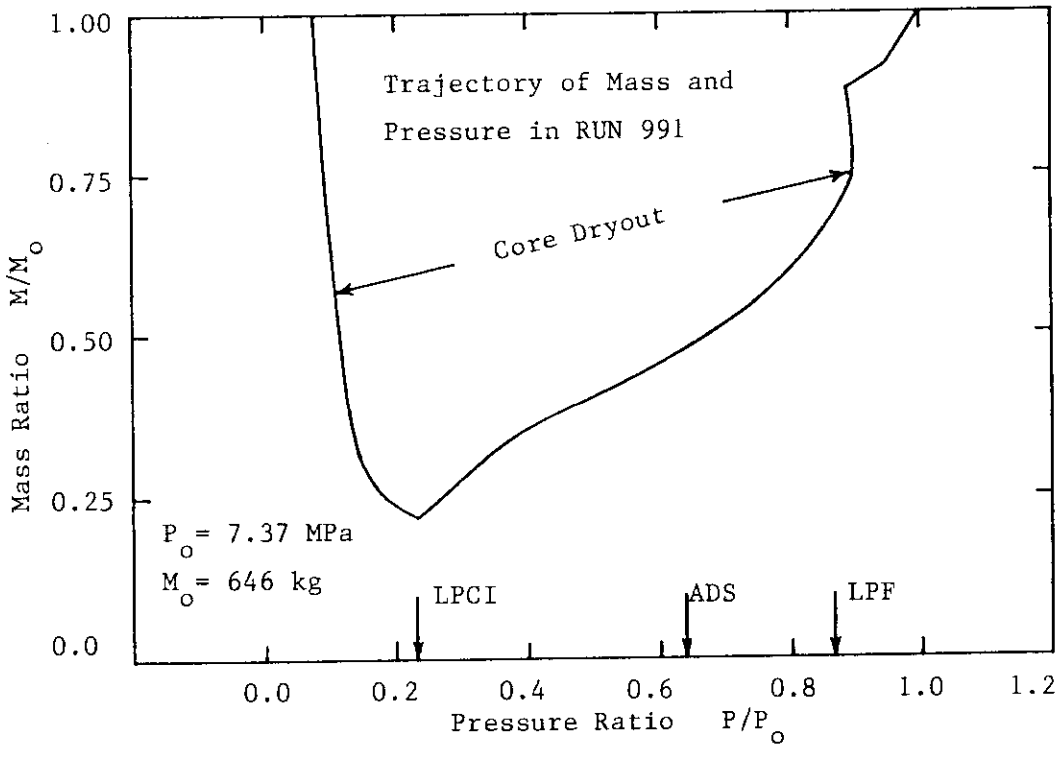

Fig. 5.12 Transient mass inventory related to time and pressure in RUN 991

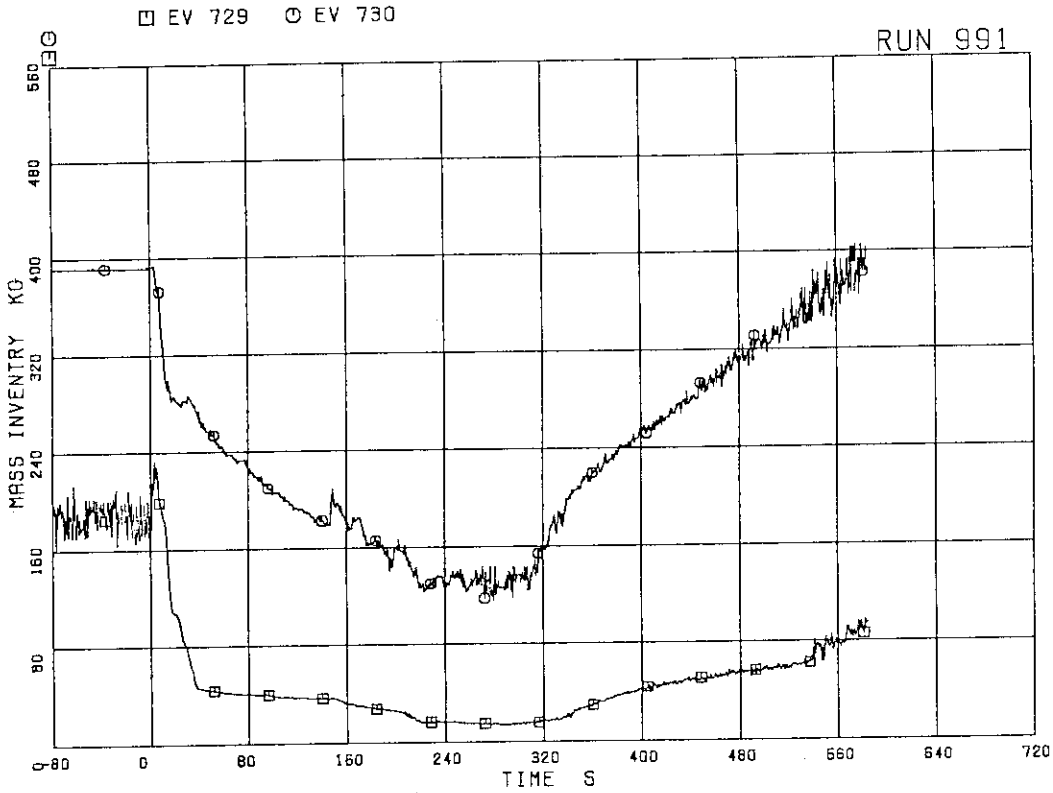

Fig. 5.13 Fluid inventory in downcomer and shroud in RUN 991

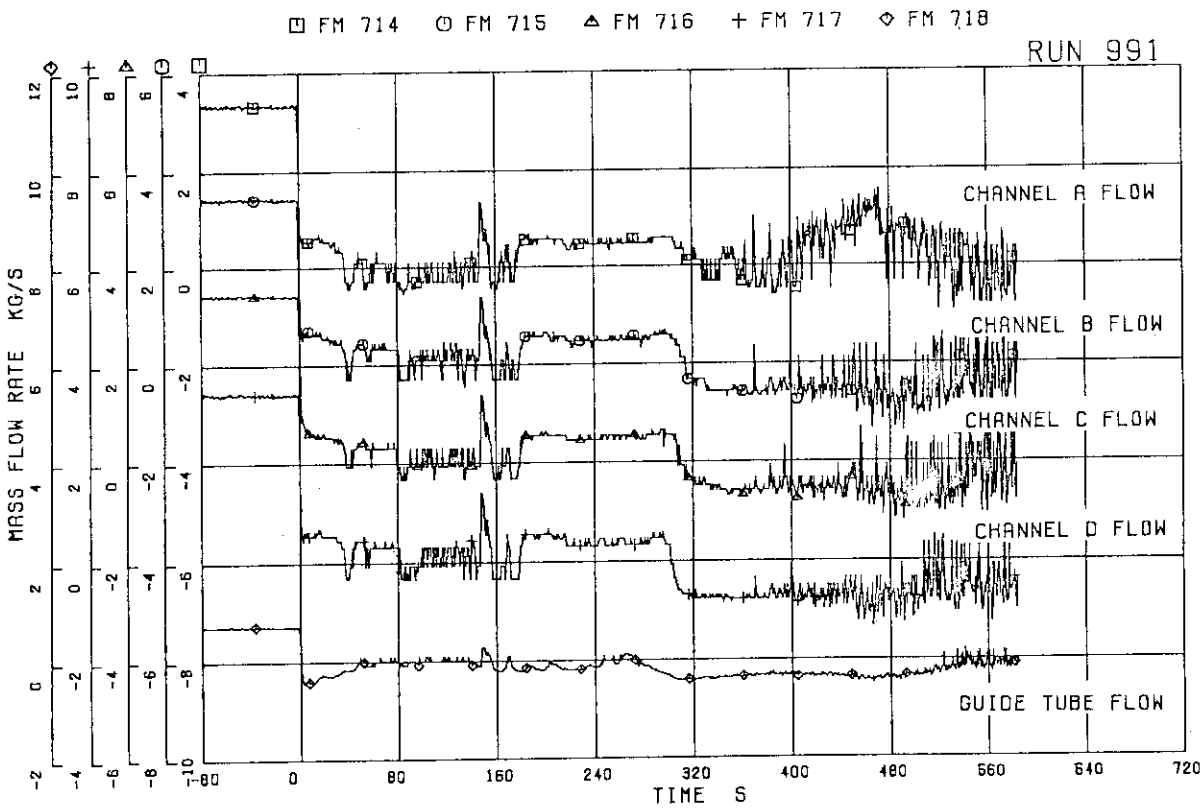

Fig. 5.14 Flow rates at core inlet orifices and bottom of guide tube in RUN 991

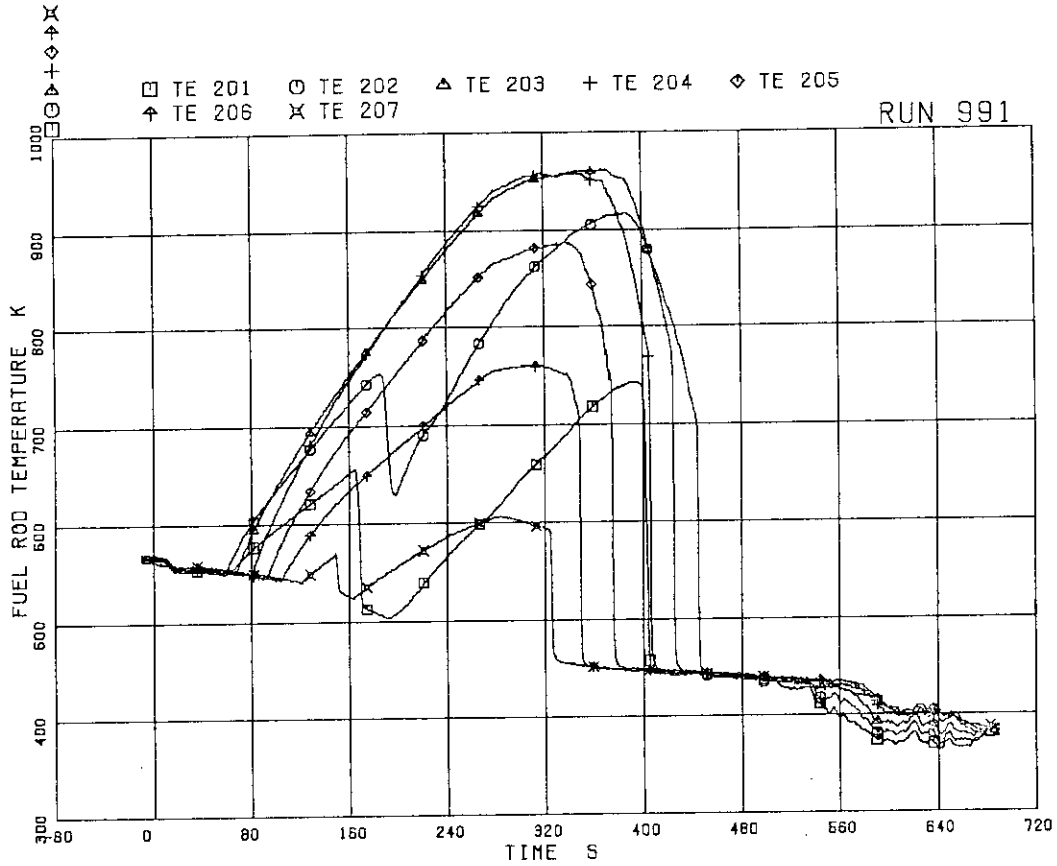

Fig. 5.15 Surface temperatures at A11 rod in RUN 991

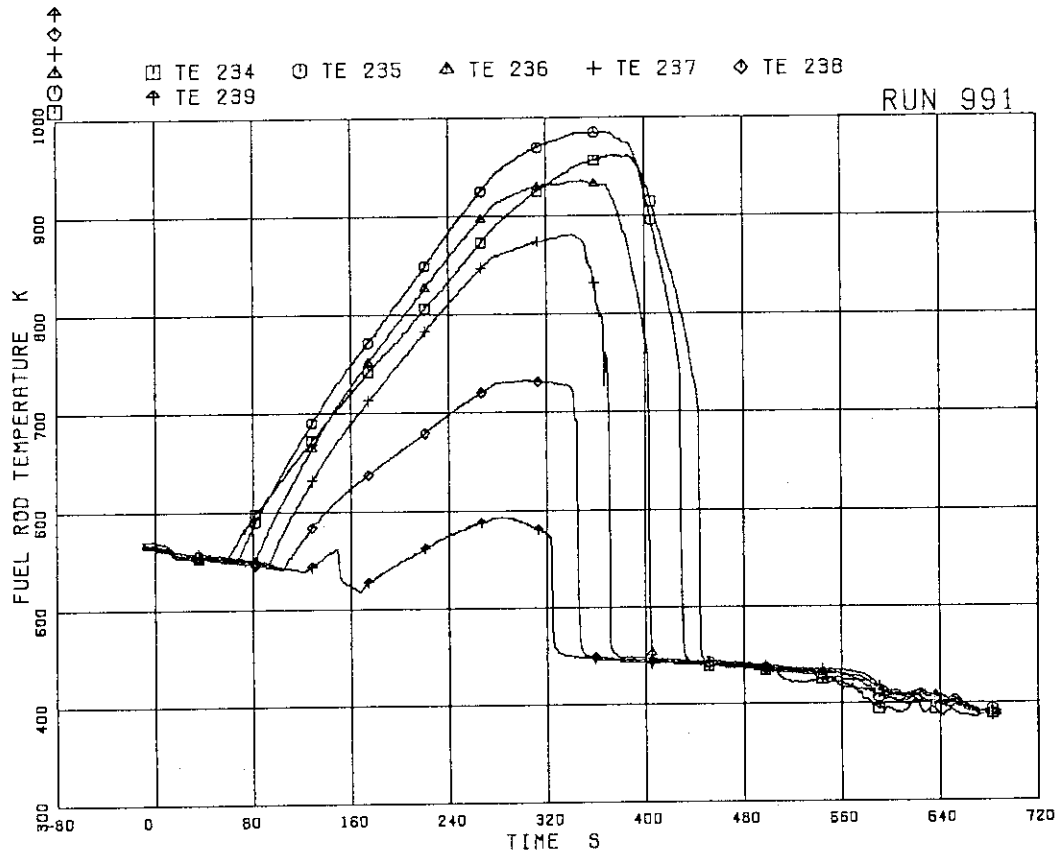

Fig. 5.16 Surface temperatures at A22 rod in RUN 991

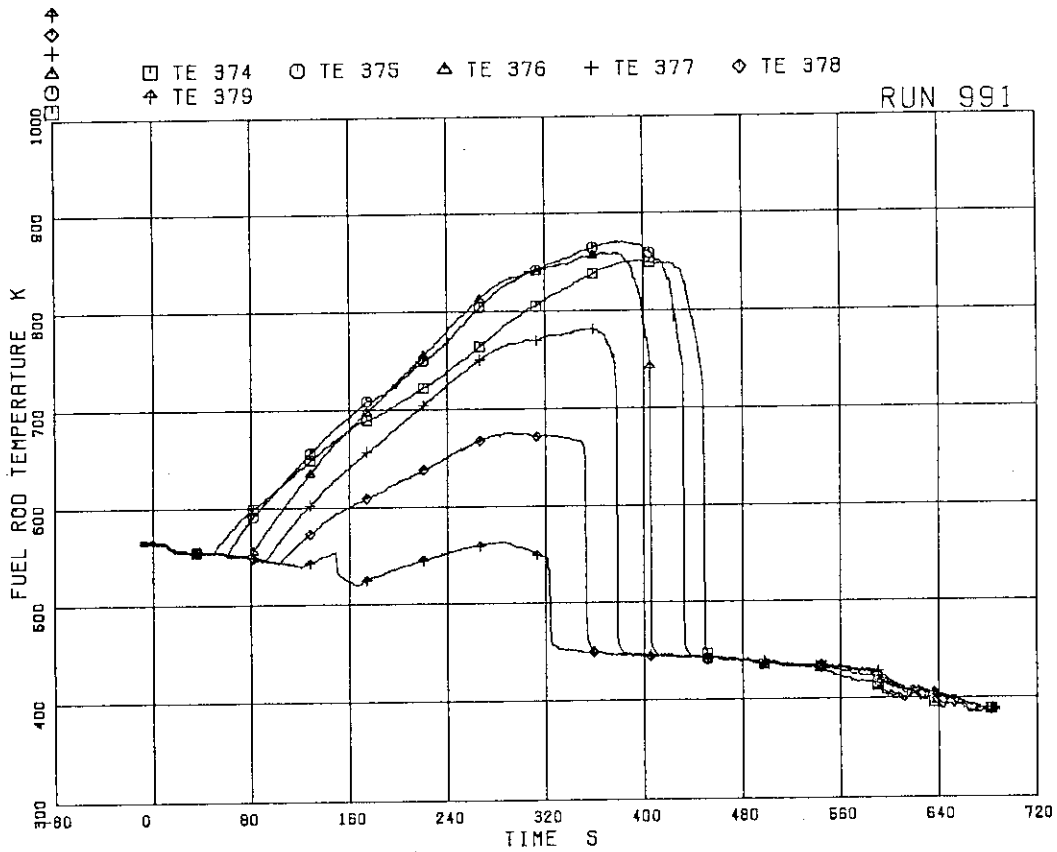

Fig. 5.17 Surface temperatures at C22 rod in RUN 991

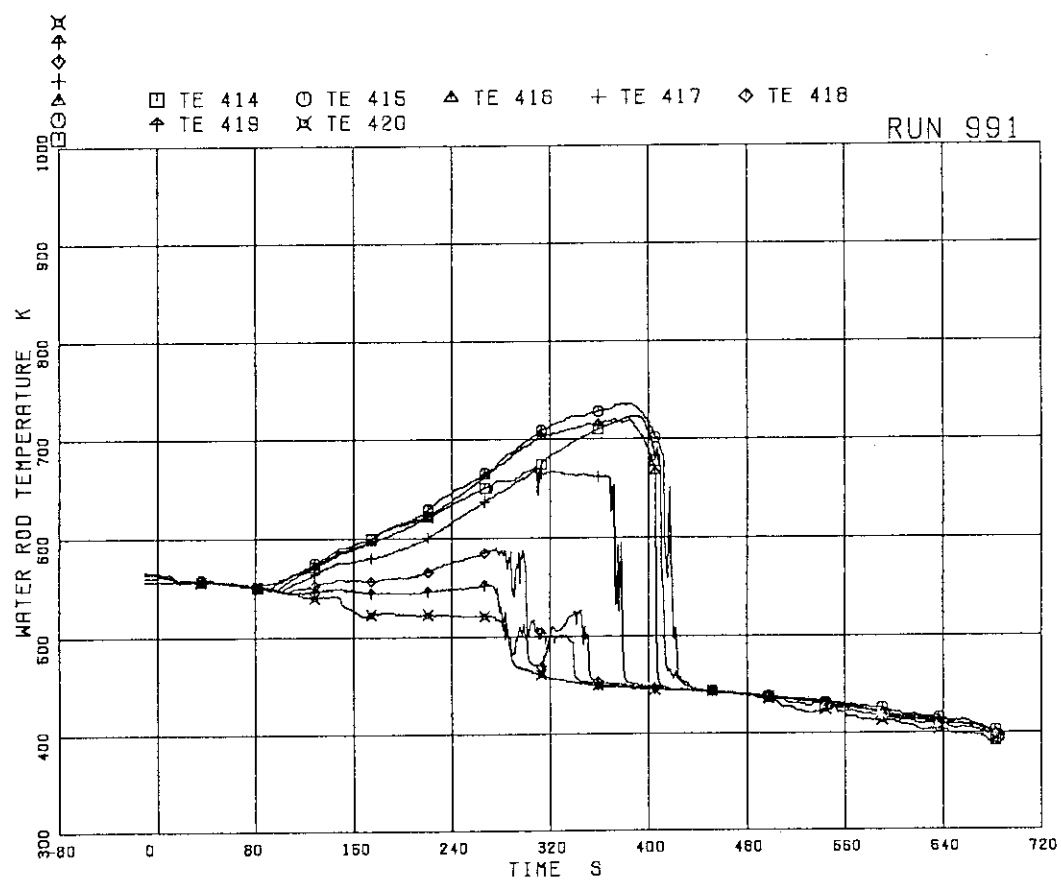

Fig. 5.18 Surface temperatures at A45 rod in RUN 991

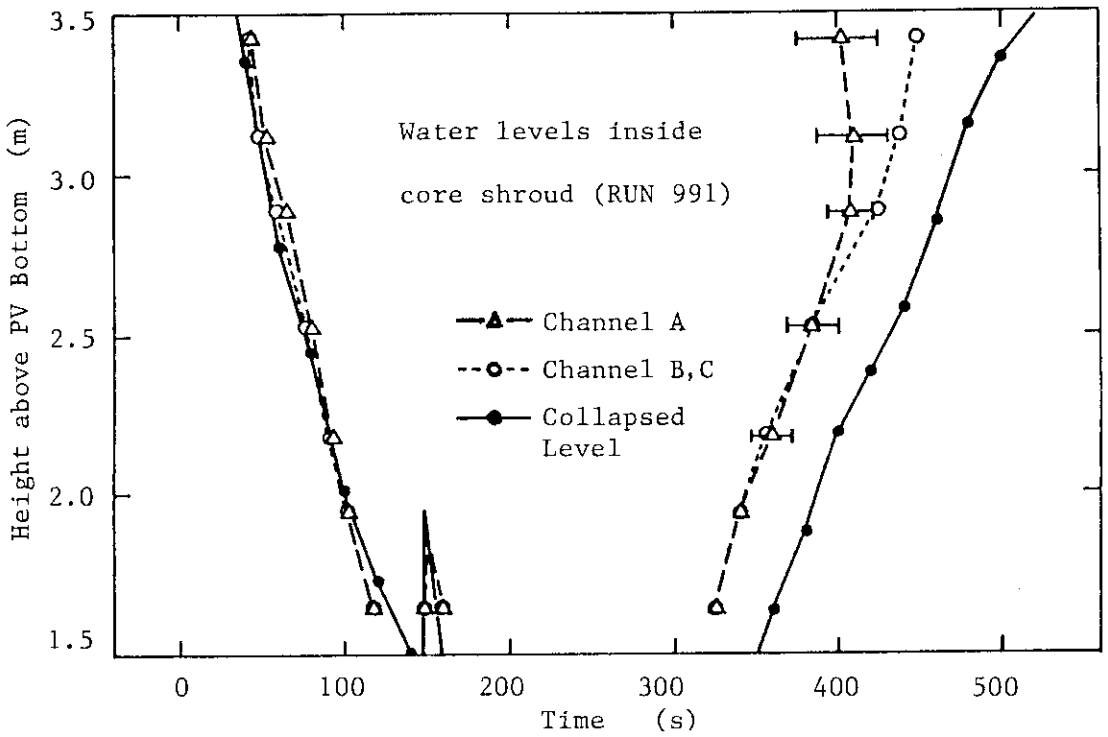

Fig. 5.19 Liquid level signals in four channel boxes in RUN 991

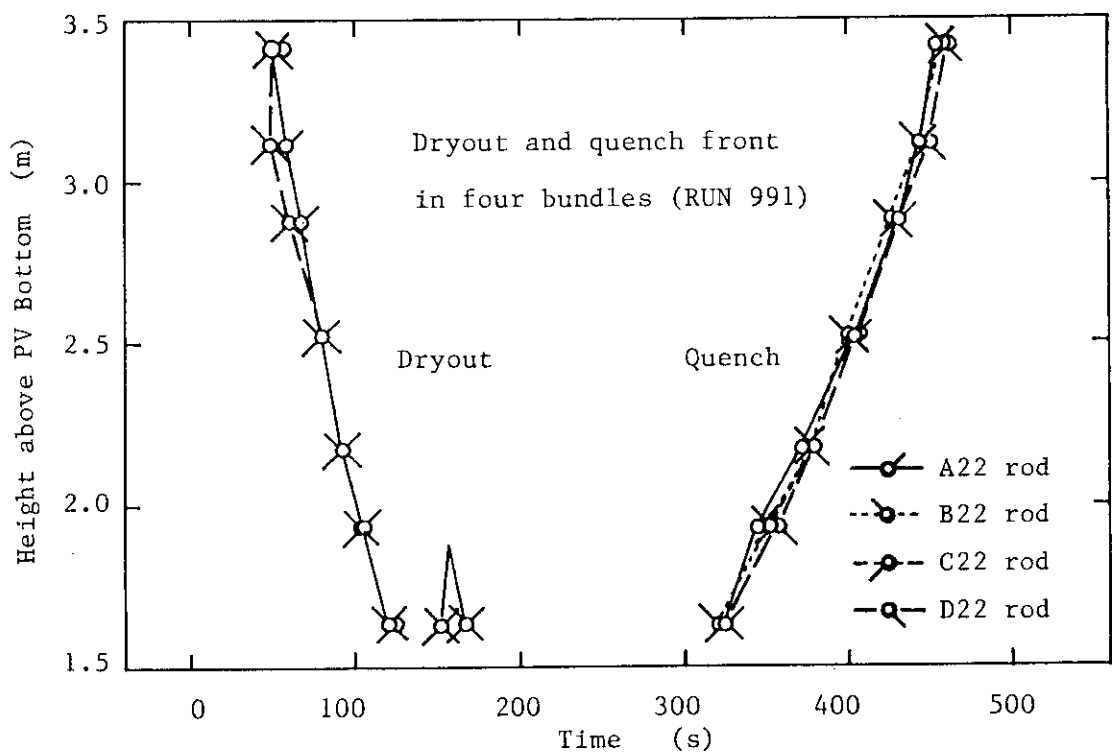

Fig. 5.20 Dryout and quench timings of heater rods in four bundles in RUN 991

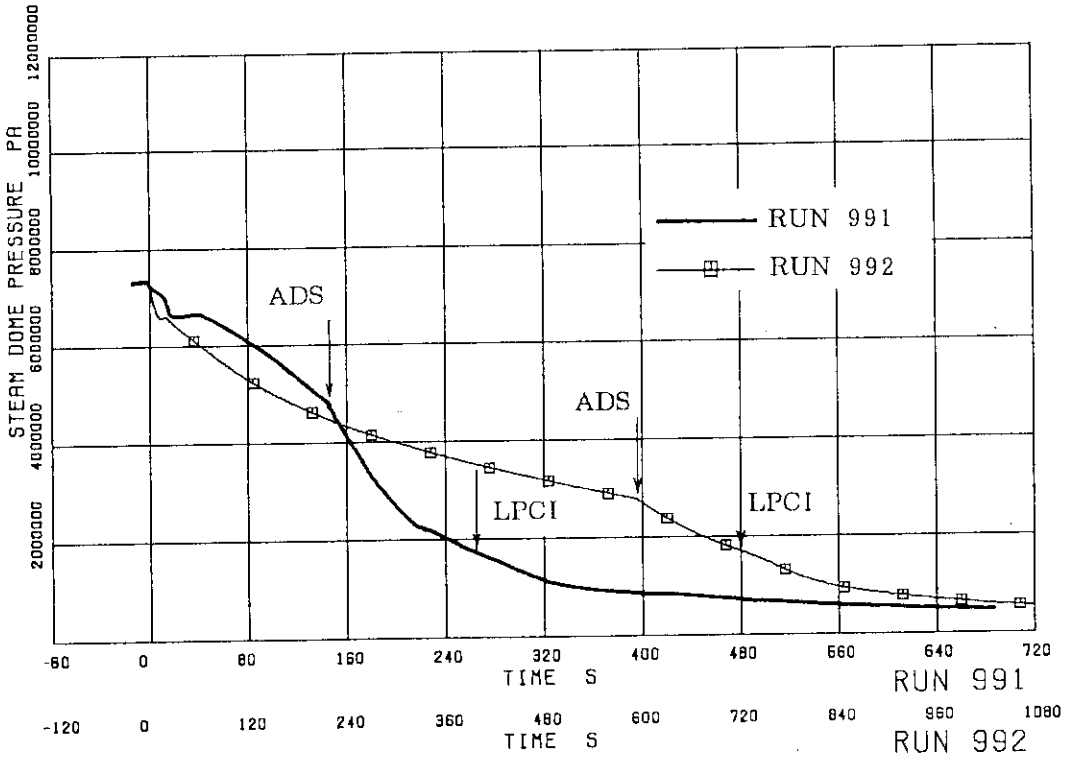

Fig. 6.1 Comparison of pressure responses between RUNs 991 and 992

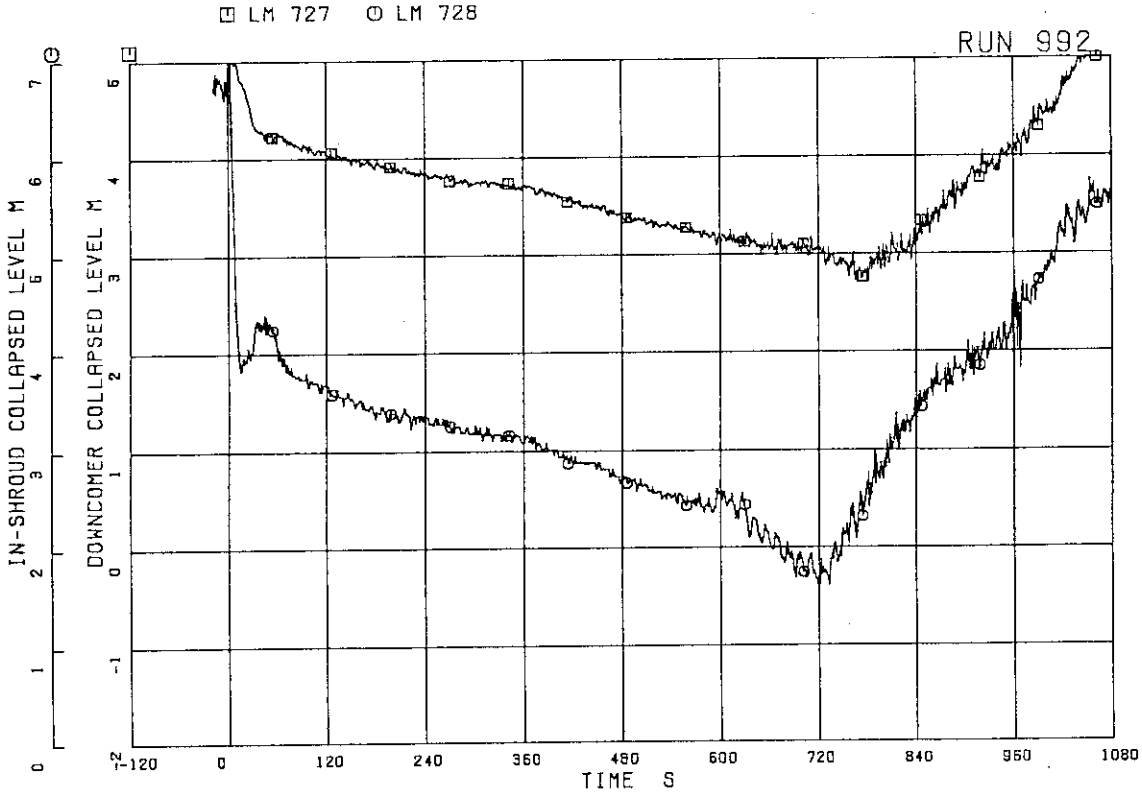

Fig. 6.2 Collapsed levels in downcomer and shroud in RUN 992

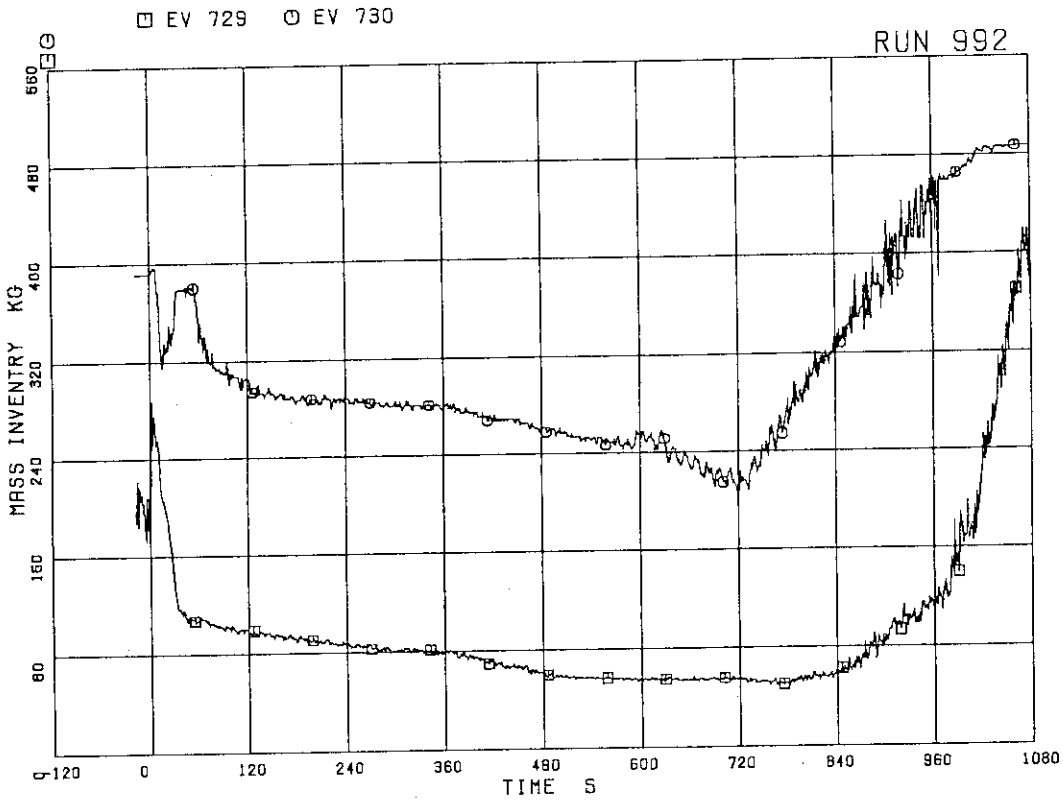

Fig. 6.3 Fluid inventory in downcomer and shroud in RUN 992

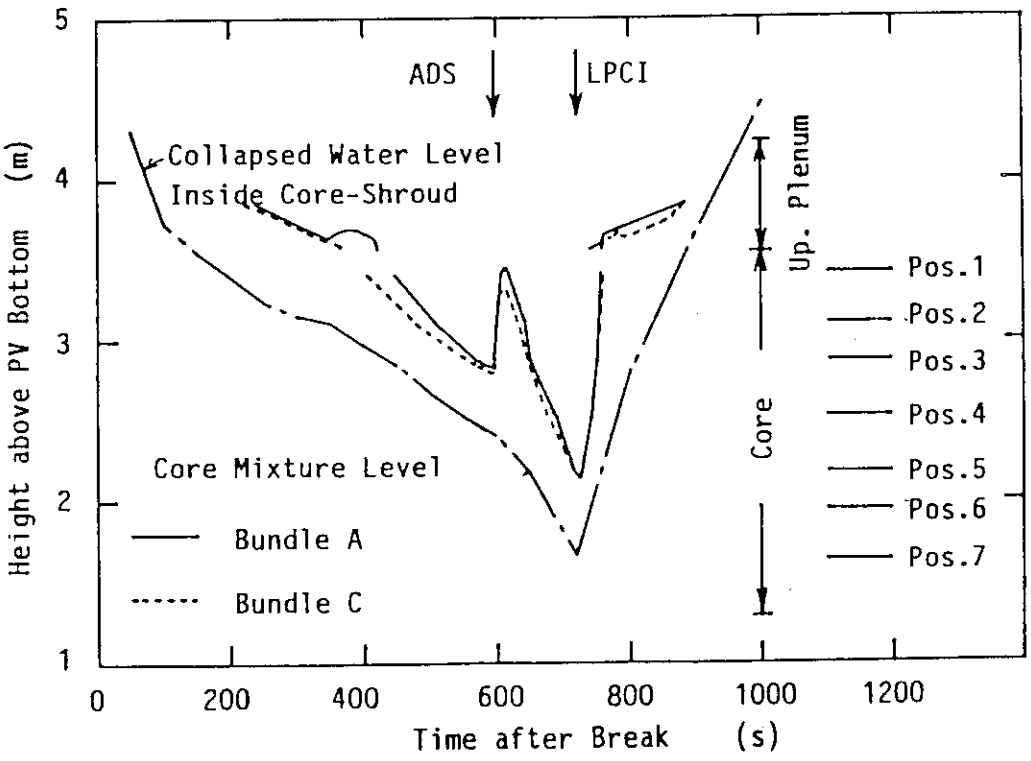

Fig. 6.4 Mixture levels in PV in RUN 992

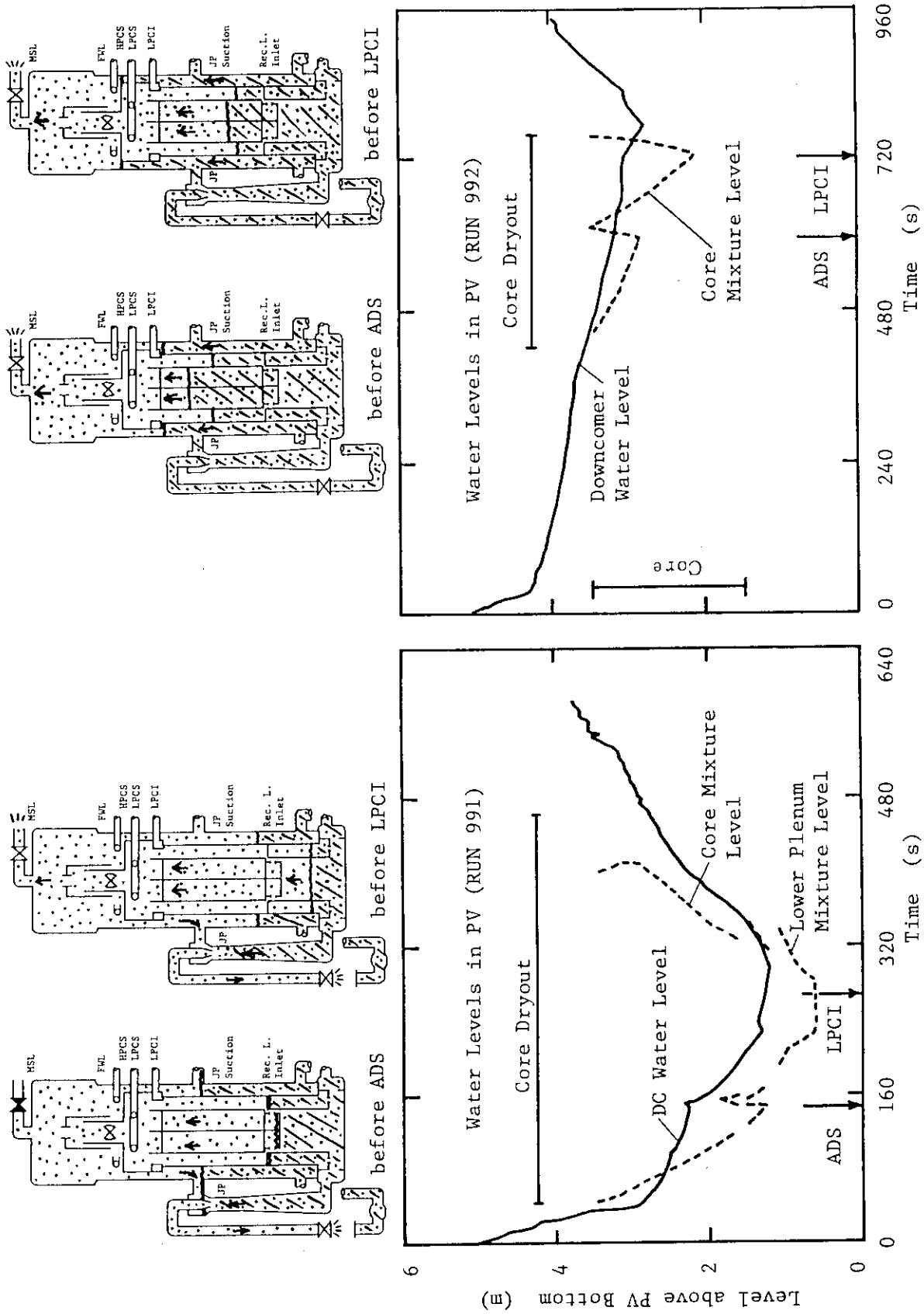

Fig. 6.5 Comparison of downcomer water level and core mixture level in RUNs 991 and 992

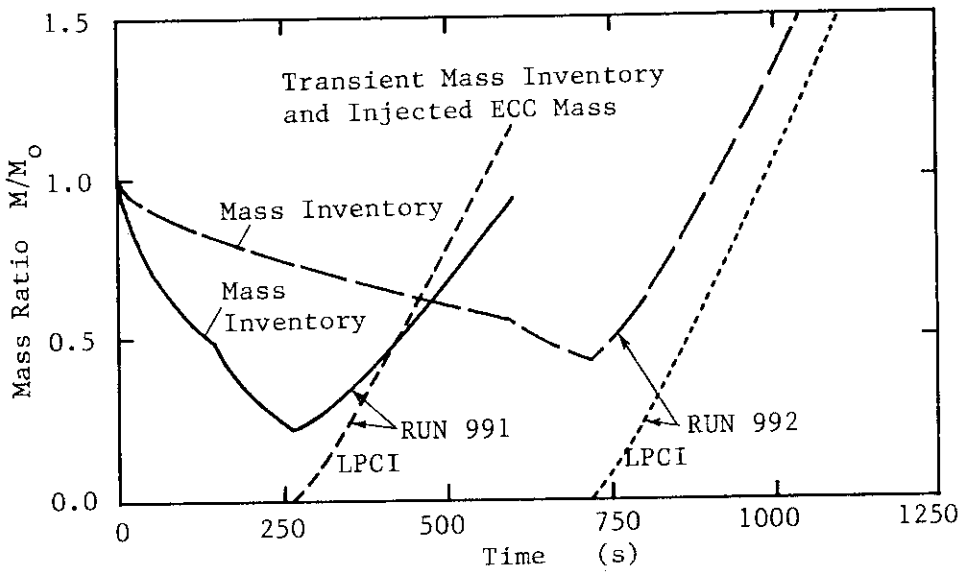

Fig. 6.6 Comparison of mass inventory between RUNs 991 and 992

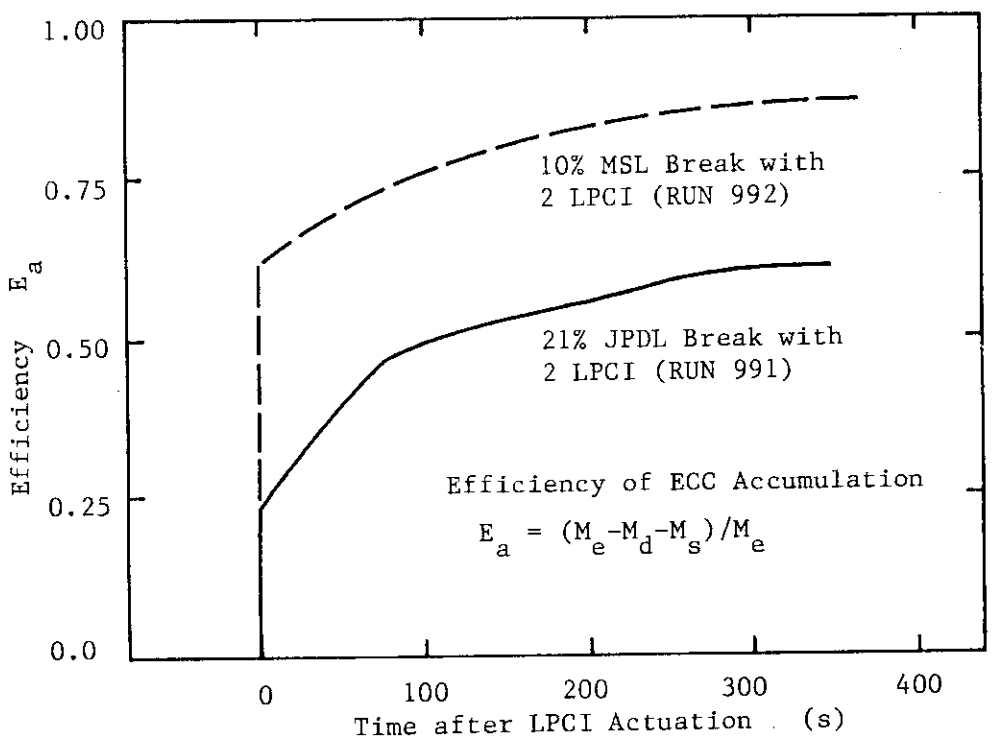

Fig. 6.7 Comparison of ECC accumulation in system between RUNs 991 and 992

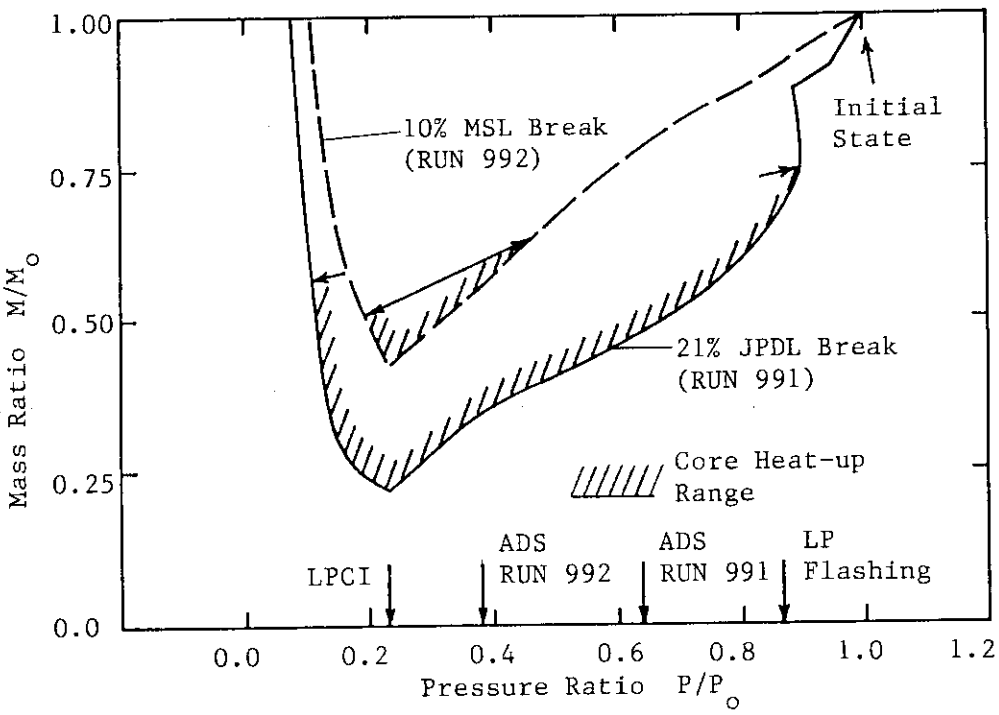

Fig. 6.8 Comparison of mass-pressure trajectory between RUNs 991 and 992

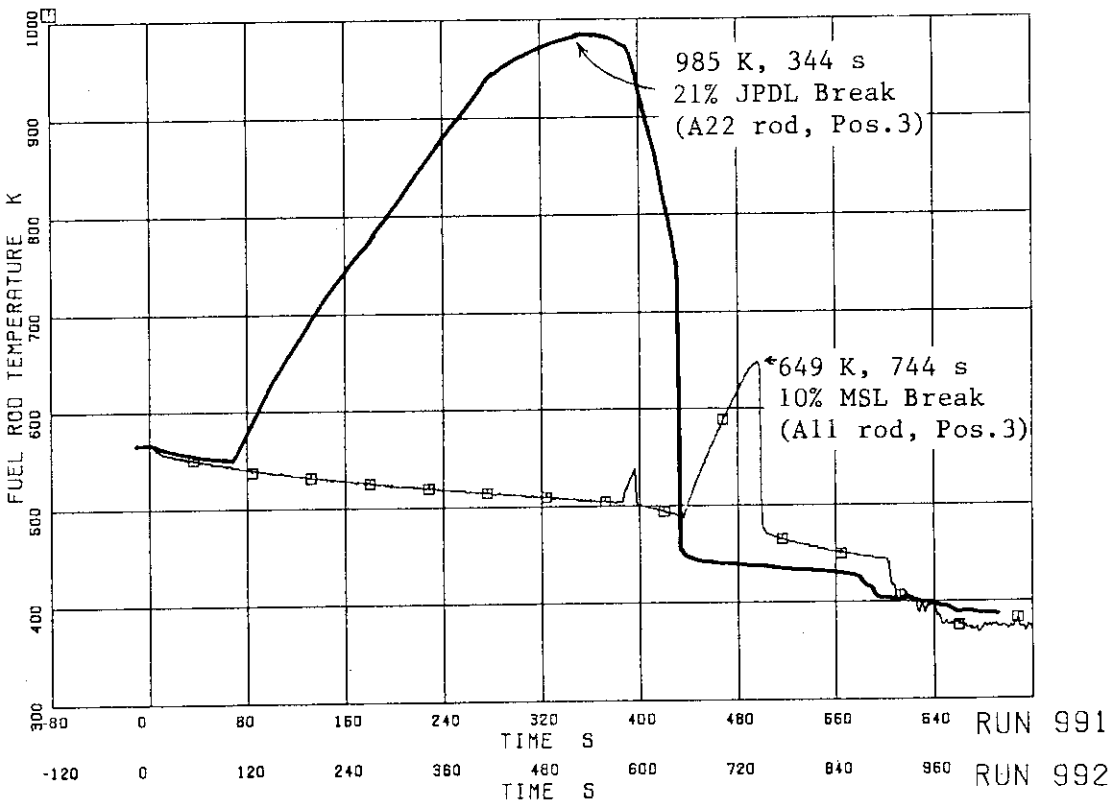

Fig. 6.9 Comparison of PCT between RUNs 991 and 992

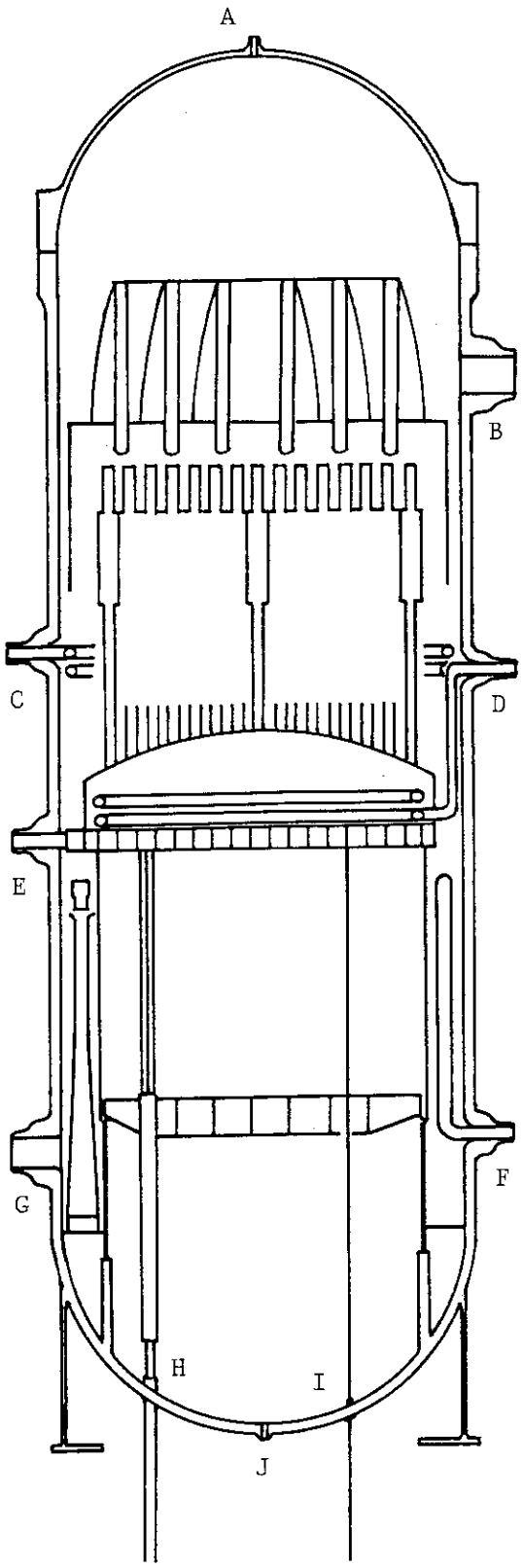

List of Vessel Nozzles

A : Vent Nozzle (Instrument)
B : Main Steam Line
C : Feedwater Line
D : ECCS Line (HPCS,LPCS)
E : ECCS Line (LPCI)
F : Rec. Coolant Inlet Line
G : Rec. Coolant Outlet Line
H : Stub Tube (Control Rod)
I : Stub (In-Core Monitor)
J : Drain Line Nozzle

Fig. 6.10 Illustration of various nozzles through a jet pump type BWR/5 vessel

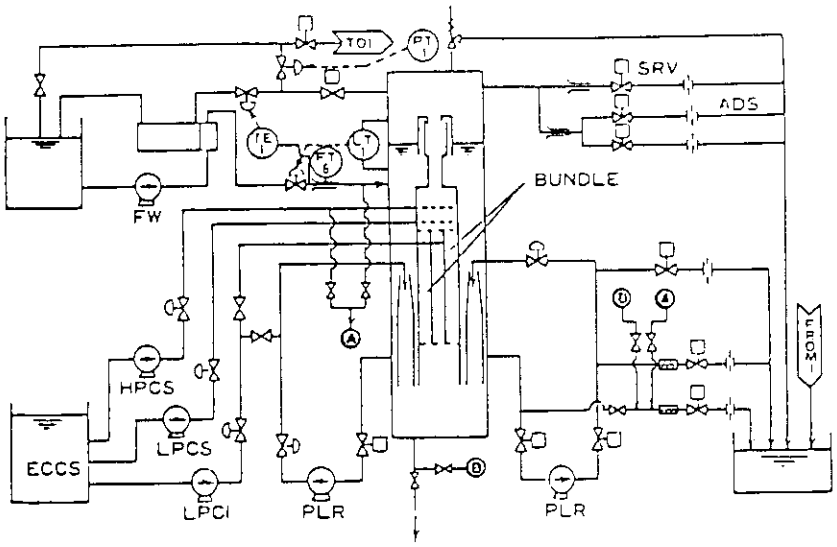

(a) Schematic diagram of TBL (Ref.61)

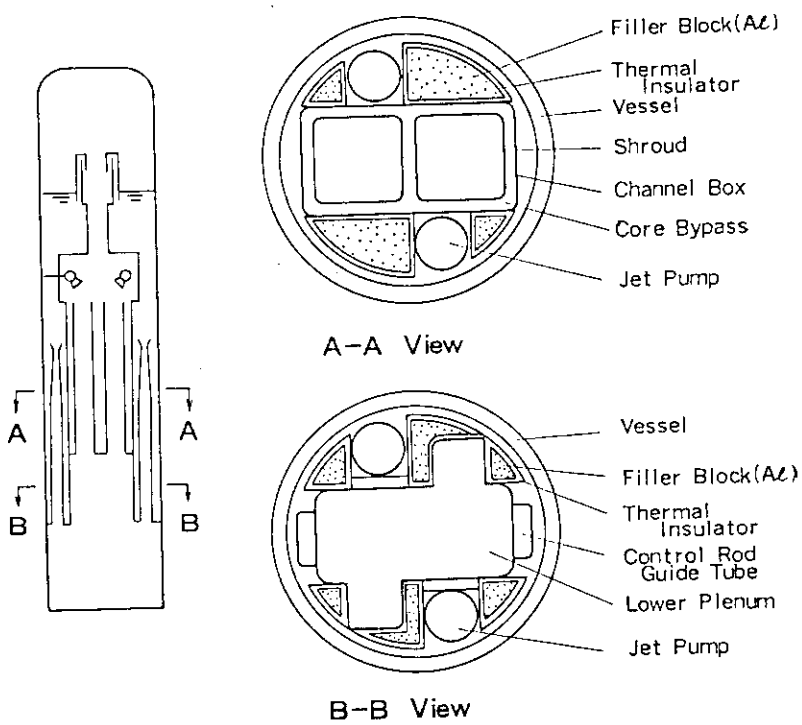

(b) Arrangement of vessel internals (Reference 62)

Fig. 6.11 Test facility of Two Bundle Loop (TBL)

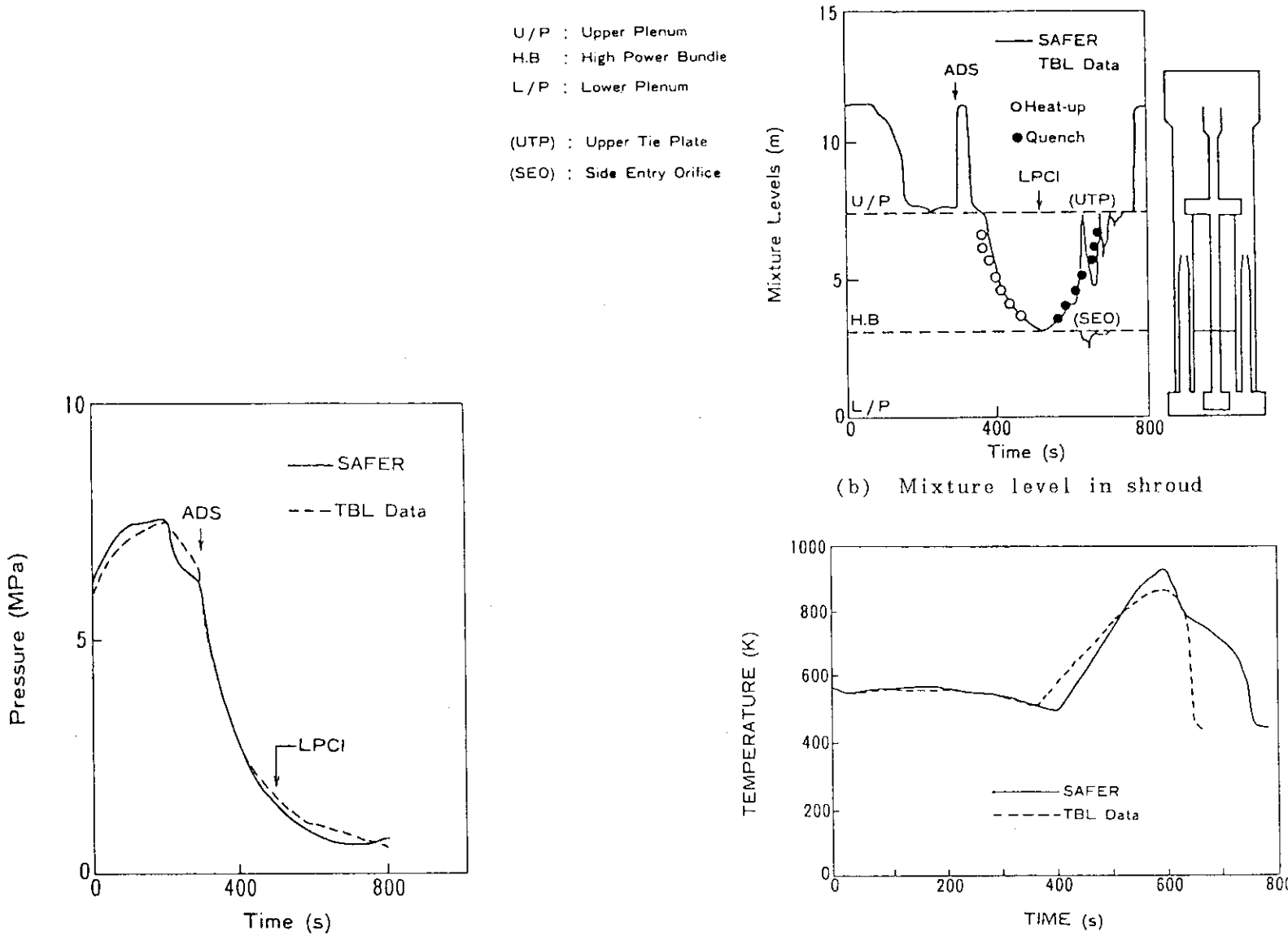

(a) Pressure in steam dome

(b) Mixture level in shroud

(c) Peak cladding temperature

Fig. 6.12 TBL HPCS line break test results (Reference 61)

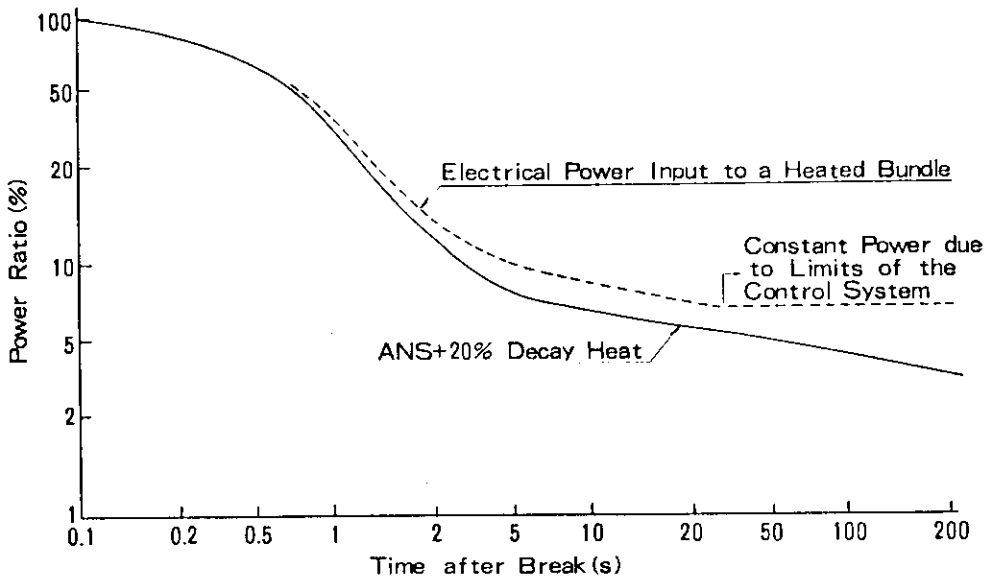

Fig. 6.13 Electrical power input to a heated bundle of TBL test (Reference 62)

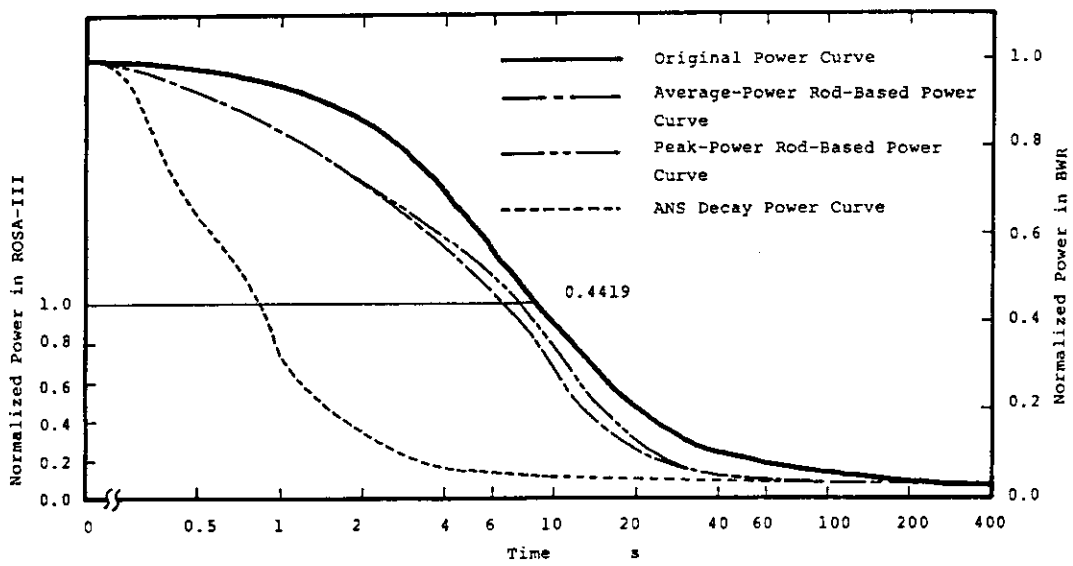

Fig. 6.14 Updated core power curve in ROSA-III tests

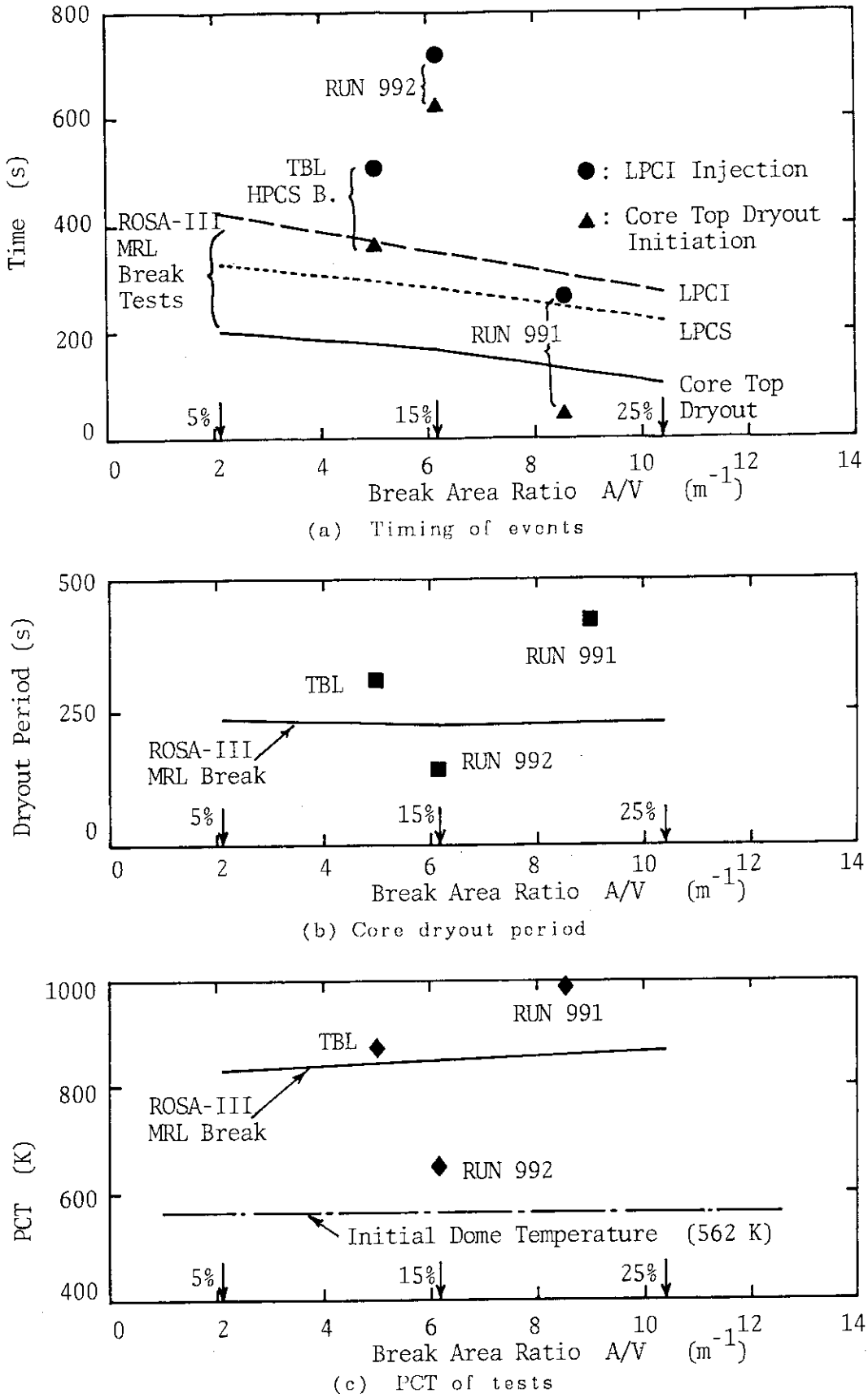

Fig. 6.15 Effect of break location on core dryout period and PCT in intermediate break LOCA tests

Appendix I List of Measurements and Calculated Data in RUN 991

Almost all of the measurements (Channels 1 through 698) in RUN 991 941 are listed in Table A.1 (in figure numbers of A.1 through A.137). However, approximately a half of the total measurements were not used or not measured in RUN 991. Some measurements are shown in Chapters 5 and 6. The blank data in Table A.1 mean that the recorded data were not shown in this report because those data were similar and could be represented by the other data shown in this report. Shown in Table A.2 is a list of calculated data by using the experimental results shown in Table A.1. The core instrumentations including the heater rod surface temperatures and fluid mixture level are listed in Table A.3.

Table A.1 Measurement List for RUN 991

Table A.2 Calculated Data in RUN 991

Table A.3 Core Instrumentation List

Table A.1 Measurement list for RUN 991

1Ch.- 50Ch.

Ch.	Item	Symbol	ID.		Location	Fig.No.	Range			Unit	Accuracy
1	Press.	P- 1	PA	1	Lower Plenum	Fig.A. 1	0.100	-	10.0	MPa	1.08%FS
2	Press.	P- 2	PA	2	Upper Plenum	Fig.A. 1	0.100	-	10.0	MPa	1.08%FS
3	Press.	P- 3	PA	3	Steam Dome	Fig.A. 1	0.100	-	10.0	MPa	1.08%FS
4	Press.	P- 4	PA	4	Downcomer Bottom	Fig.A. 1	0.100	-	10.0	MPa	1.08%FS
5	Press.	P- 5	PA	5	JP-3 Drive	Fig.A. 2	0.100	-	10.0	MPa	1.08%FS
6	Press.	P- 6	PA	6	JP-4 Drive	Fig.A. 2	0.100	-	10.0	MPa	1.08%FS
7	Press.	P- 7	PA	7	JP-3 Suction	Fig.A. 2	0.100	-	10.0	MPa	1.08%FS
8	Press.	P- 8	PA	8	JP-4 Suction	Fig.A. 2	0.100	-	10.0	MPa	1.08%FS
9	Press.	P- 9	PA	9	MRP-1 Suction	Fig.A. 3	0.100	-	10.0	MPa	1.08%FS
10	Press.	P-10	PA	10	MRP-2 Suction	Fig.A. 3	0.100	-	10.0	MPa	1.08%FS
11	Press.	P-11	PA	11	MRP-2 Delivery	Fig.A. 3	0.100	-	10.0	MPa	1.08%FS
12	Press.	P-12	PA	12	Break A Upstream	Fig.A. 4	0.100	-	10.0	MPa	1.08%FS
13	Press.	P-13	PA	13	Break A Downstream	Fig.A. 4	0.100	-	10.0	MPa	1.08%FS
14	Press.	P-14	PA	14	Break B Upstream	Not Used	0.100	-	10.0	MPa	1.08%FS
15	Press.	P-15	PA	15	Break B Downstream	Not Used	0.100	-	10.0	MPa	1.08%FS
16	Press.	P-16	PA	16	Steam Line		0.100	-	10.0	MPa	1.08%FS
17	Press.	P-17	PA	17	JP-1,2 Outlet Spool		0.100	-	10.0	MPa	1.08%FS
18	Press.	P-18	PA	18	JP-3,4 Outlet Spool		0.100	-	10.0	MPa	1.08%FS
19	Press.	P-19	PA	19	Break A Spool Piece	Fig.A. 4	0.100	-	10.0	MPa	1.08%FS
20	Press.	P-30	PA	20	Break B Spool Piece		0.100	-	10.0	MPa	1.08%FS
21	Diff.P.	D- 1	PD	21	Lower Pl.-Upper Pl.	Fig.5. 9	-50.0	-	350.	kPa	0.63%FS
22	Diff.P.	D- 2	PD	22	Upper Pl.-Steam Dome	Fig.5. 9	-10.0	-	90.0	kPa	0.63%FS
23	Diff.P.	D- 3	PD	23	Lower Plenum Head	Not Measured					
24	Diff.P.	D- 4	PD	24	Downcomer Head	Fig.A. 5	0.0	-	100.	kPa	0.63%FS
25	Diff.P.	D- 5	PD	25	PV Bottom-Top	Fig.A. 6	-100.	-	900.	kPa	0.63%FS
26	Diff.P.	D- 6	PD	26	JP-1 Disch.-Suction	Fig.A. 7	-100.	-	300.	kPa	0.63%FS
27	Diff.P.	D- 7	PD	27	JP-1 Drive -Suction	Fig.A. 8	0.0	-	2.50	MPa	0.63%FS
28	Diff.P.	D- 8	PD	28	JP-2 Disch.-Suction	Fig.A. 7	-100.	-	300.	kPa	0.63%FS
29	Diff.P.	D- 9	PD	29	JP-2 Drive -Suction	Fig.A. 8	0.0	-	2.50	MPa	0.63%FS
30	Diff.P.	D-10	PD	30	JP-3 Disch.-Suction	Fig.A. 9	-100.	-	300.	kPa	0.63%FS
31	Diff.P.	D-11	PD	31	JP-3 Drive -Suction	Fig.A.10	-4.00	-	2.00	MPa	0.63%FS
32	Diff.P.	D-12	PD	32	JP-4 Disch.-Suction	Fig.A. 9	-100.	-	300.	kPa	0.63%FS
33	Diff.P.	D-13	PD	33	JP-4 Drive -Suction	Fig.A.10	-4.00	-	2.00	MPa	0.63%FS
34	Diff.P.	D-14	PD	34	MRP-1 Deliv.-Suction	Fig.A.11	-0.100	-	2.50	MPa	0.63%FS
35	Diff.P.	D-15	PD	35	MRP-2 Deliv.-Suction	Fig.A.11	-0.100	-	2.50	MPa	0.63%FS
36	Diff.P.	D-16	PD	36	DC Bottom- MRP-1 Suc.	Fig.A.12	-50.0	-	50.0	kPa	0.63%FS
37	Diff.P.	D-17	PD	37	MRP1 Deliv.-JP1 Drive	Fig.A.13	0.0	-	250.	kPa	0.63%FS
38	Diff.P.	D-18	PD	38	MRP1 Deliv.-JP2 Drive	Fig.A.13	0.0	-	250.	kPa	0.63%FS
39	Diff.P.	D-19	PD	39	DC Middle-JP1 Suction	Fig.A.14	0.0	-	250.	kPa	0.63%FS
40	Diff.P.	D-20	PD	40	DC Middle-JP2 Suction	Fig.A.14	0.0	-	250.	kPa	0.63%FS
41	Diff.P.	D-21	PD	41	JP1 Disch.-Lower Pl.	Fig.A.15	-100.	-	100.	kPa	0.63%FS
42	Diff.P.	D-22	PD	42	JP2 Disch.-Lower Pl.	Fig.A.15	-100.	-	100.	kPa	0.63%FS
43	Diff.P.	D-23	PD	43	DC Bottom- Break B	Fig.A.16	-60.0	-	540.	kPa	0.63%FS
44	Diff.P.	D-24	PD	44	Break B- Break A		0.0	-	100.	kPa	0.63%FS
45	Diff.P.	D-25	PD	45	Break A- MRP2 Suction	Not Measured	-500.	-	100.	kPa	0.63%FS
46	Diff.P.	D-26	PD	46	MRP2 Deliv.-JP3 Drive	Fig.A.17	-500.	-	500.	kPa	0.63%FS
47	Diff.P.	D-27	PD	47	MRP2 Deliv.-JP4 Drive	Fig.A.17	-500.	-	500.	kPa	0.63%FS
48	Diff.P.	D-28	PD	48	DC Middle-JP3 Suction	Fig.A.18	-250.	-	250.	kPa	0.63%FS
49	Diff.P.	D-29	PD	49	DC Middle-JP4 Suction	Fig.A.18	-250.	-	250.	kPa	0.63%FS
50	Diff.P.	D-30	PD	50	JP3 Disch.-Confluence	Fig.A.19	-100.	-	100.	kPa	0.63%FS

Table A.1 Measurement list for RUN 991 (Cont'd)

51Ch.- 100Ch.

Ch.	Item	Symbol	ID.		Location	Fig.No.	Range			Unit	Accuracy
51	Diff.P.	D-31	PD	51	JP4 Disch.-Confluence	Fig.A.19	-100.	-	100.	kPa	0.63%FS
52	Diff.P.	D-32	PD	52	Confluence -Lower Pl.	Fig.A.20	-50.0	-	50.0	kPa	0.63%FS
53	Diff.P.	D-33	PD	53	Lower Pl.-DC Middle	Fig.A.21	-250.	-	250.	kPa	0.63%FS
54	Diff.P.	D-34	PD	54	Lower Pl.-DC Bottom	Fig.A.22	-250.	-	250.	kPa	0.63%FS
55	Diff.P.	D-35	PD	55	DC Bottom-DC Middle	Fig.A.23	-50.0	-	50.0	kPa	0.63%FS
56	Diff.P.	D-36	PD	56	DC Middle-Steam Dome	Fig.A.24	-50.0	-	50.0	kPa	0.63%FS
57	Diff.P.	D-37	PD	57	Lower Pl.Mid-Upper PL	Not Measured					
58	Diff.P.	D-38	PD	58	Lower Pl.Bottom-Mid.	Fig.A.25	0.0	-	50.0	kPa	0.63%FS
59	Diff.P.	D-39	PD	59	Upper Pl.-DC High		-20.0	-	100.	kPa	0.63%FS
60	Diff.P.	D-40	PD	60	Channel Orifice A		-50.0	-	50.0	kPa	0.63%FS
61	Diff.P.	D-41	PD	61	Channel Orifice B		-50.0	-	50.0	kPa	0.63%FS
62	Diff.P.	D-42	PD	62	Channel Orifice C		-25.0	-	75.0	kPa	0.63%FS
63	Diff.P.	D-43	PD	63	Channel Orifice D		-50.0	-	50.0	kPa	0.63%FS
64	Diff.P.	D-44	PD	64	Bypass Hole		-100.	-	100.	KPA	0.63%FS
65	Level	WL- 1	LM	65	HPCS Tank	Not Used	0.0	-	2.30	m	1.00%FS
66	Level	WL- 2	LM	66	LPCS Tank	Not Used	0.0	-	2.30	m	1.00%FS
67	Level	WL- 3	LM	67	LPCI Tank	Fig.A.26	0.0	-	4.25	m	1.00%FS
68	Level	WL- 4	LM	68	Upper Downcomer	Fig.A.27	3.90	-	6.04	m	1.00%FS
69	Level	WL- 5	LM	69	Lower Downcomer	Fig.A.27	0.938	-	3.90	m	1.00%FS
70	Mass.F.	F- 1	FM	70	Steam Line (Low Range)	Fig.A.28	0.0	-	1.13	kg/s	0.92%FS
71	Mass.F.	F- 2	FM	71	Steam Line(High Range)	Fig.A.28	0.0	-	3.00	kg/s	0.92%FS
72	Mass.F.	F- 3	FM	72	Steam Line (Mid Range)	Fig.A.28	0.0	-	1.94	kg/s	1.40%FS
73	Vol.F.	F- 7	FV	73	HPCS (Upper Plenum)	Not Used	0.0	-	0.250E-02	m3/s	0.79%FS
74	Vol.F.	F- 9	FV	74	LPCS (Upper Plenum)	Not Used	0.0	-	0.250E-02	m3/s	0.79%FS
75	Vol.F.	F-11	FV	75	LPCI (Core Bypass)	Fig.5. 6	0.0	-	0.830E-02	m3/s	0.79%FS
76	Vol.F.	F-15	FV	76	Feedwater	Fig.A.29	0.0	-	0.100E-01	m3/s	0.79%FS
77	Vol.F.	F-16	FV	77	PWT Flow		0.0	-	0.420E-02	m3/s	0.79%FS
78	Vol.F.	F-17	FV	78	JP1 Discharge	Fig.A.30	0.0	-	0.170E-01	m3/s	0.88%FS
79	Vol.F.	F-18	FV	79	JP2 Discharge	Fig.A.30	0.0	-	0.170E-01	m3/s	0.88%FS
80	Vol.F.	F-19	FV	80	JP3 Disch. Positive	Fig.A.31	0.0	-	0.170E-01	m3/s	0.92%FS
81	Vol.F.	F-20	FV	81	JP3 Disch. Negative	Fig.A.32	0.0	-	0.500E-02	m3/s	0.92%FS
82	Vol.F.	F-21	FV	82	JP4 Disch. Positive	Fig.A.31	0.0	-	0.170E-01	m3/s	0.92%FS
83	Vol.F.	F-22	FV	83	JP4 Disch. Negative	Fig.A.32	0.0	-	0.500E-02	m3/s	0.92%FS
84	Mass.F.	F-23	FM	84	JP1,2 Outlet Spool	Not Measured	0.0	-	30.0	kg/s	1.40%FS
85	Mass.F.	F-24	FM	85	JP3,4 Outlet Spool	Not Measured	0.0	-	30.0	kg/s	1.40%FS
86	Mass.F.	F-25	FM	86	Break A Spool Piece	Not Measured	0.0	-	30.0	kg/s	1.40%FS
87	Mass.F.	F-26	FM	87	Break B Spool Piece	Not Measured	0.0	-	30.0	kg/s	1.40%FS
88	Vol.F.	F-27	FV	88	MRP-1	Fig.A.33	0.0	-	0.120E-01	m3/s	0.88%FS
89	Vol.F.	F-28	FV	89	MRP-2	Fig.A.33	0.0	-	0.120E-01	m3/s	0.63%FS
90	Diff.P.	D-F1	PD	90	F1 Orifice		0.0	-	4.90	kPa	0.63%FS
91	Diff.P.	D-F2	PD	91	F2 Orifice		0.0	-	34.9	kPa	0.63%FS
92	Diff.P.	D-F3	PD	92	F3 Orifice		0.0	-	14.6	kPa	0.63%FS
93	Diff.P.	D-F17	PD	93	F17 Venturi		0.0	-	98.1	kPa	0.63%FS
94	Diff.P.	D-F18	PD	94	F18 Venturi		0.0	-	98.1	kPa	0.63%FS
95	Diff.P.	D-F19	PD	95	F19 Orifice		0.0	-	147.	kPa	0.63%FS
96	Diff.P.	D-F20	PD	96	F20 Orifice		0.0	-	13.2	kPa	0.63%FS
97	Diff.P.	D-F21	PD	97	F21 Orifice		0.0	-	147.	kPa	0.63%FS
98	Diff.P.	D-F22	PD	98	F22 Orifice		0.0	-	13.2	kPa	0.63%FS
99	Diff.P.	D-F27	PD	99	F27 Venturi		0.0	-	200.	kPa	0.63%FS
100	Diff.P.	D-F28	PD	100	F28 Venturi		0.0	-	200.	kPa	0.63%FS

Table A.1 Measurement list for RUN 991 (Cont'd)

101Ch.- 150Ch.

Ch.	Item	Symbol	ID.		Location	Fig.No.	Range			Unit	Accuracy
101	Power	W- 1	WE	101	2100 kW Power Supplier	Fig.5. 4	0.0	-	0.210E+04	kW	1.00%FS
102	Power	W- 2	WE	102	3150 kW Power Supplier	Fig.5. 4	0.0	-	0.315E+04	kW	1.00%FS
103											
104	Rev.	N- 1	SR	104	MRP-1 Revolution	Fig.A.34	0.0	-	0.500E+04	RPM	1.08%FS
105	Rev.	N- 2	SR	105	MRP-2 Revolution	Fig.A.34	0.0	-	0.500E+04	RPM	1.08%FS
106	Signal	S- 1	EV	106	Break Signal A	Fig.A.35					
107	Signal	S- 2	EV	107	Break Signal B	Fig.A.35					
108	Signal	S- 3	EV	108	QSV Signal	Fig.A.35					
109	Signal	S- 6	EV	109	HPCS Valve	Not Used					
110	Signal	S- 7	EV	110	LPCS Valve	Not Used					
111	Signal	S- 8	EV	111	LPCI Valve	Fig.A.36					
112	Signal	S- 9	EV	112	Feedwater Control	Fig.A.35					
113	Signal	S-10	EV	113	MSIV Signal						
114	Signal	S-11	EV	114	Steam Line Valve	Not Used					
115	Signal	S-12	EV	115	ADS Valve	Fig.A.36					
116	Signal	S-13	EV	116	MRP-1 Power OFF	Fig.A.37					
117	Signal	S-14	EV	117	MRP-2 Power OFF	Fig.A.37					
118	Signal	RD- 1	EV	118	MRP-1 Rev. Direction	Failure					
119	Signal	RD- 2	EV	119	MRP-2 Rev. Direction	Failure					
120	Density	DF- 1	DE	120	JP1,2 Outlet Beam A	Not Measured	0.0	-	0.100E+04	kg/m3	1.00%FS
121	Density	DF- 2	DE	121	JP1,2 Outlet Beam B	Not Measured	0.0	-	0.100E+04	kg/m3	1.00%FS
122	Density	DF- 3	DE	122	JP1,2 Outlet Beam C	Not Measured	0.0	-	0.100E+04	kg/m3	1.00%FS
123	Density	DF- 4	DE	123	JP3,4 Outlet Beam A	Not Measured	0.0	-	0.100E+04	kg/m3	1.00%FS
124	Density	DF- 5	DE	124	JP3,4 Outlet Beam B	Not Measured	0.0	-	0.100E+04	kg/m3	1.00%FS
125	Density	DF- 6	DE	125	JP3,4 Outlet Beam C	Not Measured	0.0	-	0.100E+04	kg/m3	1.00%FS
126	Density	DF- 7	DE	126	Break A Beam A	Fig.A.38	0.0	-	0.100E+04	kg/m3	1.00%FS
127	Density	DF- 8	DE	127	Break A Beam B	Fig.A.39	0.0	-	0.100E+04	kg/m3	1.00%FS
128	Density	DF- 9	DE	128	Break B Beam A	Fig.A.40	0.0	-	0.100E+04	kg/m3	1.00%FS
129	Density	DF-10	DE	129	Break B Beam B	Fig.A.41	0.0	-	0.100E+04	kg/m3	1.00%FS
130	Mo.Flux	M- 1	MF	130	JP1,2 Outlet Spool	Fig.A.42	0.0	-	0.220E+05	kg/ms2	1.00%FS
131	Mo.Flux	M- 2	MF	131	JP3,4 Outlet Spool	Fig.A.43	0.0	-	0.220E+05	kg/ms2	1.00%FS
132	Mo.Flux	M- 3	MF	132	Break A (Low Range)	Fig.A.44	0.0	-	0.220E+05	kg/ms2	1.00%FS
133	Mo.Flux	M- 4	MF	133	Break B (Low Range)	Not Measured	0.0	-	0.220E+05	kg/ms2	1.00%FS
134	Mo.Flux	M- 5	MF	134	Break A (High Range)	Fig.A.45	0.0	-	0.220E+06	kg/ms2	1.00%FS
135	Mo.Flux	M- 6	MF	135	Break B (High Range)	Not Measured	0.0	-	0.220E+06	kg/ms2	1.00%FS
136	Mo.Flux	M- 7	MF	136	Break Orifice	Not Measured	0.0	-	0.220E+05	kg/ms2	1.00%FS
137											
138	Fluid T.	T- 1	TE	138	Lower Plenum	Fig.A.46	273.	-	673.	K	0.64%FS
139	Fluid T.	T- 2	TE	139	Upper Plenum	Fig.A.46	273.	-	673.	K	0.64%FS
140	Fluid T.	T- 3	TE	140	Steam Dome	Fig.A.47	273.	-	673.	K	0.64%FS
141	Fluid T.	T- 4	TE	141	Upper Downcomer	Fig.A.48	273.	-	673.	K	0.64%FS
142	Fluid T.	T- 5	TE	142	Lower Downcomer	Fig.A.48	273.	-	673.	K	0.64%FS
143	Fluid T.	T- 6	TE	143	JP-1 Drive	Fig.A.49	273.	-	673.	K	0.64%FS
144	Fluid T.	T- 7	TE	144	JP-2 Drive	Fig.A.49	273.	-	673.	K	0.64%FS
145	Fluid T.	T- 8	TE	145	JP-3 Drive	Fig.A.50	273.	-	673.	K	0.64%FS
146	Fluid T.	T- 9	TE	146	JP-4 Drive	Fig.A.50	273.	-	673.	K	0.64%FS
147	Fluid T.	T-10	TE	147	JP-1 Discharge	Fig.A.51	273.	-	673.	K	0.64%FS
148	Fluid T.	T-11	TE	148	JP-2 Discharge	Fig.A.51	273.	-	673.	K	0.64%FS
149	Fluid T.	T-12	TE	149	JP-3 Discharge	Fig.A.52	273.	-	673.	K	0.64%FS
150	Fluid T.	T-13	TE	150	JP-4 Discharge	Fig.A.52	273.	-	673.	K	0.64%FS

Table A.1 Measurement list for RUN 991 (Cont'd)

151Ch.- 200Ch.

Ch.	Item	Symbol	ID.		Location	Fig.No.	Range			Unit	Accuracy
151	Fluid T.	T-14	TE	151	MRP-1 Suction	Fig.A.49	273.	-	673.	K	0.64%FS
152	Fluid T.	T-15	TE	152	MRP-1 Delivery	Fig.A.49	273.	-	673.	K	0.64%FS
153	Fluid T.	T-16	TE	153	MRP-2 Suction	Fig.A.50	273.	-	673.	K	0.64%FS
154	Fluid T.	T-17	TE	154	MRP-2 Delivery	Fig.A.50	273.	-	673.	K	0.64%FS
155	Fluid T.	T-18	TE	155	Break A Upstream	Fig.A.53	273.	-	673.	K	0.64%FS
156	Fluid T.	T-19	TE	156	Break B Upstream	Fig.A.53	273.	-	673.	K	0.64%FS
157	Fluid T.	T-20	TE	157	RCN A Condenced Water	Not Used	273.	-	698.	K	0.64%FS
158	Fluid T.	T-21	TE	158	RCN B Condenced Water	Not Used	273.	-	698.	K	0.64%FS
159	Fluid T.	T-22	TE	159	Discharged Steam	Fig.A.47	273.	-	673.	K	0.64%FS
160	Fluid T.	T-24	TE	160	JP-1,2 Outlet Spool	Fig.A.51	273.	-	763.	K	0.64%FS
161	Fluid T.	T-25	TE	161	JP-3,4 Outlet Spool	Fig.A.52	273.	-	763.	K	0.64%FS
162	Fluid T.	T-26	TE	162	Break A Spool Piece	Fig.A.53	273.	-	763.	K	0.64%FS
163	Fluid T.	T-27	TE	163	Break B Spool Piece	Fig.A.53	273.	-	763.	K	0.64%FS
164	Fluid T.	T-28	TE	164	Feedwater	Fig.A.54	273.	-	673.	K	0.64%FS
165	Fluid T.	T-29	TE	165	Break Orifice 1		273.	-	673.	K	0.64%FS
166	Fluid T.	T-30	TE	166	Break Orifice 2		273.	-	673.	K	0.64%FS
167	Fluid T.	T-31	TE	167	Break A Down DD(Low)	Not Measured	273.	-	673.	K	0.64%FS
168	Fluid T.	T-32	TE	168	Break B Down DD(Low)	Not Measured	273.	-	673.	K	0.64%FS
169	Fluid T.	T-33	TE	169	Break A Up. DD(High)		273.	-	673.	K	0.64%FS
170	Fluid T.	T-34	TE	170	Break B Up. DD(High)		273.	-	673.	K	0.64%FS
171	Fluid T.	T-F17	TE	171	JP1 Fluid D. Correc.		273.	-	673.	K	0.64%FS
172	Fluid T.	T-F18	TE	172	JP2 Fluid D. Correc.		273.	-	673.	K	0.64%FS
173	Fluid T.	T-F19	TE	173	JP3 Fluid D. Correc.		273.	-	673.	K	0.64%FS
174	Fluid T.	T-F21	TE	174	JP4 Fluid D. Correc.		273.	-	673.	K	0.64%FS
175	Slab T.	TS-11	TE	175	Core Barrel A Pos.5		273.	-	673.	K	0.64%FS
176	Slab T.	TS-12	TE	176	Core Barrel A Pos.6		273.	-	673.	K	0.64%FS
177	Slab T.	TS-13	TE	177	Filler Block C Pos.1	Not Measured	273.	-	673.	K	0.64%FS
178	Slab T.	TS-14	TE	178	Filler Block C Pos.2	Not Measured	273.	-	673.	K	0.64%FS
179	Slab T.	TS-15	TE	179	Filler Block C Pos.3		273.	-	673.	K	0.64%FS
180	Slab T.	TS-16	TE	180	Filler Block C Pos.4	Not Measured	273.	-	673.	K	0.64%FS
181	Slab T.	TS-17	TE	181	Filler Block C Pos.5	Not Measured	273.	-	673.	K	0.64%FS
182	Slab T.	TS-18	TE	182	Filler Block C Pos.6		273.	-	673.	K	0.64%FS
183	Slab T.	TS-19	TE	183	Filler Block A Pos.1	Not Measured	273.	-	673.	K	0.64%FS
184	Slab T.	TS-20	TE	184	Filler Block A Pos.2	Not Measured	273.	-	673.	K	0.64%FS
185	Slab T.	TS-21	TE	185	Filler Block A Pos.3	Not Measured	273.	-	673.	K	0.64%FS
186	Slab T.	TS-22	TE	186	Filler Block A Pos.4	Not Measured	273.	-	673.	K	0.64%FS
187	Slab T.	TS-23	TE	187	Filler Block A Pos.5	Not Measured	273.	-	673.	K	0.64%FS
188	Slab T.	TS-24	TE	188	Filler Block A Pos.6	Not Measured	273.	-	673.	K	0.64%FS
189	Slab T.	TS-25	TE	189	JP-1 Diffuser Wall	Not Measured	273.	-	673.	K	0.64%FS
190	Slab T.	TS-26	TE	190	JP-2 Diffuser Wall	Not Measured	273.	-	673.	K	0.64%FS
191	Slab T.	TS-27	TE	191	JP-3 Diffuser Wall	Not Measured	273.	-	673.	K	0.64%FS
192	Slab T.	TS-28	TE	192	JP-4 Diffuser Wall	Not Measured	273.	-	673.	K	0.64%FS
193	Slab T.	TS-29	TE	193	PV Wall Inside 1-1		273.	-	673.	K	0.64%FS
194	Slab T.	TS-30	TE	194	PV Inner Surface 1-2	Not Measured	273.	-	673.	K	0.64%FS
195	Slab T.	TS-31	TE	195	PV Inner Surface 1-3		273.	-	673.	K	0.64%FS
196	Slab T.	TS-32	TE	196	PV Wall Inside 2		273.	-	673.	K	0.64%FS
197	Slab T.	TS-33	TE	197	PV Wall Inside 3		273.	-	673.	K	0.64%FS
198	Slab T.	TS-34	TE	198	PV Wall Inside 4		273.	-	673.	K	0.64%FS
199	Slab T.	TS-35	TE	199	L.P. Inner Surface	Not Measured	273.	-	673.	K	0.64%FS
200	Slab T.	TS-36	TE	200	L.P. Wall Inside		273.	-	673.	K	0.64%FS

Table A.1 Measurement list for RUN 991 (Cont'd)

201Ch.- 250Ch.

Ch.	Item	Symbol	ID.	Location	Fig.No.	Range	Unit	Accuracy
201	Temp.	TF- 1	TE 201	A11 Fuel Rod Pos.1	Fig.A.55, 71	273. - 0.147E+04	K	0.64%FS
202	Temp.	TF- 2	TE 202	A11 Fuel Rod Pos.2	Fig.A.55, 72	273. - 0.147E+04	K	0.64%FS
203	Temp.	TF- 3	TE 203	A11 Fuel Rod Pos.3	Fig.A.55, 73	273. - 0.147E+04	K	0.64%FS
204	Temp.	TF- 4	TE 204	A11 Fuel Rod Pos.4	Fig.A.55, 74	273. - 0.147E+04	K	0.64%FS
205	Temp.	TF- 5	TE 205	A11 Fuel Rod Pos.5	Fig.A.55, 75	273. - 0.147E+04	K	0.64%FS
206	Temp.	TF- 6	TE 206	A11 Fuel Rod Pos.6	Fig.A.55, 76	273. - 0.147E+04	K	0.64%FS
207	Temp.	TF- 7	TE 207	A11 Fuel Rod Pos.7	Fig.A.55, 77	273. - 0.147E+04	K	0.64%FS
208	Temp.	TF- 8	TE 208	A12 Fuel Rod Pos.1	Fig.A.56, 71	273. - 0.147E+04	K	0.64%FS
209	Temp.	TF- 9	TE 209	A12 Fuel Rod Pos.2	Fig.A.56, 72	273. - 0.147E+04	K	0.64%FS
210	Temp.	TF- 10	TE 210	A12 Fuel Rod Pos.3	Fig.A.56, 73	273. - 0.147E+04	K	0.64%FS
211	Temp.	TF- 11	TE 211	A12 Fuel Rod Pos.4	Fig.A.56, 74	273. - 0.147E+04	K	0.64%FS
212	Temp.	TF- 12	TE 212	A12 Fuel Rod Pos.5	Fig.A.56, 75	273. - 0.147E+04	K	0.64%FS
213	Temp.	TF- 13	TE 213	A12 Fuel Rod Pos.6	Fig.A.56, 76	273. - 0.147E+04	K	0.64%FS
214	Temp.	TF- 14	TE 214	A12 Fuel Rod Pos.7	Fig.A.56, 77	273. - 0.147E+04	K	0.64%FS
215	Temp.	TF- 15	TE 215	A13 Fuel Rod Pos.1	Fig.A.57, 71	273. - 0.147E+04	K	0.64%FS
216	Temp.	TF- 16	TE 216	A13 Fuel Rod Pos.2	Fig.A.57, 72	273. - 0.147E+04	K	0.64%FS
217	Temp.	TF- 17	TE 217	A13 Fuel Rod Pos.3	Fig.A.57, 73	273. - 0.147E+04	K	0.64%FS
218	Temp.	TF- 18	TE 218	A13 Fuel Rod Pos.4	Fig.A.57, 74	273. - 0.147E+04	K	0.64%FS
219	Temp.	TF- 19	TE 219	A13 Fuel Rod Pos.5	Fig.A.57, 75	273. - 0.147E+04	K	0.64%FS
220	Temp.	TF- 20	TE 220	A13 Fuel Rod Pos.6	Fig.A.57, 76	273. - 0.147E+04	K	0.64%FS
221	Temp.	TF- 21	TE 221	A13 Fuel Rod Pos.7	Fig.A.57, 77	273. - 0.147E+04	K	0.64%FS
222	Temp.	TF- 22	TE 222	A14 Fuel Rod Pos.1	Not Measured	273. - 0.147E+04	K	0.64%FS
223	Temp.	TF- 23	TE 223	A14 Fuel Rod Pos.2	Not Measured	273. - 0.147E+04	K	0.64%FS
224	Temp.	TF- 24	TE 224	A14 Fuel Rod Pos.3	Not Measured	273. - 0.147E+04	K	0.64%FS
225	Temp.	TF- 25	TE 225	A14 Fuel Rod Pos.4	Not Measured	273. - 0.147E+04	K	0.64%FS
226	Temp.	TF- 26	TE 226	A14 Fuel Rod Pos.5	Not Measured	273. - 0.147E+04	K	0.64%FS
227	Temp.	TF- 27	TE 227	A14 Fuel Rod Pos.6	Not Measured	273. - 0.147E+04	K	0.64%FS
228	Temp.	TF- 28	TE 228	A14 Fuel Rod Pos.7	Not Measured	273. - 0.147E+04	K	0.64%FS
229	Temp.	TF- 29	TE 229	A15 Fuel Rod Pos.1	Not Measured	273. - 0.147E+04	K	0.64%FS
230	Temp.	TF- 30	TE 230	A15 Fuel Rod Pos.4	Not Measured	273. - 0.147E+04	K	0.64%FS
231	Temp.	TF- 31	TE 231	A17 Fuel Rod Pos.1	Not Measured	273. - 0.147E+04	K	0.64%FS
232	Temp.	TF- 32	TE 232	A17 Fuel Rod Pos.4		273. - 0.147E+04	K	0.64%FS
233	Temp.	TF- 33	TE 233	A22 Fuel Rod Pos.1	Fig.A.58, 78	273. - 0.147E+04	K	0.64%FS
234	Temp.	TF- 34	TE 234	A22 Fuel Rod Pos.2	Fig.A.58, 79	273. - 0.147E+04	K	0.64%FS
235	Temp.	TF- 35	TE 235	A22 Fuel Rod Pos.3	Fig.A.58, 80	273. - 0.147E+04	K	0.64%FS
236	Temp.	TF- 36	TE 236	A22 Fuel Rod Pos.4	Fig.A.58, 81	273. - 0.125E+04	K	0.64%FS
237	Temp.	TF- 37	TE 237	A22 Fuel Rod Pos.5	Fig.A.58, 82	273. - 0.125E+04	K	0.64%FS
238	Temp.	TF- 38	TE 238	A22 Fuel Rod Pos.6	Fig.A.58, 83	273. - 0.125E+04	K	0.64%FS
239	Temp.	TF- 39	TE 239	A22 Fuel Rod Pos.7	Fig.A.58, 84	273. - 0.125E+04	K	0.64%FS
240	Temp.	TF- 40	TE 240	A24 Fuel Rod Pos.1		273. - 0.125E+04	K	0.64%FS
241	Temp.	TF- 41	TE 241	A24 Fuel Rod Pos.2		273. - 0.125E+04	K	0.64%FS
242	Temp.	TF- 42	TE 242	A24 Fuel Rod Pos.3		273. - 0.125E+04	K	0.64%FS
243	Temp.	TF- 43	TE 243	A24 Fuel Rod Pos.4		273. - 0.125E+04	K	0.64%FS
244	Temp.	TF- 44	TE 244	A24 Fuel Rod Pos.5		273. - 0.125E+04	K	0.64%FS
245	Temp.	TF- 45	TE 245	A24 Fuel Rod Pos.6		273. - 0.125E+04	K	0.64%FS
246	Temp.	TF- 46	TE 246	A24 Fuel Rod Pos.7		273. - 0.125E+04	K	0.64%FS
247	Temp.	TF- 47	TE 247	A26 Fuel Rod Pos.1		273. - 0.125E+04	K	0.64%FS
248	Temp.	TF- 48	TE 248	A26 Fuel Rod Pos.4	Not Measured	273. - 0.125E+04	K	0.64%FS
249	Temp.	TF- 49	TE 249	A28 Fuel Rod Pos.1	Not Measured	273. - 0.125E+04	K	0.64%FS
250	Temp.	TF- 50	TE 250	A28 Fuel Rod Pos.4		273. - 0.125E+04	K	0.64%FS

Table A.1 Measurement list for RUN 991 (Cont'd)

251Ch.- 300Ch.

Ch.	Item	Symbol	ID.	Location	Fig.No.	Range	Unit	Accuracy
251	Temp.	TF- 51	TE 251	A31 Fuel Rod Pos.1	Not Measured	273. - 0.125E+04	K	0.64%FS
252	Temp.	TF- 52	TE 252	A31 Fuel Rod Pos.4		273. - 0.125E+04	K	0.64%FS
253	Temp.	TF- 53	TE 253	A33 Fuel Rod Pos.1	Fig.A.59	273. - 0.125E+04	K	0.64%FS
254	Temp.	TF- 54	TE 254	A33 Fuel Rod Pos.2	Fig.A.59	273. - 0.125E+04	K	0.64%FS
255	Temp.	TF- 55	TE 255	A33 Fuel Rod Pos.3	Fig.A.59	273. - 0.125E+04	K	0.64%FS
256	Temp.	TF- 56	TE 256	A33 Fuel Rod Pos.4	Fig.A.59	273. - 0.125E+04	K	0.64%FS
257	Temp.	TF- 57	TE 257	A33 Fuel Rod Pos.5	Fig.A.59	273. - 0.125E+04	K	0.64%FS
258	Temp.	TF- 58	TE 258	A33 Fuel Rod Pos.6	Fig.A.59	273. - 0.125E+04	K	0.64%FS
259	Temp.	TF- 59	TE 259	A33 Fuel Rod Pos.7	Fig.A.59	273. - 0.125E+04	K	0.64%FS
260	Temp.	TF- 60	TE 260	A34 Fuel Rod Pos.1	Not Measured	273. - 0.125E+04	K	0.64%FS
261	Temp.	TF- 61	TE 261	A34 Fuel Rod Pos.2	Not Measured	273. - 0.125E+04	K	0.64%FS
262	Temp.	TF- 62	TE 262	A34 Fuel Rod Pos.3	Not Measured	273. - 0.125E+04	K	0.64%FS
263	Temp.	TF- 63	TE 263	A34 Fuel Rod Pos.4	Not Measured	273. - 0.125E+04	K	0.64%FS
264	Temp.	TF- 64	TE 264	A34 Fuel Rod Pos.5	Not Measured	273. - 0.125E+04	K	0.64%FS
265	Temp.	TF- 65	TE 265	A34 Fuel Rod Pos.6	Not Measured	273. - 0.125E+04	K	0.64%FS
266	Temp.	TF- 66	TE 266	A34 Fuel Rod Pos.7	Not Measured	273. - 0.125E+04	K	0.64%FS
267	Temp.	TF- 67	TE 267	A37 Fuel Rod Pos.1	Not Measured	273. - 0.125E+04	K	0.64%FS
268	Temp.	TF- 68	TE 268	A37 Fuel Rod Pos.4	Not Measured	273. - 0.125E+04	K	0.64%FS
269	Temp.	TF- 69	TE 269	A42 Fuel Rod Pos.1	Not Measured	273. - 0.125E+04	K	0.64%FS
270	Temp.	TF- 70	TE 270	A42 Fuel Rod Pos.4	Not Measured	273. - 0.125E+04	K	0.64%FS
271	Temp.	TF- 71	TE 271	A44 Fuel Rod Pos.1	Not Measured	273. - 0.125E+04	K	0.64%FS
272	Temp.	TF- 72	TE 272	A44 Fuel Rod Pos.2	Not Measured	273. - 0.125E+04	K	0.64%FS
273	Temp.	TF- 73	TE 273	A44 Fuel Rod Pos.3	Not Measured	273. - 0.125E+04	K	0.64%FS
274	Temp.	TF- 74	TE 274	A44 Fuel Rod Pos.4	Not Measured	273. - 0.125E+04	K	0.64%FS
275	Temp.	TF- 75	TE 275	A44 Fuel Rod Pos.5	Not Measured	273. - 0.125E+04	K	0.64%FS
276	Temp.	TF- 76	TE 276	A44 Fuel Rod Pos.6	Not Measured	273. - 0.125E+04	K	0.64%FS
277	Temp.	TF- 77	TE 277	A44 Fuel Rod Pos.7	Not Measured	273. - 0.125E+04	K	0.64%FS
278	Temp.	TF- 78	TE 278	A48 Fuel Rod Pos.1	Not Measured	273. - 0.125E+04	K	0.64%FS
279	Temp.	TF- 79	TE 279	A48 Fuel Rod Pos.4	Not Measured	273. - 0.125E+04	K	0.64%FS
280	Temp.	TF- 80	TE 280	A51 Fuel Rod Pos.1	Not Measured	273. - 0.125E+04	K	0.64%FS
281	Temp.	TF- 81	TE 281	A51 Fuel Rod Pos.4	Not Measured	273. - 0.125E+04	K	0.64%FS
282	Temp.	TF- 82	TE 282	A53 Fuel Rod Pos.1	Not Measured	273. - 0.125E+04	K	0.64%FS
283	Temp.	TF- 83	TE 283	A53 Fuel Rod Pos.4	Not Measured	273. - 0.125E+04	K	0.64%FS
284	Temp.	TF- 84	TE 284	A57 Fuel Rod Pos.1	Not Measured	273. - 0.125E+04	K	0.64%FS
285	Temp.	TF- 85	TE 285	A57 Fuel Rod Pos.4		273. - 0.125E+04	K	0.64%FS
286	Temp.	TF- 86	TE 286	A62 Fuel Rod Pos.1	Not Measured	273. - 0.125E+04	K	0.64%FS
287	Temp.	TF- 87	TE 287	A62 Fuel Rod Pos.4	Not Measured	273. - 0.125E+04	K	0.64%FS
288	Temp.	TF- 88	TE 288	A66 Fuel Rod Pos.1	Not Measured	273. - 0.125E+04	K	0.64%FS
289	Temp.	TF- 89	TE 289	A66 Fuel Rod Pos.4	Not Measured	273. - 0.125E+04	K	0.64%FS
290	Temp.	TF- 90	TE 290	A68 Fuel Rod Pos.1	Not Measured	273. - 0.125E+04	K	0.64%FS
291	Temp.	TF- 91	TE 291	A68 Fuel Rod Pos.4		273. - 0.125E+04	K	0.64%FS
292	Temp.	TF- 92	TE 292	A71 Fuel Rod Pos.1	Not Measured	273. - 0.125E+04	K	0.64%FS
293	Temp.	TF- 93	TE 293	A71 Fuel Rod Pos.4		273. - 0.125E+04	K	0.64%FS
294	Temp.	TF- 94	TE 294	A73 Fuel Rod Pos.1	Not Measured	273. - 0.125E+04	K	0.64%FS
295	Temp.	TF- 95	TE 295	A73 Fuel Rod Pos.4		273. - 0.125E+04	K	0.64%FS
296	Temp.	TF- 96	TE 296	A75 Fuel Rod Pos.1	Not Measured	273. - 0.125E+04	K	0.64%FS
297	Temp.	TF- 97	TE 297	A75 Fuel Rod Pos.4	Not Measured	273. - 0.125E+04	K	0.64%FS
298	Temp.	TF- 98	TE 298	A77 Fuel Rod Pos.1	Fig.A.60, 85	273. - 0.125E+04	K	0.64%FS
299	Temp.	TF- 99	TE 299	A77 Fuel Rod Pos.2	Fig.A.60, 86	273. - 0.125E+04	K	0.64%FS
300	Temp.	TF-100	TE 300	A77 Fuel Rod Pos.3	Fig.A.60, 87	273. - 0.125E+04	K	0.64%FS

Table A.1 Measurement list for RUN 991 (Cont'd)

301Ch.- 350Ch.

Ch.	Item	Symbol	ID.	Location	Fig.No.	Range	Unit	Accuracy
301	Temp.	TF-101	TE 301	A77 Fuel Rod Pos.4	Fig.A.60, 88	273. - 0.125E+04	K	0.64%FS
302	Temp.	TF-102	TE 302	A77 Fuel Rod Pos.5	Fig.A.60, 89	273. - 0.125E+04	K	0.64%FS
303	Temp.	TF-103	TE 303	A77 Fuel Rod Pos.6	Fig.A.60, 90	273. - 0.125E+04	K	0.64%FS
304	Temp.	TF-104	TE 304	A77 Fuel Rod Pos.7	Failure	273. - 0.125E+04	K	0.64%FS
305	Temp.	TF-105	TE 305	A82 Fuel Rod Pos.1	Not Measured	273. - 0.125E+04	K	0.64%FS
306	Temp.	TF-106	TE 306	A82 Fuel Rod Pos.4	Not Measured	273. - 0.125E+04	K	0.64%FS
307	Temp.	TF-107	TE 307	A84 Fuel Rod Pos.1		273. - 0.125E+04	K	0.64%FS
308	Temp.	TF-108	TE 308	A84 Fuel Rod Pos.4		273. - 0.125E+04	K	0.64%FS
309	Temp.	TF-109	TE 309	A85 Fuel Rod Pos.1	Not Measured	273. - 0.125E+04	K	0.64%FS
310	Temp.	TF-110	TE 310	A85 Fuel Rod Pos.2	Not Measured	273. - 0.125E+04	K	0.64%FS
311	Temp.	TF-111	TE 311	A85 Fuel Rod Pos.3	Not Measured	273. - 0.125E+04	K	0.64%FS
312	Temp.	TF-112	TE 312	A85 Fuel Rod Pos.4	Not Measured	273. - 0.125E+04	K	0.64%FS
313	Temp.	TF-113	TE 313	A85 Fuel Rod Pos.5	Not Measured	273. - 0.125E+04	K	0.64%FS
314	Temp.	TF-114	TE 314	A85 Fuel Rod Pos.6	Not Measured	273. - 0.125E+04	K	0.64%FS
315	Temp.	TF-115	TE 315	A85 Fuel Rod Pos.7	Not Measured	273. - 0.125E+04	K	0.64%FS
316	Temp.	TF-116	TE 316	A87 Fuel Rod Pos.1		273. - 0.125E+04	K	0.64%FS
317	Temp.	TF-117	TE 317	A87 Fuel Rod Pos.2		273. - 0.125E+04	K	0.64%FS
318	Temp.	TF-118	TE 318	A87 Fuel Rod Pos.3		273. - 0.125E+04	K	0.64%FS
319	Temp.	TF-119	TE 319	A87 Fuel Rod Pos.4		273. - 0.125E+04	K	0.64%FS
320	Temp.	TF-120	TE 320	A87 Fuel Rod Pos.5		273. - 0.125E+04	K	0.64%FS
321	Temp.	TF-121	TE 321	A87 Fuel Rod Pos.6		273. - 0.125E+04	K	0.64%FS
322	Temp.	TF-122	TE 322	A87 Fuel Rod Pos.7		273. - 0.125E+04	K	0.64%FS
323	Temp.	TF-123	TE 323	A88 Fuel Rod Pos.1	Fig.A.61, 71	273. - 0.125E+04	K	0.64%FS
324	Temp.	TF-124	TE 324	A88 Fuel Rod Pos.2	Fig.A.61, 72	273. - 0.125E+04	K	0.64%FS
325	Temp.	TF-125	TE 325	A88 Fuel Rod Pos.3	Fig.A.61, 73	273. - 0.125E+04	K	0.64%FS
326	Temp.	TF-126	TE 326	A88 Fuel Rod Pos.4	Fig.A.61, 74	273. - 0.125E+04	K	0.64%FS
327	Temp.	TF-127	TE 327	A88 Fuel Rod Pos.5	Fig.A.61, 75	273. - 0.125E+04	K	0.64%FS
328	Temp.	TF-128	TE 328	A88 Fuel Rod Pos.6	Fig.A.61, 76	273. - 0.125E+04	K	0.64%FS
329	Temp.	TF-129	TE 329	A88 Fuel Rod Pos.7	Fig.A.61, 77	273. - 0.125E+04	K	0.64%FS
330	Temp.	TF-130	TE 330	B11 Fuel Rod Pos.1		273. - 0.125E+04	K	0.64%FS
331	Temp.	TF-131	TE 331	B11 Fuel Rod Pos.2		273. - 0.125E+04	K	0.64%FS
332	Temp.	TF-132	TE 332	B11 Fuel Rod Pos.3		273. - 0.125E+04	K	0.64%FS
333	Temp.	TF-133	TE 333	B11 Fuel Rod Pos.4		273. - 0.125E+04	K	0.64%FS
334	Temp.	TF-134	TE 334	B11 Fuel Rod Pos.5		273. - 0.125E+04	K	0.64%FS
335	Temp.	TF-135	TE 335	B11 Fuel Rod Pos.6		273. - 0.125E+04	K	0.64%FS
336	Temp.	TF-136	TE 336	B11 Fuel Rod Pos.7	Not Measured	273. - 0.125E+04	K	0.64%FS
337	Temp.	TF-137	TE 337	B13 Fuel Rod Pos.4		273. - 0.125E+04	K	0.64%FS
338	Temp.	TF-138	TE 338	B22 Fuel Rod Pos.1	Fig.A.62, 78	273. - 0.125E+04	K	0.64%FS
339	Temp.	TF-139	TE 339	B22 Fuel Rod Pos.2	Fig.A.62, 79	273. - 0.125E+04	K	0.64%FS
340	Temp.	TF-140	TE 340	B22 Fuel Rod Pos.3	Fig.A.62, 80	273. - 0.125E+04	K	0.64%FS
341	Temp.	TF-141	TE 341	B22 Fuel Rod Pos.4	Fig.A.62 81	273. - 0.125E+04	K	0.64%FS
342	Temp.	TF-142	TE 342	B22 Fuel Rod Pos.5	Fig.A.62, 82	273. - 0.125E+04	K	0.64%FS
343	Temp.	TF-143	TE 343	B22 Fuel Rod Pos.6	Fig.A.62, 83	273. - 0.125E+04	K	0.64%FS
344	Temp.	TF-144	TE 344	B22 Fuel Rod Pos.7	Fig.A.62, 84	273. - 0.125E+04	K	0.64%FS
345	Temp.	TF-145	TE 345	B31 Fuel Rod Pos.4	Not Measured	273. - 0.125E+04	K	0.64%FS
346	Temp.	TF-146	TE 346	B33 Fuel Rod Pos.4	Not Measured	273. - 0.125E+04	K	0.64%FS
347	Temp.	TF-147	TE 347	B51 Fuel Rod Pos.4	Not Measured	273. - 0.125E+04	K	0.64%FS
348	Temp.	TF-148	TE 348	B53 Fuel Rod Pos.4	Not Measured	273. - 0.125E+04	K	0.64%FS
349	Temp.	TF-149	TE 349	B66 Fuel Rod Pos.4	Not Measured	273. - 0.125E+04	K	0.64%FS
350	Temp.	TF-150	TE 350	B77 Fuel Rod Pos.1	Fig.A. 85	273. - 0.125E+04	K	0.64%FS

Table A.1 Measurement list for RUN 991 (Cont'd)

351Ch.- 400Ch.

Ch.	Item	Symbol	ID.	Location	Fig.No.	Range	Unit	Accuracy
351	Temp.	TF-151	TE 351	B77 Fuel Rod Pos.2	Fig.A. 86	273. - 0.125E+04	K	0.64%FS
352	Temp.	TF-152	TE 352	B77 Fuel Rod Pos.3	Fig.A. 87	273. - 0.125E+04	K	0.64%FS
353	Temp.	TF-153	TE 353	B77 Fuel Rod Pos.4	Fig.A. 88	273. - 0.125E+04	K	0.64%FS
354	Temp.	TF-154	TE 354	B77 Fuel Rod Pos.5	Fig.A. 89	273. - 0.125E+04	K	0.64%FS
355	Temp.	TF-155	TE 355	B77 Fuel Rod Pos.6	Fig.A. 90	273. - 0.125E+04	K	0.64%FS
356	Temp.	TF-156	TE 356	B77 Fuel Rod Pos.7	Fig.A. 91	273. - 0.125E+04	K	0.64%FS
357	Temp.	TF-157	TE 357	B86 Fuel Rod Pos.4	Not Measured	273. - 0.125E+04	K	0.64%FS
358	Temp.	TF-158	TE 358	C11 Fuel Rod Pos.1	Failure	273. - 0.125E+04	K	0.64%FS
359	Temp.	TF-159	TE 359	C11 Fuel Rod Pos.2	Fig.A.63	273. - 0.125E+04	K	0.64%FS
360	Temp.	TF-160	TE 360	C11 Fuel Rod Pos.3	Fig.A.63	273. - 0.125E+04	K	0.64%FS
361	Temp.	TF-161	TE 361	C11 Fuel Rod Pos.4	Fig.A.63	273. - 0.125E+04	K	0.64%FS
362	Temp.	TF-162	TE 362	C11 Fuel Rod Pos.5	Fig.A.63	273. - 0.125E+04	K	0.64%FS
363	Temp.	TF-163	TE 363	C11 Fuel Rod Pos.6	Fig.A.63	273. - 0.125E+04	K	0.64%FS
364	Temp.	TF-164	TE 364	C11 Fuel Rod Pos.7	Fig.A.63	273. - 0.125E+04	K	0.64%FS
365	Temp.	TF-165	TE 365	C13 Fuel Rod Pos.1	Fig.A.64	273. - 0.125E+04	K	0.64%FS
366	Temp.	TF-166	TE 366	C13 Fuel Rod Pos.2	Fig.A.64	273. - 0.125E+04	K	0.64%FS
367	Temp.	TF-167	TE 367	C13 Fuel Rod Pos.3	Fig.A.64	273. - 0.125E+04	K	0.64%FS
368	Temp.	TF-168	TE 368	C13 Fuel Rod Pos.4	Fig.A.64	273. - 0.125E+04	K	0.64%FS
369	Temp.	TF-169	TE 369	C13 Fuel Rod Pos.5	Fig.A.64	273. - 0.125E+04	K	0.64%FS
370	Temp.	TF-170	TE 370	C13 Fuel Rod Pos.6	Fig.A.64	273. - 0.125E+04	K	0.64%FS
371	Temp.	TF-171	TE 371	C13 Fuel Rod Pos.7	Fig.A.64	273. - 0.125E+04	K	0.64%FS
372	Temp.	TF-172	TE 372	C15 Fuel Rod Pos.4	Not Measured	273. - 0.125E+04	K	0.64%FS
373	Temp.	TF-173	TE 373	C22 Fuel Rod Pos.1	Fig.A.65, 78	273. - 0.125E+04	K	0.64%FS
374	Temp.	TF-174	TE 374	C22 Fuel Rod Pos.2	Fig.A.65, 79	273. - 0.125E+04	K	0.64%FS
375	Temp.	TF-175	TE 375	C22 Fuel Rod Pos.3	Fig.A.65, 80	273. - 0.125E+04	K	0.64%FS
376	Temp.	TF-176	TE 376	C22 Fuel Rod Pos.4	Fig.A.65, 81	273. - 0.125E+04	K	0.64%FS
377	Temp.	TF-177	TE 377	C22 Fuel Rod Pos.5	Fig.A.65, 82	273. - 0.125E+04	K	0.64%FS
378	Temp.	TF-178	TE 378	C22 Fuel Rod Pos.6	Fig.A.65, 83	273. - 0.125E+04	K	0.64%FS
379	Temp.	TF-179	TE 379	C22 Fuel Rod Pos.7	Fig.A.65, 84	273. - 0.125E+04	K	0.64%FS
380	Temp.	TF-180	TE 380	C31 Fuel Rod Pos.4	Not Measured	273. - 0.125E+04	K	0.64%FS
381	Temp.	TF-181	TE 381	C33 Fuel Rod Pos.1	Fig.A.66	273. - 0.125E+04	K	0.64%FS
382	Temp.	TF-182	TE 382	C33 Fuel Rod Pos.2	Fig.A.66	273. - 0.125E+04	K	0.64%FS
383	Temp.	TF-183	TE 383	C33 Fuel Rod Pos.3	Fig.A.66	273. - 0.125E+04	K	0.64%FS
384	Temp.	TF-184	TE 384	C33 Fuel Rod Pos.4	Fig.A.66	273. - 0.125E+04	K	0.64%FS
385	Temp.	TF-185	TE 385	C33 Fuel Rod Pos.5	Fig.A.66	273. - 0.125E+04	K	0.64%FS
386	Temp.	TF-186	TE 386	C33 Fuel Rod Pos.6	Fig.A.66	273. - 0.125E+04	K	0.64%FS
387	Temp.	TF-187	TE 387	C33 Fuel Rod Pos.7	Fig.A.66	273. - 0.125E+04	K	0.64%FS
388	Temp.	TF-188	TE 388	C35 Fuel Rod Pos.4	Not Measured	273. - 0.125E+04	K	0.64%FS
389	Temp.	TF-189	TE 389	C66 Fuel Rod Pos.4	Not Measured	273. - 0.125E+04	K	0.64%FS
390	Temp.	TF-190	TE 390	C68 Fuel Rod Pos.4	Not Measured	273. - 0.125E+04	K	0.64%FS
391	Temp.	TF-191	TE 391	C77 Fuel Rod Pos.1	Fig.A.67, 85	273. - 0.125E+04	K	0.64%FS
392	Temp.	TF-192	TE 392	C77 Fuel Rod Pos.2	Fig.A.67, 86	273. - 0.125E+04	K	0.64%FS
393	Temp.	TF-193	TE 393	C77 Fuel Rod Pos.3	Fig.A.67, 87	273. - 0.125E+04	K	0.64%FS
394	Temp.	TF-194	TE 394	C77 Fuel Rod Pos.4	Fig.A.67, 88	273. - 0.125E+04	K	0.64%FS
395	Temp.	TF-195	TE 395	C77 Fuel Rod Pos.5	Fig.A.67, 89	273. - 0.125E+04	K	0.64%FS
396	Temp.	TF-196	TE 396	C77 Fuel Rod Pos.6	Fig.A.67, 90	273. - 0.125E+04	K	0.64%FS
397	Temp.	TF-197	TE 397	C77 Fuel Rod Pos.7	Fig.A.67, 91	273. - 0.125E+04	K	0.64%FS
398	Temp.	TF-198	TE 398	D11 Fuel Rod Pos.4		273. - 0.125E+04	K	0.64%FS
399	Temp.	TF-199	TE 399	D13 Fuel Rod Pos.4		273. - 0.125E+04	K	0.64%FS
400	Temp.	TF-200	TE 400	D22 Fuel Rod Pos.1	Fig.A.68, 78	273. - 0.125E+04	K	0.64%FS

Table A.1 Measurement list for RUN 991 (Cont'd)

401Ch.- 450Ch.

Ch.	Item	Symbol	ID.	Location	Fig.No.	Range	Unit	Accuracy
401	Temp.	TF-201	TE 401	D22 Fuel Rod Pos.2	Fig.A.68, 79	273. - 0.125E+04	K	0.64%FS
402	Temp.	TF-202	TE 402	D22 Fuel Rod Pos.3	Fig.A.68, 80	273. - 0.125E+04	K	0.64%FS
403	Temp.	TF-203	TE 403	D22 Fuel Rod Pos.4	Fig.A.68, 81	273. - 0.125E+04	K	0.64%FS
404	Temp.	TF-204	TE 404	D22 Fuel Rod Pos.5	Fig.A.68, 82	273. - 0.125E+04	K	0.64%FS
405	Temp.	TF-205	TE 405	D22 Fuel Rod Pos.6	Fig.A.68, 83	273. - 0.125E+04	K	0.64%FS
406	Temp.	TF-206	TE 406	D22 Fuel Rod Pos.7	Fig.A.68, 84	273. - 0.125E+04	K	0.64%FS
407	Temp.	TF-207	TE 407	D31 Fuel Rod Pos.4	Not Measured	273. - 0.125E+04	K	0.64%FS
408	Temp.	TF-208	TE 408	D33 Fuel Rod Pos.4	Not Measured	273. - 0.125E+04	K	0.64%FS
409	Temp.	TF-209	TE 409	D51 Fuel Rod Pos.4	Not Measured	273. - 0.125E+04	K	0.64%FS
410	Temp.	TF-210	TE 410	D53 Fuel Rod Pos.4	Not Measured	273. - 0.125E+04	K	0.64%FS
411	Temp.	TF-211	TE 411	D66 Fuel Rod Pos.4	Not Measured	273. - 0.125E+04	K	0.64%FS
412	Temp.	TF-212	TE 412	D77 Fuel Rod Pos.4		273. - 0.125E+04	K	0.64%FS
413	Temp.	TF-213	TE 413	D86 Fuel Rod Pos.4		273. - 0.125E+04	K	0.64%FS
414	Fluid T.	TW- 1	TE 414	A45 Tie Rod Pos.1	Fig.A.69	273. - 0.125E+04	K	0.64%FS
415	Fluid T.	TW- 2	TE 415	A45 Tie Rod Pos.2	Fig.A.69	273. - 0.125E+04	K	0.64%FS
416	Fluid T.	TW- 3	TE 416	A45 Tie Rod Pos.3	Fig.A.69	273. - 0.125E+04	K	0.64%FS
417	Fluid T.	TW- 4	TE 417	A45 Tie Rod Pos.4	Fig.A.69	273. - 0.125E+04	K	0.64%FS
418	Fluid T.	TW- 5	TE 418	A45 Tie Rod Pos.5	Fig.A.69	273. - 0.125E+04	K	0.64%FS
419	Fluid T.	TW- 6	TE 419	A45 Tie Rod Pos.6	Fig.A.69	273. - 0.125E+04	K	0.64%FS
420	Fluid T.	TW- 7	TE 420	A45 Tie Rod Pos.7	Fig.A.69	273. - 0.125E+04	K	0.64%FS
421	Fluid T.	TW- 8	TE 421	B45 Tie Rod Pos.1	Not Measured	273. - 0.125E+04	K	0.64%FS
422	Fluid T.	TW- 9	TE 422	B45 Tie Rod Pos.2	Not Measured	273. - 0.125E+04	K	0.64%FS
423	Fluid T.	TW-10	TE 423	B45 Tie Rod Pos.3	Not Measured	273. - 0.125E+04	K	0.64%FS
424	Fluid T.	TW-11	TE 424	B45 Tie Rod Pos.4	Not Measured	273. - 0.125E+04	K	0.64%FS
425	Fluid T.	TW-12	TE 425	B45 Tie Rod Pos.5	Not Measured	273. - 0.125E+04	K	0.64%FS
426	Fluid T.	TW-13	TE 426	B45 Tie Rod Pos.6	Not Measured	273. - 0.125E+04	K	0.64%FS
427	Fluid T.	TW-14	TE 427	B45 Tie Rod Pos.7	Not Measured	273. - 0.125E+04	K	0.64%FS
428	Fluid T.	TW-15	TE 428	C45 Tie Rod Pos.1	Fig.A.70	273. - 0.125E+04	K	0.64%FS
429	Fluid T.	TW-16	TE 429	C45 Tie Rod Pos.2	Fig.A.70	273. - 0.125E+04	K	0.64%FS
430	Fluid T.	TW-17	TE 430	C45 Tie Rod Pos.3	Fig.A.70	273. - 0.125E+04	K	0.64%FS
431	Fluid T.	TW-18	TE 431	C45 Tie Rod Pos.4	Fig.A.70	273. - 0.125E+04	K	0.64%FS
432	Fluid T.	TW-19	TE 432	C45 Tie Rod Pos.5	Fig.A.70	273. - 0.125E+04	K	0.64%FS
433	Fluid T.	TW-20	TE 433	C45 Tie Rod Pos.6	Fig.A.70	273. - 0.125E+04	K	0.64%FS
434	Fluid T.	TW-21	TE 434	C45 Tie Rod Pos.7	Fig.A.70	273. - 0.125E+04	K	0.64%FS
435	Fluid T.	TW-22	TE 435	D45 Tie Rod Pos.1	Not Measured	273. - 0.125E+04	K	0.64%FS
436	Fluid T.	TW-23	TE 436	D45 Tie Rod Pos.2	Not Measured	273. - 0.125E+04	K	0.64%FS
437	Fluid T.	TW-24	TE 437	D45 Tie Rod Pos.3	Not Measured	273. - 0.125E+04	K	0.64%FS
438	Fluid T.	TW-25	TE 438	D45 Tie Rod Pos.4	Not Measured	273. - 0.125E+04	K	0.64%FS
439	Fluid T.	TW-26	TE 439	D45 Tie Rod Pos.5	Not Measured	273. - 0.125E+04	K	0.64%FS
440	Fluid T.	TW-27	TE 440	D45 Tie Rod Pos.6	Not Measured	273. - 0.125E+04	K	0.64%FS
441	Fluid T.	TW-28	TE 441	D45 Tie Rod Pos.7	Not Measured	273. - 0.125E+04	K	0.64%FS
442	Fluid T.	TC- 1	TE 442	Channel Box A Inlet	Fig.A. 92	273. - 0.125E+04	K	0.64%FS
443	Fluid T.	TC- 2	TE 443	Channel Box B Inlet	Fig.A. 92	273. - 0.125E+04	K	0.64%FS
444	Fluid T.	TC- 3	TE 444	Channel Box C Inlet	Fig.A. 92	273. - 0.125E+04	K	0.64%FS
445	Fluid T.	TC- 4	TE 445	Channel Box D Inlet	Fig.A. 92	273. - 0.125E+04	K	0.64%FS
446	Fluid T.	TC- 5	TE 446	Channel Box Outlet A-1	Fig.A. 93	273. - 0.125E+04	K	0.64%FS
447	Fluid T.	TC- 6	TE 447	Channel Box Outlet A-2	Fig.A. 93	273. - 0.125E+04	K	0.64%FS
448	Fluid T.	TC- 7	TE 448	Channel Box Outlet A-3	Fig.A. 93	273. - 0.125E+04	K	0.64%FS
449	Fluid T.	TC- 8	TE 449	Channel Box Outlet A-4	Fig.A. 93	273. - 0.125E+04	K	0.64%FS
450	Fluid T.	TC- 9	TE 450	Channel Box Outlet A-6	Fig.A. 93	273. - 0.125E+04	K	0.64%FS

Table A.1 Measurement list for RUN 991 (Cont'd)

451Ch.- 500Ch.

Ch.	Item	Symbol	ID.	Location	Fig.No.	Range	Unit	Accuracy
451	Fluid T.	TC-10	TE 451	Channel Box Outlet C-1	Fig.A. 94	273. - 0.125E+04	K	0.64%FS
452	Fluid T.	TC-11	TE 452	Channel Box Outlet C-2	Fig.A. 94	273. - 0.125E+04	K	0.64%FS
453	Fluid T.	TC-12	TE 453	Channel Box Outlet C-3	Fig.A. 94	273. - 0.125E+04	K	0.64%FS
454	Fluid T.	TC-13	TE 454	Channel Box Outlet C-4	Fig.A. 94	273. - 0.125E+04	K	0.64%FS
455	Fluid T.	TC-14	TE 455	Channel Box Outlet C-6	Fig.A. 94	273. - 0.125E+04	K	0.64%FS
456	Fluid T.	TG- 1	TE 456	Upper Tieplate A Up.1	Fig.A. 95, 97	273. - 0.125E+04	K	0.64%FS
457	Fluid T.	TG- 2	TE 457	Upper Tieplate A Up.2	Not Measured	273. - 0.125E+04	K	0.64%FS
458	Fluid T.	TG- 3	TE 458	Upper Tieplate A Up.3	Not Measured	273. - 0.125E+04	K	0.64%FS
459	Fluid T.	TG- 4	TE 459	Upper Tieplate A Up.4	Fig.A. 95, 98	273. - 0.125E+04	K	0.64%FS
460	Fluid T.	TG- 5	TE 460	Upper Tieplate A Up.5	Not Measured	273. - 0.125E+04	K	0.64%FS
461	Fluid T.	TG- 6	TE 461	Upper Tieplate A Up.6	Not Measured	273. - 0.125E+04	K	0.64%FS
462	Fluid T.	TG- 7	TE 462	Upper Tieplate A Up.7	Not Measured	273. - 0.125E+04	K	0.64%FS
463	Fluid T.	TG- 8	TE 463	Upper Tieplate A Up.8	Not Measured	273. - 0.125E+04	K	0.64%FS
464	Fluid T.	TG- 9	TE 464	Upper Tieplate A Up.9	Not Measured	273. - 0.125E+04	K	0.64%FS
465	Fluid T.	TG-10	TE 465	Upper Tieplate A Up.10	Fig.A. 95, 99	273. - 0.125E+04	K	0.64%FS
466	Fluid T.	TG-11	TE 466	Upper Tieplate A Lo.1	Fig.A. 96, 97	273. - 0.125E+04	K	0.64%FS
467	Fluid T.	TG-12	TE 467	Upper Tieplate A Lo.2	Not Measured	273. - 0.125E+04	K	0.64%FS
468	Fluid T.	TG-13	TE 468	Upper Tieplate A Lo.3	Not Measured	273. - 0.125E+04	K	0.64%FS
469	Fluid T.	TG-14	TE 469	Upper Tieplate A Lo.4	Fig.A. 96, 98	273. - 0.125E+04	K	0.64%FS
470	Fluid T.	TG-15	TE 470	Upper Tieplate A Lo.5	Not Measured	273. - 0.125E+04	K	0.64%FS
471	Fluid T.	TG-16	TE 471	Upper Tieplate A Lo.6	Not Measured	273. - 0.125E+04	K	0.64%FS
472	Fluid T.	TG-17	TE 472	Upper Tieplate A Lo.7	Not Measured	273. - 0.125E+04	K	0.64%FS
473	Fluid T.	TG-18	TE 473	Upper Tieplate A Lo.8	Not Measured	273. - 0.125E+04	K	0.64%FS
474	Fluid T.	TG-19	TE 474	Upper Tieplate A Lo.9	Not Measured	273. - 0.125E+04	K	0.64%FS
475	Fluid T.	TG-20	TE 475	Upper Tieplate A Lo.10	Fig.A. 96, 99	273. - 0.125E+04	K	0.64%FS
476	Fluid T.	TG-21	TE 476	Upper Tieplate C Up.1	Fig.A.100,102	273. - 0.125E+04	K	0.64%FS
477	Fluid T.	TG-22	TE 477	Upper Tieplate C Up.2	Not Measured	273. - 0.125E+04	K	0.64%FS
478	Fluid T.	TG-23	TE 478	Upper Tieplate C Up.3	Not Measured	273. - 0.125E+04	K	0.64%FS
479	Fluid T.	TG-24	TE 479	Upper Tieplate C Up.4	Fig.A.100,103	273. - 0.125E+04	K	0.64%FS
480	Fluid T.	TG-25	TE 480	Upper Tieplate C Up.5	Not Measured	273. - 0.125E+04	K	0.64%FS
481	Fluid T.	TG-26	TE 481	Upper Tieplate C Up.6	Not Measured	273. - 0.125E+04	K	0.64%FS
482	Fluid T.	TG-27	TE 482	Upper Tieplate C Up.7	Not Measured	273. - 0.125E+04	K	0.64%FS
483	Fluid T.	TG-28	TE 483	Upper Tieplate C Up.8	Not Measured	273. - 0.125E+04	K	0.64%FS
484	Fluid T.	TG-29	TE 484	Upper Tieplate C Up.9	Not Measured	273. - 0.125E+04	K	0.64%FS
485	Fluid T.	TG-30	TE 485	Upper Tieplate C Up.10	Fig.A.100,104	273. - 0.125E+04	K	0.64%FS
486	Fluid T.	TG-31	TE 486	Upper Tieplate C Lo.1	Fig.A.101,102	273. - 0.125E+04	K	0.64%FS
487	Fluid T.	TG-32	TE 487	Upper Tieplate C Lo.2	Not Measured	273. - 0.125E+04	K	0.64%FS
488	Fluid T.	TG-33	TE 488	Upper Tieplate C Lo.3	Not Measured	273. - 0.125E+04	K	0.64%FS
489	Fluid T.	TG-34	TE 489	Upper Tieplate C Lo.4	Fig.A.101,103	273. - 0.125E+04	K	0.64%FS
490	Fluid T.	TG-35	TE 490	Upper Tieplate C Lo.5	Not Measured	273. - 0.125E+04	K	0.64%FS
491	Fluid T.	TG-36	TE 491	Upper Tieplate C Lo.6	Not Measured	273. - 0.125E+04	K	0.64%FS
492	Fluid T.	TG-37	TE 492	Upper Tieplate C Lo.7	Not Measured	273. - 0.125E+04	K	0.64%FS
493	Fluid T.	TG-38	TE 493	Upper Tieplate C Lo.8	Not Measured	273. - 0.125E+04	K	0.64%FS
494	Fluid T.	TG-39	TE 494	Upper Tieplate C Lo.9	Not Measured	273. - 0.125E+04	K	0.64%FS
495	Fluid T.	TG-40	TE 495	Upper Tieplate C Lo.10	Fig.A.101,104	273. - 0.125E+04	K	0.64%FS
496	Slab T.	TB- 1	TE 496	C.B. A1 Inner ,Pos.1	Not Measured	273. - 0.125E+04	K	0.64%FS
497	Slab T.	TB- 2	TE 497	C.B. A1 Inner ,Pos.2	Not Measured	273. - 0.125E+04	K	0.64%FS
498	Slab T.	TB- 3	TE 498	C.B. A1 Inner ,Pos.3	Not Measured	273. - 0.125E+04	K	0.64%FS
499	Slab T.	TB- 4	TE 499	C.B. A1 Inner ,Pos.4	Not Measured	273. - 0.125E+04	K	0.64%FS
500	Slab T.	TB- 5	TE 500	C.B. A1 Inner ,Pos.5	Not Measured	273. - 0.125E+04	K	0.64%FS

Table A.1 Measurement list for RUN 991 (Cont'd)

501Ch.- 550Ch.

Ch.	Item	Symbol	ID.	Location	Fig.No.	Range	Unit	Accuracy
501	Slab T.	TB- 6	TE 501	C.B. A1 Inner ,Pos.6	Not Measured	273. - 0.125E+04	K	0.64%FS
502	Slab T.	TB- 7	TE 502	C.B. A1 Inner ,Pos.7	Not Measured	273. - 0.125E+04	K	0.64%FS
503	Slab T.	TB- 8	TE 503	C.B. A2 Inner ,Pos.1	Not Measured	273. - 0.125E+04	K	0.64%FS
504	Slab T.	TB- 9	TE 504	C.B. A2 Inner ,Pos.2	Not Measured	273. - 0.125E+04	K	0.64%FS
505	Slab T.	TB-10	TE 505	C.B. A2 Inner ,Pos.3	Not Measured	273. - 0.125E+04	K	0.64%FS
506	Slab T.	TB-11	TE 506	C.B. A2 Inner ,Pos.4	Not Measured	273. - 0.125E+04	K	0.64%FS
507	Slab T.	TB-12	TE 507	C.B. A2 Inner ,Pos.5	Not Measured	273. - 0.125E+04	K	0.64%FS
508	Slab T.	TB-13	TE 508	C.B. A2 Inner ,Pos.6	Not Measured	273. - 0.125E+04	K	0.64%FS
509	Slab T.	TB-14	TE 509	C.B. A2 Inner ,Pos.7	Not Measured	273. - 0.125E+04	K	0.64%FS
510	Slab T.	TB-15	TE 510	C.B. B Inner ,Pos.1	Not Measured	273. - 0.125E+04	K	0.64%FS
511	Slab T.	TB-16	TE 511	C.B. B Inner ,Pos.2	Not Measured	273. - 0.125E+04	K	0.64%FS
512	Slab T.	TB-17	TE 512	C.B. B Inner ,Pos.3	Not Measured	273. - 0.125E+04	K	0.64%FS
513	Slab T.	TB-18	TE 513	C.B. B Inner ,Pos.4	Not Measured	273. - 0.125E+04	K	0.64%FS
514	Slab T.	TB-19	TE 514	C.B. B Inner ,Pos.5	Not Measured	273. - 0.125E+04	K	0.64%FS
515	Slab T.	TB-20	TE 515	C.B. B Inner ,Pos.6	Not Measured	273. - 0.125E+04	K	0.64%FS
516	Slab T.	TB-21	TE 516	C.B. B Inner ,Pos.7	Not Measured	273. - 0.125E+04	K	0.64%FS
517	Slab T.	TB-22	TE 517	C.B. C Inner ,Pos.1	Not Measured	273. - 0.125E+04	K	0.64%FS
518	Slab T.	TB-23	TE 518	C.B. C Inner ,Pos.2	Not Measured	273. - 0.125E+04	K	0.64%FS
519	Slab T.	TB-24	TE 519	C.B. C Inner ,Pos.3	Not Measured	273. - 0.125E+04	K	0.64%FS
520	Slab T.	TB-25	TE 520	C.B. C Inner ,Pos.4	Not Measured	273. - 0.125E+04	K	0.64%FS
521	Slab T.	TB-26	TE 521	C.B. C Inner ,Pos.5	Not Measured	273. - 0.125E+04	K	0.64%FS
522	Slab T.	TB-27	TE 522	C.B. C Inner ,Pos.6	Not Measured	273. - 0.125E+04	K	0.64%FS
523	Slab T.	TB-28	TE 523	C.B. C Inner ,Pos.7	Not Measured	273. - 0.125E+04	K	0.64%FS
524	Slab T.	TB-29	TE 524	C.B. D Inner ,Pos.1	Not Measured	273. - 0.125E+04	K	0.64%FS
525	Slab T.	TB-30	TE 525	C.B. D Inner ,Pos.2	Not Measured	273. - 0.125E+04	K	0.64%FS
526	Slab T.	TB-31	TE 526	C.B. D Inner ,Pos.3	Not Measured	273. - 0.125E+04	K	0.64%FS
527	Slab T.	TB-32	TE 527	C.B. D Inner ,Pos.4	Not Measured	273. - 0.125E+04	K	0.64%FS
528	Slab T.	TB-33	TE 528	C.B. D Inner ,Pos.5	Not Measured	273. - 0.125E+04	K	0.64%FS
529	Slab T.	TB-34	TE 529	C.B. D Inner ,Pos.6	Not Measured	273. - 0.125E+04	K	0.64%FS
530	Slab T.	TB-35	TE 530	C.B. D Inner ,Pos.7	Not Measured	273. - 0.125E+04	K	0.64%FS
531	Fluid T.	TB-36	TE 531	C.B. A Outer ,Pos.1	Fig.A.105	273. - 0.125E+04	K	0.64%FS
532	Fluid T.	TB-37	TE 532	C.B. A Outer ,Pos.2	Fig.A.105	273. - 0.125E+04	K	0.64%FS
533	Fluid T.	TB-38	TE 533	C.B. A Outer ,Pos.3	Fig.A.105	273. - 0.125E+04	K	0.64%FS
534	Fluid T.	TB-39	TE 534	C.B. A Outer ,Pos.4	Fig.A.105	273. - 0.125E+04	K	0.64%FS
535	Fluid T.	TB-40	TE 535	C.B. A Outer ,Pos.5	Fig.A.105	273. - 0.125E+04	K	0.64%FS
536	Fluid T.	TB-41	TE 536	C.B. A Outer ,Pos.6	Fig.A.105	273. - 0.125E+04	K	0.64%FS
537	Fluid T.	TB-42	TE 537	C.B. A Outer ,Pos.7	Fig.A.105	273. - 0.125E+04	K	0.64%FS
538	Fluid T.	TB-43	TE 538	C.B. C Outer ,Pos.1	Not Measured	273. - 0.125E+04	K	0.64%FS
539	Fluid T.	TB-44	TE 539	C.B. C Outer ,Pos.2	Not Measured	273. - 0.125E+04	K	0.64%FS
540	Fluid T.	TB-45	TE 540	C.B. C Outer ,Pos.3	Not Measured	273. - 0.125E+04	K	0.64%FS
541	Fluid T.	TB-46	TE 541	C.B. C Outer ,Pos.4	Not Measured	273. - 0.125E+04	K	0.64%FS
542	Fluid T.	TB-47	TE 542	C.B. C Outer ,Pos.5	Not Measured	273. - 0.125E+04	K	0.64%FS
543	Fluid T.	TB-48	TE 543	C.B. C Outer ,Pos.6	Not Measured	273. - 0.125E+04	K	0.64%FS
544	Fluid T.	TB-49	TE 544	C.B. C Outer ,Pos.7	Not Measured	273. - 0.125E+04	K	0.64%FS
545	Fluid T.	TP- 1	TE 545	Lower Pl. Center 1	Fig.A.106	273. - 0.125E+04	K	0.64%FS
546	Fluid T.	TP- 2	TE 546	Lower Pl. Center 2	Fig.A.106	273. - 0.125E+04	K	0.64%FS
547	Fluid T.	TP- 3	TE 547	Lower Pl. Center 3	Fig.A.106	273. - 0.125E+04	K	0.64%FS
548	Fluid T.	TP- 4	TE 548	Lower Pl. Center 4	Fig.A.106	273. - 0.125E+04	K	0.64%FS
549	Fluid T.	TP- 5	TE 549	Lower Pl. Center 5	Fig.A.106	273. - 0.125E+04	K	0.64%FS
550	Fluid T.	TP- 6	TE 550	Lower Pl. Center 7	Fig.A.106	273. - 0.125E+04	K	0.64%FS

Table A.1 Measurement list for RUN 991 (Cont'd)

551Ch.- 600Ch.

Ch.	Item	Symbol	ID.		Location	Fig.No.	Range			Unit	Accuracy
551	Slab T.	TP- 7	TE	551	Lower Pl. North 1	Not Measured	273.	-	0.125E+04	K	0.64%FS
552	Slab T.	TP- 8	TE	552	Lower Pl. North 2	Not Measured	273.	-	673.	K	0.64%FS
553	Slab T.	TP- 9	TE	553	Lower Pl. North 4	Not Measured	273.	-	673.	K	0.64%FS
554	Slab T.	TP-10	TE	554	Lower Pl. North 6	Not Measured	273.	-	673.	K	0.64%FS
555	Slab T.	TP-11	TE	555	Lower Pl. South 1	Not Measured	273.	-	673.	K	0.64%FS
556	Slab T.	TP-12	TE	556	Lower Pl. South 2	Not Measured	273.	-	673.	K	0.64%FS
557	Slab T.	TP-13	TE	557	Lower Pl. South 4	Not Measured	273.	-	673.	K	0.64%FS
558	Slab T.	TP-14	TE	558	Lower Pl. South 6	Not Measured	273.	-	673.	K	0.64%FS
559	Level	LB- 1	LM	559	C.B.Liquid Level A1-1	Not Measured					
560	Level	LB- 2	LM	560	C.B.Liquid Level A1-2	Not Measured					
561	Level	LB- 3	LM	561	C.B.Liquid Level A1-3	Not Measured					
562	Level	LB- 4	LM	562	C.B.Liquid Level A1-4	Not Measured					
563	Level	LB- 5	LM	563	C.B.Liquid Level A1-5	Not Measured					
564	Level	LB- 6	LM	564	C.B.Liquid Level A1-6	Not Measured					
565	Level	LB- 7	LM	565	C.B.Liquid Level A1-7	Not Measured					
566	Level	LB- 8	LM	566	C.B.Liquid Level A2-1	Fig.A.107					
567	Level	LB- 9	LM	567	C.B.Liquid Level A2-2	Fig.A.107					
568	Level	LB-10	LM	568	C.B.Liquid Level A2-3	Fig.A.107					
569	Level	LB-11	LM	569	C.B.Liquid Level A2-4	Fig.A.107					
570	Level	LB-12	LM	570	C.B.Liquid Level A2-5	Fig.A.107					
571	Level	LB-13	LM	571	C.B.Liquid Level A2-6	Fig.A.107					
572	Level	LB-14	LM	572	C.B.Liquid Level A2-7	Fig.A.107					
573	Level	LB-15	LM	573	C.B.Liquid Level B-1	Fig.A.108					
574	Level	LB-16	LM	574	C.B.Liquid Level B-2	Fig.A.108					
575	Level	LB-17	LM	575	C.B.Liquid Level B-3	Fig.A.108					
576	Level	LB-18	LM	576	C.B.Liquid Level B-4	Fig.A.108					
577	Level	LB-19	LM	577	C.B.Liquid Level B-5	Fig.A.108					
578	Level	LB-20	LM	578	C.B.Liquid Level B-6	Fig.A.108					
579	Level	LB-21	LM	579	C.B.Liquid Level B-7	Fig.A.108					
580	Level	LB-22	LM	580	C.B.Liquid Level C-1	Failure					
581	Level	LB-23	LM	581	C.B.Liquid Level C-2	Fig.A.109					
582	Level	LB-24	LM	582	C.B.Liquid Level C-3	Fig.A.109					
583	Level	LB-25	LM	583	C.B.Liquid Level C-4	Failure					
584	Level	LB-26	LM	584	C.B.Liquid Level C-5	Fig.A.109					
585	Level	LB-27	LM	585	C.B.Liquid Level C-6	Fig.A.109					
586	Level	LB-28	LM	586	C.B.Liquid Level C-7	Fig.A.109					
587	Level	LB-29	LM	587	C.B.Liquid Level D-1	Not Measured					
588	Level	LB-30	LM	588	C.B.Liquid Level D-2	Not Measured					
589	Level	LB-31	LM	589	C.B.Liquid Level D-3	Not Measured					
590	Level	LB-32	LM	590	C.B.Liquid Level D-4	Not Measured					
591	Level	LB-33	LM	591	C.B.Liquid Level D-5	Not Measured					
592	Level	LB-34	LM	592	C.B.Liquid Level D-6	Not Measured					
593	Level	LB-35	LM	593	C.B.Liquid Level D-7	Not Measured					
594	Level	LL- 1	LM	594	Ch.Box Outlet A1-5	Not Measured					
595	Level	LL- 2	LM	595	Ch.Box Outlet A1-6	Not Measured					
596	Level	LL- 3	LM	596	Ch.Box Outlet A1-7	Not Measured					
597	Level	LL- 4	LM	597	Ch.Box Outlet A2-5	Fig.A.110					
598	Level	LL- 5	LM	598	Ch.Box Outlet A2-6	Fig.A.110					
599	Level	LL- 6	LM	599	Ch.Box Outlet A2-7	Fig.A.110					
600	Level	LL- 7	LM	600	Ch.Box Outlet A-1	Fig.A.111					

Table A.1 Measurement list for RUN 991 (Cont'd)

601Ch.- 650Ch.

Ch.	Item	Symbol	ID.		Location	Fig.No.	Range	Unit	Accuracy
601	Level	LL- 8	LM	601	Ch.Box Outlet A-2	Not Measured			
602	Level	LL- 9	LM	602	Ch.Box Outlet A-3	Fig.A.111			
603	Level	LL-10	LM	603	Ch.Box Outlet A-4	Fig.A.111			
604	Level	LL-11	LM	604	Ch.Box Outlet A-6	Not Measured			
605	Level	LL-12	LM	605	Ch.Box Outlet C1-5				
606	Level	LL-13	LM	606	Ch.Box Outlet C1-6	Failure			
607	Level	LL-14	LM	607	Ch.Box Outlet C1-7	Fig.A.112			
608	Level	LL-15	LM	608	Ch.Box Outlet C2-5	Not Measured			
609	Level	LL-16	LM	609	Ch.Box Outlet C2-6	Not Measured			
610	Level	LL-17	LM	610	Ch.Box Outlet C2-7	Not Measured			
611	Level	LL-18	LM	611	Ch.Box Outlet C-1	Fig.A.113			
612	Level	LL-19	LM	612	Ch.Box Outlet C-2	Fig.A.113			
613	Level	LL-20	LM	613	Ch.Box Outlet C-3	Fig.A.113			
614	Level	LL-21	LM	614	Ch.Box Outlet C-4	Fig.A.113			
615	Level	LL-22	LM	615	Ch.Box Outlet C-6	Fig.A.113			
616	Level	LL-23	LM	616	Ch.Box Inlet A-1	Fig.A.114			
617	Level	LL-24	LM	617	Ch.Box Inlet A-2	Fig.A.114			
618	Level	LL-25	LM	618	Ch.Box Inlet B-1	Not Measured			
619	Level	LL-26	LM	619	Ch.Box Inlet B-2	Not Measured			
620	Level	LL-27	LM	620	Ch.Box Inlet C-1	Fig.A.115			
621	Level	LL-28	LM	621	Ch.Box Inlet C-2	Fig.A.115			
622	Level	LL-29	LM	622	Ch.Box Inlet D-1	Not Measured			
623	Level	LL-30	LM	623	Ch.Box Inlet D-2	Not Measured			
624	Level	LL-31	LM	624	Lower Pl. North 1	Fig.A.116			
625	Level	LL-32	LM	625	Lower Pl. North 2	Fig.A.116			
626	Level	LL-33	LM	626	Lower Pl. North 3	Fig.A.116			
627	Level	LL-34	LM	627	Lower Pl. North 4	Failure			
628	Level	LL-35	LM	628	Lower Pl. North 5	Fig.A.116			
629	Level	LL-36	LM	629	Lower Pl. North 6	Fig.A.116			
630	Level	LL-37	LM	630	Lower Pl. South 1	Not Measured			
631	Level	LL-38	LM	631	Lower Pl. South 2	Not Measured			
632	Level	LL-39	LM	632	Lower Pl. South 3	Not Measured			
633	Level	LL-40	LM	633	Lower Pl. South 4	Not Measured			
634	Level	LL-41	LM	634	Lower Pl. South 5	Not Measured			
635	Level	LL-42	LM	635	Lower Pl. South 6	Not Measured			
636	Level	LL-43	LM	636	Guide Tube North 0	Fig.A.117			
637	Level	LL-44	LM	637	Guide Tube North 1	Fig.A.117			
638	Level	LL-45	LM	638	Guide Tube North 3	Fig.A.117			
639	Level	LL-46	LM	639	Guide Tube North 6	Fig.A.117			
640	Level	LL-47	LM	640	Guide Tube South 0	Not Measured			
641	Level	LL-48	LM	641	Guide Tube South 1	Not Measured			
642	Level	LL-49	LM	642	Guide Tube South 3	Not Measured			
643	Level	LL-50	LM	643	Guide Tube South 6	Not Measured			
644	Level	L- 1	LM	644	Downcomer D-Side 1	Fig.A.118			
645	Level	L- 2	LM	645	Downcomer D-Side 2	Fig.A.118			
646	Level	L- 3	LM	646	Downcomer D-Side 3	Fig.A.118			
647	Level	L- 4	LM	647	Downcomer D-Side 4	Fig.A.118			
648	Level	L- 5	LM	648	Downcomer D-Side 5	Failure			
649	Level	L- 6	LM	649	Downcomer B-Side 1	Not Measured			
650	Level	L- 7	LM	650	Downcomer B-Side 2	Not Measured			

Table A.1 Measurement list for RUN 991 (Cont'd)

651Ch.- 700Ch.

Ch.	Item	Symbol	ID.		Location	Fig.No.	Range			Unit	Accuracy
651	Level	L- 8	LM	651	Downcomer B-Side 3	Not Measured					
652	Level	L- 9	LM	652	Downcomer B-Side 4	Not Measured					
653	Level	L-10	LM	653	Downcomer B-Side 5	Not Measured					
654	Void	VF- 1	VD	654	A54 Tie Rod Pos.1	Not Measured	0.0	-	1.00		
655	Void	VF- 2	VD	655	A54 Tie Rod Pos.2	Not Measured	0.0	-	1.00		
656	Void	VF- 3	VD	656	A54 Tie Rod Pos.3	Not Measured	0.0	-	1.00		
657	Void	VF- 4	VD	657	A54 Tie Rod Pos.4	Not Measured	0.0	-	1.00		
658	Void	VF- 5	VD	658	A54 Tie Rod Pos.5	Not Measured	0.0	-	1.00		
659	Void	VF- 6	VD	659	A54 Tie Rod Pos.6	Not Measured	0.0	-	1.00		
660	Void	VF- 7	VD	660	A54 Tie Rod Pos.7	Not Measured	0.0	-	1.00		
661	Void	VF- 8	VD	661	B54 Tie Rod Pos.1	Not Measured	0.0	-	1.00		
662	Void	VF- 9	VD	662	B54 Tie Rod Pos.2	Not Measured	0.0	-	1.00		
663	Void	VF-10	VD	663	B54 Tie Rod Pos.3	Not Measured	0.0	-	1.00		
664	Void	VF-11	VD	664	B54 Tie Rod Pos.4	Not Measured	0.0	-	1.00		
665	Void	VF-12	VD	665	B54 Tie Rod Pos.5	Not Measured	0.0	-	1.00		
666	Void	VF-13	VD	666	B54 Tie Rod Pos.6	Not Measured	0.0	-	1.00		
667	Void	VF-14	VD	667	B54 Tie Rod Pos.7	Not Measured	0.0	-	1.00		
668	Void	VF-15	VD	668	C54 Tie Rod Pos.1	Not Measured	0.0	-	1.00		
669	Void	VF-16	VD	669	C54 Tie Rod Pos.2	Not Measured	0.0	-	1.00		
670	Void	VF-17	VD	670	C54 Tie Rod Pos.3	Not Measured	0.0	-	1.00		
671	Void	VF-18	VD	671	C54 Tie Rod Pos.4	Not Measured	0.0	-	1.00		
672	Void	VF-19	VD	672	C54 Tie Rod Pos.5	Not Measured	0.0	-	1.00		
673	Void	VF-20	VD	673	C54 Tie Rod Pos.6	Not Measured	0.0	-	1.00		
674	Void	VF-21	VD	674	C54 Tie Rod Pos.7	Not Measured	0.0	-	1.00		
675	Void	VF-22	VD	675	D54 Tie Rod Pos.7	Not Measured	0.0	-	1.00		
676	Void	VF-23	VD	676	D54 Tie Rod Pos.7	Not Measured	0.0	-	1.00		
677	Void	VF-24	VD	677	D54 Tie Rod Pos.7	Not Measured	0.0	-	1.00		
678	Void	VF-25	VD	678	D54 Tie Rod Pos.7	Not Measured	0.0	-	1.00		
679	Void	VF-26	VD	679	D54 Tie Rod Pos.7	Not Measured	0.0	-	1.00		
680	Void	VF-27	VD	680	D54 Tie Rod Pos.7	Not Measured	0.0	-	1.00		
681	Void	VF-28	VD	681	D54 Tie Rod Pos.7	Not Measured	0.0	-	1.00		
682	Void	VE- 1	VD	682	Channel A Outlet 1	Not Measured	0.0	-	1.00		
683	Void	VE- 2	VD	683	Channel A Outlet 2	Not Measured	0.0	-	1.00		
684	Void	VE- 3	VD	684	Channel A Outlet 3	Not Measured	0.0	-	1.00		
685	Void	VE- 4	VD	685	Channel B Outlet 1	Not Measured	0.0	-	1.00		
686	Void	VE- 5	VD	686	Channel B Outlet 2	Not Measured	0.0	-	1.00		
687	Void	VE- 6	VD	687	Channel B Outlet 3	Not Measured	0.0	-	1.00		
688	Void	VE- 7	VD	688	Channel C Outlet 1	Not Measured	0.0	-	1.00		
689	Void	VE- 8	VD	689	Channel C Outlet 2	Not Measured	0.0	-	1.00		
690	Void	VE- 9	VD	690	Channel C Outlet 3	Not Measured	0.0	-	1.00		
691	Void	VE-10	VD	691	Channel D Outlet 1	Not Measured	0.0	-	1.00		
692	Void	VE-11	VD	692	Channel D Outlet 2	Not Measured	0.0	-	1.00		
693	Void	VE-12	VD	693	Channel D Outlet 3	Not Measured	0.0	-	1.00		
694	Void	VE-13	VD	694	Lower Plenum Bottom 1	Not Measured	0.0	-	1.00		
695	Void	VE-14	VD	695	Lower Plenum Bottom 2	Not Measured	0.0	-	1.00		
696	Void	VE-15	VD	696	Lower Plenum Bottom 3	Not Measured	0.0	-	1.00		
697	Void	VP- 1	VD	697	Lower Plenum Inlet	Not Measured	0.0	-	1.00		
698	Void	VP- 2	VD	698	Lower Plenum Inlet	Not Measured	0.0	-	1.00		

Table A.2 Calculated Data in RUN 991

No.	Item	Symbol	Location	Fig. No.	Unit
1	Density	DE 701	JP1,2 Outlet, Average	NU	kg/m^3
2	Density	DE 702	JP3,4 Outlet, Average	NU	kg/m^3
3	Density	DE 703	MRP-Side Break, Average	A.119	kg/m^3
4	Density	DE 704	PV-Side loop, Average		kg/m^3
5	Flow Rate	FM 705	MRP-Side Break, (Low)	A.120	kg/s
6	Flow Rate	FM 706	PV-Side Break, (Low)	NU	kg/s
7	Flow Rate	FM 707	MRP-Side Break, (High)	A.121	kg/s
8	Flow Rate	FM 708	PV-Side Break, (High)	NU	kg/s
9	Flow Rate	FM 709	Total Break Flow (Low)	NU	kg/s
10	Flow Rate	FM 710	Total Break Flow (High)	NU	kg/s
11	Flow Rate	FM 711	Steam Flow (Low)	A.122	kg/s
12	Flow Rate	FM 712	Steam Flow (High)	A.122	kg/s
13	Flow Rate	FM 713	Steam Flow (Middle)	A.122	kg/s
14	Flow Rate	FM 714	Channel A Inlet	A.123	kg/s
15	Flow Rate	FM 715	Channel B Inlet	A.124	kg/s
16	Flow Rate	FM 716	Channel C Inlet	A.125	kg/s
17	Flow Rate	FM 717	Channel D Inlet	A.126	kg/s
18	Flow Rate	FM 718	Bypass Hole Flow	A.127	kg/s
19	Flow Rate	FM 719	Total Core Flow	A.128	kg/s
20	Flow Rate	FM 720	JP1 Outlet (Pos. Flow)	A.129	kg/s
21	Flow Rate	FM 721	JP2 Outlet (Pos. Flow)	A.129	kg/s
22	Flow Rate	FM 722	JP3 Outlet (Pos. Flow)	A.130	kg/s
23	Flow Rate	FM 723	JP3 Outlet (Neg. Flow)	A.131	kg/s
24	Flow Rate	FM 724	JP4 Outlet (Pos. Flow)	A.130	kg/s
25	Flow Rate	FM 725	JP4 Outlet (Neg. FLow)	A.131	kg/s
26	Flow Rate	FM 726	Total JP Outlet Flow	A.132	kg/s
27	Water Level	LM 727	Collapsed DC Level	A.133	m
28	Water Level	LM 728	Collapsed In-Shroud Level	A.134	m
29	Fluid Mass	EV 729	Downcomer Mass	A.135	kg
30	Fluid Mass	EV 730	In-Shroud Mass	A.136	kg
31	Fluid Mass	EV 731	Total Mass in PV	A.137	kg
32	Fluid Mass	EV 732	Mass Balance in PV		kg
33	Fluid Mass	EV 733	Discharged Mass		kg
34	Flow Rate	FM 734	Discharged Flow Rate		kg/s
35	Flow Rate	FM 735	Discharged Flow Rate		kg/s

Table A.3 Core Instrumentation List

Item	Pos. / DL / Rod NO.	Core Outlet	Pos.1	Pos.2	Pos.3	Pos.4	Pos.5	Pos.6	Pos.7	Core Inlet
		3660	3417	3114.5	2879.5	2527	2174.5	1939.5	1637	1454
Surface Temp.	A11		TF 1	TF 2	TF 3	TF 4	TF 5	TF 6	TF 7	
	A12		TF 8	TF 9	TF 10	TF 11	TF 12	TF 13	TF 14	
	A13		TF 15	TF 16	TF 17	TF 18	TF 19	TF 20	TF 21	
	A14		TF 22	TF 23	TF 24	TF 25	TF 26	TF 27	TF 28	
	A15		TF 29			TF 30				
	A17		TF 31			TF 32				
	A22		TF 33	TF 34	TF 35	TF 36	TF 37	TF 38	TF 39	
	A23		TF 40	TF 41	TF 42	TF 43	TF 44	TF 45	TF 46	
	A24		TF 47	TF 48	TF 49	TF 50	TF.51	TF 52	TF 53	
	A26		TF 54			TF 55				
	A28		TF 56			TF 57				
	A31		TF 58			TF 59				
	A33		TF 60	TF 61	TF 62	TF 63	TF 64	TF 65	TF 66	
	A34		TF 67	TF 68	TF 69	TF 70	TF 71	TF 72	TF 73	
	A35		TF 74			TF 75				
	A37		TF 76			TF 77				
	A42		TF 78			TF 79				
Fluid Temp.	A44	TC 1	TF180	TF181	TF182	TF183	TF184	TF185	TF186	TC 2
Surface Temp.	A45		TF 80			TF 81				
	A46		TF 82			TF 83				
	A48		TF 84			TF 85				
	A51		TF 86			TF 87				
	A53		TF 88			TF 89				
	A54		TF 90							
	A57		TF 91			TF 92				
	A62		TF 93			TF 94				
	A64		TF 95			TF 96				
	A66		TF 97			TF 98				
	A68		TF 99			TF100				
	A71		TF101			TF102				
	A73		TF103			TF104				
	A75		TF105			TF106				
	A77		TF107			TF108				

Table A.3 Core Instrumentation List (Cont'd)

Item	Pos. / DL / Rod NO.	Core Outlet	Pos.1	Pos.2	Pos.3	Pos.4	Pos.5	Pos.6	Pos.7	Core Inlet
		3660	3417	3114.5	2879.5	2527	2174.5	1939.5	1637	1454
Surface Temp.	A82		TF109			TF110				
	A84		TF111			TF112				
	A86		TF113			TF114				
	A88		TF115			TF116				
	B11					TF117				
	B13					TF118				
	B15		TF119	TF120	TF121	TF122	TF123	TF124	TF125	
	B31					TF126				
	B33					TF127				
	B35					TF128				
Fluid Temp.	B44	TC 3	TF187	TF188	TF189	TF190	TF191	TF192	TF193	TC 4
Surface Temp.	B51					TF129				
	B53					TF130				
	B85		TF131	TF132	TF133	TF134	TF135	TF136	TF137	
	C11					TF138				
	C13					TF139				
	C15					TF140				
	C31					TF141				
	C33		TF142	TF143	TF144	TF145	TF146	TF147	TF148	
	C35					TF149				
Fluid Temp.	C44	TC 5	TF194	TF195	TF196	TF197	TF198	TF199	TF200	TC 6
Surface Temp.	C51					TF150				
	C53					TF151				
	C77		TF152	TF153	TF154	TF155	TF156	TF157	TF158	
	D11					TF159				
	D13					TF160				
	D27		TF161	TF162	TF163	TF164	TF165	TF166	TF167	
	D31					TF168				
	D33					TF169				
	D35					TF170				
Fluid Temp.	D44	TC 7	TF201	TF202	TF203	TF204	TF205	TF206	TF207	TC 8
Surface Temp.	D51					TF171				
	D53					TF172				
	D88		TF173	TF174	TF175	TF176	TF177	TF178	TF179	

Table A.3 Core Instrumentation List (Cont'd)

Item	Pos. / DL / Rod NO.	Core Outlet	Pos.1	Pos.2	Pos.3	Pos.4	Pos.5	Pos.6	Pos.7	Core Inlet
		3660	3417	3114.5	2879.5	2527	2174.5	1939.5	1673	1454
Void	A55		VF 1	VF 2	VF 3	VF 4	VF 5	VF 6	VF 7	
	B55		VF 8	VF 9	VF 10	VF 11	VF 12	VF 13	VF 14	
	C55		VF 15	VF 16	VF 17	VF 18	VF 19	VF 20	VF 21	
	D55		VF 22	VF 23	VF 24	VF 25	VF 26	VF 27	VF 28	
Channel Box Surface Temp.	A1*		TB 1	TB 2	TB 3	TB 4	TB 5	TB 6	TB 7	
	A2*		TB 8	TB 9	TB 10	TB 11	TB 12	TB 13	TB 14	
	B*		TB 15	TB 16	TB 17	TB 18	TB 19	TB 20	TB 21	
	C*		TB 22	TB 23	TB 24	TB 25	TB 26	TB 27	TB 28	
	D*		TB 29	TB 30	TB 31	TB 32	TB 33	TB 34	TB 35	
Liquid Level in the Channel Box	A1*		LB 1	LB 2	LB 3	LB 4	LB 5	LB 6	LB 7	
	A2*		LB 8	LB 9	LB 10	LB 11	LB 12	LB 13	LB 14	
	B*		LB 15	LB 16	LB 17	LB 18	LB 19	LB 20	LB 21	
	C*		LB 22	LB 23	LB 24	LB 25	LB 26	LB 27	LB 28	
	D*		LB 29	LB 30	LB 31	LB 32	LB 33	LB 34	LB 35	

Appendix II Data Processing and Experiment Data for RUN 991

List of Figures of Experiment Data for RUN 991 (Appendix II)

Data Processing and Experiment Data for RUN 991

In Appendix II, most of the measured data of RUN 991 and their data processing methods are shown. Some of the experiment data are also shown in Chapters 5 and 6. The data acquisition frequency was 10 Hz. The test data were processed and reduced to 1000 data points in each data channel for computer plotting.

The test data of RUN 991 are shown in Figs. A.1 through A.137. In these figures, the measured quantity is identified by the channel number and the alphabetic characters (ref. Table A.1).

(1) Experiment Data of RUN 991

Figures A.1 through A.4 show the pressure data in the pressure vessel (PV) and recirculation loops. Figures A.5 through A.25 show differential pressure data between various positions in the pressure vessel and the recirculation loops. Figures A.26 and A.27 show the liquid levels in the ECCS tank and downcomer. Figures A.28 through A.33 show flow rates at the main steam line (MSL), feedwater, jet pump discharge flows and recirculation line flows. The pump speed of the recirculation pump is shown in Fig.A.34. The trip signals such as the break initiation signal and the valve positioning signals are shown in Figs. A.35 through A.37. Figures A.38 through A.41 show the fluid densities measured by the gamma densitometer at the break unit and the single-ended recirculation loop. The fluid density data at the break unit are corrected at two known points, one is the initial condition and another is a steam-phase condition or a water single phase condition and are used for calculation of the average fluid density (see Fig.A.119). However, the density data of DE 128 and DE 129 in Figs.A.40 and A.41 are not corrected and can be used as only the qualitative data to show the flashing initiation timing in the recirculation loop.

Figures A.42 through A.45 show momentum fluxes measured by drag-disks at the break unit and the PV-side of the single-ended recirculation loop. The drag-disk data are similarly corrected as the fluid density at two

known points, one is the initial condition, in which the volumetric flow rate for the initial water flow is known, and another one is the final test condition, in which the recirculation flow was terminated by closing the QSV after the end of test period. Figures A.46 through A.54 show the fluid temperatures at various positions in the system. The surface temperatures of heater rods and water rods are measured at positions 1 through 7 as given in Figs. A.55 through A.70.

Figures A.71 through A.91 show the heater rod temperatures in the common vertical axis. Figures A.92 through A.94 show the fluid temperatures at both outlet and inlet of the channel boxes. The fluid temperatures above and below the upper tieplate (UTP) in both A and C channels are shown in Figs.A.95 through A.104 (thermocouple locations of these are shown in Fig.3.6). The channel box surface temperatures on the outer wall are compared each other in Fig.A.105. Fluid temperatures in the lower plenum are compared in Fig.A.106. The liquid level signals in the core, the upper and lower plena, the guide tube and the downcomer are shown in Figs. A.107 through A.118.

Quantities reduced from the test data are shown in Figs. A.119 through A.139. The average density of Fig.A.119 is calculated as an arithmetic mean of the densities in multi-directions with the weight of each cord length (ref. Figs.A.38 and A.39).

For the three-beam densitometer at the jet pump outlet spool (these are not used in RUN 991),

$$\rho_{av} = 0.3221\rho_A + 0.43\rho_B + 0.2479\rho_C \qquad (A.1)$$

where,

ρ_{av}: average density obtained from the three-beam gamma densitometer,

ρ_A : density measured by beam A (bottom),

ρ_B : density measured by beam B (middle).

ρ_C : density measured by beam C (top).

For the two-beam densitometer at the break spool piece,

$$\rho_{av} = 0.5863\rho_A + 0.4137\rho_B \qquad (A.2)$$

where,

ρ_{av}: average density obtained from the two-beam gamma densitometer,

ρ_A : density measured by beam A (bottom),

ρ_B : density measured by beam B (top).

Figures A.120 and A.121 show flow rates measured by the low and high-range drag-disks. The flow rates are computed from the drag-disk data and the gamma densitometer data by using the following equation,

$$G = C_D \cdot A \cdot \sqrt{\rho_{av} \cdot \rho V^2} \qquad (A.3)$$

where,

G : mass flow rate,

C_D : drag coefficient (= 1.13),

A : flow area (= 1.923×10^{-3} m^2),

ρ_{av} : average density from gamma densitometer,

ρV^2 : momentum flux from drag disk.

The fluid flow rates at the main steam line, channel inlet orifices, bypass hole and jet pump outlets shown in Figs.A.122 through A.132 are calculated from the test data which are the pressure drop across the orifices or venturi flow meters and the liquid density obtained from the temperature and the pressure condition. The equation used for the calculation is as follows :

$$G = C_D \cdot A \cdot \sqrt{2g \cdot \rho_l \cdot \Delta P} \qquad (A.4)$$

where,

G : flow rate,

ΔP : pressure drop across the orifice,

C_D : discharge coefficient,

= 0.6552 (the orifice to measure the steam discharge flow rate)

= 0.4761 (the channel inlet orifice)

= 0.8032 (the bypass hole)

= 0.7383 (the orifice to measure jet pump outlet flow)

= 1.1260 (the venturi to measure jet pump outlet flow)

A : flow area (m^2)

= 2.875×10^{-3} (the orifice to measure the steam discharge flow rate)

= 1.521×10^{-3} (the channel inlet orifice)

= 1.758×10^{-4} (the bypass hole)

$= 1.133 \times 10^{-3}$ (the jet pump outlet orifice)
$= 9.095 \times 10^{-4}$ (the jet pump outlet venturi)

g : gravitational acceleration ($= 9.807$ m/s^2),
ρ_l : density of the single-phase liquid (kg/m^3).

This calculation method is not applicable for two-phase flow condition after the LPF initiation at the channel inlet orifice and the bypass hole. Those calculated values show only a trend in two-phase flow condition. Total channel inlet flow rate presents the sum of four channel inlet flow rates and a bypass hole flow rate.

Figures A.133 and A.134 show the collapsed water levels in downcomer and inside the core-shroud, respectively. Each level is obtained from the corresponding differential pressure. The differential pressure may include the flow resistance effect, however, the flow resistance becomes negligible after slowdown of the recirculation pump speed and lower plenum flashing.

Figure A.135 shows the fluid mass inventory in downcomer. The fluid mass inventory is determined from the density and configurational data outside the core shroud,

$$M = \rho_l \cdot Q \qquad (A.5)$$

where,

M : fluid inventory,
ρ_l : liquid density estimated from the satulation temperature and/or pressure,
Q : liquid volume calculated from the liquid level.

The volume Q (m^3) inside the shroud is also given as a function of collapsed water level in downcomer (L),

$$\begin{aligned}
Q &= 0.0 && (L \leqq 0.494) \\
Q &= 0.0225L - 0.0111 && (0.494 < L \leqq 1.384) \\
Q &= 0.0697L - 0.0769 && (1.384 < L \leqq 1.519) \\
Q &= 0.0225L - 0.0048 && (1.519 < L \leqq 3.355) \\
Q &= 0.0801L - 0.1980 && (3.355 < L \leqq 4.250) \\
Q &= 0.2443L - 0.8959 && (4.250 < L \leqq 4.413) \qquad (A.6)
\end{aligned}$$

$$Q = 0.2611L - 0.9700 \quad (4.413 < L \leqq 4.578)$$
$$Q = 0.2504L - 0.9211 \quad (4.578 < L \leqq 4.654)$$
$$Q = 0.2375L - 0.8610 \quad (4.654 < L \leqq 4.815)$$
$$Q = 0.2866L - 1.0974 \quad (4.815 < L \leqq 4.915)$$
$$Q = 0.3396L - 1.3580 \quad (4.915 < L \leqq 5.143)$$
$$Q = 0.3607L - 1.4665 \quad (5.143 < L \leqq 5.365)$$
$$Q = 0.3848L - 1.5960 \quad (5.365 < L \leqq 5.995)$$
$$Q = 0.7111 \quad (5.995 < L)$$

Figure A.136 shows the fluid mass inventory inside core shroud. The fluid mass inventory is determined from the density and configurational data inside the core-shroud,

$$M = \rho_l \cdot Q \tag{A.7}$$

where,

M : fluid inventory,

ρ_l : liquid density estimated from the saturation temperature and/or pressure,

Q : liquid volume calculated from the liquid level.

The volume Q (m^3) inside the shroud is also given as a function of collapsed water level inside core-shroud (L),

$$\begin{aligned}
Q &= 0.0 && (L \leqq 0.0) \\
Q &= 0.2350L && (0.0 < L \leqq 0.497) \\
Q &= 0.1245L + 0.0549 && (0.497 < L \leqq 1.354) \\
Q &= 0.0698L + 0.1290 && (1.354 < L \leqq 3.589) \\
Q &= 0.1648L - 0.2120 && (3.589 < L \leqq 3.744) \\
Q &= 0.1963L - 0.3299 && (3.744 < L \leqq 4.243) \\
Q &= 0.0196L + 0.4199 && (4.243 < L \leqq 4.578) \\
Q &= 0.0186L + 0.4244 && (4.578 < L \leqq 4.654) \\
Q &= 0.0410L + 0.3201 && (4.654 < L \leqq 5.099) \\
Q &= 0.0196L + 0.4292 && (5.099 < L \leqq 5.365) \\
Q &= 0.5344 && (5.365 < L)
\end{aligned} \tag{A.8}$$

Figure A.137 shows a total fluid inventory in PV, which is a sum of fluid mass in downcomer (see Fig. A.135) and inside core-shroud (see Fig. A.136).

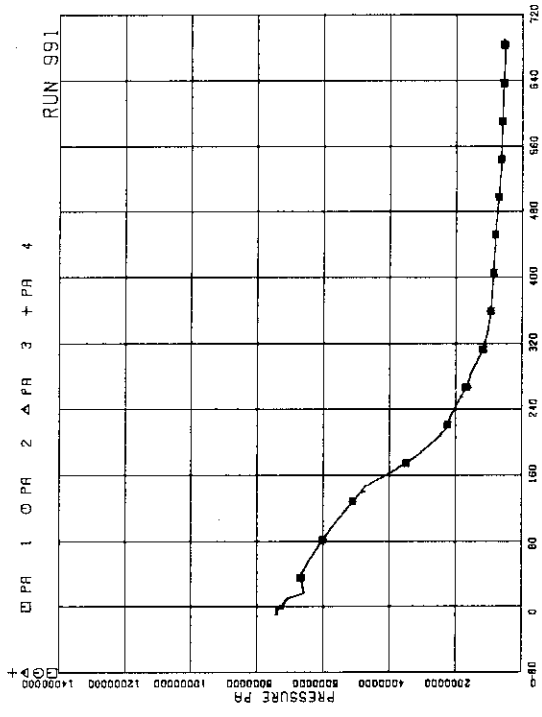

FIG.A. 1 PRESSURE IN PV (PRESSURE VESSEL)

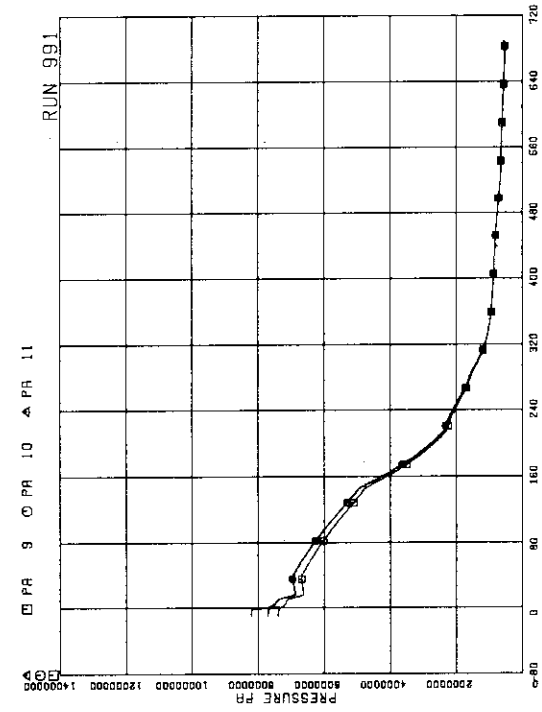

FIG.A. 2 PRESSURE IN BROKEN LOOP JP (JET PUMP)

FIG.A. 3 PRESSURE NEAR MRP (MAIN RECIRCULATION PUMP)

FIG.A. 4 PRESSURE AT JP SIDE OF BREAK

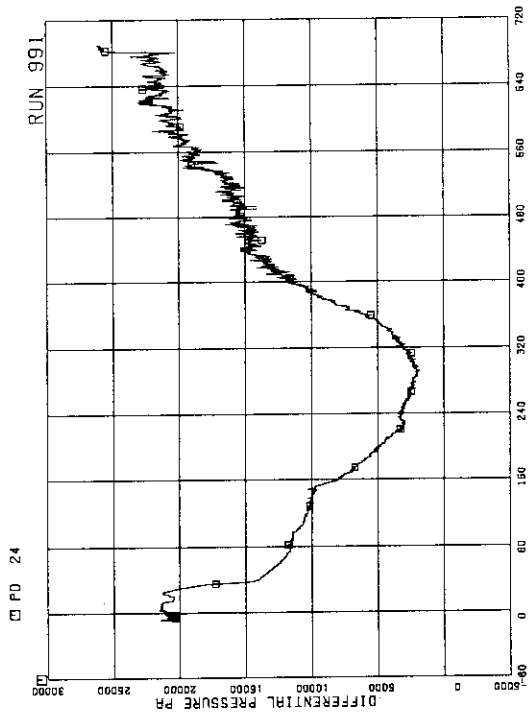

FIG.A. 5 DC (DOWNCOMER) HEAD

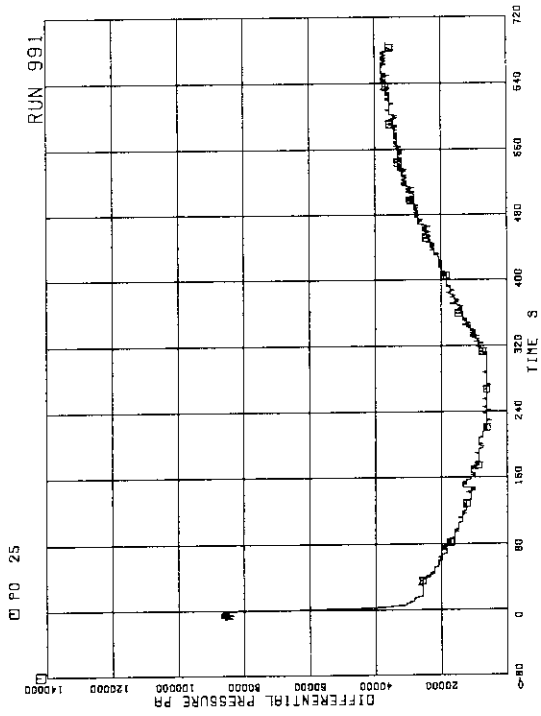

FIG.A. 6 DIFFERENTIAL PRESSURE BETWEEN PV BOTTOM AND TOP

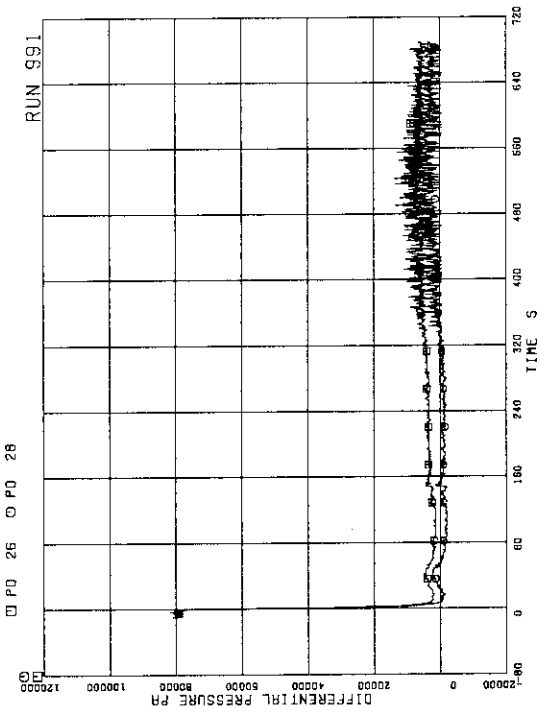

FIG.A. 7 DIFFERENTIAL PRESSURE BETWEEN JP-1.2 DISCHARGE AND SUCTION

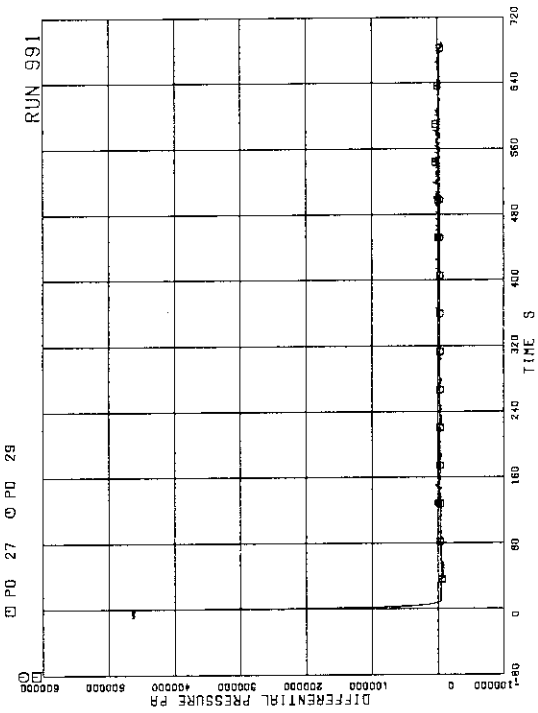

FIG.A. 8 DIFFERENTIAL PRESSURE BETWEEN JP-1.2 DRIVE AND SUCTION

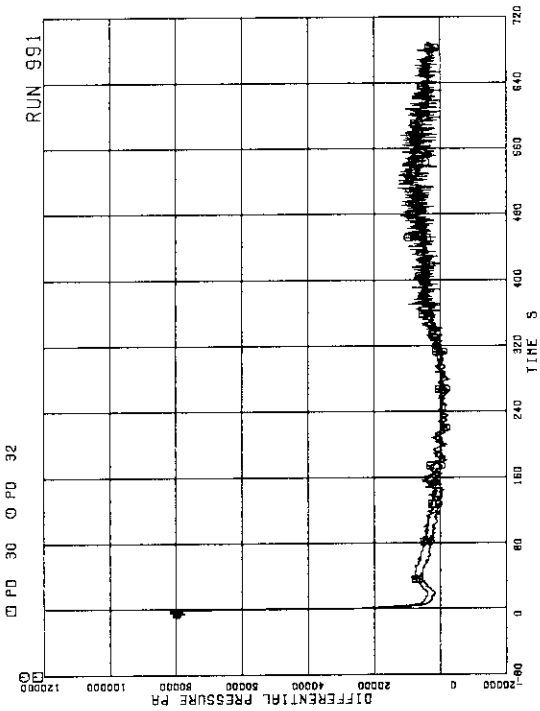

FIG.A. 9 DIFFERENTIAL PRESSURE BETWEEN JP-3,4 DISCHARGE AND SUCTION

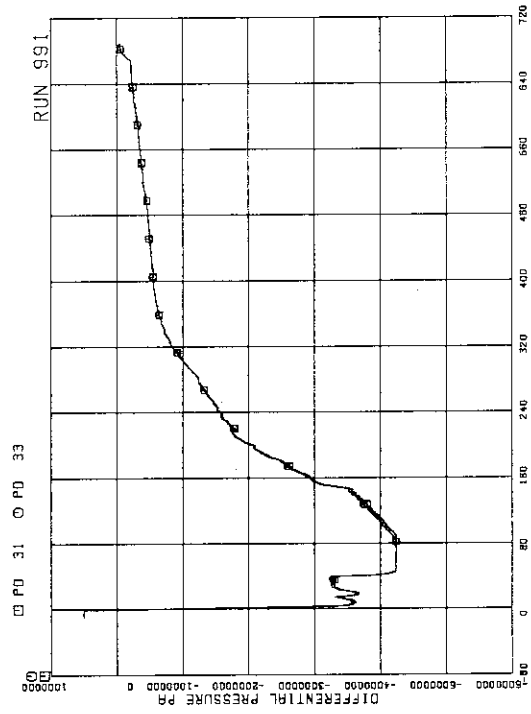

FIG.A. 10 DIFFERENTIAL PRESSURE BETWEEN JP-3,4 DRIVE AND SUCTION

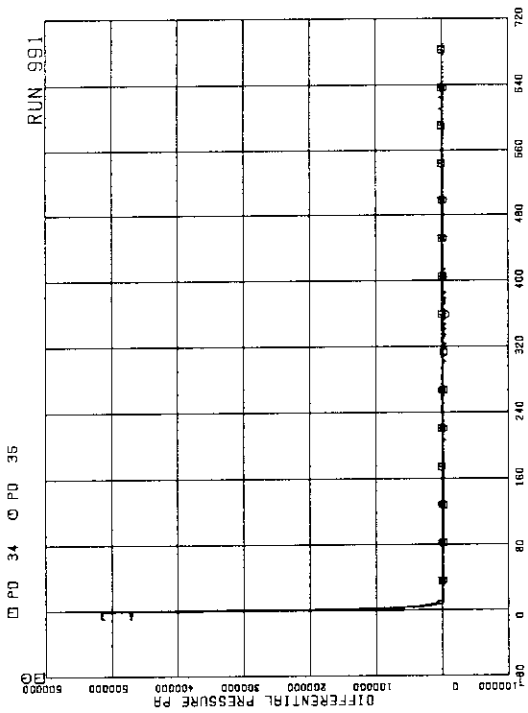

FIG.A. 11 DIFFERENTIAL PRESSURE BETWEEN MRP DELIVERY AND SUCTION

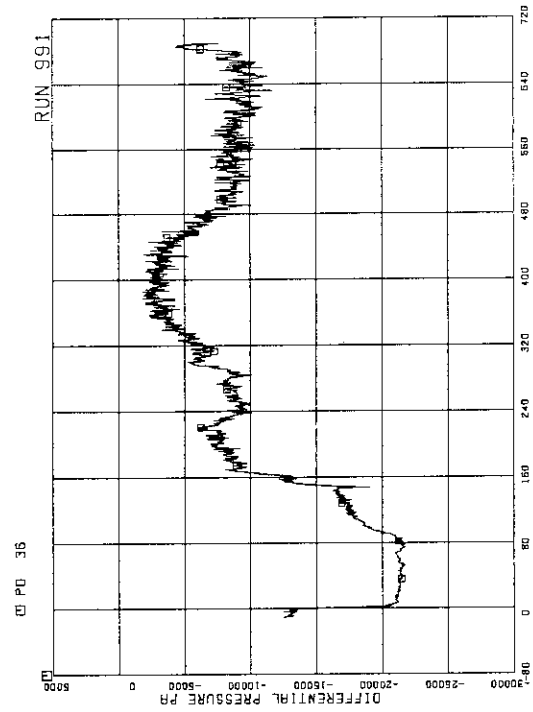

FIG.A. 12 DIFFERENTIAL PRESSURE BETWEEN DOWNCOMER BOTTOM AND MRP1 SUCTION

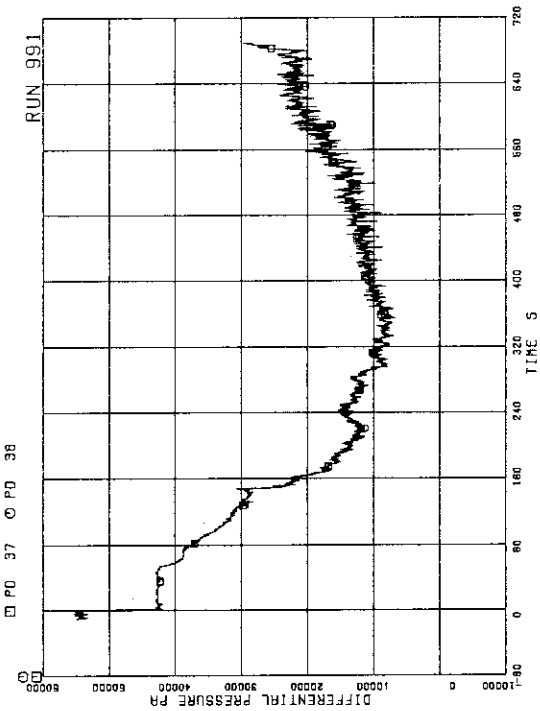

FIG.A. 13 DIFFERENTIAL PRESSURE BETWEEN MRP1 DELIVERY AND JP-1,2 DRIVE

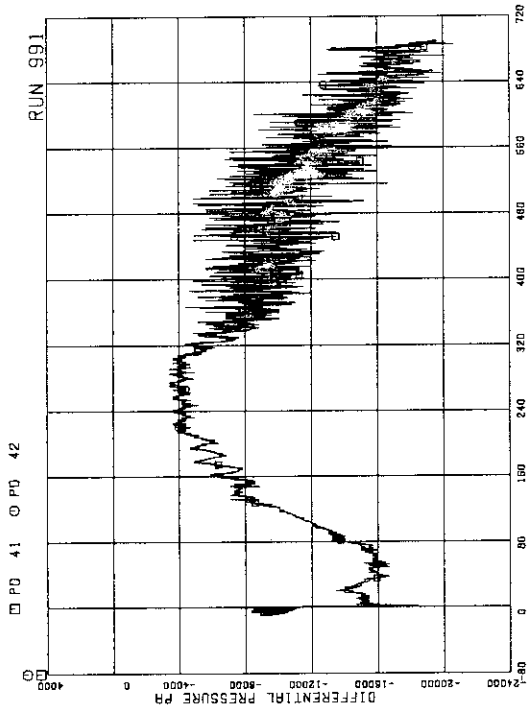

FIG.A. 15 DIFFERENTIAL PRESSURE BETWEEN JP-1,2 DISCHARGE AND LOWER PLENUM

FIG.A. 14 DIFFERENTIAL PRESSURE BETWEEN DOWNCOMER MIDDLE AND JP-1,2 SUCTION

FIG.A. 16 DIFFERENTIAL PRESSURE BETWEEN DOWNCOMER BOTTOM AND BREAK B

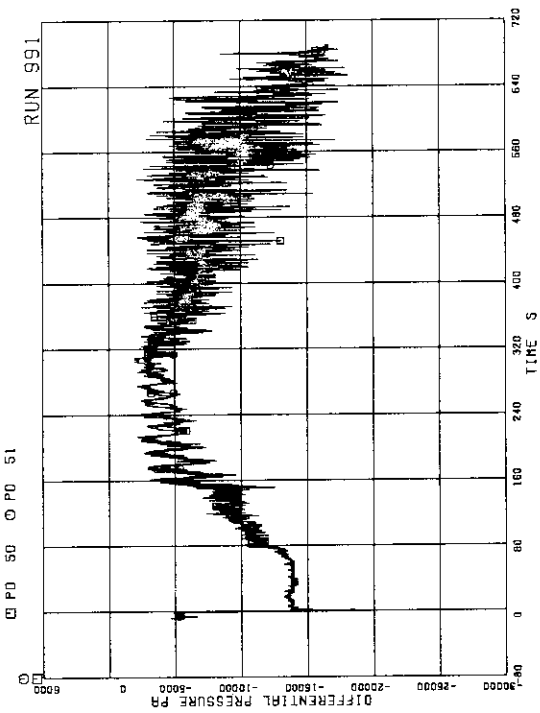

FIG.A. 19 DIFFERENTIAL PRESSURE BETWEEN JP-3,4 DISCHARGE AND CONFLURNCE

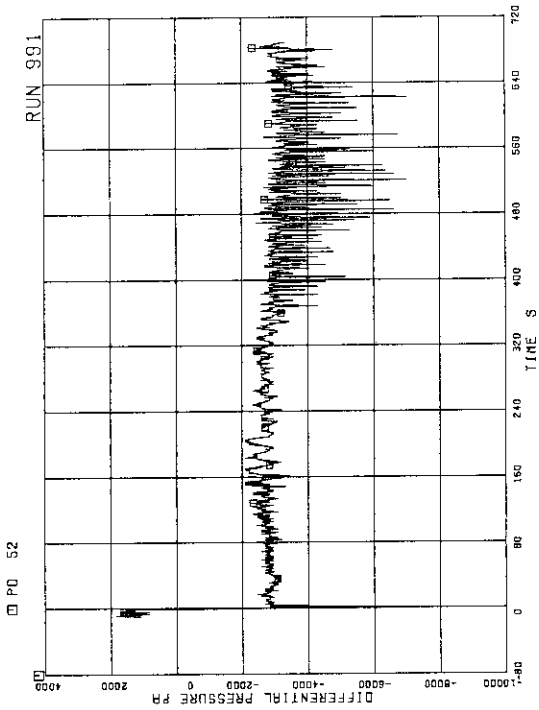

FIG.A. 20 DIFFERENTIAL PRESSURE BETWEEN JP-3,4 CONFLUENCE IN BROKEN LOOP AND LP

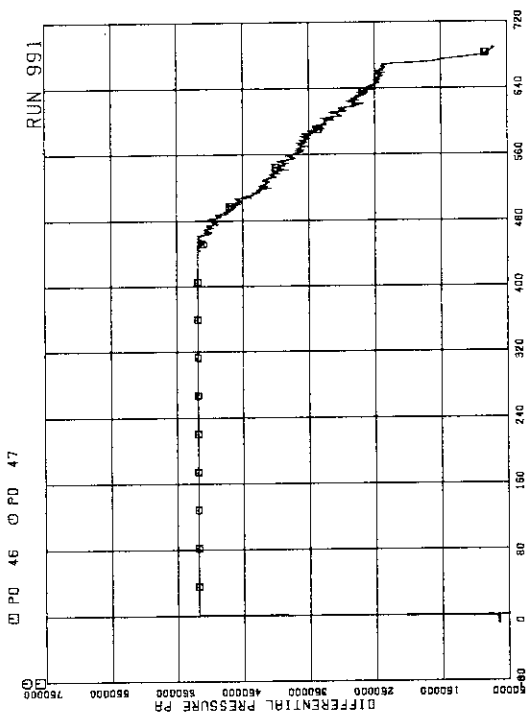

FIG.A. 17 DIFFERENTIAL PRESSURE BETWEEN MRP2 DELIVERY AND JP-3,4 DRIVE

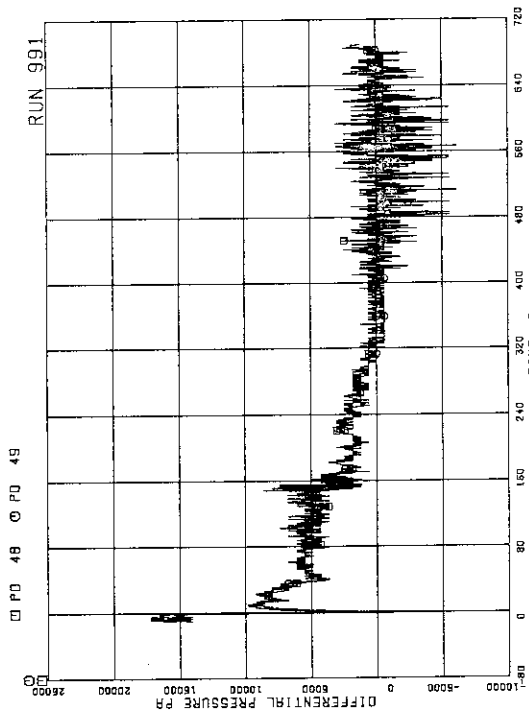

FIG.A. 18 DIFFERENTIAL PRESSURE BETWEEN DOWNCOMER MIDDLE AND JP-3,4 SUCTION

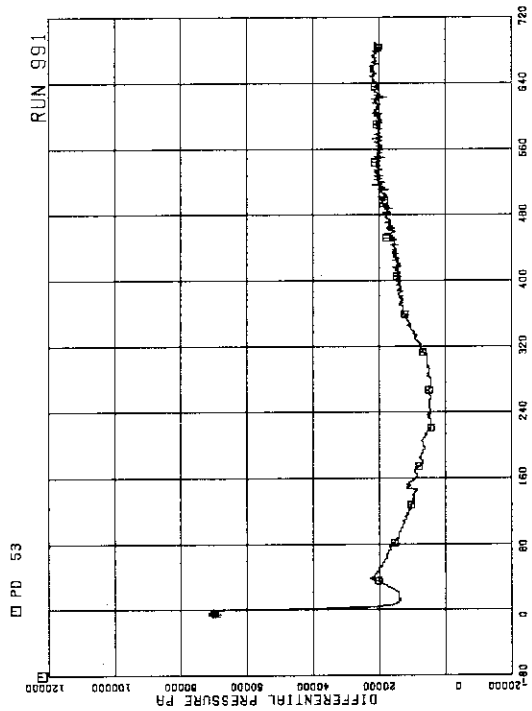

FIG.A. 21 DIFFERENTIAL PRESSURE BETWEEN LOWER PLENUM AND DOWNCOMER MIDDLE

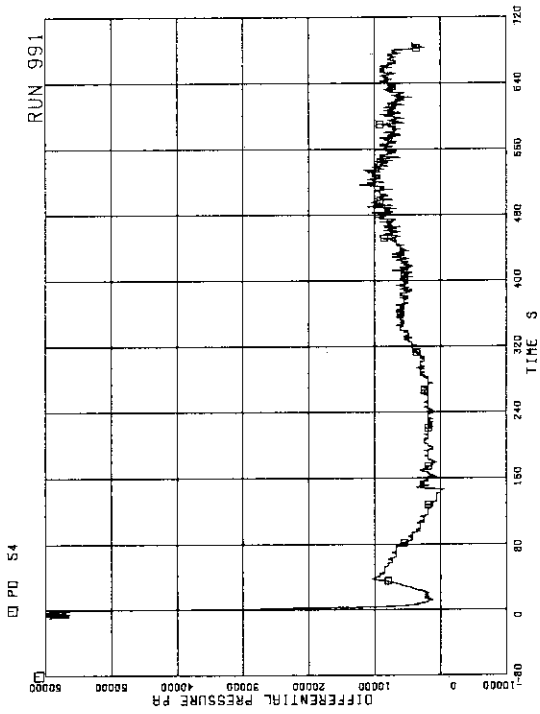

FIG.A. 22 DIFFERENTIAL PRESSURE BETWEEN LOWER PLENUM AND DOWNCOMER BOTTOM

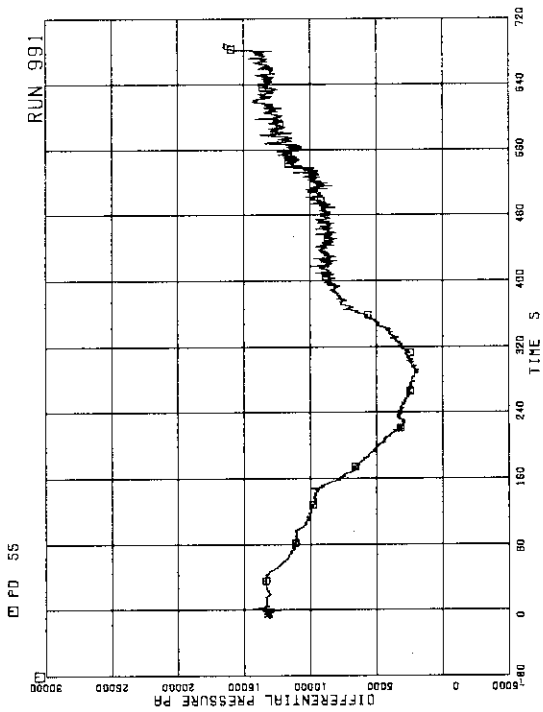

FIG.A. 23 DIFFERENTIAL PRESSURE BETWEEN DOWNCOMER BOTTOM AND DOWNCOMER MIDDLE

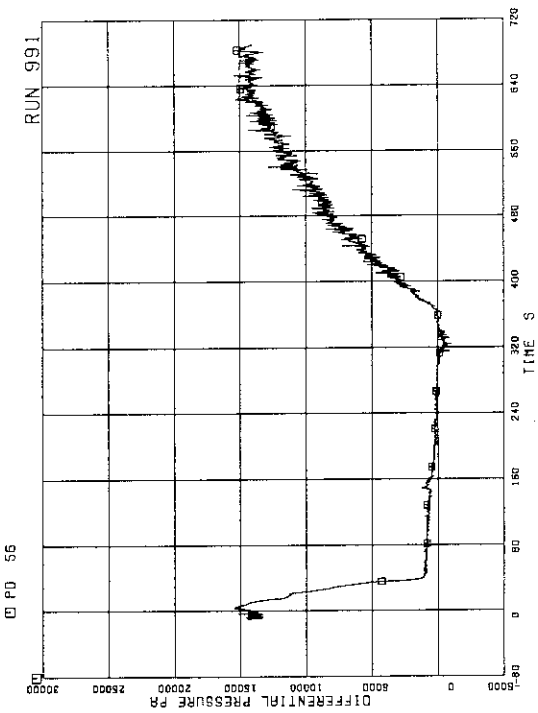

FIG.A. 24 DIFFERENTIAL PRESSURE BETWEEN DOWNCOMER MIDDLE AND STEAM DOME

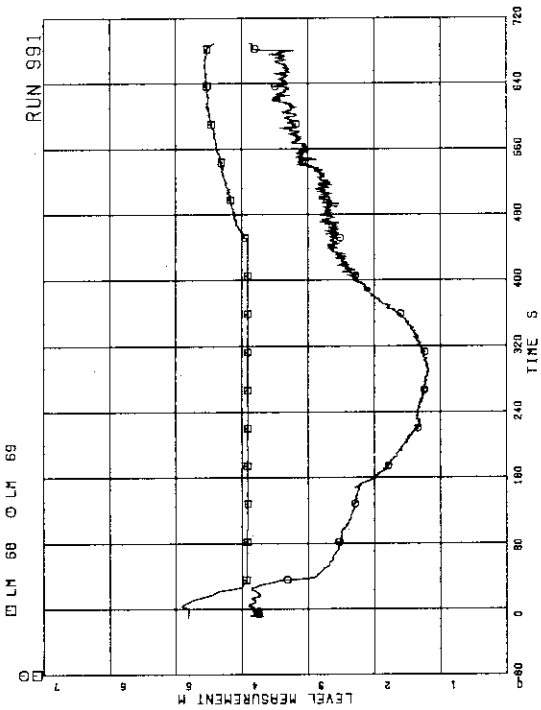

FIG.A. 27 LIQUID LEVEL IN DOWNCOMER

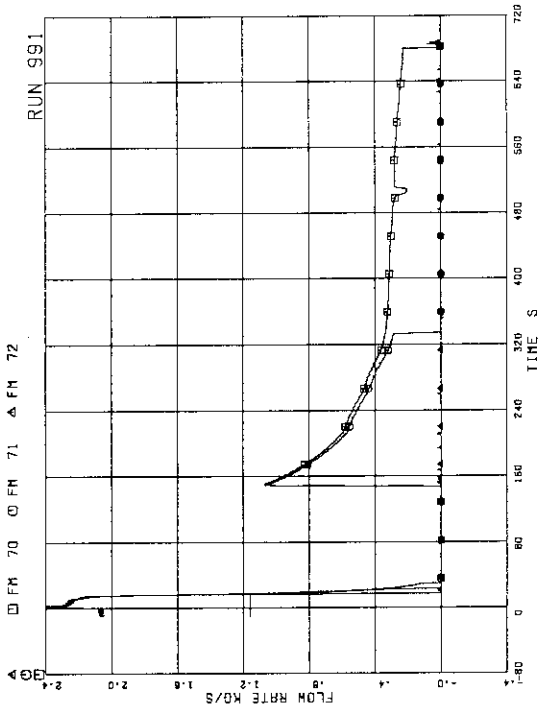

FIG.A. 28 MASS FLOW RATE IN MSL

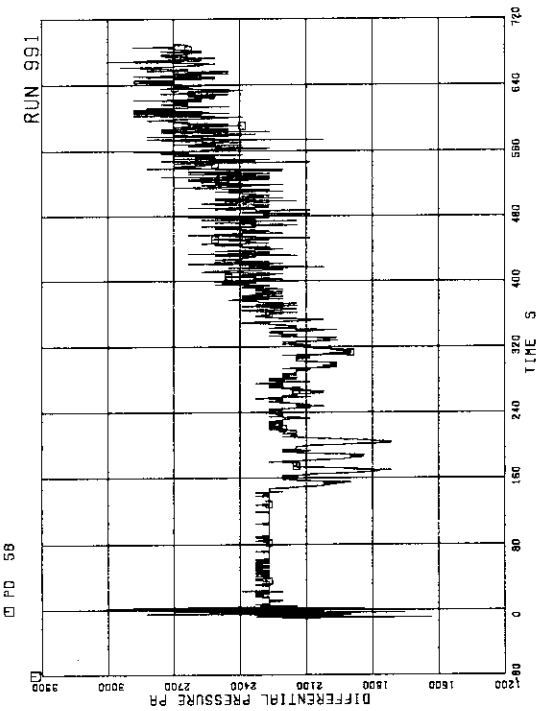

FIG.A. 25 DIFFERENTIAL PRESSURE BETWEEN LP BOTTOM AND LP MIDDLE

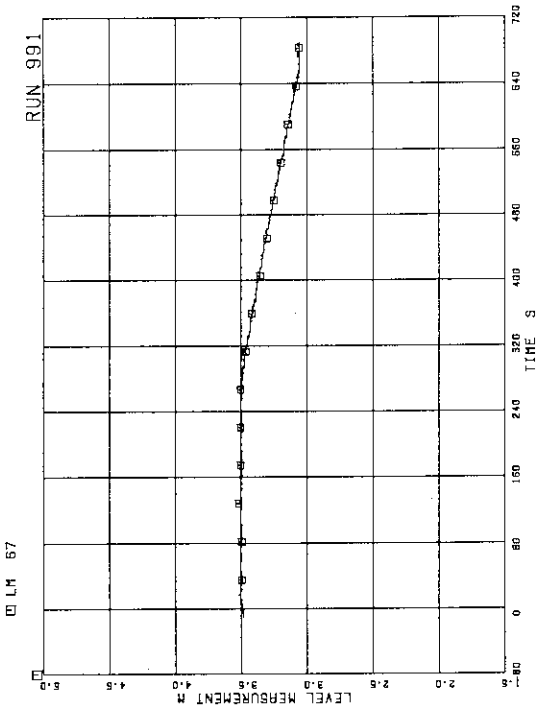

FIG.A. 26 LIQUID LEVEL IN ECCS TANK

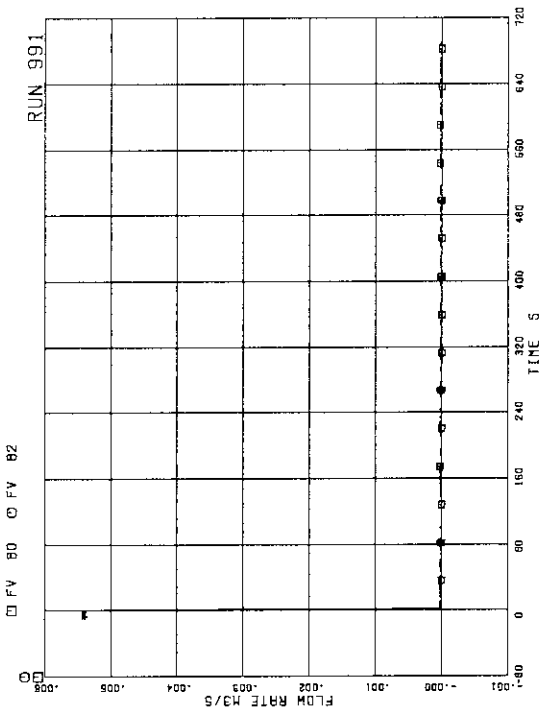

FIG.A. 31 JP-3.4 DISCHARGE FLOW RATE (POS. FLOW)

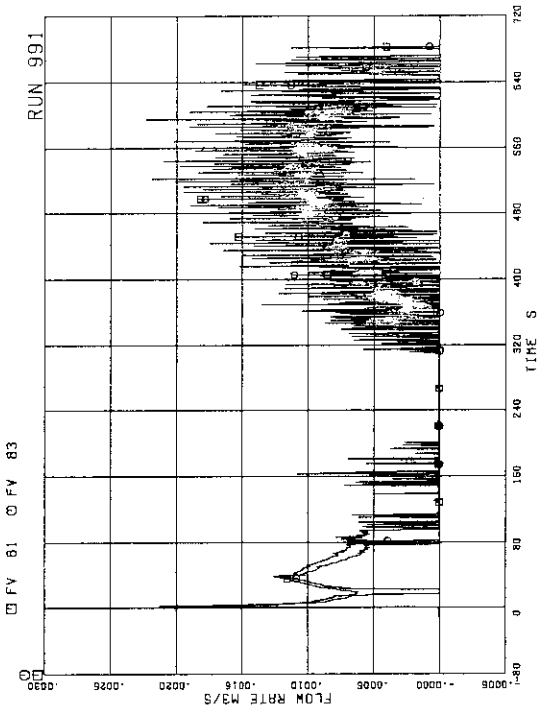

FIG.A. 32 JP-3.4 DISCHARGE FLOW RATE (NEG. FLOW)

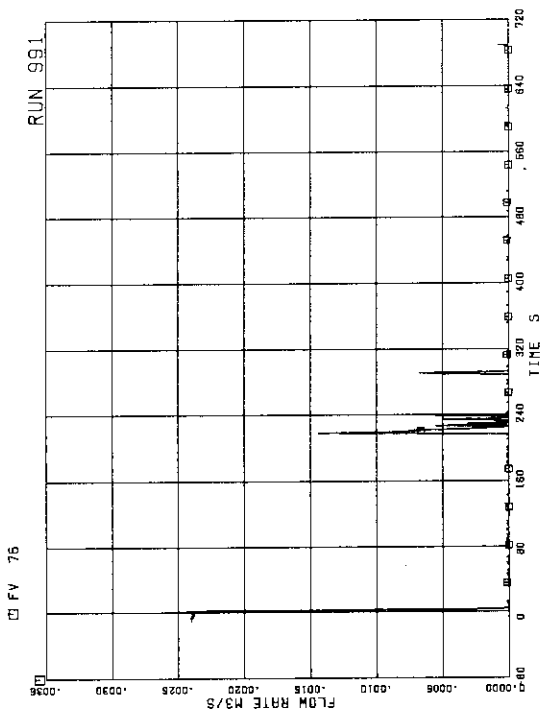

FIG.A. 29 FEEDWATER FLOW RATE

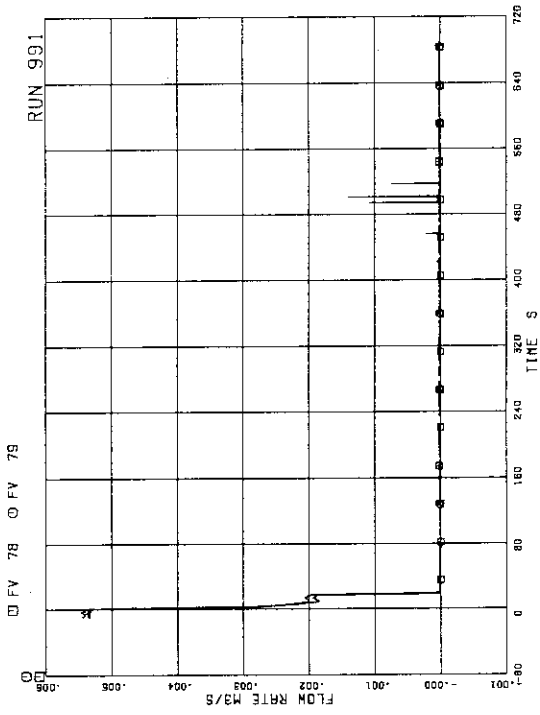

FIG.A. 30 JP-1.2 DISCHARGE FLOW RATE (POS. FLOW)

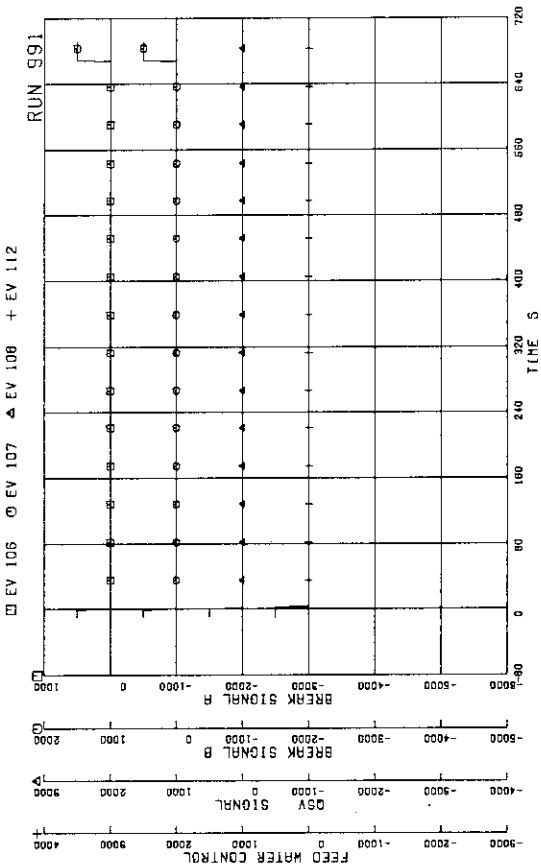

FIG.A. 35 VALVE OPERATION SIGNAL

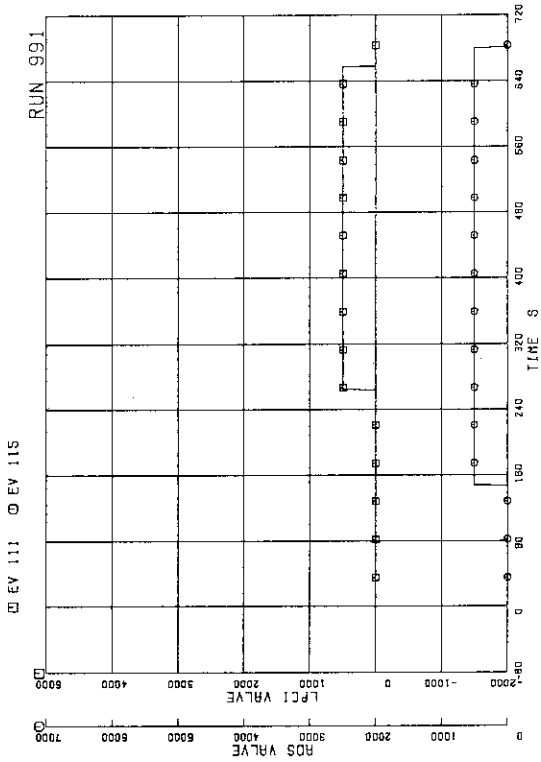

FIG.A. 36 ECCS OPERATION SIGNAL

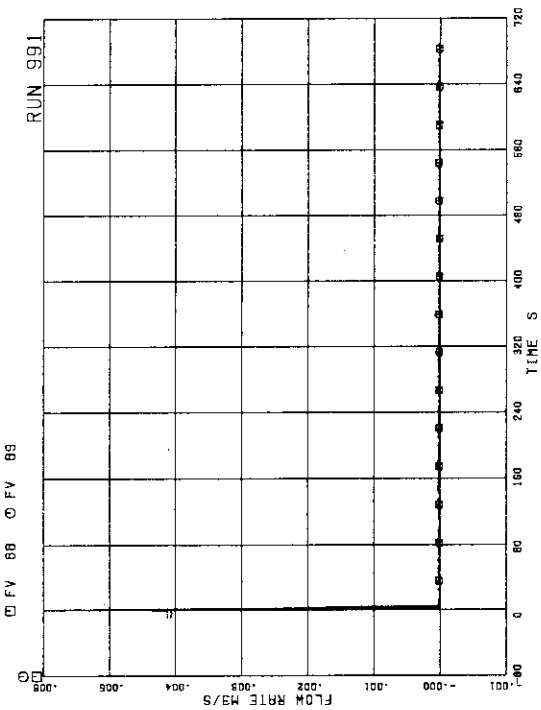

FIG.A. 33 MRP DISCHARGE FLOW RATE

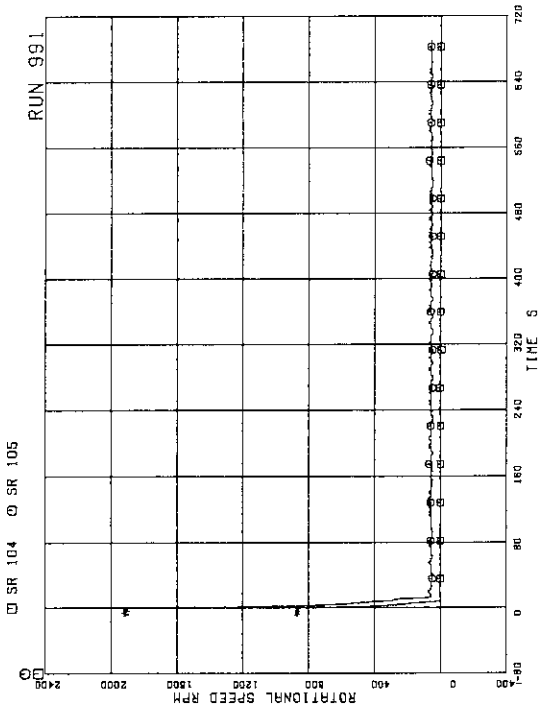

FIG.A. 34 MRP PUMP SPEED

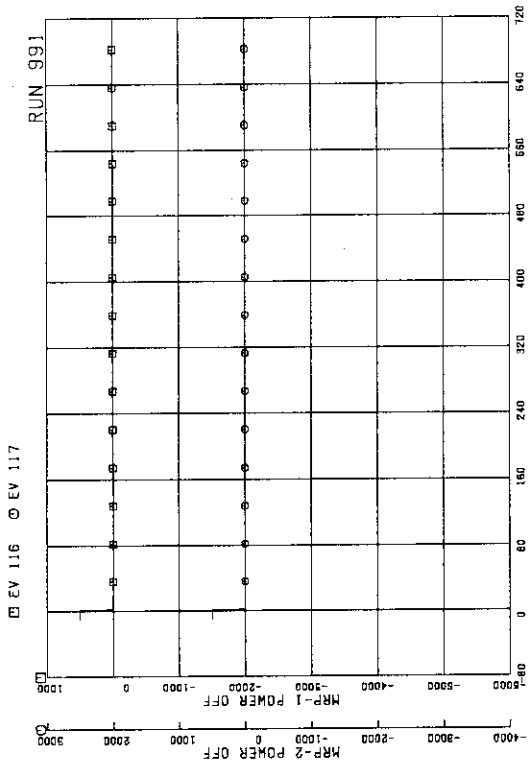

FIG.A. 37 MRP OPERATION SIGNAL

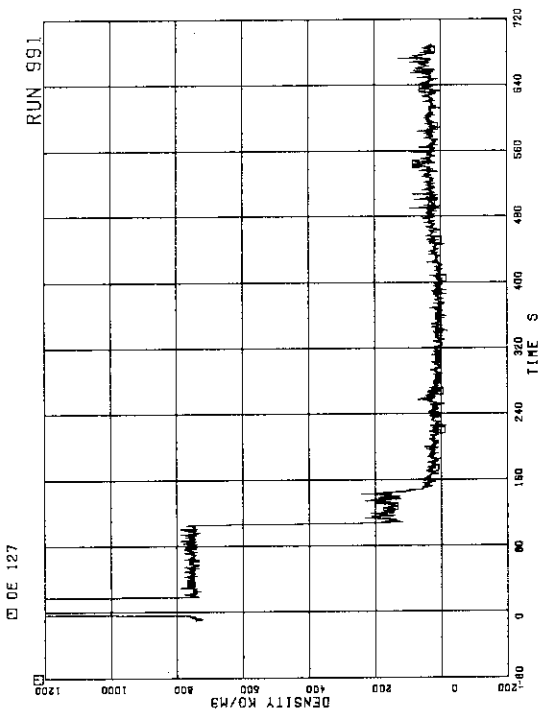

FIG.A. 39 FLUID DENSITY AT BREAK A UPSTREAM, BEAM B

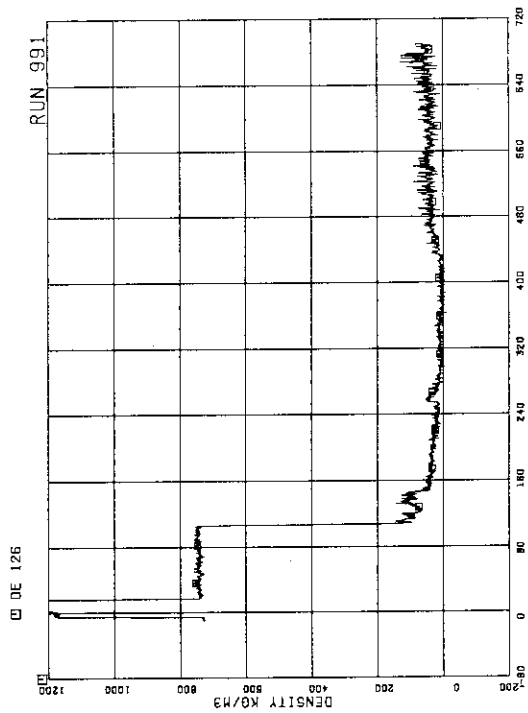

FIG.A. 38 FLUID DENSITY AT BREAK A UPSTREAM, BEAM A

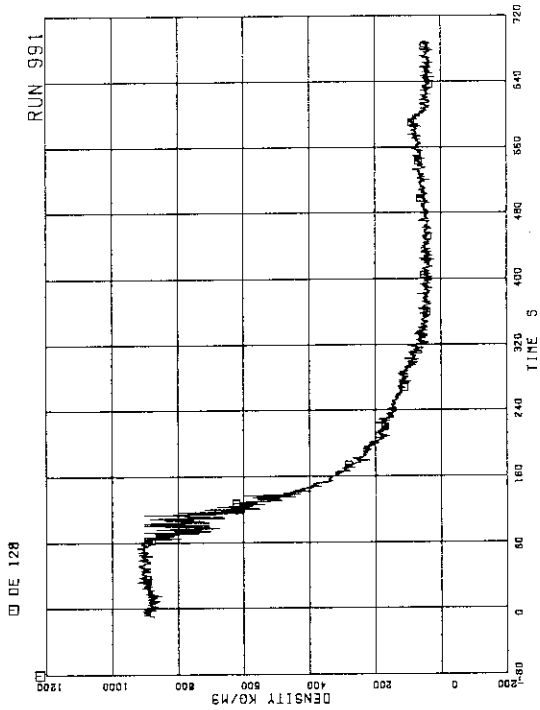

FIG.A. 40 FLUID DENSITY IN RECIRCULATION LOOP, BEAM A (DATA ARE NOT QUALIFIED)

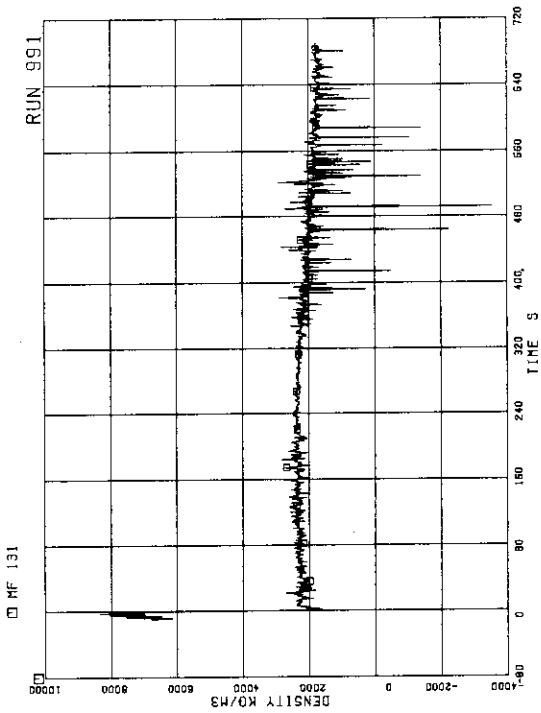

FIG.A. 43 MOMENTUM FLUX AT JP-3,4 OUTLET SPOOL

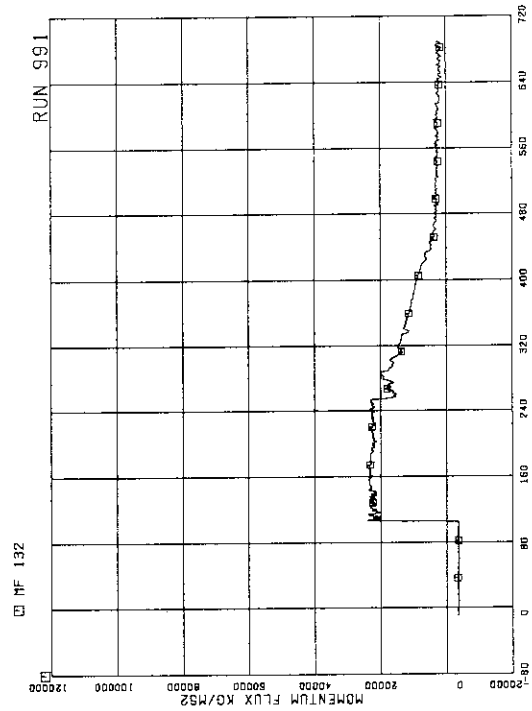

FIG.A. 44 MOMENTUM FLUX AT BREAK A SPOOL PIECE (LOW RANGE)

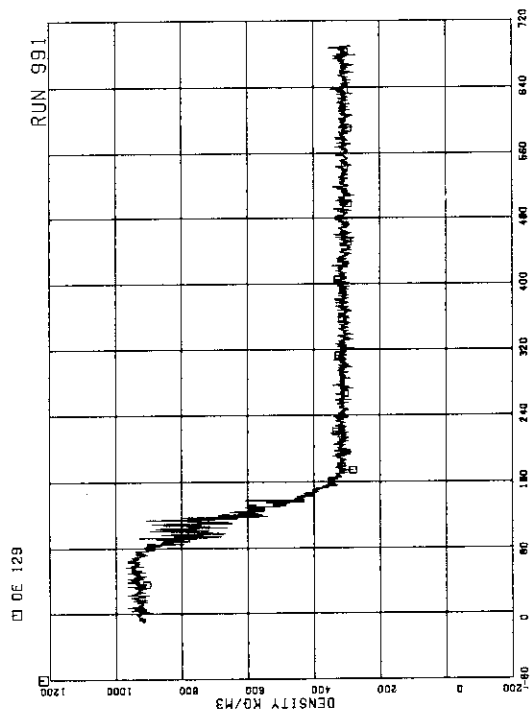

FIG.A. 41 FLUID DENSITY IN RECIRCULATION LOOP, BEAM B (DATA ARE NOT QUALIFIED)

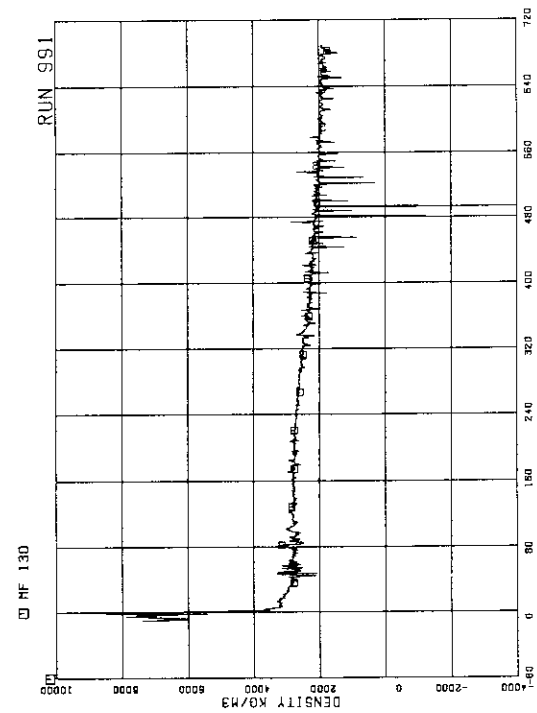

FIG.A. 42 MOMENTUM FLUX AT JP-1,2 OUTLET SPOOL

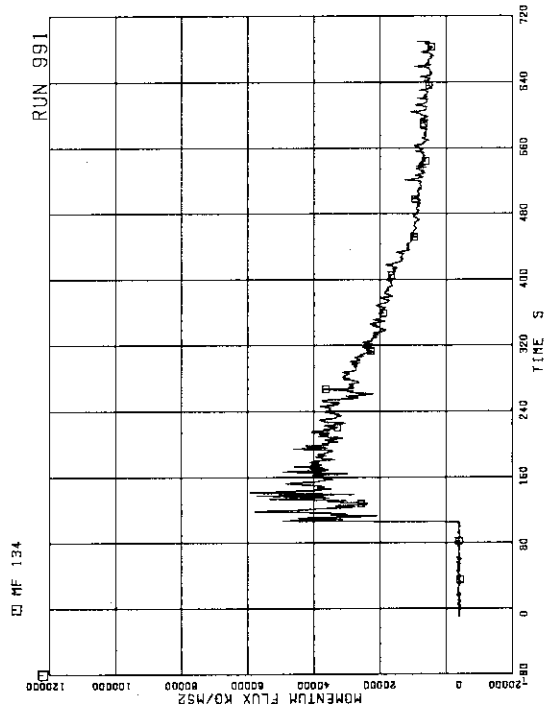

FIG.A. 45 MOMENTUM FLUX AT BREAK A SPOOL PIECE (HIGH RANGE)

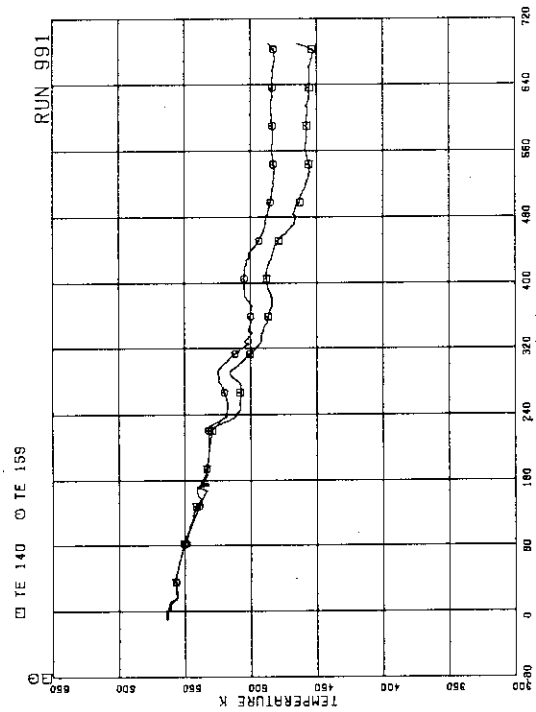

FIG.A. 47 FLUID TEMPERATURE IN STEAM DOME AND MSL

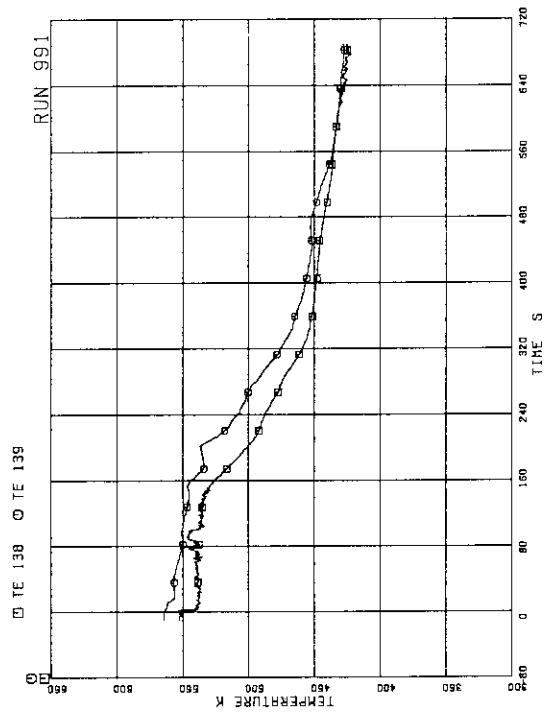

FIG.A. 46 FLUID TEMPERATURE IN LOWER PLENUM AND UPPER PLENUM

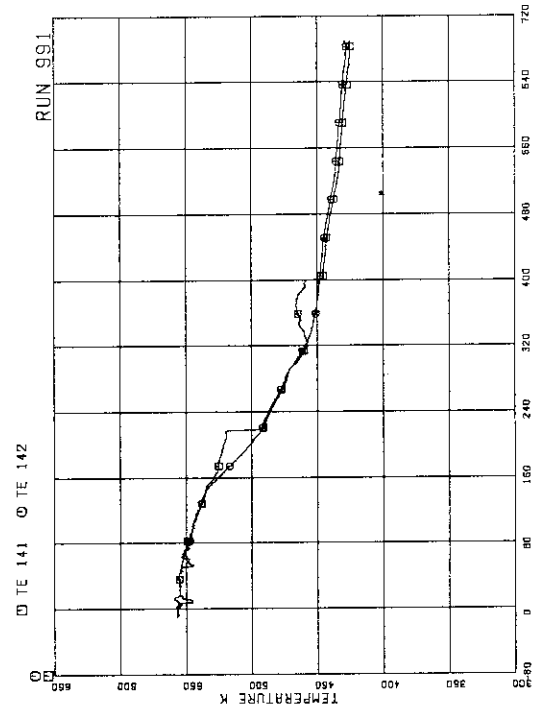

FIG.A. 48 FLUID TEMPERATURE IN DOWNCOMER

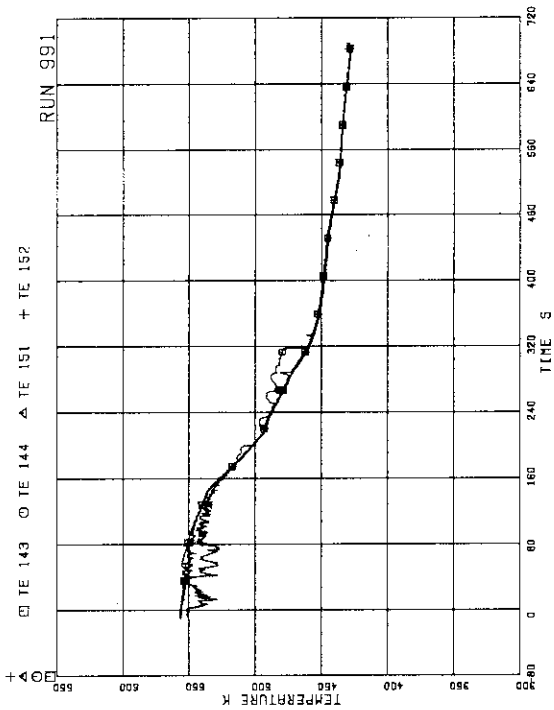

FIG.A. 49 FLUID TEMPERATURE IN INTACT RECIRCULATION LOOP

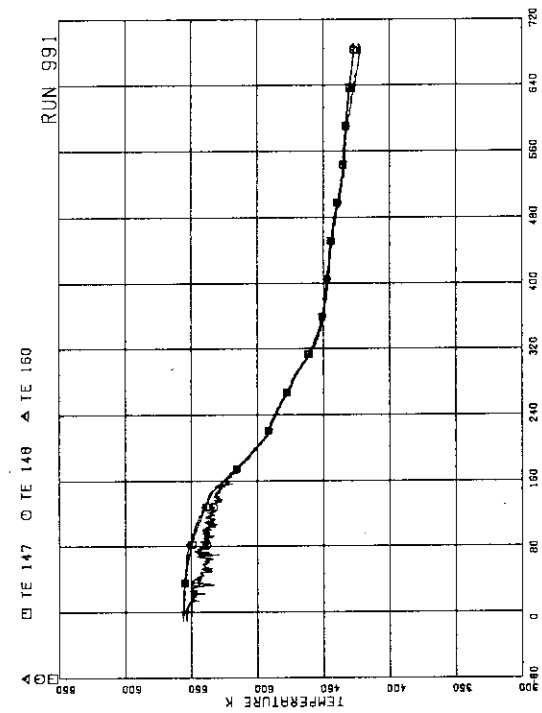

FIG.A. 51 FLUID TEMPERATURE AT JP-1,2 OUTLET

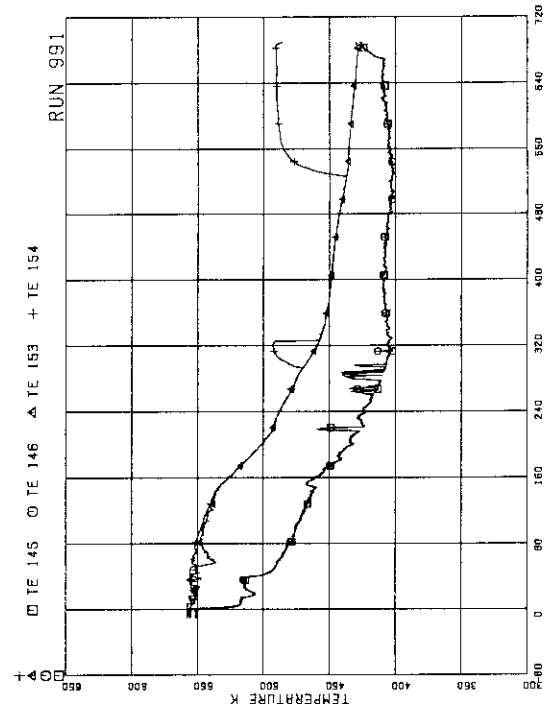

FIG.A. 50 FLUID TEMPERATURE IN BROKEN RECIRCULATION LOOP

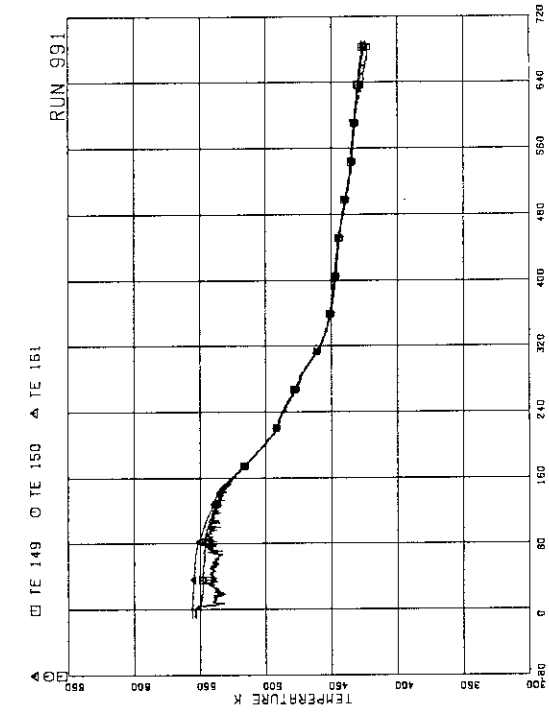

FIG.A. 52 FLUID TEMPERATURE AT JP-3,4 OUTLET

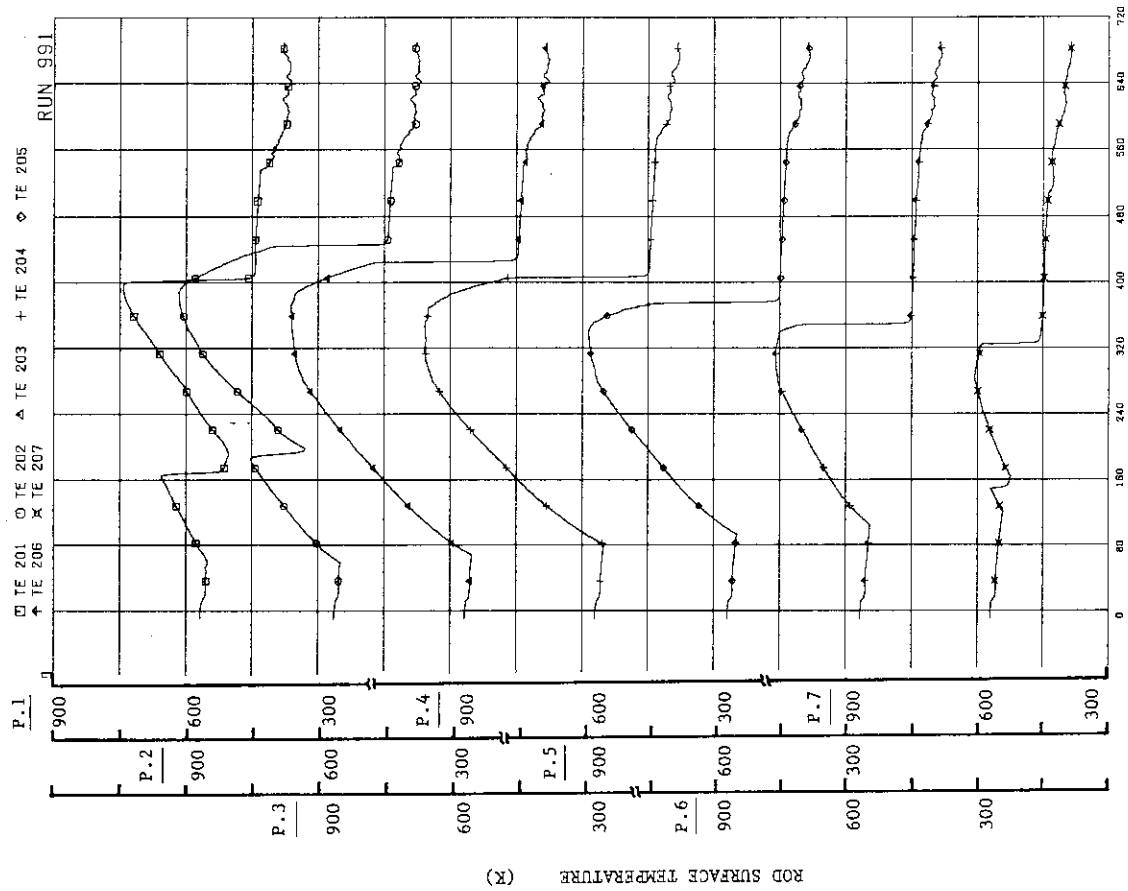

FIG.A. 55 SURFACE TEMPERATURE OF FUEL ROD A11

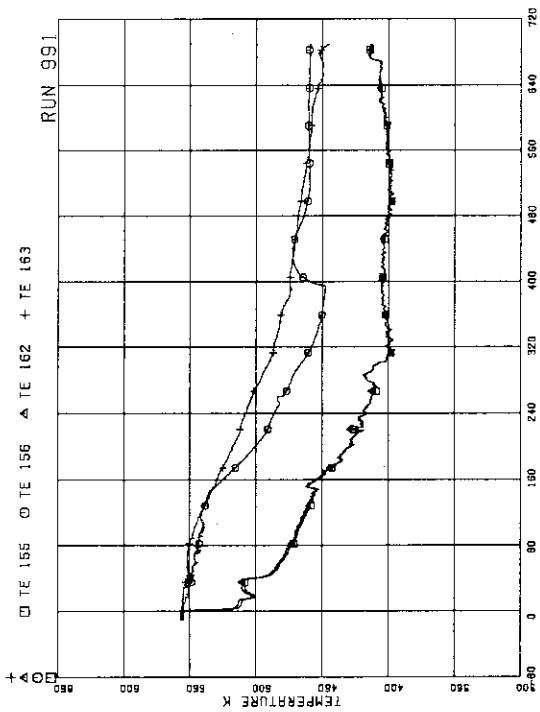

FIG.A. 53 FLUID TEMPERATURE NEAR BREAKS A AND B

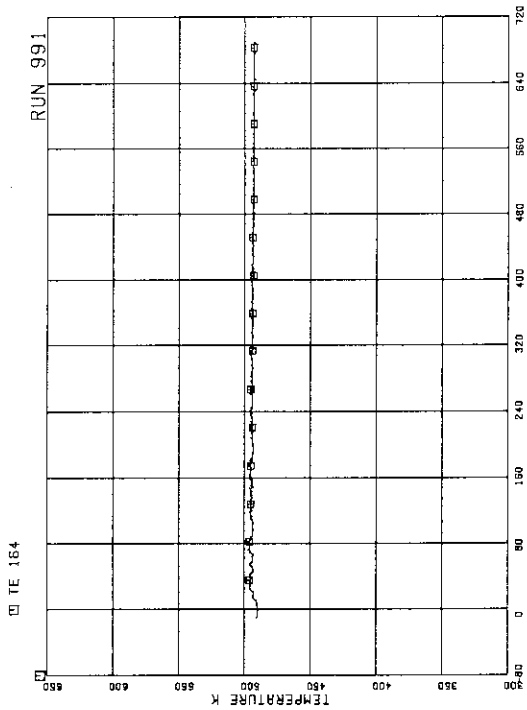

FIG.A. 54 FEEDWATER TEMPERATURE

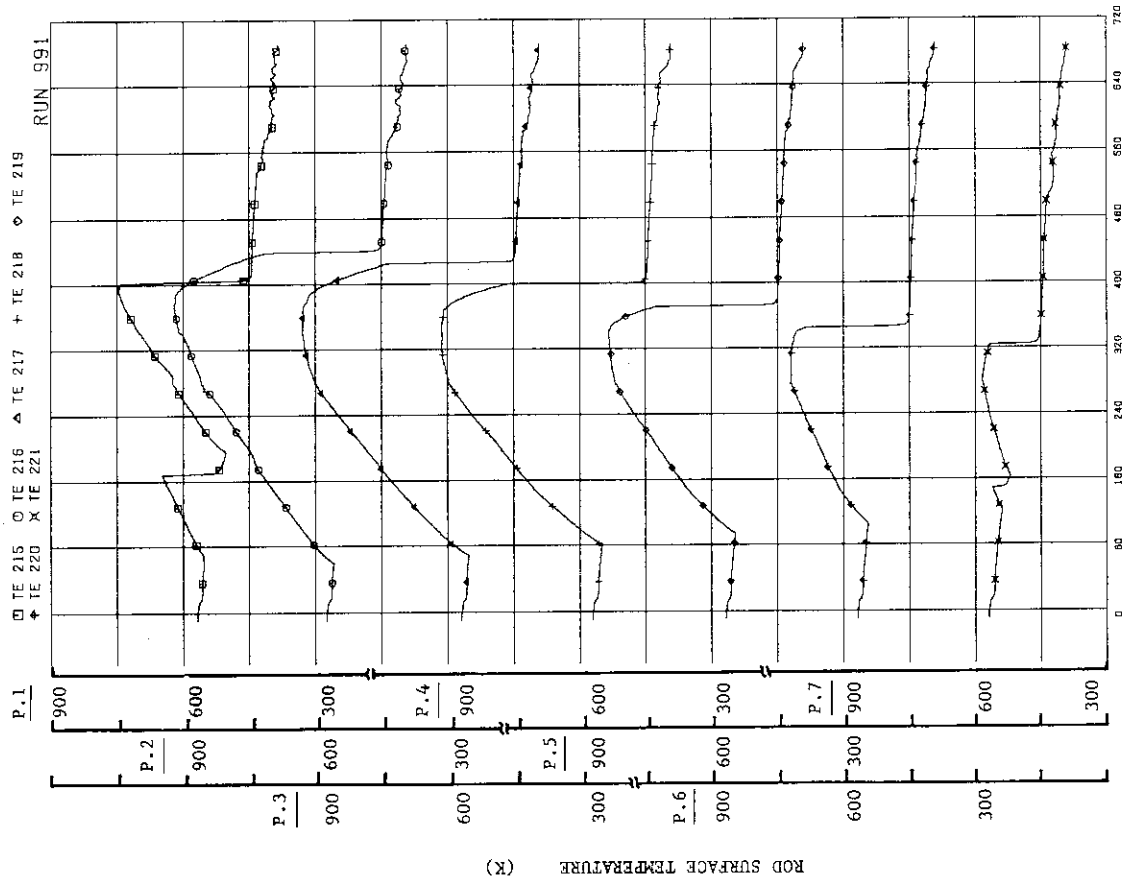

FIG.A. 57 SURFACE TEMPERATURE OF FUEL ROD A13

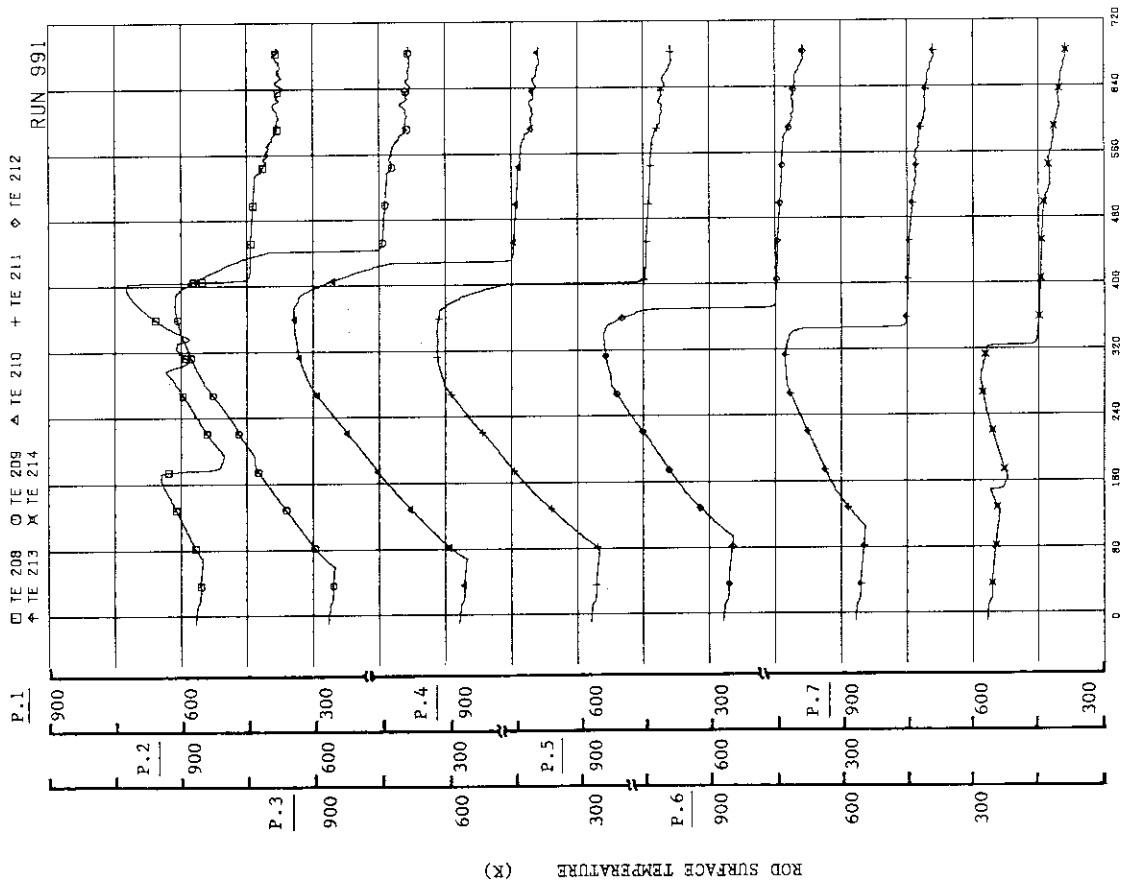

FIG.A. 56 SURFACE TEMPERATURE OF FUEL ROD A12

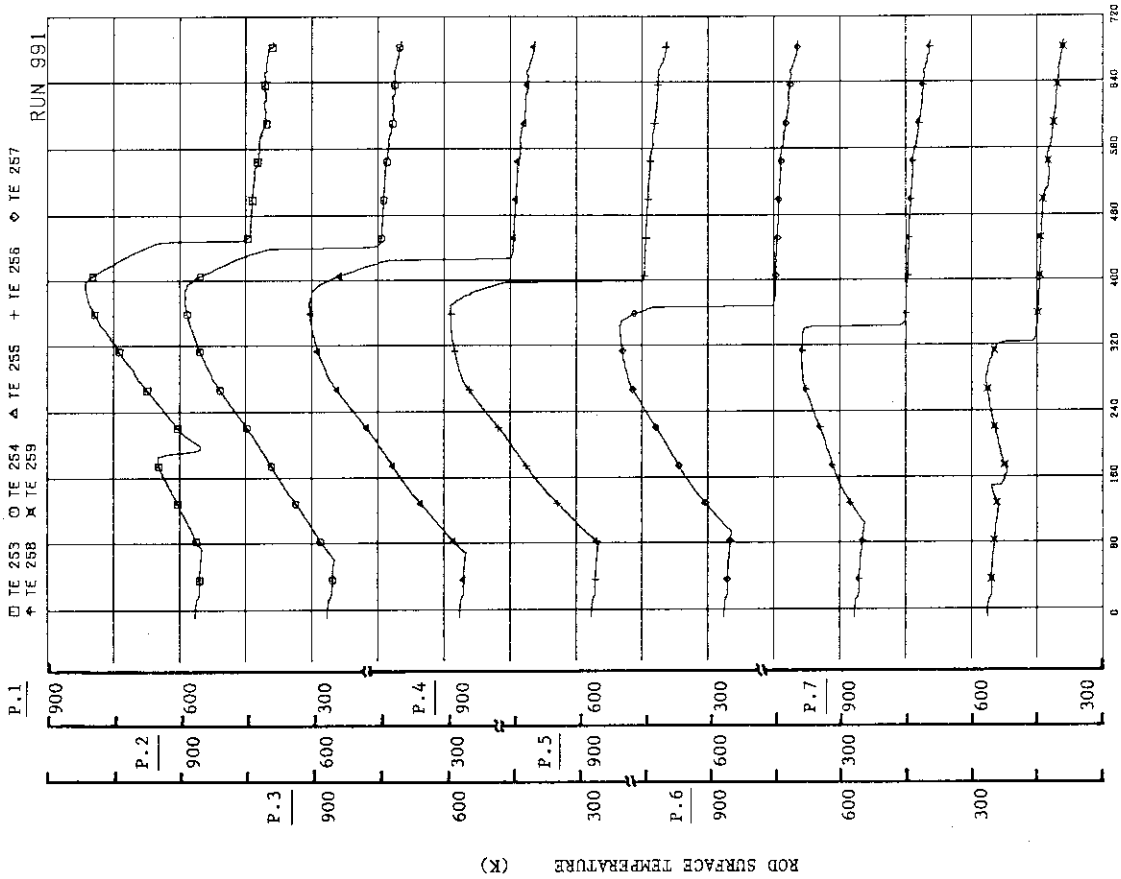

FIG.A. 59 SURFACE TEMPERATURE OF FUEL ROD A33

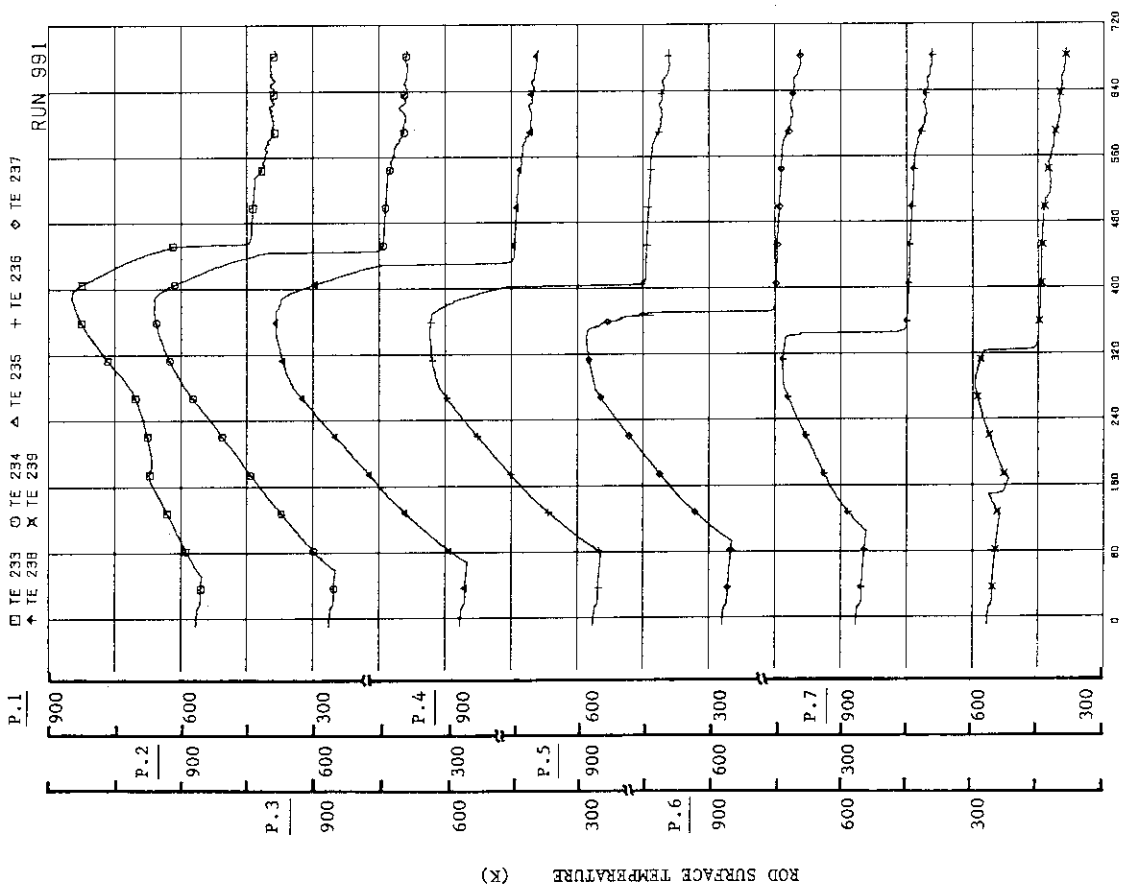

FIG.A. 58 SURFACE TEMPERATURE OF FUEL ROD A22

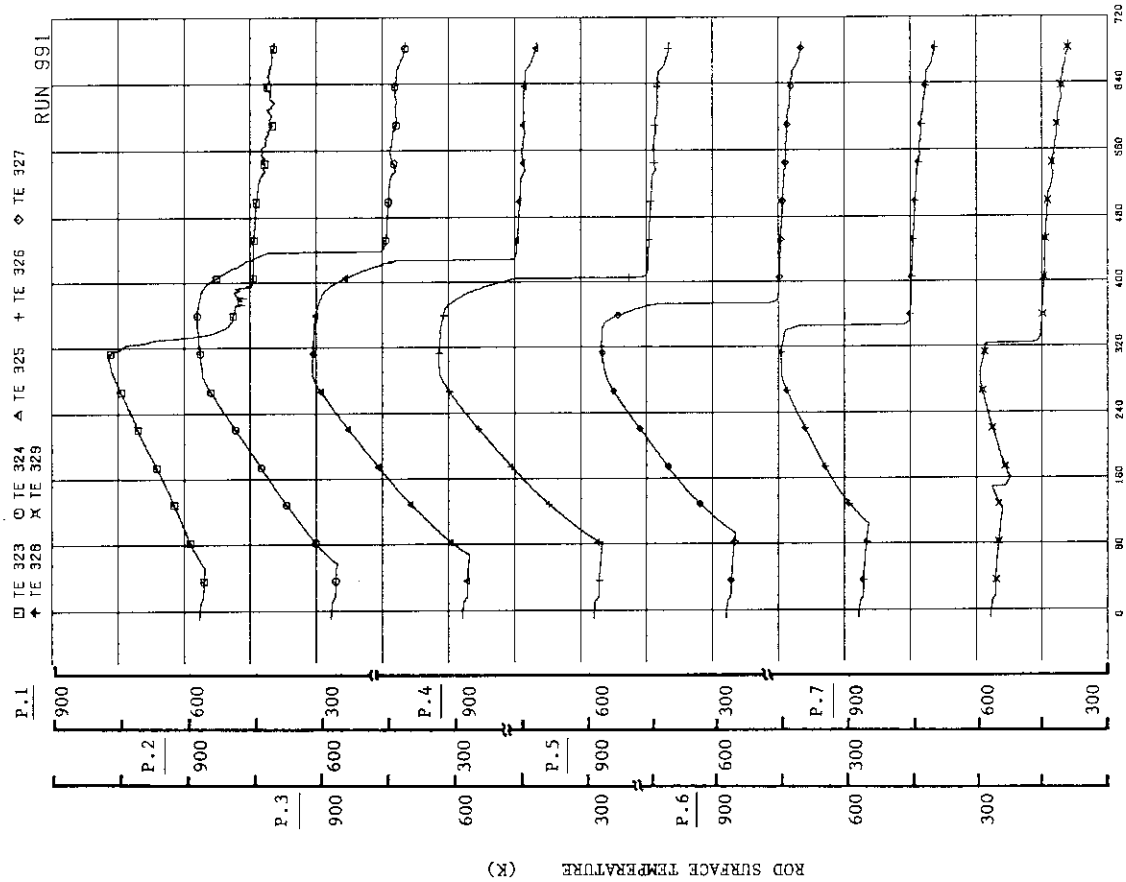

FIG.A. 61 SURFACE TEMPERATURE OF FUEL ROD A88

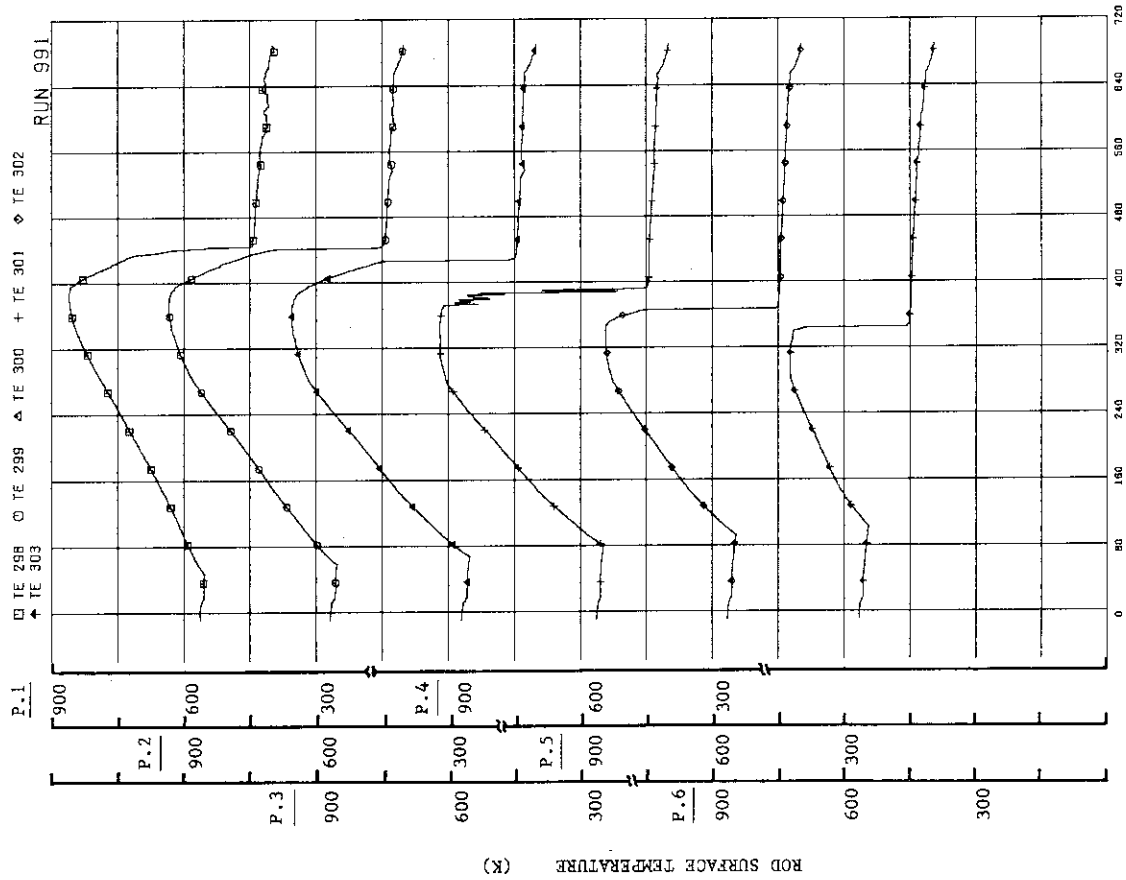

FIG.A. 60 SURFACE TEMPERATURE OF FUEL ROD A77

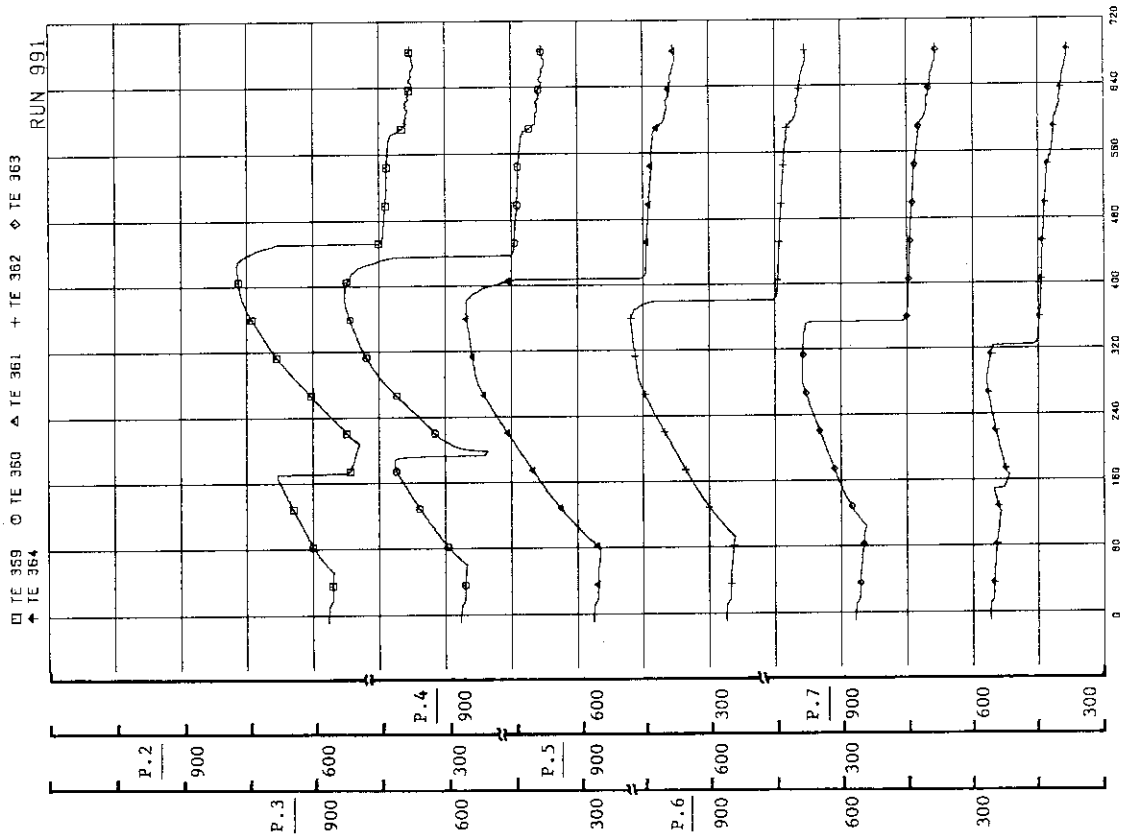

FIG.A- 63 SURFACE TEMPERATURE OF FUEL ROD C11

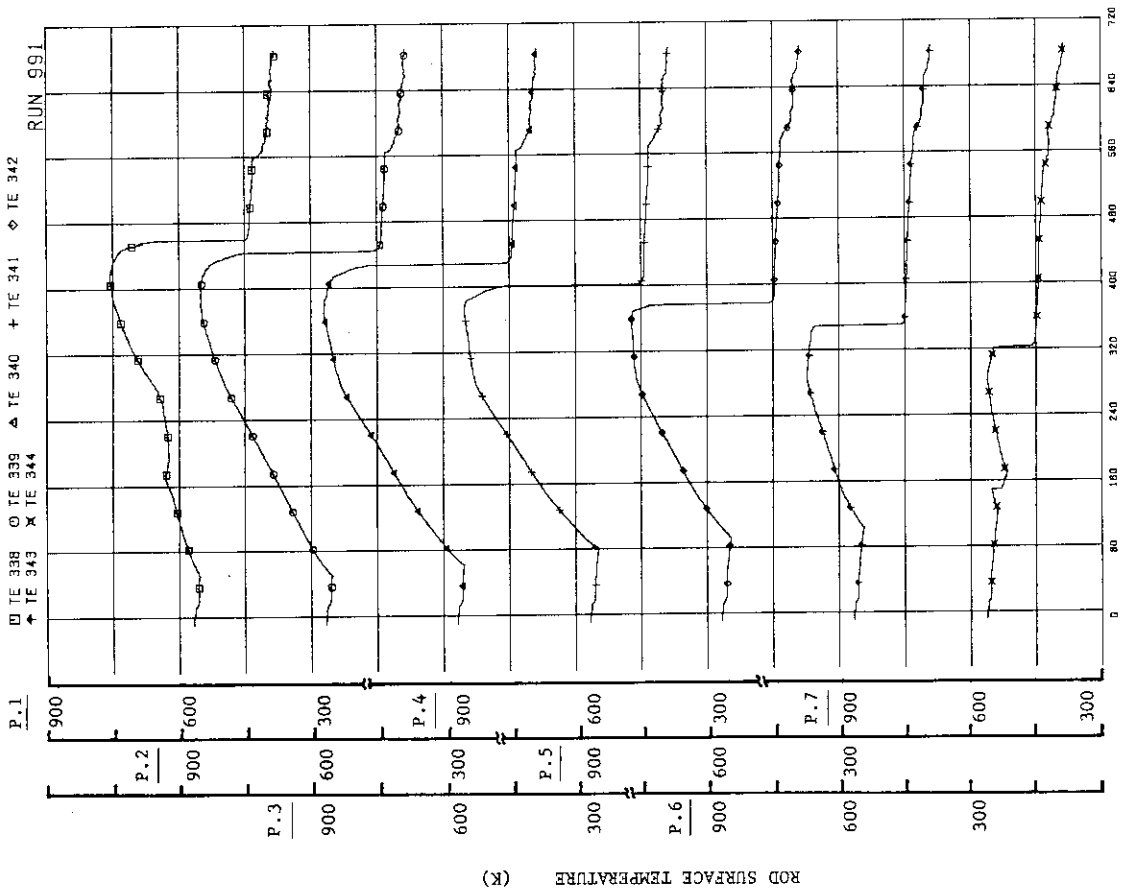

FIG.A- 62 SURFACE TEMPERATURE OF FUEL ROD B22

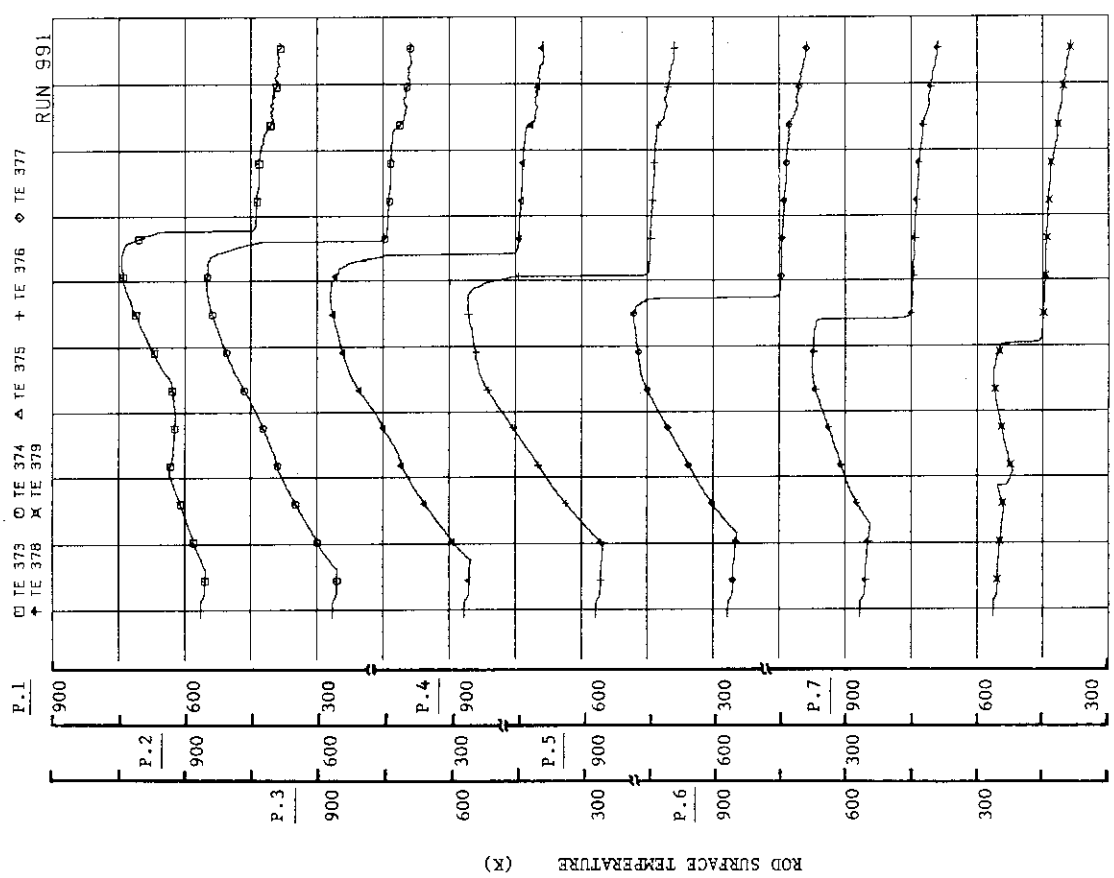

FIG.A. 65 SURFACE TEMPERATURE OF FUEL ROD C22

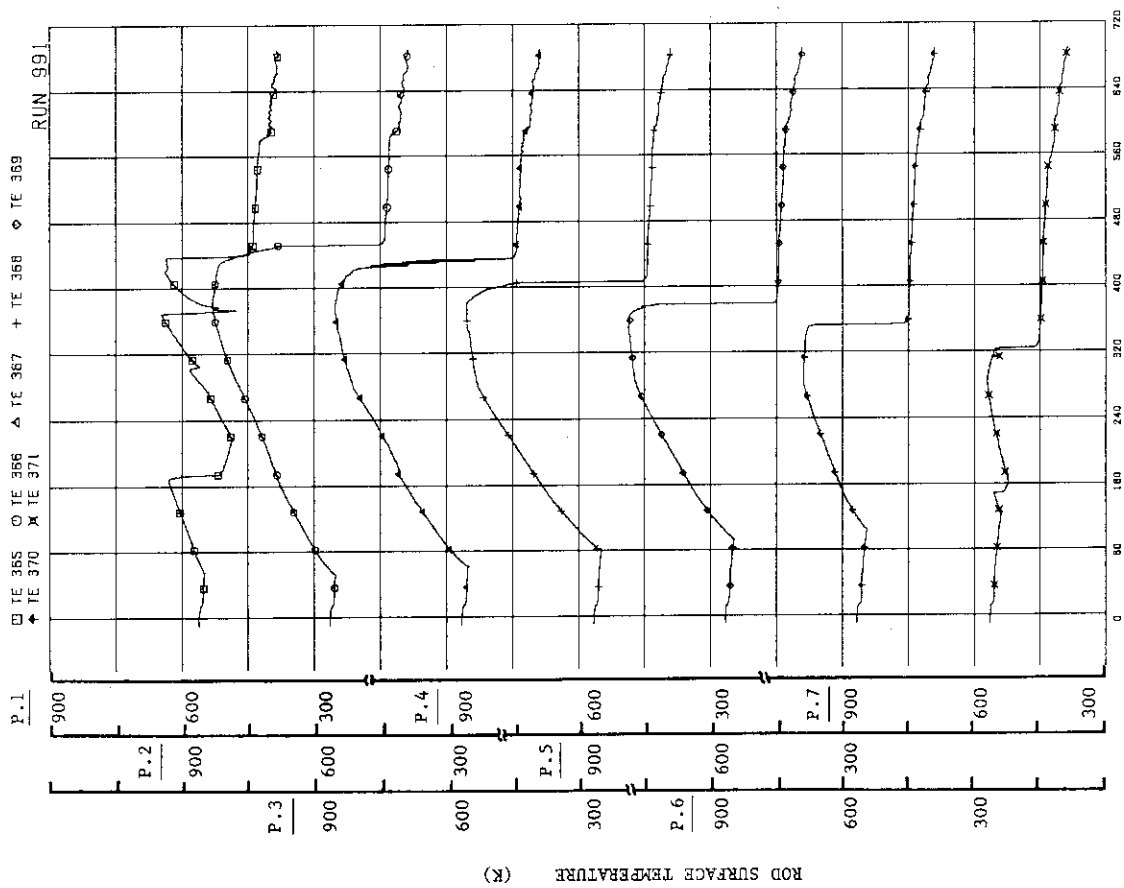

FIG.A. 64 SURFACE TEMPERATURE OF FUEL ROD C13

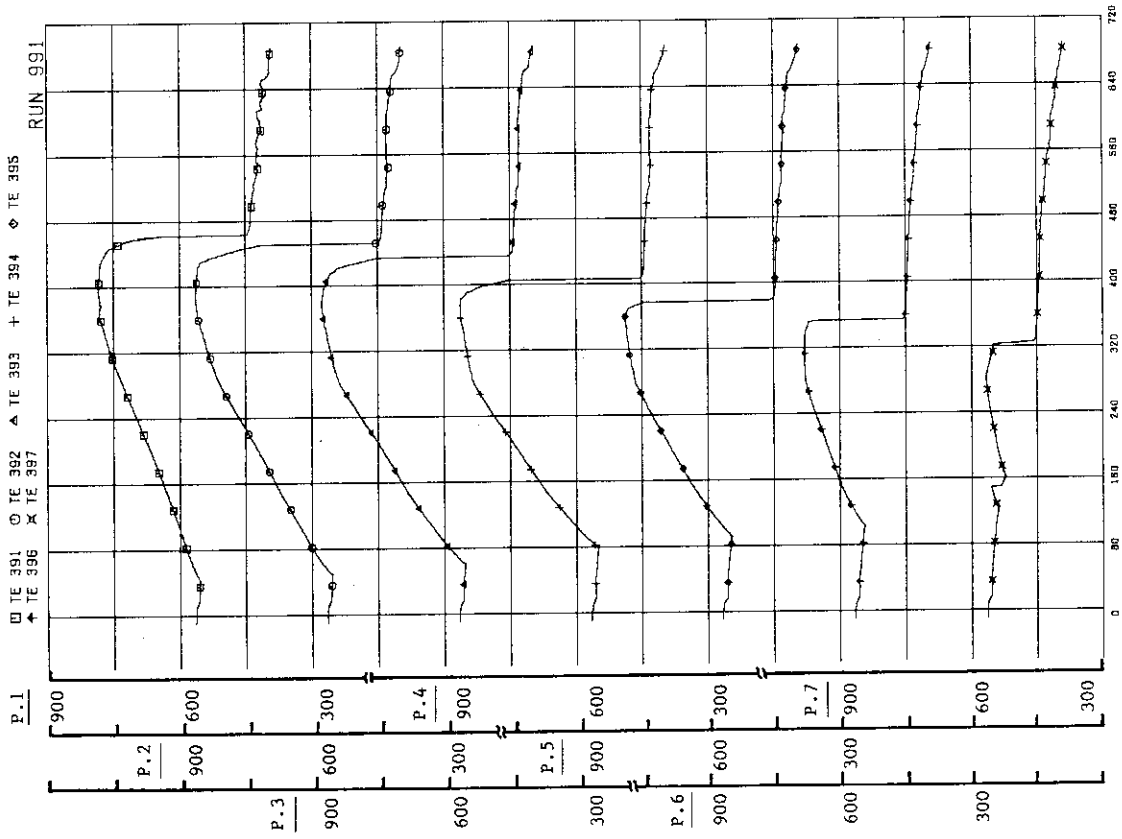

FIG.A. 67 SURFACE TEMPERATURE OF FUEL ROD C77

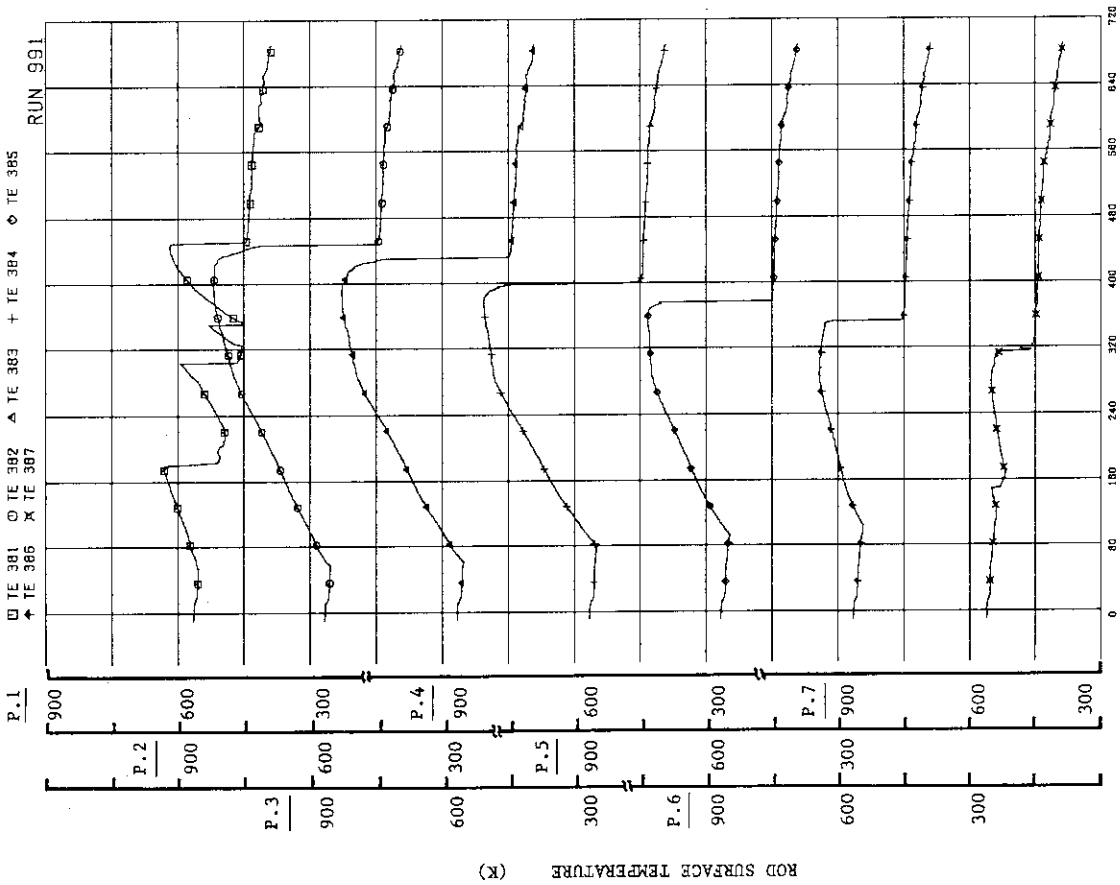

FIG.A. 66 SURFACE TEMPERATURE OF FUEL ROD C33

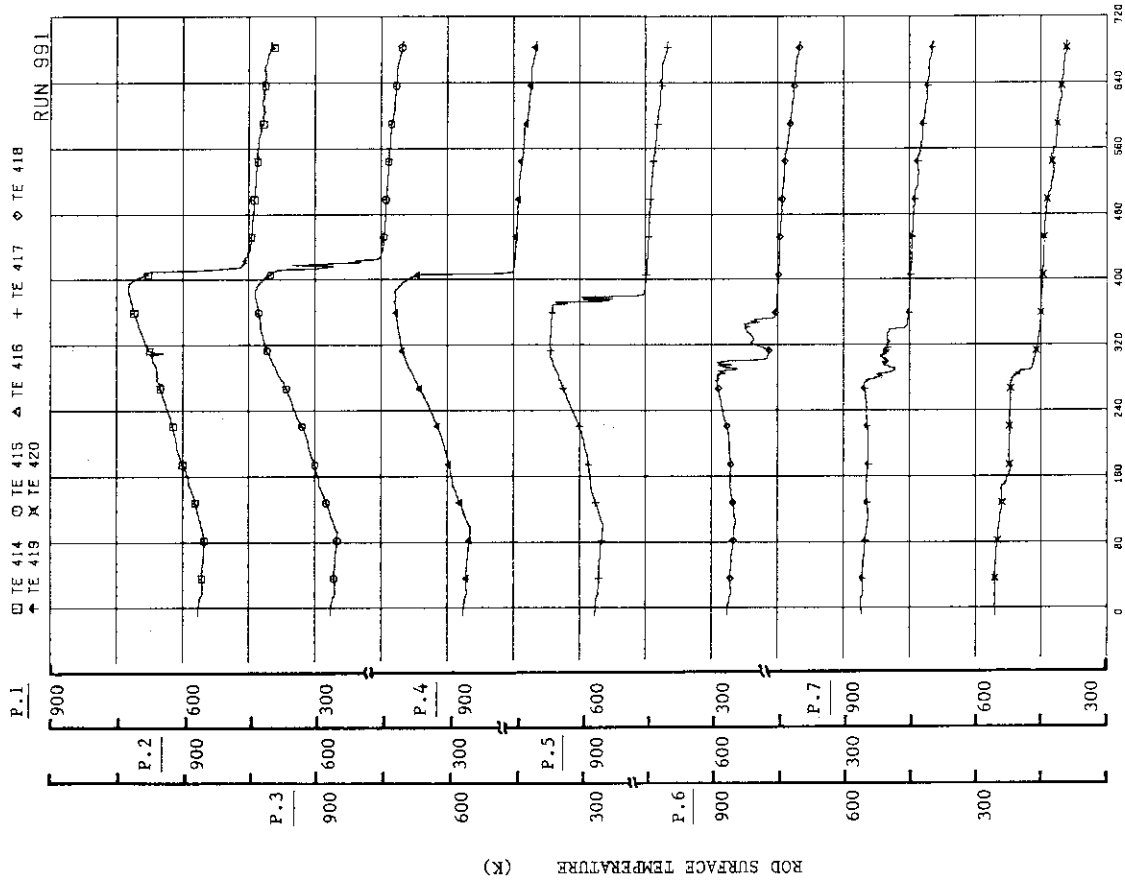

FIG.A. 69 SURFACE TEMPERATURE OF WATER ROD SIMULATOR A45

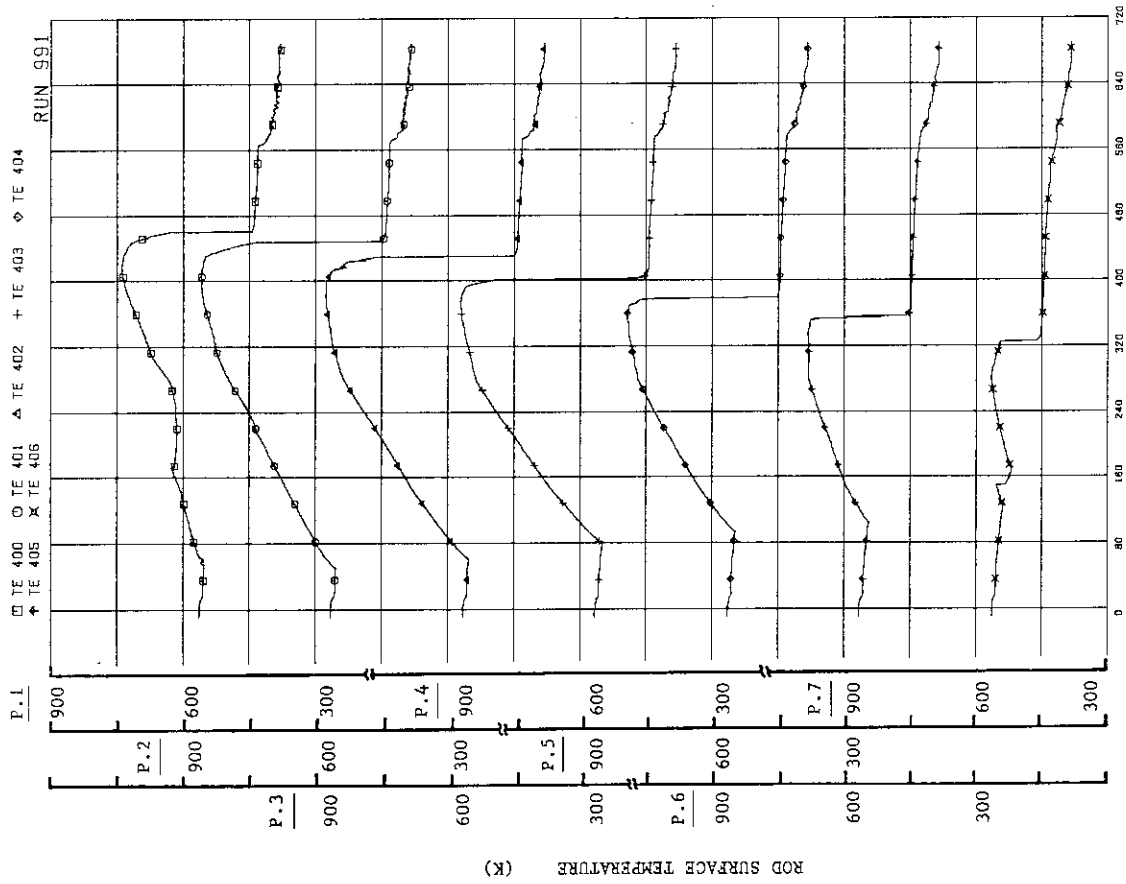

FIG.A. 68 SURFACE TEMPERATURE OF FUEL ROD D22

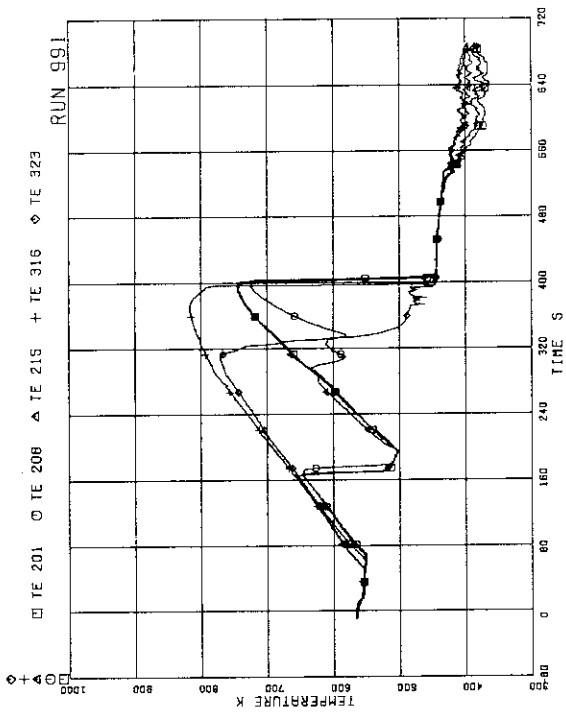

FIG.A. 71 SURFACE TEMPERATURES OF FUEL RODS A11,A12,A13,A87,A88 AT POSITION 1

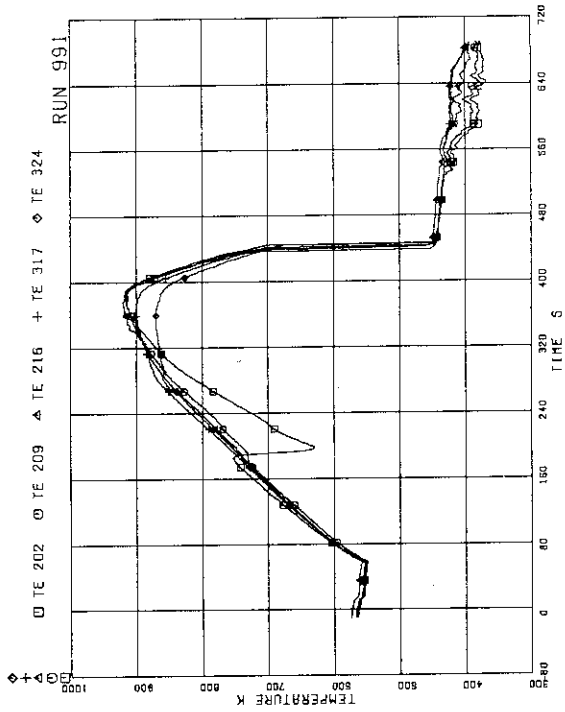

FIG.A. 72 SURFACE TEMPERATURES OF FUEL RODS A11,A12,A13,A88 AT POSITION 2

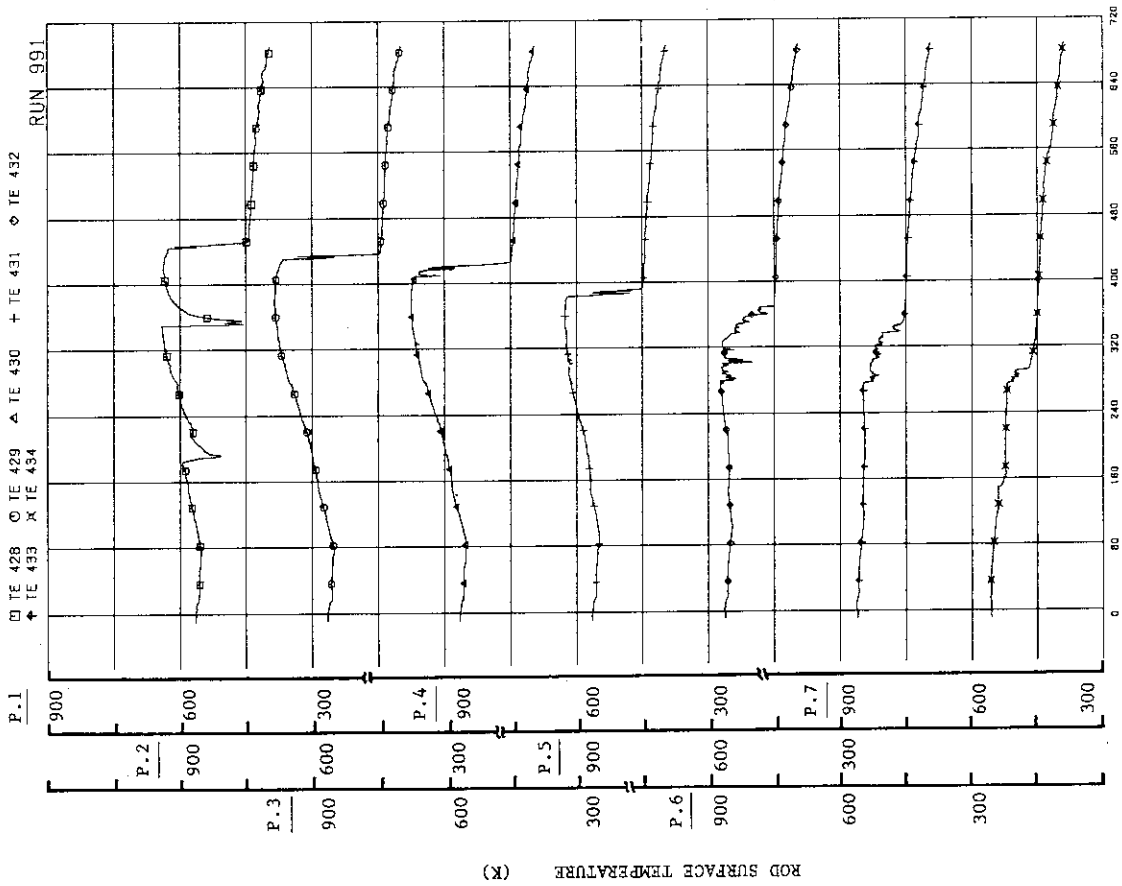

FIG.A. 70 SURFACE TEMPERATURE OF WATER ROD SIMULATOR C45

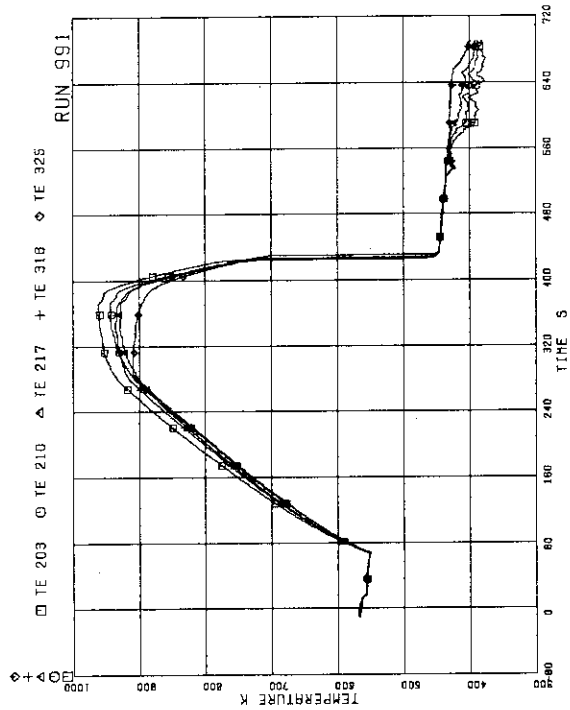

FIG.A. 73 SURFACE TEMPERATURES OF FUEL RODS A11,A12,A13,A87,A88 AT POSITION 3

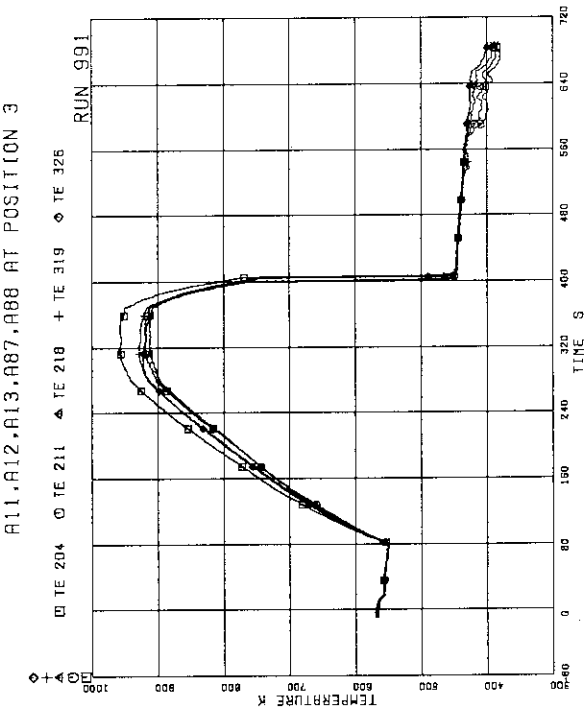

FIG.A. 74 SURFACE TEMPERATURES OF FUEL RODS A11,A12,A13,A87,A88 AT POSITION 4

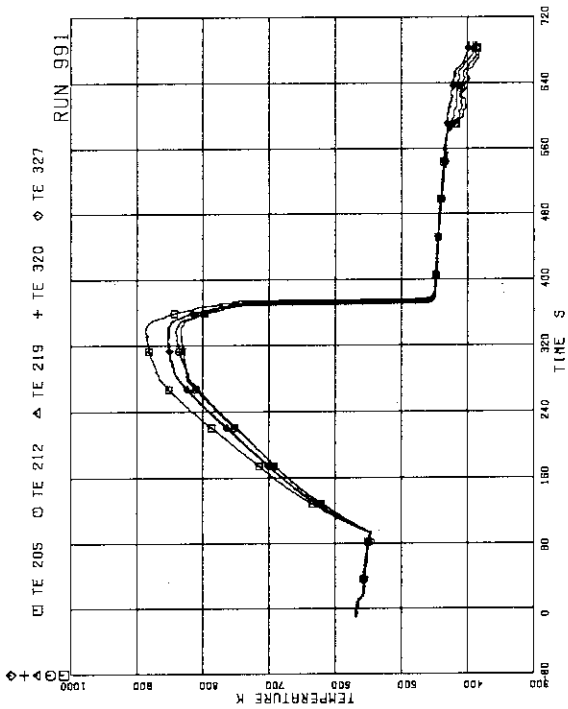

FIG.A. 75 SURFACE TEMPERATURES OF FUEL RODS A11,A12,A13,A87,A88 AT POSITION 5

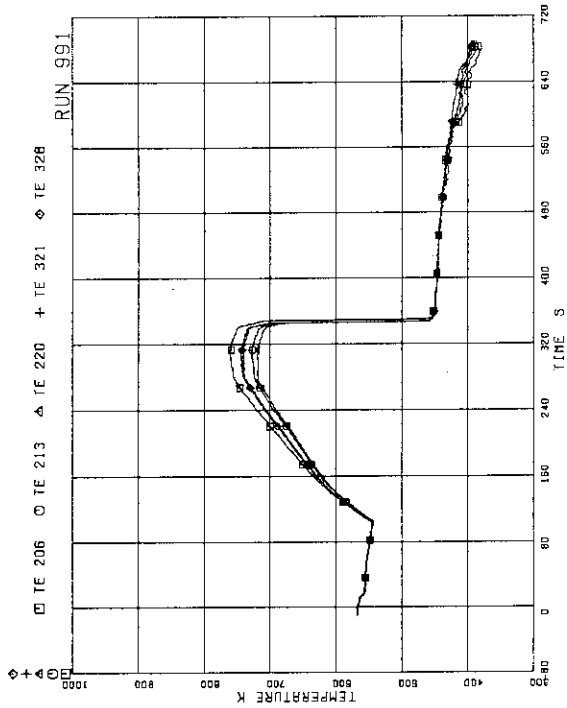

FIG.A. 76 SURFACE TEMPERATURES OF FUEL RODS A11,A12,A13,A87,A88 AT POSITION 6

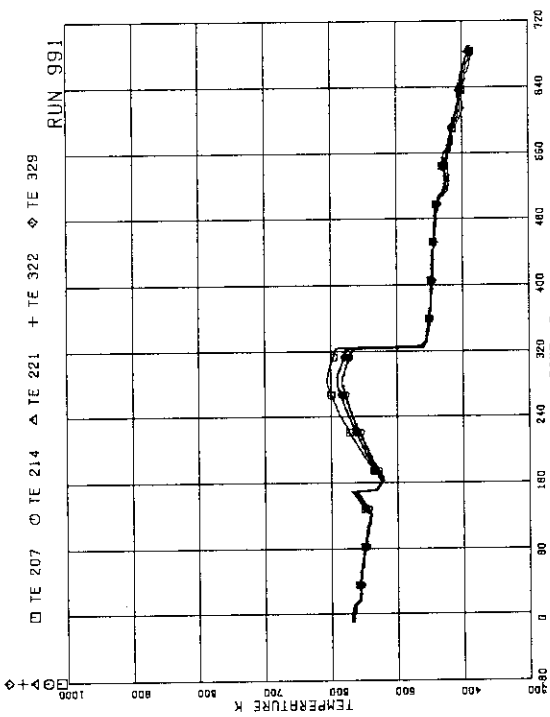

FIG.A. 77 SURFACE TEMPERATURES OF FUEL RODS A11,A12,A13,A87,A88 AT POSITION 7

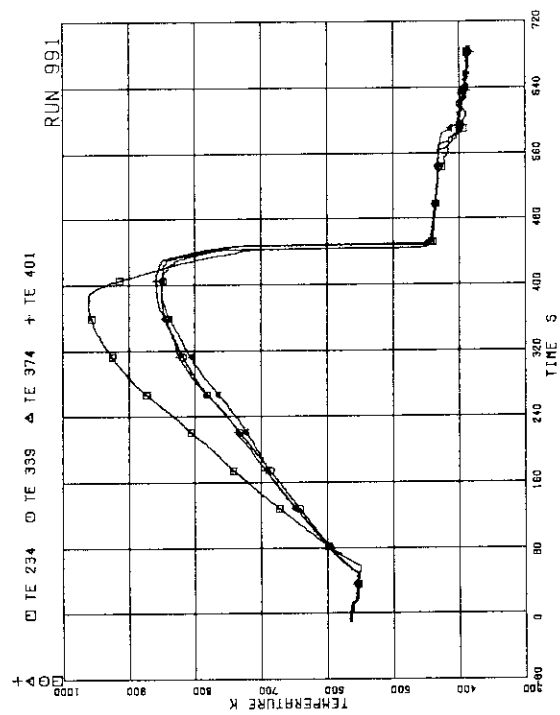

FIG.A. 78 SURFACE TEMPERATURES OF FUEL RODS A22,B22,C22,D22 AT POSITION 1

FIG.A. 79 SURFACE TEMPERATURES OF FUEL RODS A22,B22,C22,D22 AT POSITION 2

FIG.A. 80 SURFACE TEMPERATURES OF FUEL RODS A22,B22,C22,D22 AT POSITION 3

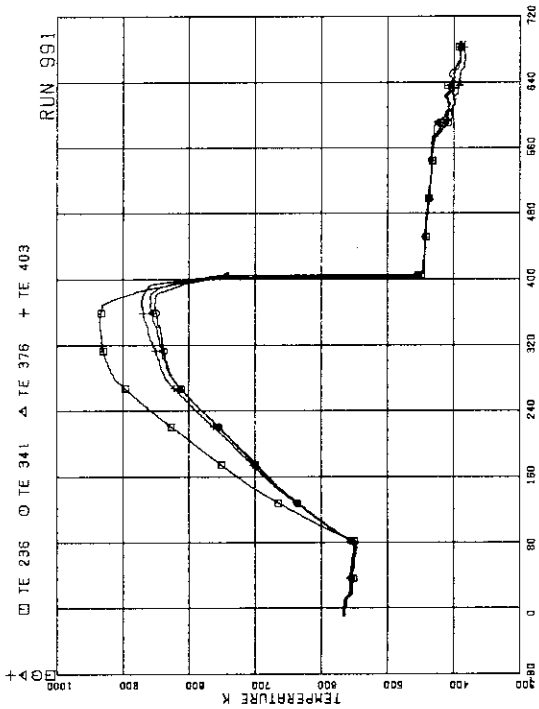

FIG.A. 81 SURFACE TEMPERATURES OF FUEL RODS A22,C22,D22 AT POSITION 4

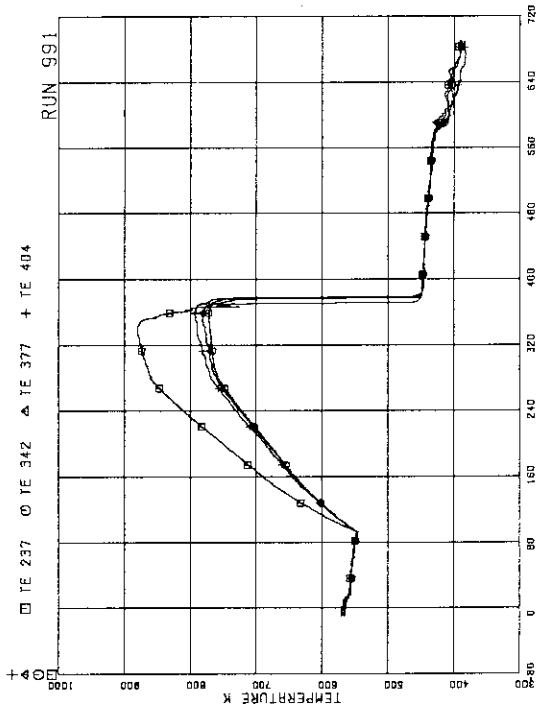

FIG.A. 82 SURFACE TEMPERATURES OF FUEL RODS A22,B22,C22,D22 AT POSITION 5

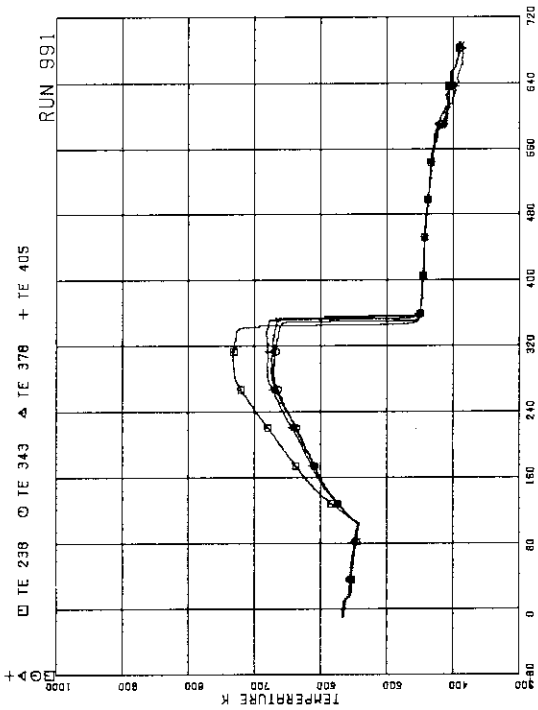

FIG.A. 83 SURFACE TEMPERATURES OF FUEL RODS A22,B22,C22,D22 AT POSITION 6

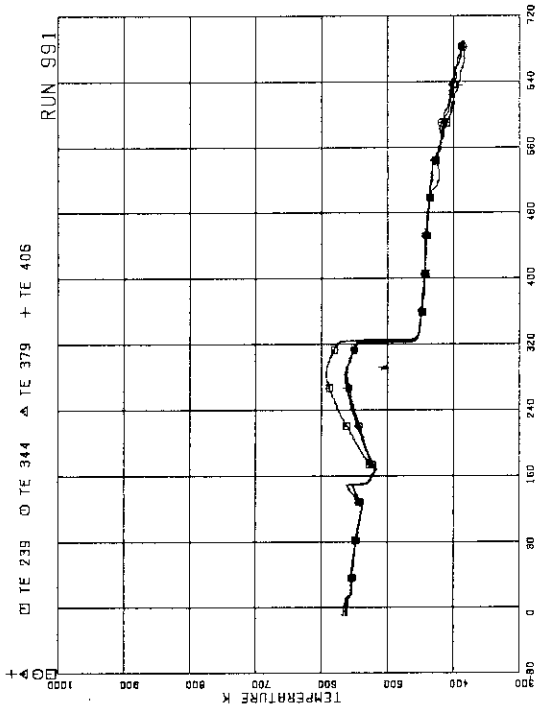

FIG.A. 84 SURFACE TEMPERATURES OF FUEL RODS A22,B22,C22,D22 AT POSITION 7

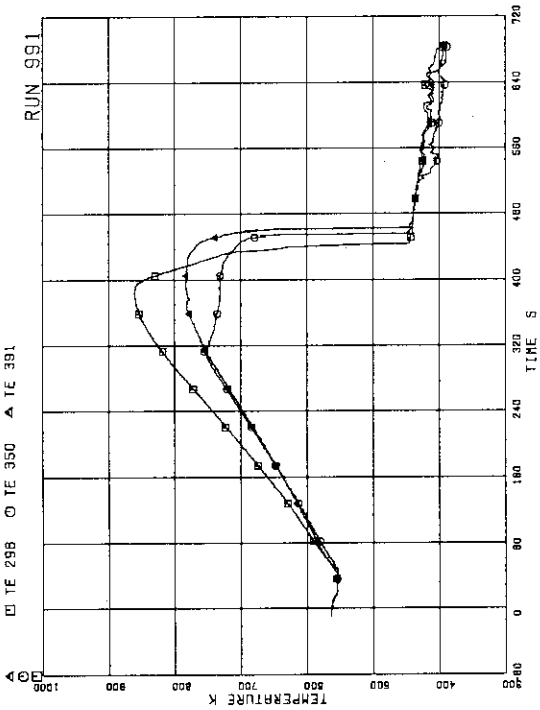

FIG.A. 85 SURFACE TEMPERATURES OF FUEL RODS A77,B77,C77 AT POSITION 1

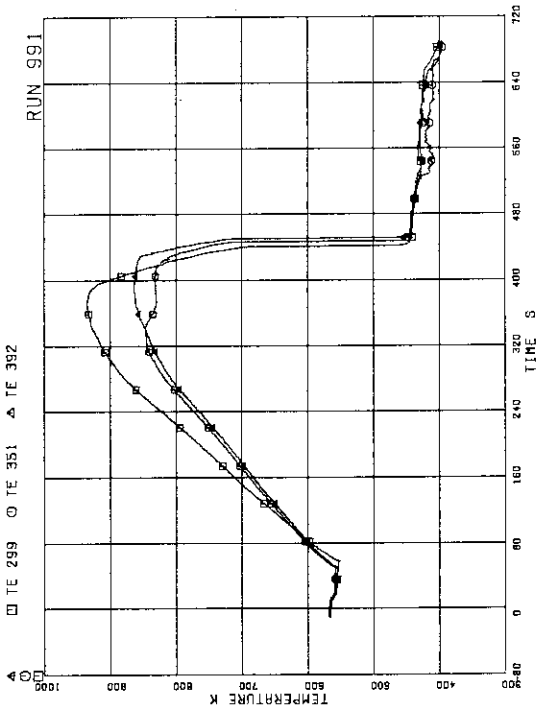

FIG.A. 86 SURFACE TEMPERATURES OF FUEL RODS A77,B77,C77 AT POSITION 2

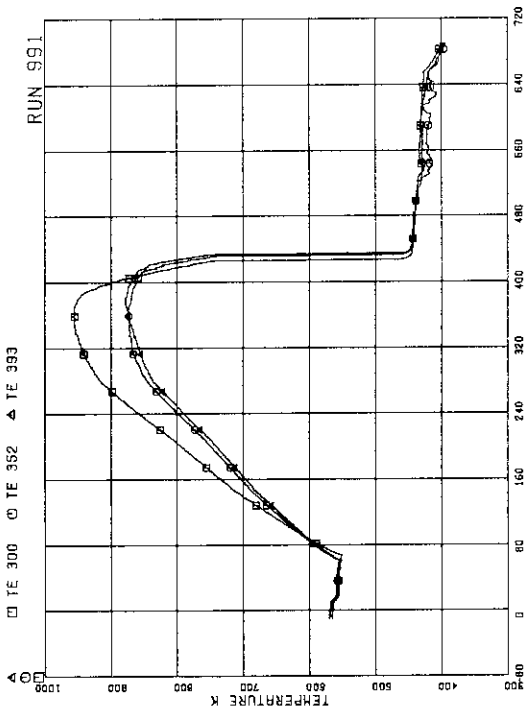

FIG.A. 87 SURFACE TEMPERATURES OF FUEL RODS A77,B77,C77 AT POSITION 3

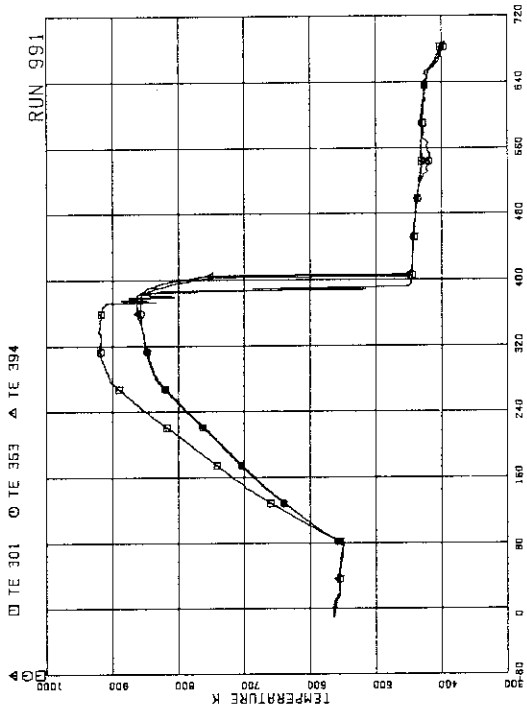

FIG.A. 88 SURFACE TEMPERATURES OF FUEL RODS A77,B77,C77 AT POSITION 4

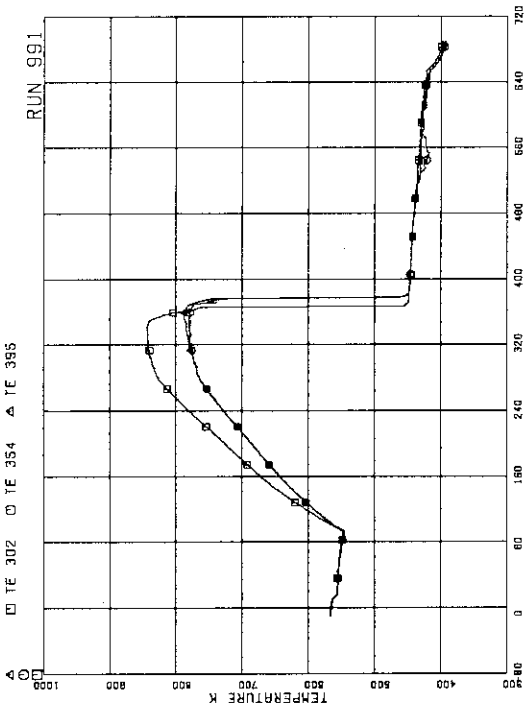

FIG.A. 89 SURFACE TEMPERATURES OF FUEL RODS A77,B77,C77 AT POSITION 5

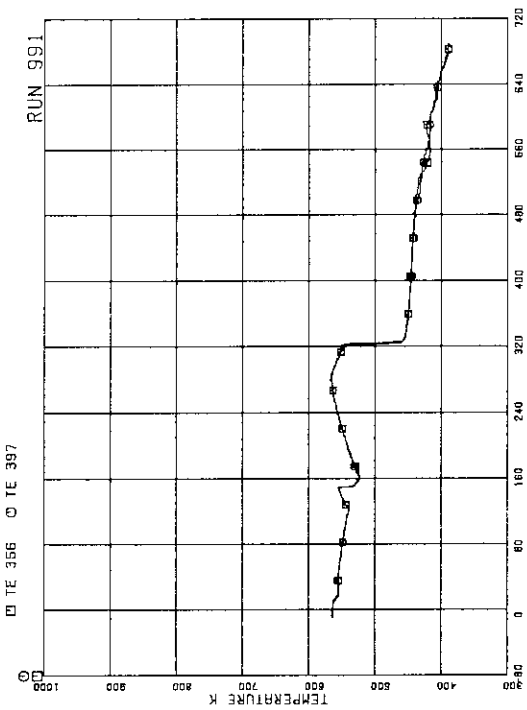

FIG.A. 91 SURFACE TEMPERATURES OF FUEL RODS B77,C77 RODS AT POSITION 7

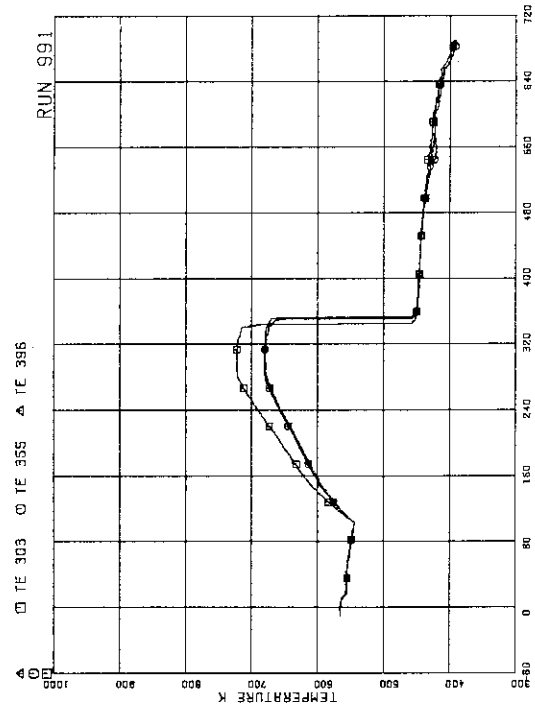

FIG.A. 90 SURFACE TEMPERATURES OF FUEL RODS A77,B77,C77 AT POSITION 6

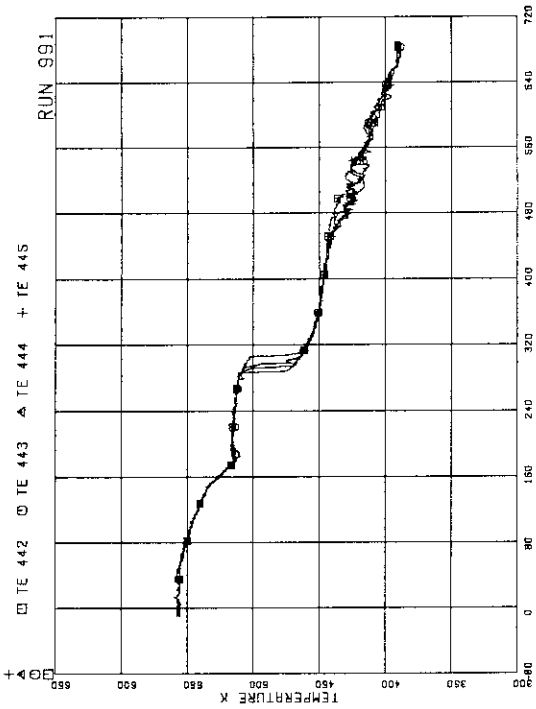

FIG.A. 92 FLUID TEMPERATURES AT CHANNEL INLET

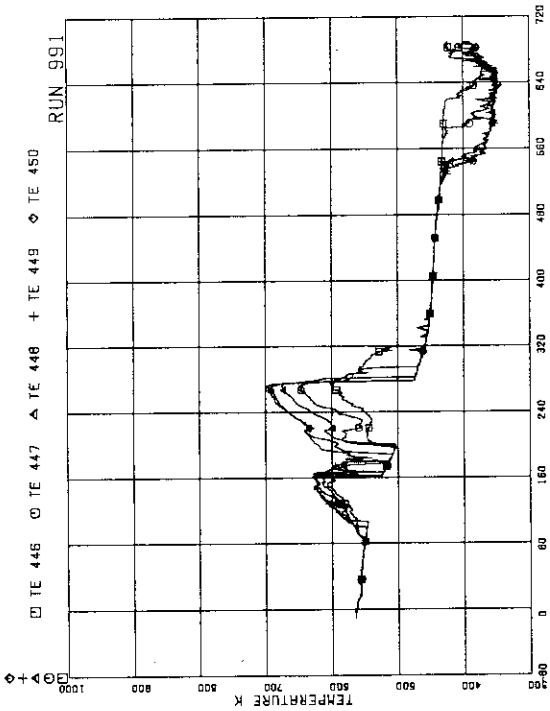

FIG.A. 93 FLUID TEMPERATURES AT CHANNEL A OUTLET

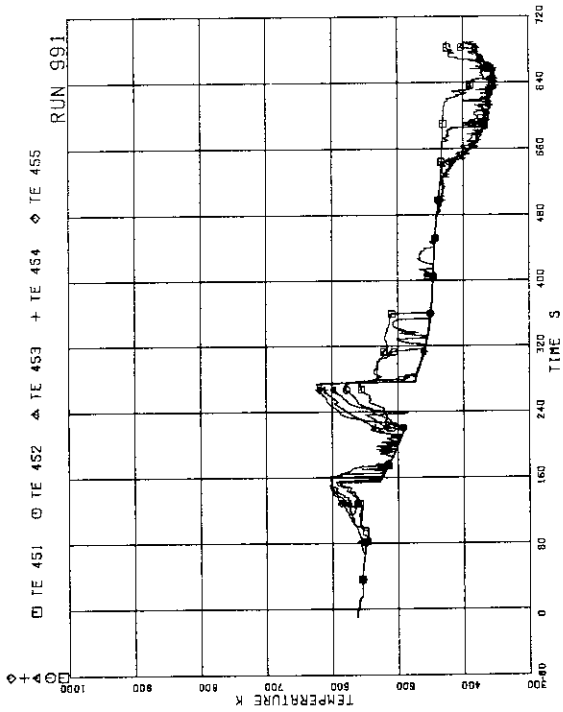

FIG.A. 94 FLUID TEMPERATURES AT CHANNEL C OUTLET

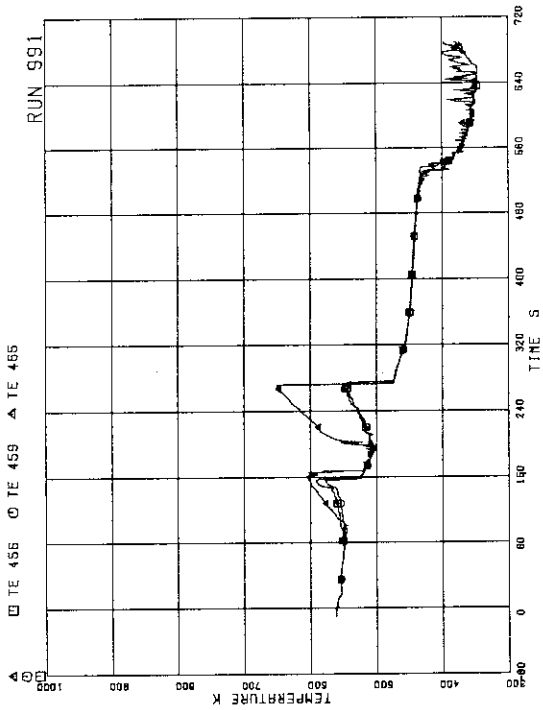

FIG.A. 95 FLUID TEMPERATURES ABOVE UTP OF CHANNEL A, OPENINGS 1,4,10

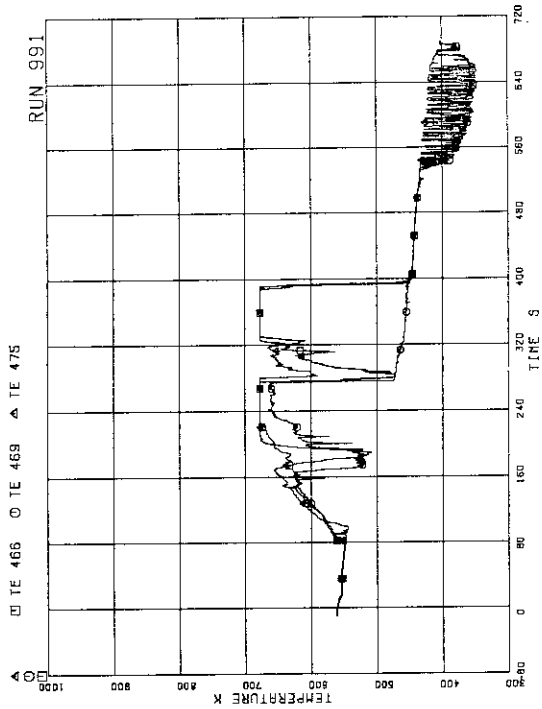

FIG.A. 96 FLUID TEMPERATURES BELOW UTP OF CHANNEL A, OPENINGS 1,4,10

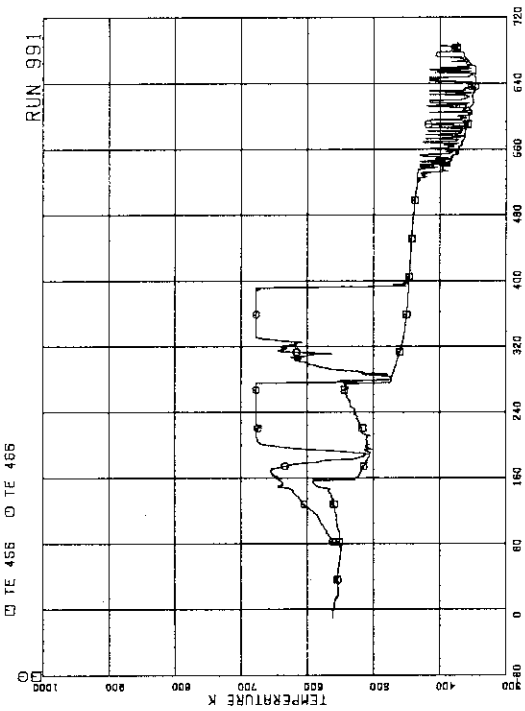

FIG.A. 97 FLUID TEMPERATURES AT UTP IN CHANNEL A, OPENING 1

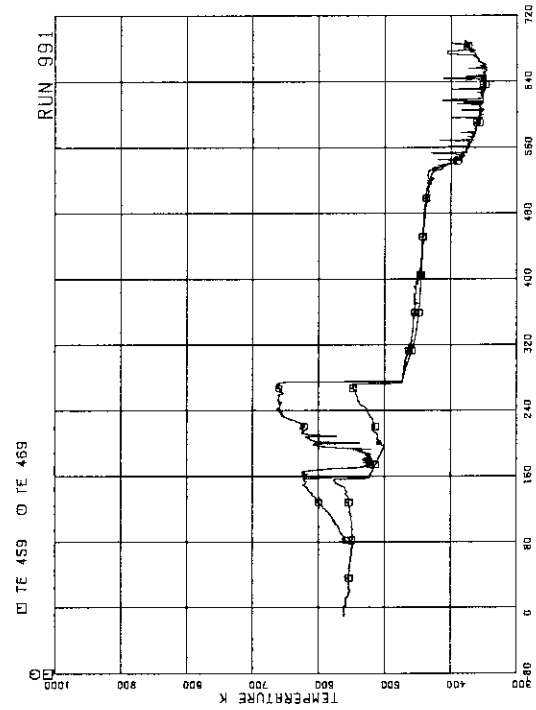

FIG.A. 98 FLUID TEMPERATURES AT UTP IN CHANNEL A, OPENING 4

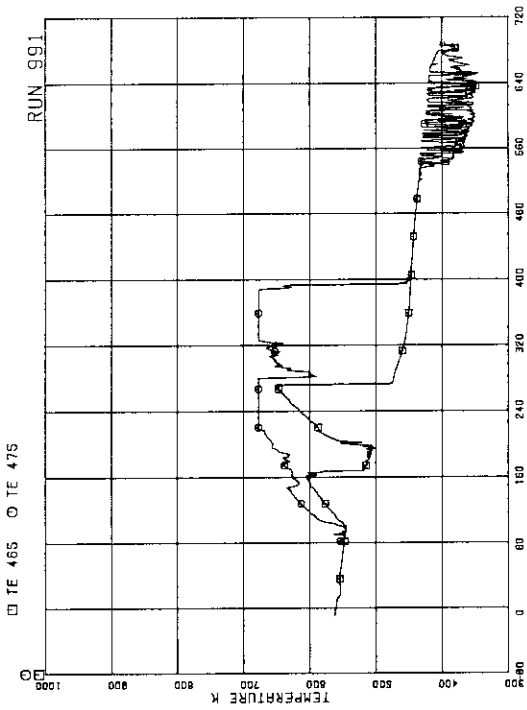

FIG.A. 99 FLUID TEMPERATURES AT UTP IN CHANNEL A, OPENING 10

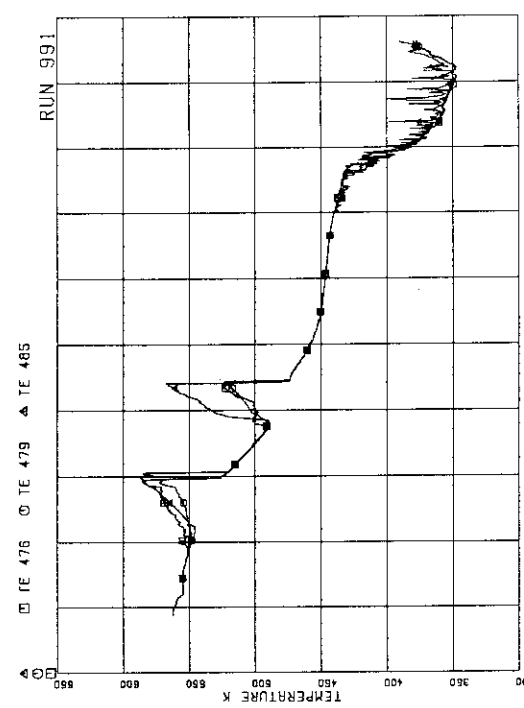

FIG.A.100 FLUID TEMPERATURES ABOVE UTP OF CHANNEL C, OPENINGS 1,4,10

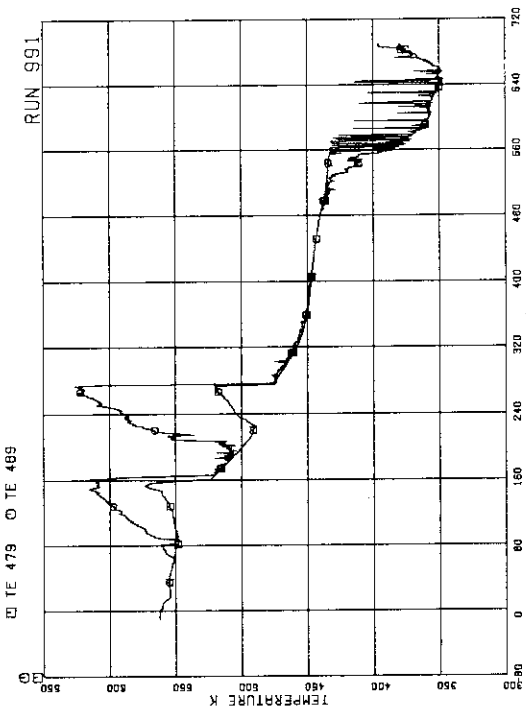

FIG.A.103 FLUID TEMPERATURES AT UTP IN CHANNEL C, OPENING 4

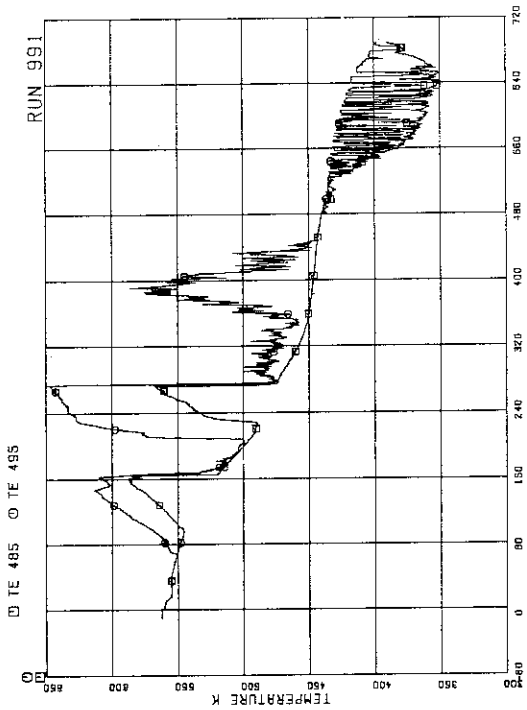

FIG.A.104 FLUID TEMPERATURES AT UTP IN CHANNEL C, OPENING 10

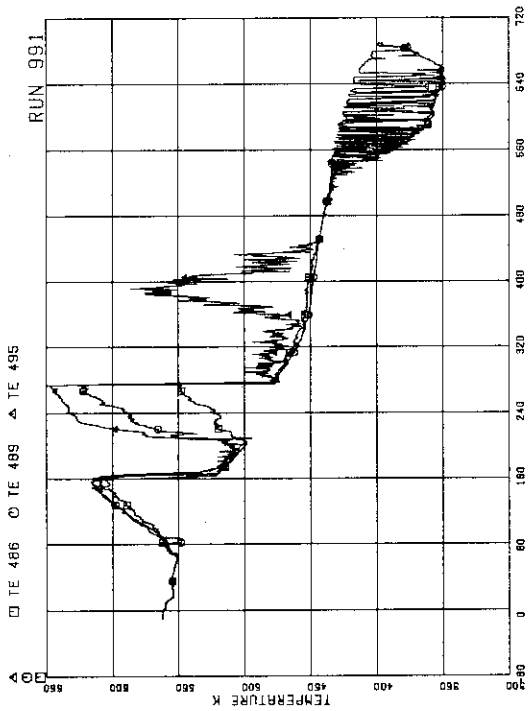

FIG.A.101 FLUID TEMPERATURES BELOW UTP OF CHANNEL C, OPENINGS 1,4,10

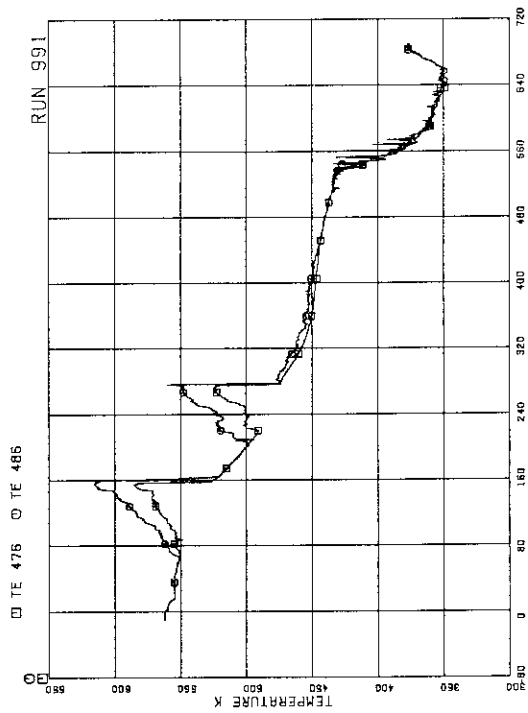

FIG.A.102 FLUID TEMPERATURES AT UTP IN CHANNEL C, OPENINGS 1

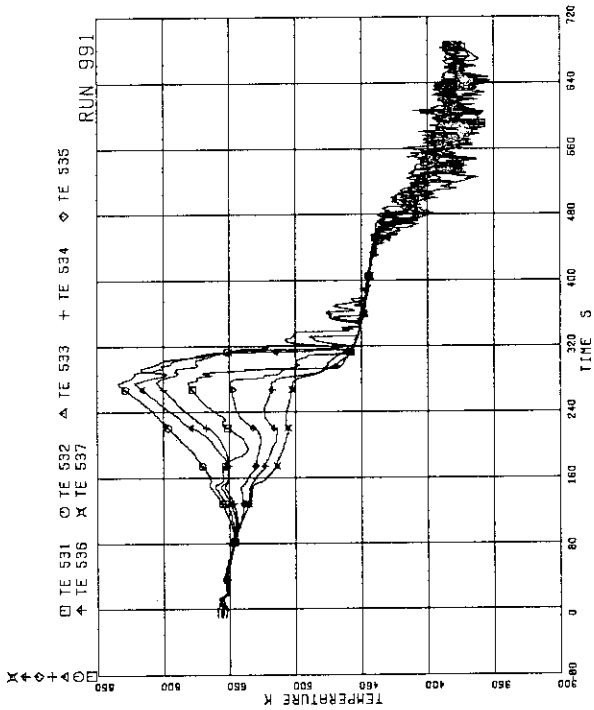

FIG.A.105 OUTER SURFACE TEMPERATURE OF CHANNEL BOX AT POS.1 THROUGH 7

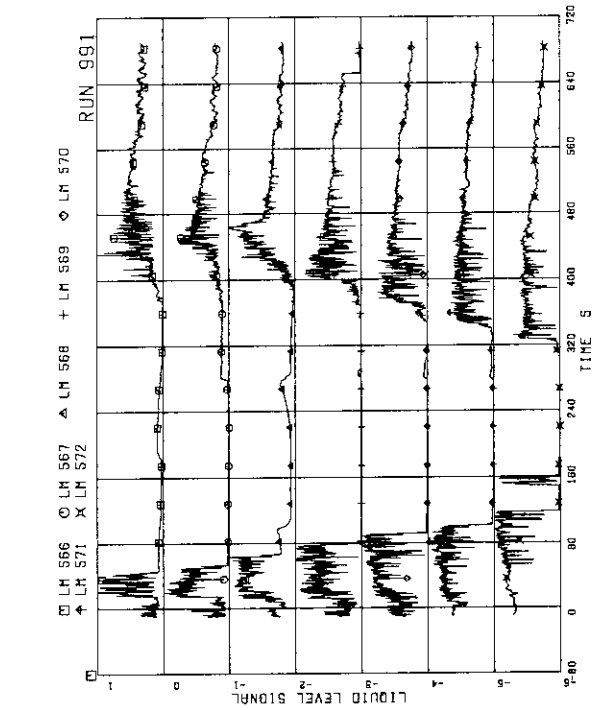

FIG.A.107 LIQUID LEVEL SIGNALS IN CHANNEL BOX A, LOCATION A2

FIG.A.106 FLUID TEMPERATURES IN LOWER PLENUM, CENTER

FIG.A.108 LIQUID LEVEL SIGNALS IN CHANNEL BOX B

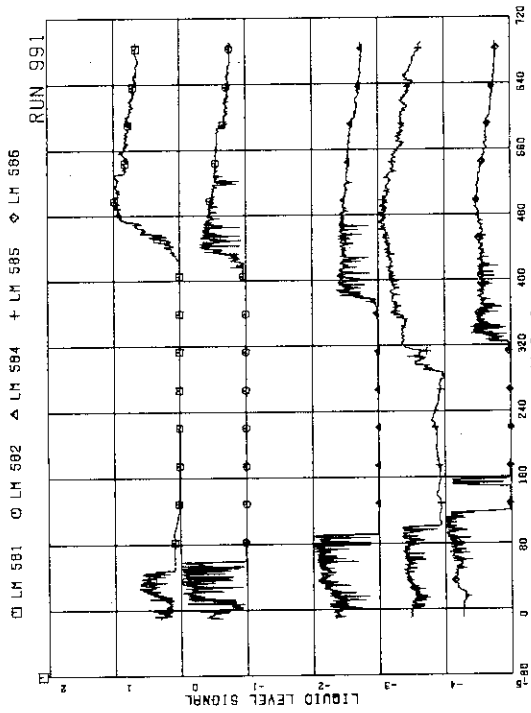

FIG.A.109 LIQUID LEVEL SIGNALS IN CHANNEL BOX C

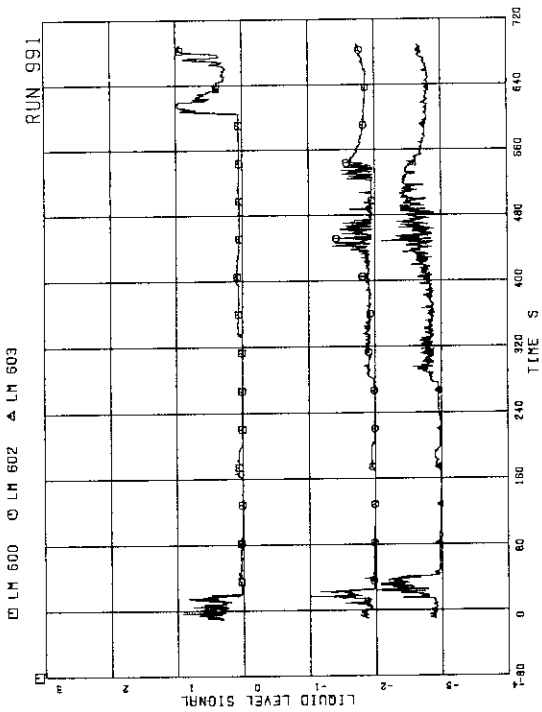

FIG.A.111 LIQUID LEVEL SIGNALS IN CHANNEL A OUTLET CENTER

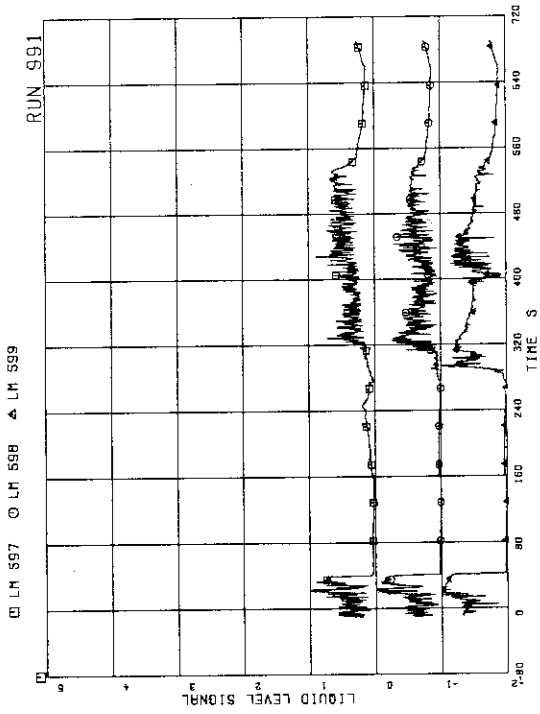

FIG.A.110 LIQUID LEVEL SIGNALS IN CHANNEL A OUTLET LOCATION A2

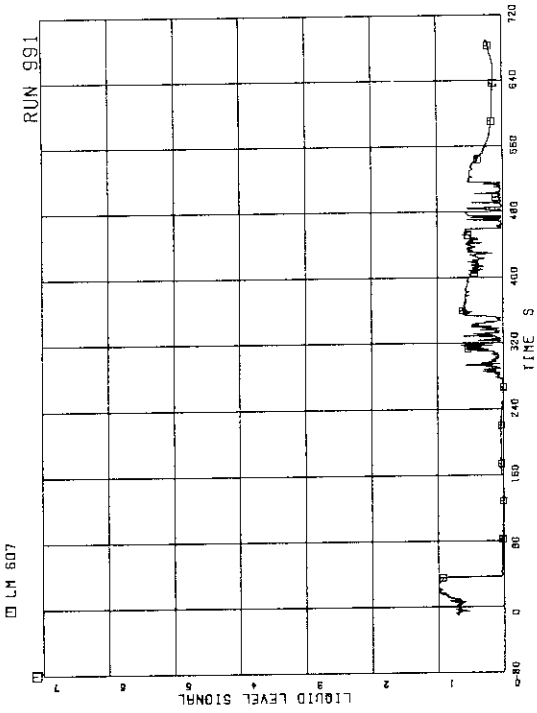

FIG.A.112 LIQUID LEVEL SIGNALS IN CHANNEL C OUTLET LOCATION C2

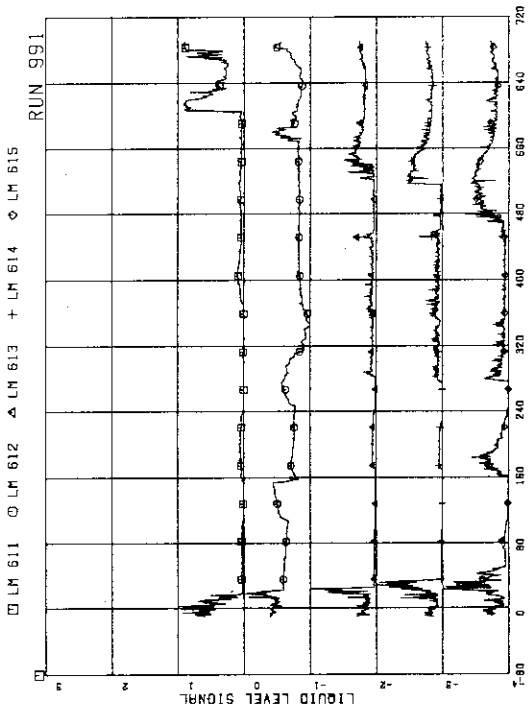

FIG.A.113 LIQUID LEVEL SIGNALS IN CHANNEL C OUTLET CENTER

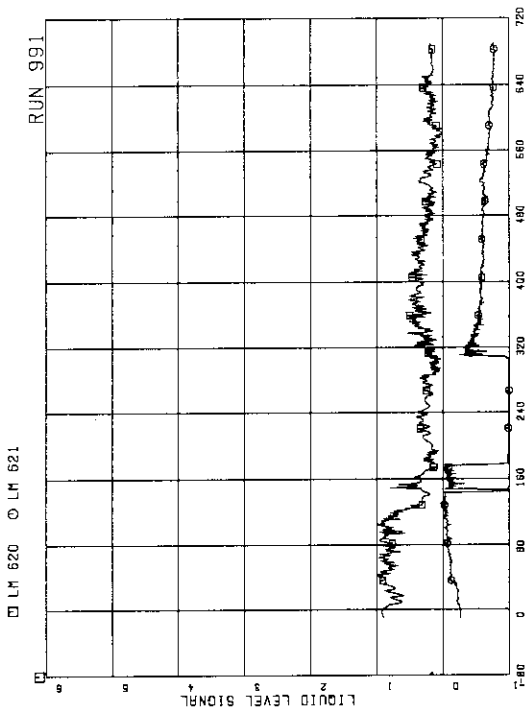

FIG.A.115 LIQUID LEVEL SIGNALS IN CHANNEL C INLET

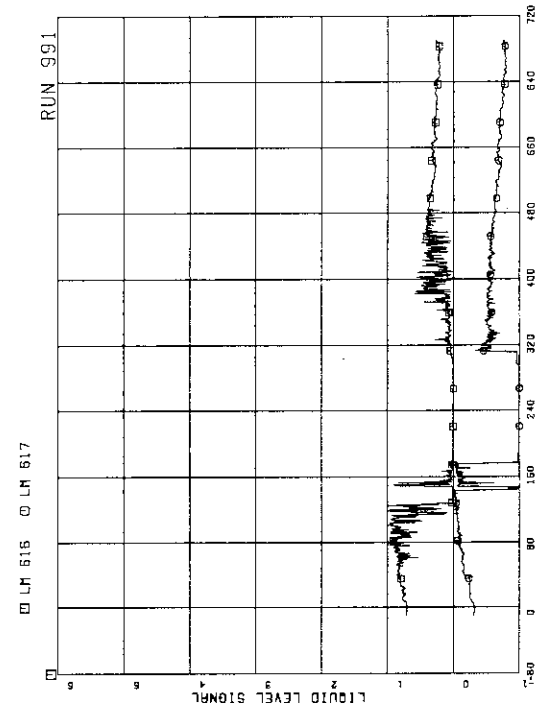

FIG.A.114 LIQUID LEVEL SIGNALS IN CHANNEL A INLET

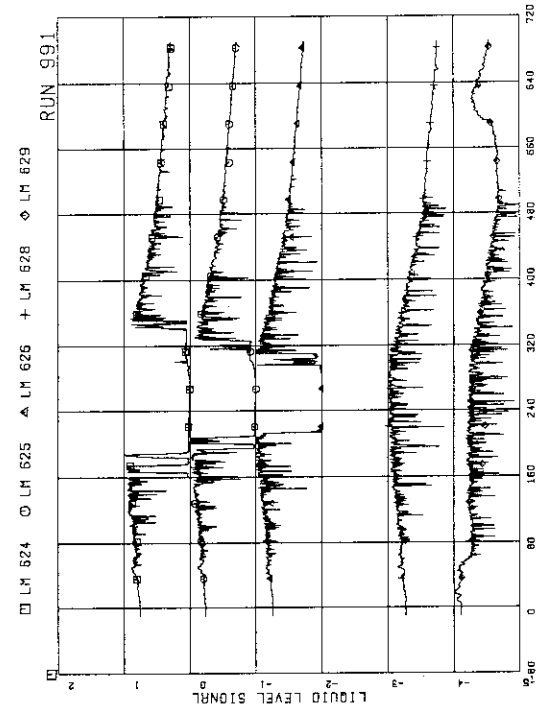

FIG.A.116 LIQUID LEVEL SIGNALS IN LOWER PLENUM, NORTH

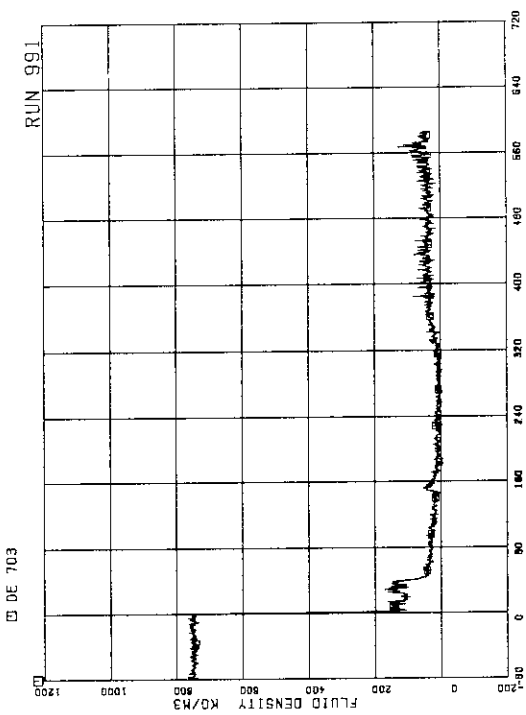

FIG.A.119 AVERAGE DENSITY AT BREAK A UPSTREAM

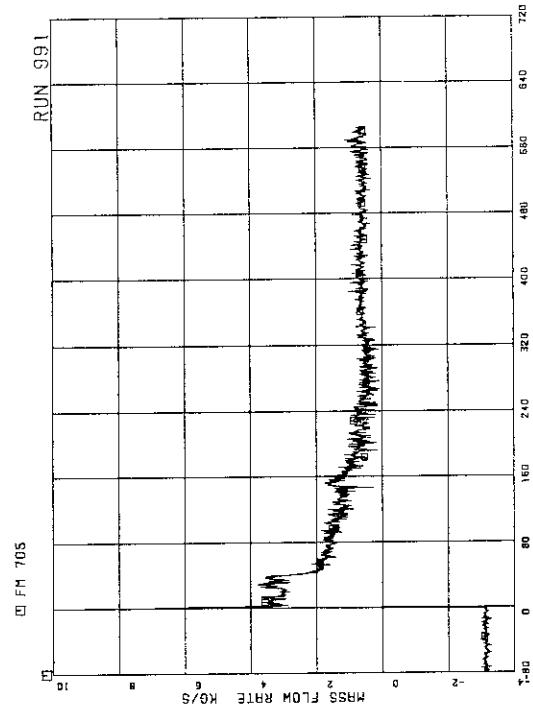

FIG.A.120 FLOW RATE AT BREAK A UPSTREAM (BASED ON LOW RANGE DRAG-DISK DATA)

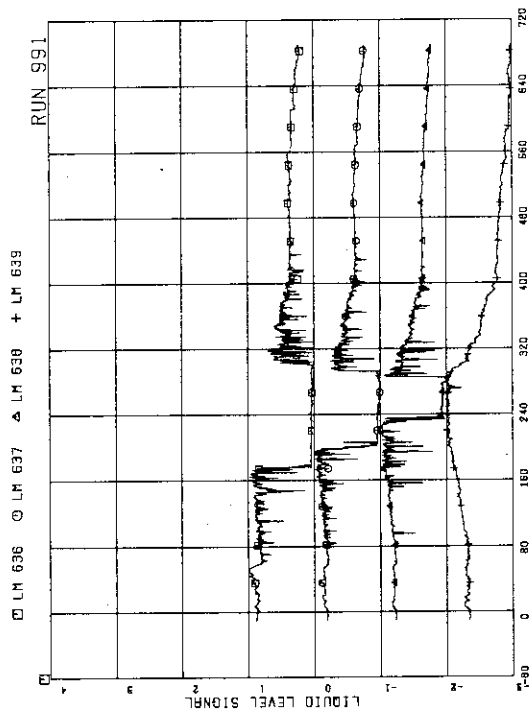

FIG.A-117 LIQUID LEVEL SIGNALS IN GUIDE TUBE, NORTH

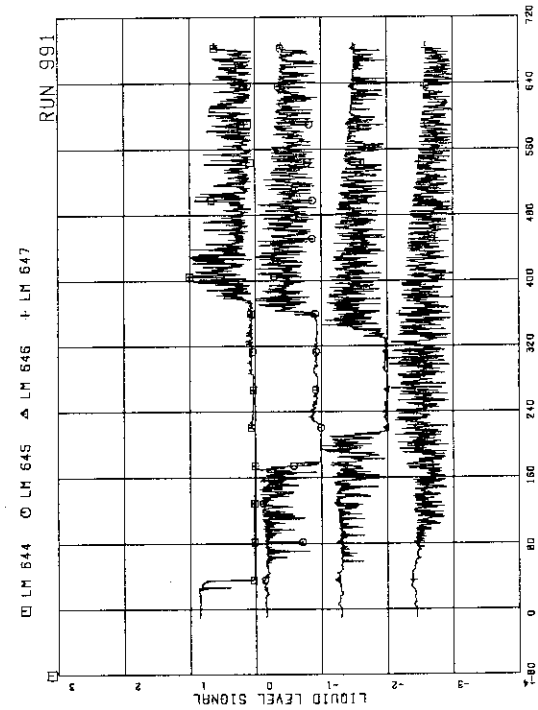

FIG.A.118 LIQUID LEVEL SIGNALS IN DOWNCOMER, D SIDE

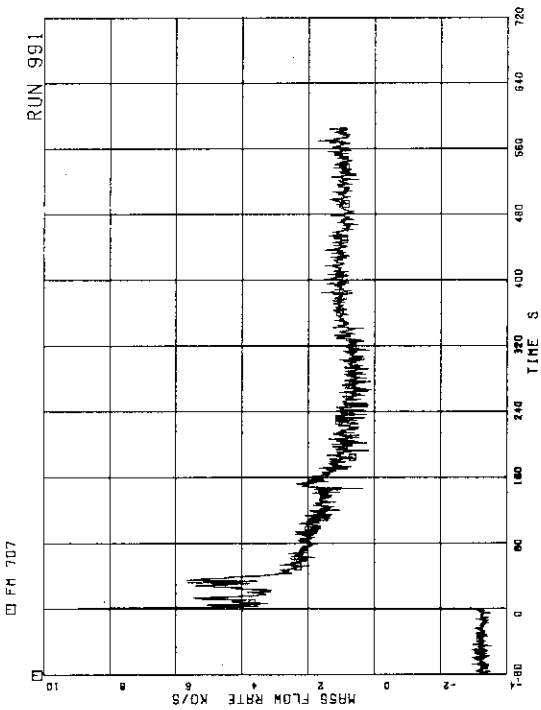

FIG.A.121 FLOW RATE AT BREAK A UPSTREAM (BASED ON HIGH RANGE DRAG-DISK DATA)

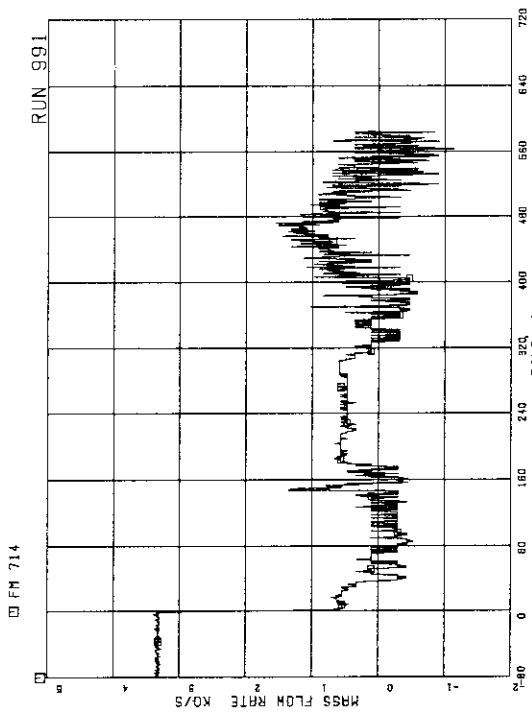

FIG.A.123 FLOW RATE AT CHANNEL A INLET

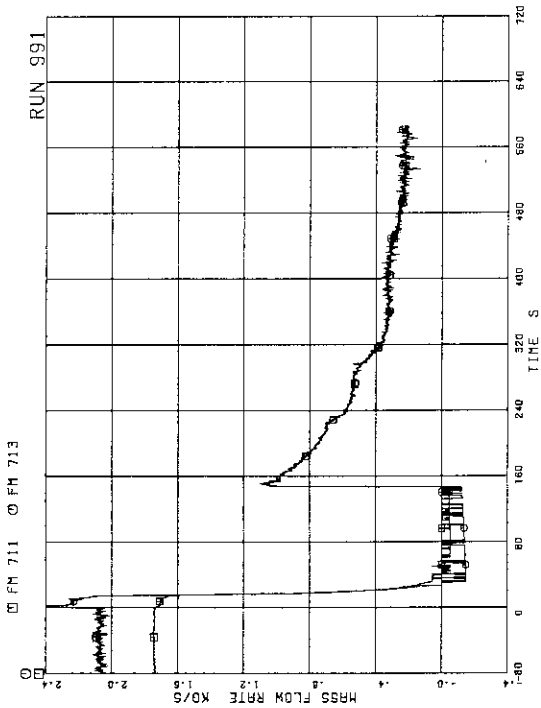

FIG.A.122 STEAM DISCHARGE FLOW RATE THROUGH MSL

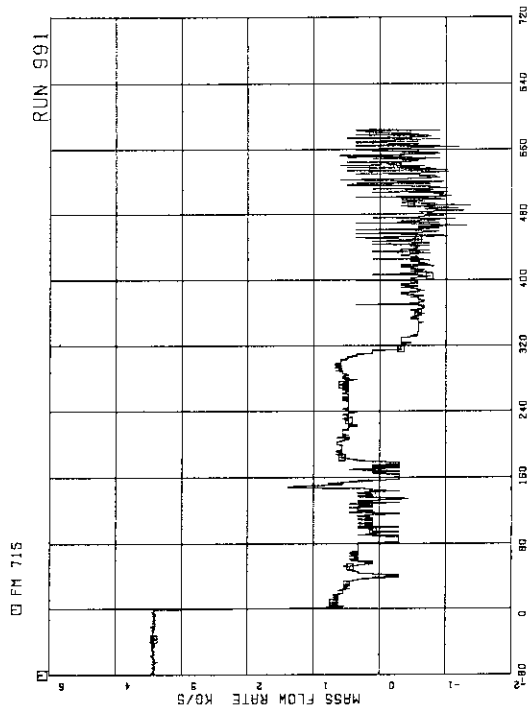

FIG.A.124 FLOW RATE AT CHANNEL B INLET

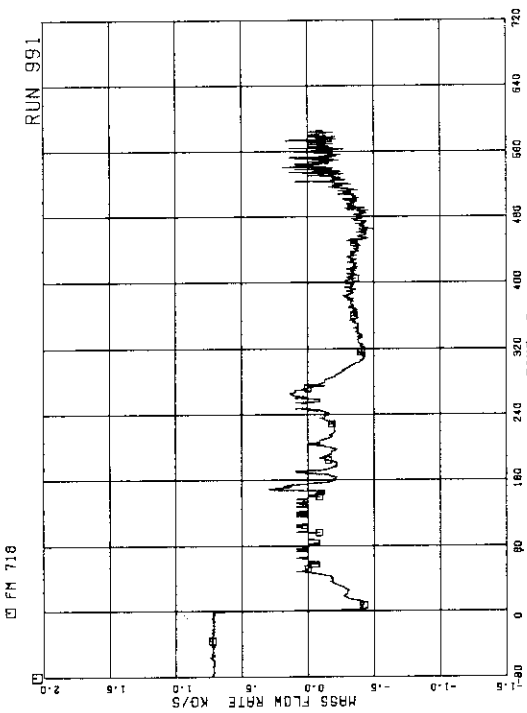

FIG.A.127 FLOW RATE AT BYPASS HOLE

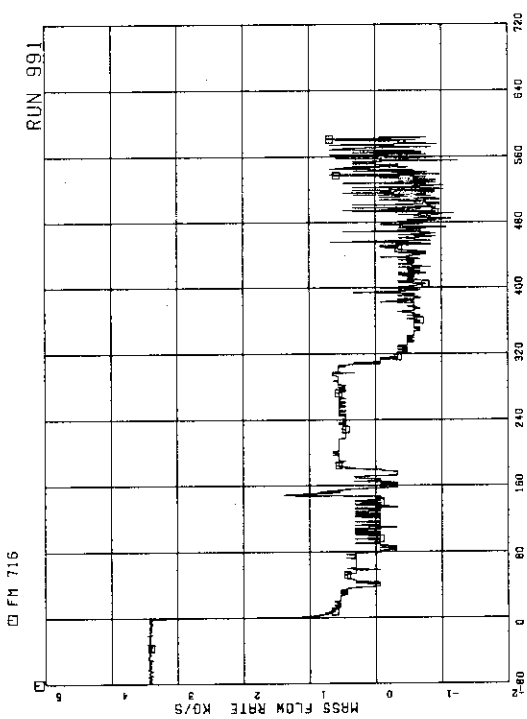

FIG.A.125 FLOW RATE AT CHANNEL C INLET

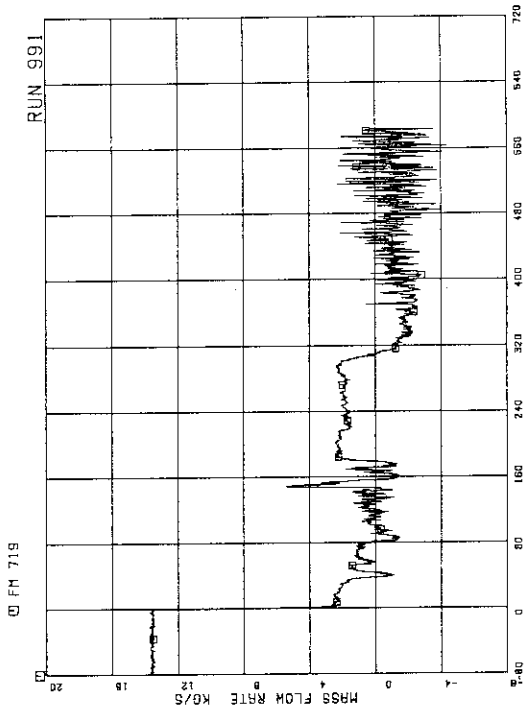

FIG.A.128 TOTAL CHANNEL INLET FLOW RATE

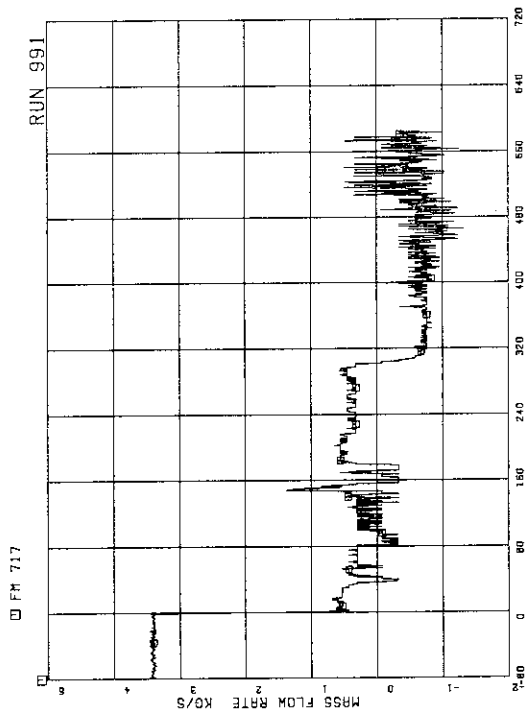

FIG.A.126 FLOW RATE AT CHANNEL D INLET

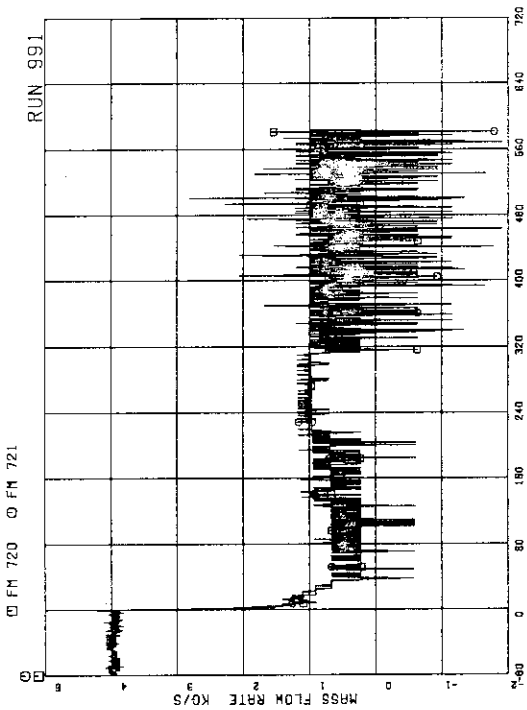

FIG.A.129 FLOW RATE AT JP-1,2 OUTLET (POS. FLOW)

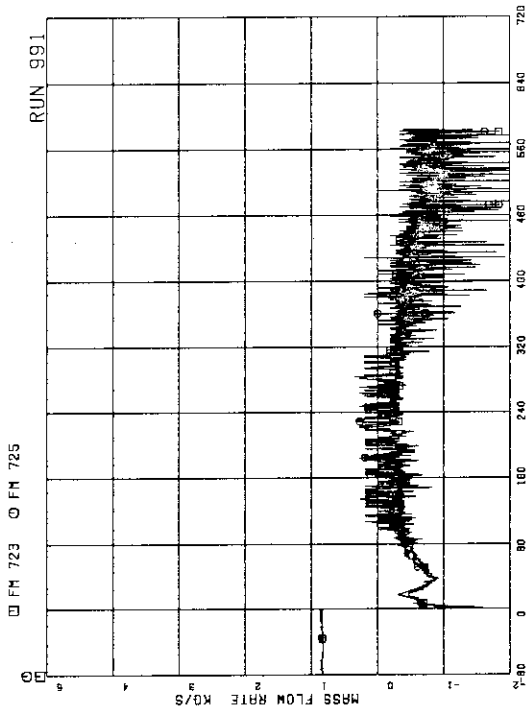

FIG.A.131 FLOW RATE AT JP-3,4 OUTLET (NEG. FLOW)

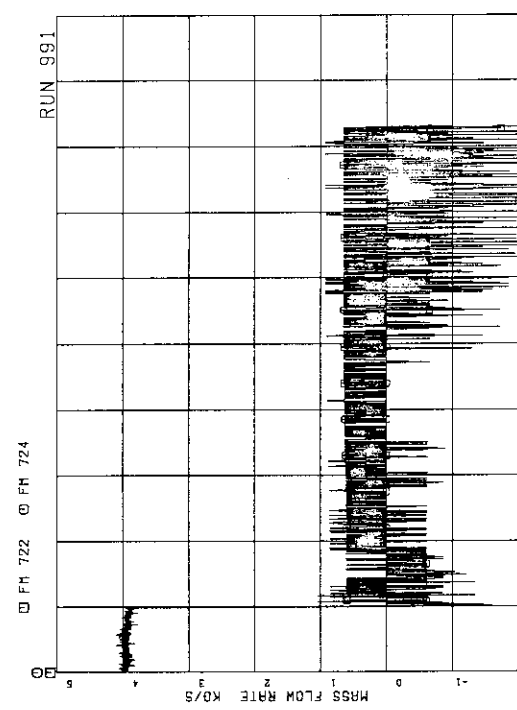

FIG.A.130 FLOW RATE AT JP-3,4 OUTLET (POS. FLOW)

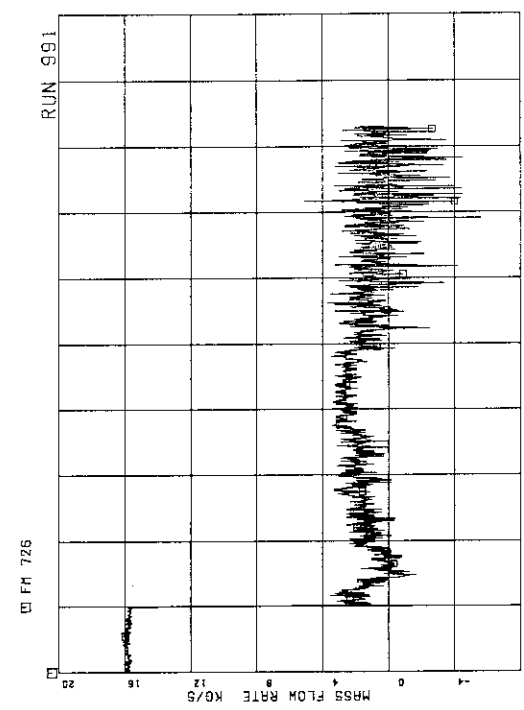

FIG.A.132 TOTAL JP OUTLET FLOW RATE (POS. FLOW)

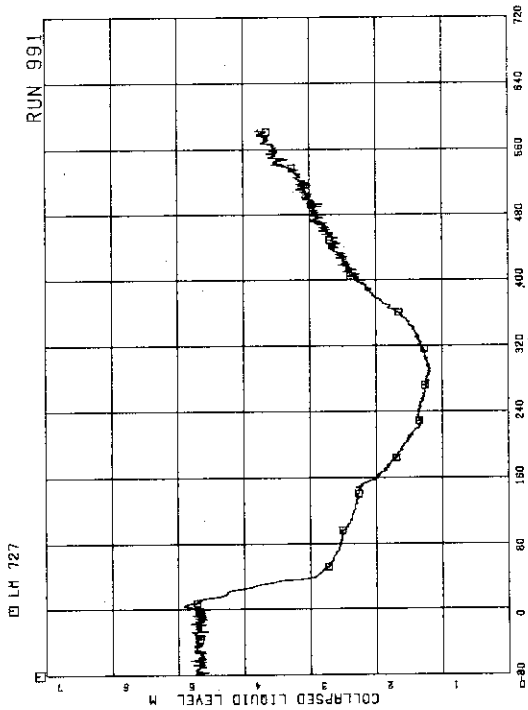

FIG.A.133 COLLAPSED LIQUID LEVEL IN DOWNCOMER

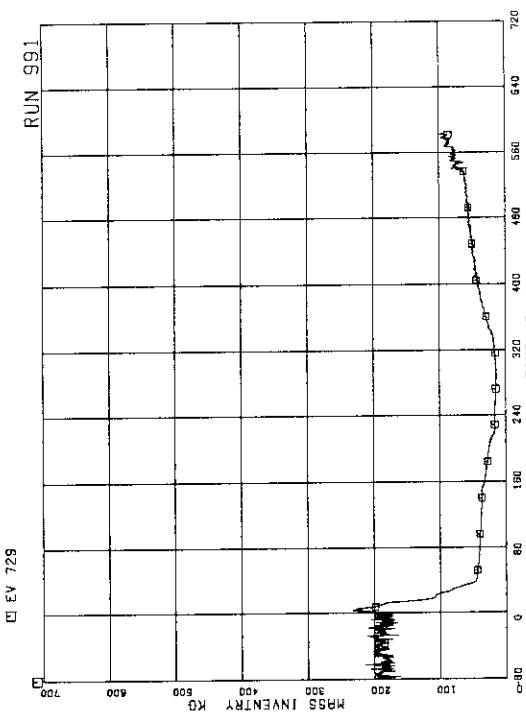

FIG.A.135 FLUID INVENTORY IN DOWNCOMER

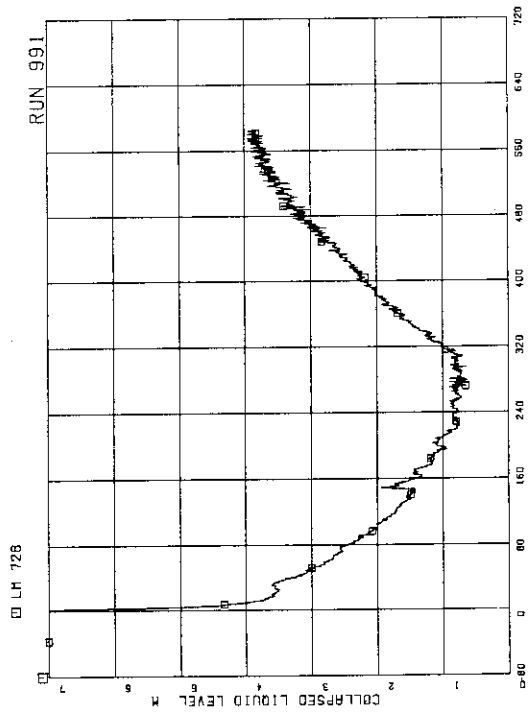

FIG.A.134 COLLAPSED LIQUID LEVEL INSIDE CORE SHROUD

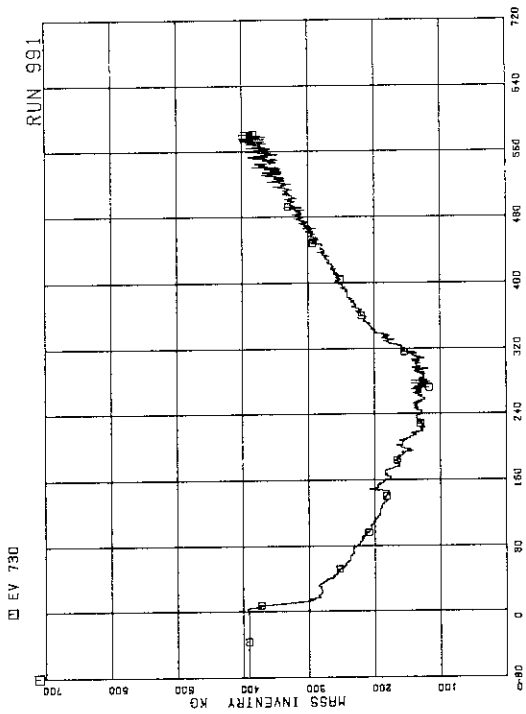

FIG.A.136 FLUID INVENTORY INSIDE CORE SHROUD

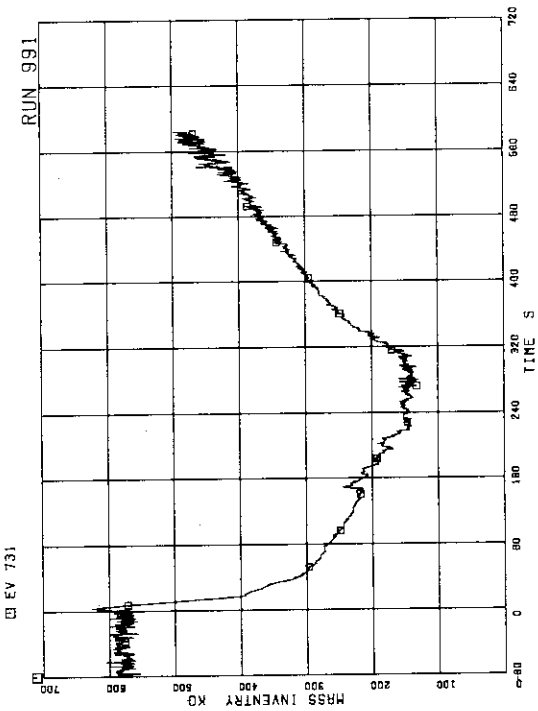

FIG.A.137 TOTAL FLUID INVENTORY IN PRESSURE VESSEL

Appendix III Maximum Cladding Temperature Distribution in RUN 991

Maximum surface temperature at each thermo-couple is searched during a time period after the break and data plotting time, and is recorded with its observation time.

Table A.4 Maximum temperature distribution for RUN 991

Table A.4 Maximum temperature distribution for RUN 991

	Pos.1	Pos.2	Pos.3	Pos.4	Pos.5	Pos.6	Pos.7
A-11 rod	TE 201	TE 202	TE 203	TE 204	TE 205	TE 206	TE 207
PCT (K)	743.5	916.3	961.9	958.3	886.3	760.3	606.7
Time (s)	391.3	382.2	366.8	315.7	331.1	301.0	282.1
A-12 rod	TE 208	TE 209	TE 210	TE 211	TE 212	TE 213	TE 214
PCT (K)	724.3	913.9	943.9	919.9	841.9	727.9	583.9
Time (s)	394.8	370.3	352.1	315.7	336.0	301.7	280.7
A-13 rod	TE 215	TE 216	TE 217	TE 218	TE 219	TE 220	TE 221
PCT (K)	744.7	919.9	929.5	913.9	833.5	723.1	583.9
Time (s)	389.9	371.0	340.2	324.8	325.5	275.8	277.2
A-14 rod	TE 222	TE 223	TE 224	TE 225	TE 226	TE 227	TE 228
PCT (K)	------	------	------	------	------	------	------
Time (s)	------	------	------	------	------	------	------
A-15 rod	TE 229			TE 230			
PCT (K)	------			------			
Time (s)	------			------			
A-17 rod	TE 231			TE 232			
PCT (K)	------			909.1			
Time (s)	------			291.2			
A-22 rod	TE 233	TE 234	TE 235	TE 236	TE 237	TE 238	TE 239
PCT (K)	846.7	960.7	984.7	936.0	880.2	732.6	594.1
Time (s)	387.1	369.6	343.7	348.6	333.9	301.0	282.8
A-24 rod	TE 240	TE 241	TE 242	TE 243	TE 244	TE 245	TE 246
PCT (K)	------	------	------	------	------	------	------
Time (s)	------	------	------	------	------	------	------

	Pos.1	Pos.2	Pos.3	Pos.4	Pos.5	Pos.6	Pos.7
A-26 rod	TE 247			TE 248			
PCT (K)	------			------			
Time (s)	------			------			
A-28 rod	TE 249			TE 250			
PCT (K)	------			908.9			
Time (s)	------			340.9			
A-31 rod	TE 251			TE 252			
PCT (K)	------			944.0			
Time (s)	------			337.4			
A-33 rod	TE 253	TE 254	TE 255	TE 256	TE 257	TE 258	TE 259
PCT (K)	814.7	888.6	906.8	885.8	801.3	687.5	567.2
Time (s)	390.6	371.0	367.5	354.2	339.5	303.8	275.1
A-34 rod	TE 260	TE 261	TE 262	TE 263	TE 264	TE 265	TE 266
PCT (K)	------	------	------	------	------	------	------
Time (s)	------	------	------	------	------	------	------
A-37 rod	TE 267			TE 268			
PCT (K)	------			------			
Time (s)	------			------			
A-42 rod	TE 269			TE 270			
PCT (K)	------			------			
Time (s)	------			------			
A-44 rod	TE 271	TE 272	TE 273	TE 274	TE 275	TE 276	TE 277
PCT (K)	------	------	------	------	------	------	------
Time (s)	------	------	------	------	------	------	------

Table A.4 Maximum temperature distribution for RUN 991 (Cont'd)

	Pos.1	Pos.2	Pos.3	Pos.4	Pos.5	Pos.6	Pos.7
A-48 rod	TE 278			TE 279			
PCT (K)	------			------			
Time (s)	------			------			
A-51 rod	TE 280			TE 281			
PCT (K)	------			------			
Time (s)	------			------			
A-53 rod	TE 282			TE 283			
PCT (K)	------			------			
Time (s)	------			------			
A-57 rod	TE 284			TE 285			
PCT (K)	------			925.5			
Time (s)	------			349.3			
A-62 rod	TE 286			TE 287			
PCT (K)	------			------			
Time (s)	------			------			
A-66 rod	TE 288			TE 289			
PCT (K)	------			------			
Time (s)	------			------			
A-68 rod	TE 290			TE 291			
PCT (K)	------			922.6			
Time (s)	------			306.6			
A-71 rod	TE 292			TE 293			
PCT (K)	------			958.7			
Time (s)	------			304.5			

	Pos.1	Pos.2	Pos.3	Pos.4	Pos.5	Pos.6	Pos.7
A-73 rod	TE 294			TE 295			
PCT (K)	------			952.0			
Time (s)	------			340.9			
A-75 rod	TE 296			TE 297			
PCT (K)	------			------			
Time (s)	------			------			
A-77 rod	TE 298	TE 299	TE 300	TE 301	TE 302	TE 303	TE 304
PCT (K)	861.4	934.9	955.8	920.7	843.5	723.3	------
Time (s)	384.3	366.8	361.9	336.7	337.4	288.4	------
A-82 rod	TE 305			TE 306			
PCT (K)	------			------			
Time (s)	------			------			
A-84 rod	TE 307			TE 308			
PCT (K)	971.0			945.4			
Time (s)	340.2			338.1			
A-85 rod	TE 309	TE 310	TE 311	TE 312	TE 313	TE 314	TE 315
PCT (K)	------	------	------	------	------	------	------
Time (s)	------	------	------	------	------	------	------
A-87 rod	TE 316	TE 317	TE 318	TE 319	TE 320	TE 321	TE 322
PCT (K)	817.2	899.9	935.9	929.2	853.9	741.2	590.3
Time (s)	365.4	368.2	338.1	312.2	326.2	298.2	283.5
A-88 rod	TE 323	TE 324	TE 325	TE 326	TE 327	TE 328	TE 329
PCT (K)	771.3	870.8	909.4	922.6	853.9	744.0	592.2
Time (s)	307.3	355.6	286.3	298.2	320.6	294.0	283.5

Table A.4 Maximum temperature distribution for RUN 991 (Cont'd)

	Pos.1	Pos.2	Pos.3	Pos.4	Pos.5	Pos.6	Pos.7
B-11 rod	TE 330	TE 331	TE 332	TE 333	TE 334	TE 335	TE 336
PCT (K)	622.9	831.3	861.4	852.9	784.4	692.2	------
Time (s)	164.5	392.7	364.0	367.5	347.9	302.4	------
B-13 rod				TE 337			
PCT (K)				855.7			
Time (s)				362.6			
B-22 rod	TE 338	TE 339	TE 340	TE 341	TE 342	TE 343	TE 344
PCT (K)	756.2	851.0	871.7	852.0	773.1	672.3	561.4
Time (s)	409.5	384.3	370.3	365.4	350.0	284.2	0.0
B-31 rod				TE 345			
PCT (K)				------			
Time (s)				------			
B-33 rod				TE 346			
PCT (K)				------			
Time (s)				------			
B-51 rod				TE 347			
PCT (K)				------			
Time (s)				------			
B-53 rod				TE 348			
PCT (K)				------			
Time (s)				------			
B-66 rod				TE 349			
PCT (K)				------			
Time (s)				------			

	Pos.1	Pos.2	Pos.3	Pos.4	Pos.5	Pos.6	Pos.7
B-77 rod	TE 350	TE 351	TE 352	TE 353	TE 354	TE 355	TE 356
PCT (K)	756.2	847.3	873.6	857.6	779.7	681.8	566.2
Time (s)	315.0	335.3	365.4	361.9	322.0	287.7	280.7
B-86 rod				TE 357			
PCT (K)				------			
Time (s)				------			
C-11 rod	TE 358	TE 359	TE 360	TE 361	TE 362	TE 363	TE 364
PCT (K)	640.0	773.1	829.4	852.9	779.7	688.4	568.1
Time (s)	159.6	424.9	385.0	366.1	354.9	286.3	278.6
C-13 rod	TE 365	TE 366	TE 367	TE 368	TE 369	TE 370	TE 371
PCT (K)	646.7	831.3	853.9	854.8	788.2	689.3	571.0
Time (s)	368.2	375.9	373.8	361.2	350.0	284.9	281.4
C-15 rod				TE 372			
PCT (K)				------			
Time (s)				------			
C-22 rod	TE 373	TE 374	TE 375	TE 376	TE 377	TE 378	TE 379
PCT (K)	744.0	851.0	870.8	858.5	782.5	676.1	563.3
Time (s)	417.9	393.4	378.0	365.4	358.4	286.3	0.0
C-31 rod				TE 380			
PCT (K)				------			
Time (s)				------			
C-33 rod	TE 381	TE 382	TE 383	TE 384	TE 385	TE 386	TE 387
PCT (K)	630.5	820.1	829.4	806.0	733.7	643.8	562.3
Time (s)	173.6	394.1	387.1	371.0	352.8	287.0	0.7

Table A.4 Maximum temperature distribution for RUN 991 (Cont'd)

	Pos.1	Pos.2	Pos.3	Pos.4	Pos.5	Pos.6	Pos.7
C-35 rod				TE 388			
PCT (K)				------			
Time (s)				------			
C-66 rod				TE 389			
PCT (K)				------			
Time (s)				------			
C-68 rod				TE 390			
PCT (K)				------			
Time (s)				------			
C-77 rod	TE 391	TE 392	TE 393	TE 394	TE 395	TE 396	TE 397
PCT (K)	783.5	864.2	878.3	864.2	789.1	679.9	567.2
Time (s)	389.9	386.4	374.5	374.5	354.2	298.9	278.6
D-11 rod				TE 398			
PCT (K)				871.7			
Time (s)				356.3			
D-13 rod				TE 399			
PCT (K)				876.4			
Time (s)				359.8			
D-22 rod	TE 400	TE 401	TE 402	TE 403	TE 404	TE 405	TE 406
PCT (K)	738.4	858.5	877.3	871.7	793.8	683.7	565.3
Time (s)	410.9	386.4	374.5	366.8	357.7	333.9	275.1
D-31 rod				TE 407			
PCT (K)				------			
Time (s)				------			

	Pos.1	Pos.2	Pos.3	Pos.4	Pos.5	Pos.6	Pos.7
D-33 rod				TE 408			
PCT (K)				------			
Time (s)				------			
D-51 rod				TE 409			
PCT (K)				------			
Time (s)				------			
D-53 rod				TE 410			
PCT (K)				------			
Time (s)				------			
D-66 rod				TE 411			
PCT (K)				------			
Time (s)				------			
D-77 rod				TE 412			
PCT (K)				------			
Time (s)				------			
D-86 rod				TE 413			
PCT (K)				850.1			
Time (s)				361.2			